POLITECNICO DI TORINO
Repository ISTITUZIONALE

Photocatalytic reduction of CO2 to valuable fuels by novel nanostructured titania materials

Original
Photocatalytic reduction of CO2 to valuable fuels by novel nanostructured titania materials / Akhter, Parveen. - (2015). [10.6092/polito/porto/2588280]

Availability:
This version is available at: 11583/2588280 since:

Publisher:
Politecnico di Torino

Published
DOI:10.6092/polito/porto/2588280

Terms of use:
Altro tipo di accesso

This article is made available under terms and conditions as specified in the corresponding bibliographic description in the repository

Publisher copyright

(Article begins on next page)

05 May 2023

POLITECNICO DI TORINO

DEPARTMENT OF APPLIED SCIENCE AND TECHNOLOGY (DISAT)

XXVII Cycle

Ph.D. Dissertation in Chemical Engineering:

Photocatalytic reduction of CO_2 to valuable fuels by novel nanostructured titania materials

Supervisor:
Prof. Nunzio Russo

Author:
Parveen Akhter

December 2014

This work is dedicated to my beloved family: especially, my husband Dr. Murid Hussain, elder son Muhammad Aayan Malik & younger one Muhammad Hassaan Malik as well as, in loving memory of my great mother.

Table of contents

Table of contents

Table of contents

Table of contents

Table of contents

Figures caption **Page No**

Figures caption

Figures caption

Figures caption

Figures caption

Figures caption

Figures, tables and schemes caption

Tables and schemes caption

Acknowledgements

"All praises and glory to ALMIGHTY ALLAH, who is most gracious and very merciful and his countless blessings on us who always helped me to complete my project"

The writing of a Ph.D. dissertation has been one of the enjoyable, sometimes frustrating experience, as well as very significant academic challenges in my life which, i have ever faced but the most important point is that, this work would have not been possible without the invaluable support, help and encouragement of an entire network of people including Professors, administrative staff, secretaries, former teachers, colleagues, friends, family and the top-most my supervisor who have helped me in this journey. So, I owe my sincere gratitude for all of them who always stay with me.

Foremost, I would like to give my immense, debt gratitude to my honorific supervisor to Prof. Dr. Nunzio Russo, who gave me a good chance to do work on this fascinating project (in Politecnico di Torino, Italy) with a constant help, guidance, and insightful discussion during my 3 years study plan. His higher standards knowledge inspired and provoked me to pursuing this work without any hesitations. He also makes my Ph.D. experience productive, stimulating and valuable.

I am also very grateful specifically for two persons, which i need to mention, one of them is Prof. Guido Saracco who is the Director of the Department of Applied Science and Technology (DISAT) of Politecnico di Torino and another is Prof. Debora Fino whose generous help, unconditional support, as well as providing me an opportunity to work with a multicultural atmosphere during my research work. I am also very thankful to former Ph.D. Coordinator, Prof. Vito Specchia, as well as the present Ph.D. Coordinator, Prof. Marco Vanni, for their necessary guidance, inspirational instruction helped me through this long but fulfilling road. This work could have not been possible without these kind people.

Acknowledgements

It is not sufficient to express my gratitude in a few words but it is very crucial to mention some of my deepest and heartfelt sincere to Dr. Murid Hussain who is not only my devoted husband but he formed the backbone and origin of my happiness by starting again my study. I have no words to state for his kindness. He mentored, encouraged and supported me in every difficulty from my 1st day of this journey to the final destination. Occasionally, when i became depressed from my work or something went wrong, he gave me his own examples during his Ph.D. study for making me strong, developing a confident and pursuing this work to go ahead to get ambitions. He always guided me the truth path and motivated me to learn things independently. However, i think after my supervisor, all my credit goes to him and i am also greatly indebted to him.

I also would like to acknowledge to all of my colleagues, lab fellows and friends for their help, discussion on lab's matters, keeping the Blu Nox lab's environment peaceful, and friendly. As we all are aware very well, that working place greatly influences the external environment, which should be more optimistic, friendly and clean to reach their final goal. However, I am so pleased to having all these opportunities throughout my study and also thank you so much for all those who are involved for making this ideal workplace.

I am thankful to SCUDO (School of Doctorates) of Polytechnic University of Torino and administrative staff, as well as my graduation committee for their positive response, valuable discussion, and input ideas for my dissertation. My sincerely gratitude goes to secretaries of the DISAT of Polytechnic University of Torino especially, to Elena Pertusato, Silvia Cerioli, and Margherita Cerrina for their cooperation and support for the management of our research group.

I also gratefully acknowledge the financial support by Politecnico di Torino during my entire research period.

How can I forgot to my former Prof. Ameen Shab from Pakistan, who just not taught me Chemistry but always encouraged me not only to grow as a chemist but also as an independent thinker. Even though, I tackled many difficulties during my study but he put only one thing in my mind, you have potential to do, you have to pursued and always advised me, be steadfast, nothing is impossible in this world. Therefore, i am very appreciative for such a sympathetic direction and instruction for making me strong.

Acknowledgements

Last but doesn't means least, and very importantly, I am very grateful to my parents, brothers and sisters, parents in law for their support, appreciation, help, love, encouragement and a lots of prayers throughout my study in direct and indirect way. I am very thankful to my very sweet family especially my two sons, elder one, Muhammad Aayan Malik and younger one, Muhammad Hassaan Malik for their sacrifices, unconditional love, great patience and help makes my work enthusiastic at all times.

Parveen Akhter

Abstract

In this study, an attempt has been made to synthesize the novel mesoporous Santa-Barbra-Amorphous-spherical shaped (SBA-15-S) and Korean Advance Institute of Science and Technology (KIT-6) mesoporous silica materials by hydrothermal treatment method. Afterward, these samples were used as support materials for synthesis of novel isolated Ti-SBA-15-S as well as Ti-KIT-6 with different Si/Ti (200, 100, 50 ratios) both in dried and calcined forms. Thereafter, the properties of the materials have been characterized through Brunner-Emmet-Teller *(BET)* to see the specific surface area, Scanning Electron Microscopy *(SEM)* to observe the surface morphology and microstructures, Ultraviolet-Visible spectroscopy *(UV-Vis)* to see the band gap energies and their corresponding wave lengths, Transmission Electron Microscopy (TEM) to investigate the behavior of Ti interaction with mesoporous materials, X-ray Photoelectron Spectroscopy (*XPS)* was done to observe the elemental composition, empirical formula as well as chemical and electronic states of the elements and Fourier-Transform Infra-Red (FT-IR) spectra to observe the Ti interaction to silica and presence of OH groups which play a significant role in photocatalytic activity. Photocatalytic activity of CO_2 reduction in Ti-KIT-6 (Si/Ti=100) showed better CH_4 production rate (*4.15 μmol·gcat.*$^{-1}$·h^{-1}) than the corresponding Ti-KIT-6-dried (*2.63 μmol·gcat.-1·h-1*) and the Ti-SBA-15-calcined/dried (*1.85, 3.45 μmol·gcat.-1·h-1*, respectively) in the initial photocatalytic reaction of CO_2 to methane. The Ti-KIT-6 (Si/Ti = 100) material also showed more OH groups, which are useful to obtain a higher production rate of the products, particularly methane, which was even higher than the best commercial TiO_2 (Aeroxide P25, Evonik Industries AG, Essen, Germany) photocatalyst. In addition, CH_3OH, H_2 and CO, are the other main fuel products produced by the Ti-KIT-6-calcined (Si/Ti=100) after optimization. The increased surface concentration of OH groups found in the Ti-KIT-6-calcined (Si/Ti=100) than the other two ratios (Si/Ti=200, 50), the presence of more accessible surface reaction active sites due to the lower numbers of Ti-O-Ti or TiO_2 agglomerates, and the more isolated Ti species which are uniformly dispersed on the 3-D KIT-6 mesoporous silica support without collapsing the mesoporous structure, have boosted the higher activity. The photocatalytic activity results of optimized Ti-KIT-6 calcined Si/Ti = 100 ratio preceded by the competitive adsorption of CO_2 and H_2O vapors towards other fuel products with *4.14, 0.029, 2.55, 1.45μmol* g_{-cat}^{-1} h^{-1} *for* CH_4, CH_3OH, H_2, *CO,* respectively.

Abstract

Similarly, various key parameters including, UV light source (300, 200W), UV light intensity, H_2O/CO_2 ratios and catalyst shapes, as well as water vapor effect, and long-term stability have been explored for optimized photocatalyst, which strongly influences the performance of the catalyst towards fuels production.

Moreover, another effort was made to synthesize the TiO_2 nanoparticles (TNPs) prepared by sol-gel method and new nanostructured Mesoporous TiO_2 by nanocasting technique or template method using KIT-6 as a template in order to establish the photocatalytic reduction of CO_2 with water vapor. In addition, commercial TiO_2 (Aeroxide P25) was used for comparison of photoactivity. Thus, the synthesized materials have been characterized by using BET, FE-SEM, XRD, SAXS, and UV-Vis, analyses techniques. TNPs have of an average 11nm TiO_2 particle size, higher surface area of ($151m^2/g$) as compared to commercial TiO_2 Aeroxide P25 i.e. ($53m^2/g$) which also demonstrate an enhance adsorption capacity. Furthermore, Meso.TiO_2 has shown a greater surface area ($190m^2/g$) along with mesoporosity with (4nm) which is much more higher than that of TNPs and also from commercial TiO_2 (Aeroxide P25). Overall, Meso. TiO_2 was superior in photocataltic activity of CO_2 reduction towards renewable fuel products than that of other TiO_2s. The photocatalytic activity of CO_2 reduction comparison with titania nanoparticles (TNPs) and Evonik P25 which showed the improved resuls towards fuel production such as *(14.01, 0.11, 83.50, 26.30 µmol* g_{-cat}^{-1} h^{-1} for CH_4, CH_3OH, H_2, CO respectively). However, various reaction factors, activation/regeneration of photocatalyst and reaction mechanism and pathways of CO_2 reduction on Meso. TiO_2 have been explored.

Finally, nanostructured TiO_2/KIT-6 series with (1, 5, 10, 20, 30, 50, 70, and 90 %) by using different titania wt% have been prepared by precipitation following the sol-gel hydrolysis and condensation of titania precursor dispersed within/surface of the mesoporous silica KIT-6. The characterization was made by N_2 adsorption/desorption isptherms, FE-SEM, XRD and UV-Vis, analyses techniques to observe the physio-chemical properties of materials and their corelation with photocatalytic activity. Furthermore, screening of the TiO_2 series showed that selectivity toward fuel products depends on the various titania loadings. However, on the basis of our required products (hydrocarbon and H_2, CO) the 20wt% TiO_2/KIT-6 nanocomposite was found to be the optimized photocatalyst with higher photocatalytic products formation than that of other wt% nanocomposites. The photocatalytic activity of CO_2 reduction for 20 wt%

Abstract

TiO_2/KIT-6 showed the production for CH_4, CH_3OH, H_2, CO with *44.55, 1.08, 9.20, and 120* $\mu mol\ g_{-cat}^{-1}\ h^{-1}$, respectively. Furthermore, the affect of thermal treatment was explored for 20% TiO_2/KIT-6 to observe the change in structure and its corealation with photocatalytic activity. The proposed reaction mechanism/pathways for CO_2 reduction with H_2O vapor on TiO_2/KIT-6 nanocomposite has also been discussed.

Keywords: Isolated Ti-oxide, Meso.TiO_2, TiO_2/KIT-6 nanocomposite, Carbon dioxide, Water vapor, Fuels; Photocatalysis

Chapter 1

1 Introduction

1.1 General principle of photocatalysis

The word "photocatalysis" has a Greek origin and comprises of two parts: the prefix Photo (phos: light) and the word catalysis (katalyo: break apart, décompose) [1]. However, an appropriate definition could be, an acceleration of chemical reaction or a change in the rate of a chemical reaction without being use of catalyst in the presence of light it can be either UV or visible light to boost the reaction. In the prescence of light, semiconductor photocatalyst undergoes to generation of a pair electron/hole **(A)** but it could only be possible if the energy of light is greater or equal to band gap energy of the photocatalyst.

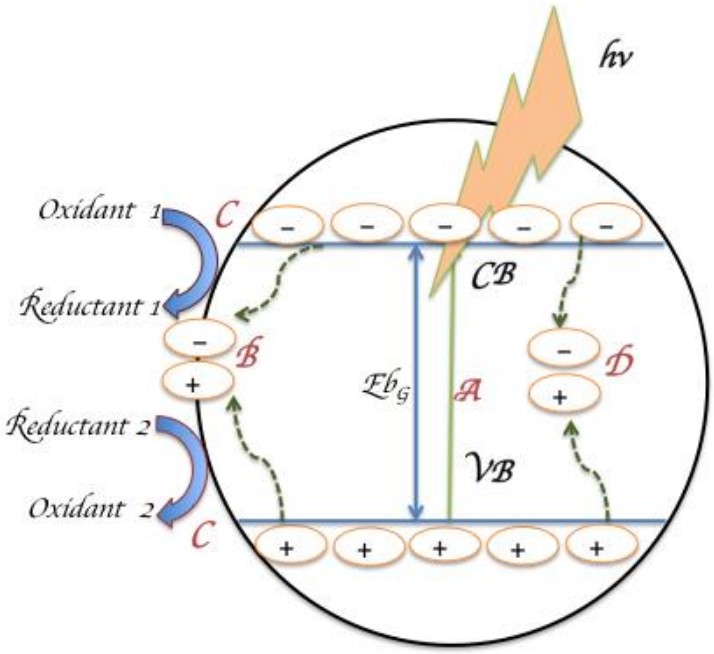

Figure: 1.1 *General principle of photocatalysis* ***(A)*** e^-/h^+ *pair generation after light illumination* ***(B)*** *surface recombination* ***(C)*** *redox reactions* ***(D)*** *volume recombination.*

However, higher energy e^- (electrons) promoted from valence band to the conduction band leaving the h^+ (holes) in the valence band. [2]

Valence band: Highest energy band in which all energy levels are occupied by electrons or all energy level are filled with electrons.

Conduction band: Lowest energy band without electrons or unfilled with electrons.

Photogenerated e^-/h^+ pairs move to the surface of the photocatalyst **(B)** where e^-/h^+ participates in the redox reaction with adsorbate having appropriate redox potentials (*called surface recombination)* **(C)**. However, in case of VB redox potential must have more positive than that of the adsorbates. Similarly, CB electrons must have more negative redox potential to reduce the adsorbate species. On the other hand, there might be a possibility that e^-/h^+ recombine in the volume of the semiconductor catalyst (*called volume recombination*) to form of unproductive products or heat **(D).** However, the pioneering work on the photocatalysis by using semiconducting catalyst done by Fujishima and Honda [3] called "Honda-Fujishima-effect" to discover the photocatalytic splitting of water on TiO_2 electrodes resulting, the formation of H_2. This happening manifests the beginning of a new area in heterogeneous photocatalysis.

1.2 Heterogeneous photocatalysis

Photocatalytic reactions may occur homogeneously or heterogeneously both are promising technologies, but most importantly "*Heterogeneous photocatalysis*" has been more extensively studied in the last few years because of its potential use for environmental problems, energy generation and synthesis of organic materials such as (methane, methanol, carbon monoxide, formic acid, formaldehyde, and other hydrocarbons *etc.,).* Additionally, there are two major types of the heterogeneous photocatalysts such as bulk semiconductor photocatalysts and matrix dispersed photocatalysts [4-8]. Most significant features about the heterogeneous photocatalysis reaction are involved in five categories [9]

i) Diffusion of reactants to the surface

ii) Adsorption of reactants onto the surface

iii) Reaction on the surface

iv) Desorption of products from the surface

v) Diffusion of products from the surface

The use of photocatalyst in any photocatalytic application is not only a crucial but also gives the expectation to get better photocatalytic products. In such a way, by modifying it with various species, which can enhance its photocatalytic performance is considered very vital step. A plenty of work has been carried out by various researchers by modification of titania but some pure and modify titania is listed below.

Cation doped titania: Au/TiO_2, Cu/TiO_2, Pt/TiO_2, Ag/TiO_2, Ru/TiO_2, Rh/TiO_2 Pd/TiO_2, and Cr/TiO_2

Anion dopted titania: Br, I, F, $S\text{-}TiO_2$, $N\text{-}TiO_2$, $C\text{-}TiO_2$

Sensitization of titania: Dye/TiO_2, $CdSe/TiO_2$, RhB/TiO_2, $AgBr/\ TiO_2$

$CdS\text{-}Pt\text{-}Fe\text{-}TiO_2$

Oxidizes catalyst: TiO_2, ZnO, FeO, ZrO, SnO, Bi WO_3, SiO_2, *TiO_2/SiO_2 (in this work).*

Non-oxidizes catalyst: TiO_2/Y-zeolite, Ti-MCM-41, Clay-TiO_2, TNTs. and novel Ti-SBA 15-S, *Ti-KIT-6 (in this study).*

The list of the TiO_2 semiconductor photocatalysts with simple, doped or isolated dispersed forms is presented in the chapter 4 and Table: 4.2. But some of the titania modification process are briefly explained and can be categories into bulk, metals and non metals doped, dye sensitization and isolated Ti-based titania.

1.2.1 Bulk titania/powder titania photocatalyst

In heterogeneous photocatalysis two or more phases are used in the photocatalytic reaction, 1) light source with semiconductor material is used to initiate the photoreaction. 2) The catalysts can carry out substrate oxidation and reduction simultaneously, 3) light source UV light or visible light. Though, bulk semiconductor photocatalyst includes metal oxides, sulphides, nitrides, oxynitrides and titanium dioxides, which is most used photocatalysts in CO_2

photoreduction. In the case of the bulk TiO_2 materials, upon the UV irradiation reduction of CO_2 with H_2O resulting in the formation of CH_4 + CH_3OH and yields of these products increased with the incresing of UV light duration. However, it is clear indication that CH_4 formation from CO_2 reduction with H_2O vapor took place in solid-gas phase system with powder TiO_2. When titania powder is illuminated by UV light, the absorption of photon having energy equal or greater than the band gap energy of the semiconductor (3.2eV for anatase) produced e^-/h^+ pairs, shown in [(Eq. (1.1)].

$$TiO_2 \ (\xrightarrow{h\nu})e^-_{cb}\,(TiO2) + \ h^+_{vb}(TiO2) \qquad (1.1)$$

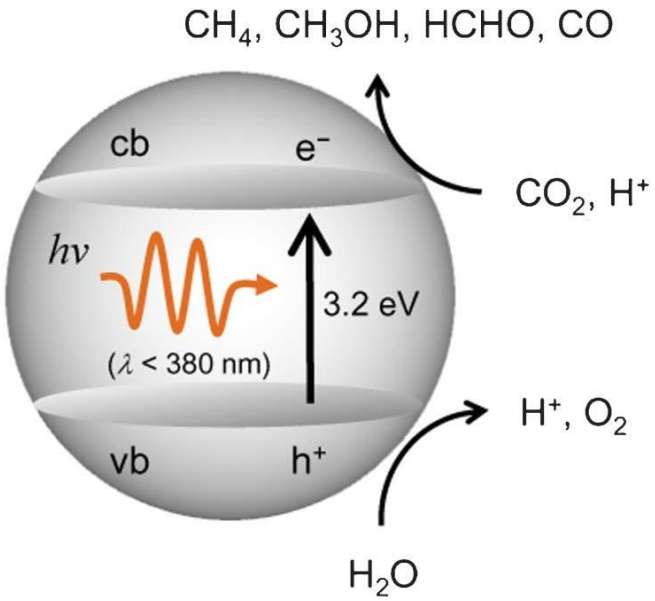

Figure: 1.2 *Reaction scheme for the photocatalytic reduction of CO_2 with H_2O on bulk TiO_2 [10].*

which lead to the promotion of electrons to CB and leaving the holes behind in the VB respectively. Consequently, the TiO_2 particle can act as either an electron donor or acceptor for molecules in the surrounding medium. Thus, the efficiency to photocatalytic activity and product selectivity of the bulk titania is lower.

Chapter 1

1.2.2 Isolated Ti-species as photocatalyst

In another type of heterogeneous photocatalyst, the isolated species, which are entrapped in an inert matrix, have lager surface area, good adsorption property of the reactants and light, which enhanced photoactivity towards fuel formation. In addition, in isolated Ti-highly dispersed species photo generated charges e^-/h^+ pairs are very close to each other, which play a very significant role in the photocatalysis process of CO_2 reduction.

$$[Ti^{4+} - O^{2-}] \xrightarrow{h\nu} [Ti^{3+} - O^{-}] \qquad (1.2)$$

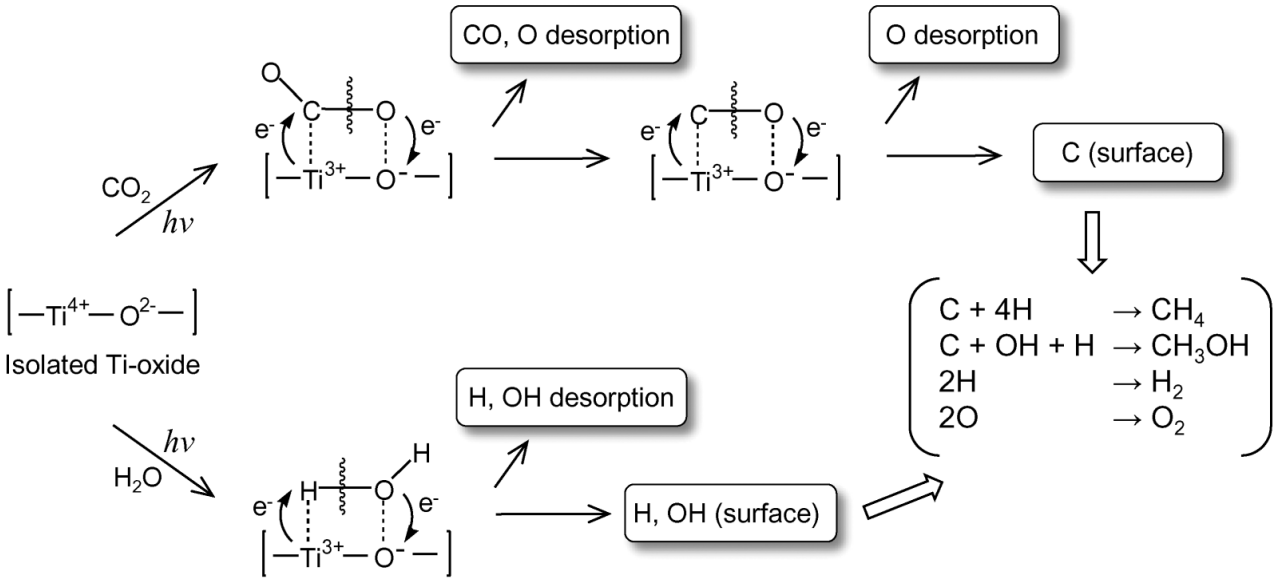

Figure: 1.3 *Schematic diagram for the photocatalytic reduction of CO_2 with H_2O on* the isolated titanium oxide species *[10]*.

In such a way, an isolated and tetrahedrally coordinated Ti–oxide species under light irradiation transfer an electron from the oxygen O^{2-} to Ti^{4+} ions, resulting in the transit state formation of a pairs of trapped hole centers $O^-$and electron centers Ti^{3+}which are localize quite near to each other compared to the electron and hole produced in semiconductor bulk titania photocatalyst [10]. Moreover, owing to this unique property Ti-isolated species play a significant

role in different photocatalytic reactions. Reaction mechanism of CO_2 reduction and H_2O oxidation is elucidated in isolated Ti-species as shown in Fig. 1.3. Currently, these procedures are widely engaged in the CO_2 reduction process while, the photocatalytic productivity and selectivity toward valuable fuel product is higher in isolated titania as compared to bulk titania.

1.2.3 Single crystal titania photocatalyst

The photocatalytic reduction of CO_2 with H_2O on rutile-type single crystal TiO_2 (100) and TiO_2(110) surfaces was performed by Yamashita et al. [11] and selectivity of the photocatalytic reactions strongly depends on the type of TiO_2 single crystal surface. UV-irradiation of the TiO_2(100) single crystal catalyst in the presence of a mixture of CO_2 and H_2O produced both hydrocarbons, CH_4 and CH_3OH with *3.5 and 2.4µmol* h^{-1} *g-cat*$^{-1}$ yields respectively but limitation for TiO_2(110) single crystal, only *0.84µmol h1*$^{-}$ *g- cat*$^{-1}$$CH_3OH$ was detected not methane. However, the photo-generated electrons localize on the surface sites of excited TiO_2 participate with CO_2 molecules to form intermediate into intermediate and surface Ti atoms acts as a reductive site. Consequently, TiO_2(100) single crystal showed the more photocatalytic activity towards hydrocarbon formation [11].

1.2.4 Doping of titania with metals (Cations doping)

The the main barrier, which reduced the photocatalytic activity of the titania catalyst, is the higher rate of recombination of (e^-) and holes (h^+) pairs. However, to overcome this problem or prevent the recombination of (e^-) and holes (h^+) pairs, the loading of photocatalysts with metals and noble metals to function as charge-carrier traps or induced it with isolated Ti-species is the best solution to reduce this risk. The surface defects and sites and inequalities, which are present on the catalyst surface as well as in the bulk participate as charge carrier traps and suppress the recombination of electron and holes, as elucidated in Fig. 1.4. However

different studies of CO_2 reduction with H_2O have been carried out in order to improve photoactivity.

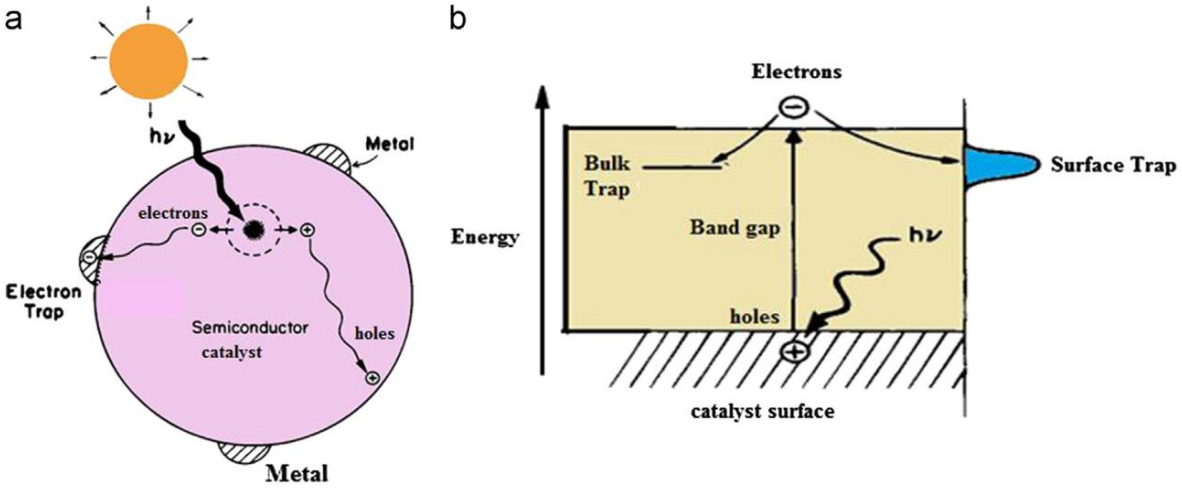

Figure: 1.4 (a) *Doping of semiconductor photocatalyst with metals for electron trapping* ***(b)*** *surface and bulk electron carrier trappings (Adapted from Ref [12]).*

Some modified titania doped with metals such as Cu/TiO_2 photocatalyst loading with 0.3 to1.0wt% reduced the CH_4 but surprisingly CH_3OH could be observed [13]. Afterward, it was suggested that by further increasing the Cu loading on the TiO_2, increased the CH_3OH yield significantly, but 3% Cu/TiO_2, was found to be optimized with maximum three times higher than the original TiO_2 but no methane at all. [14] But another group, Wu et al. observed that maximum methanol yield was obtained by (*0.45 μ mole/g-cat•h*) by using 1.2wt%Cu/TiO_2 under the increasing light intensity of light from 1 to 6 W/cm^2 [15]. Similarly, pt/TiO_2 favor to production of CH_4, which remarkably increased with increasing of pt 0.1 to 1.0% loading on titania [16].

1.2.5 Nitrogen doped titania: N/TiO_2 (Anion doping)

Photocatalytic reduction of CO_2 with H_2O vapor using nitrogen doped TiO_2 nanotube arrays co-catalyzed with copper and/or Pt nanoparticles, was investigated by Varghese et al. [17].

Methane as a main product with yield *160 μL/gh* as well as some another other hydrocarbons obtain as photocatalytic product in the presence of natural sunlight. In addition, recently nitrogen doped TiO_2 study was carried out by Michalkiewicz et al. [18], methanol was found to be a CO_2 reduction product. Its high efficiency is mainly depend on the synthesis route, higher surface area, crystal phase composition.

1.2.6 Ti/Si binary oxide/Mixed oxide titania photocatalyst

The Ti/Si binary oxide catalysts in the presence of a gaseous mixture of CO_2 and H_2O led to the formation of CH_4 and CH_3OH as the main products. Higher photocatalytic of CO_2 reduction was observed towards hydrocarbon formation. Due to this appearance of high photocatalytic activity for the binary oxides is closely associated with the formation of the charge transfer excited complex due to the highly dispersed tetrahedral Ti–oxide species. Ti–oxide species maintain tetrahedral geometry until the TiO_2 content approaches up to approximately 20wt%. Accordingly, the Ti/Si binary oxides with a high Ti content can be successfully utilized as active photocatalysts for the efficient reduction of CO_2 with H_2O in the gas-solid system. However, Wu J C S [19] noticed that methane formation increased by loading mixed oxies with metal components such as Cu (0.5wt%)–Fe (0.5wt%)/TiO_2–SiO_2-acac *(0.279* μ*mol/g-cat h*) showed higher production rate than that of undoped mixed oxides TiO_2–SiO_2-acac *(0.177* μ*mol/g-cat h).*

1.2.7 Ti–oxide anchored on porous silica glass

The anchored Ti–oxide catalysts in the presence of CO_2 reduction with H_2O led to the evolution of CH_4, CH_3OH and CO at 323 K. The total yield was larger under UV- irradiation at 323 K than at 275 K. The efficiency of the photocatalytic reaction strongly depends on the ratio of H_2O/CO_2 and its activity increases when increasing the H_2O/CO_2 ratio while an excess amount of H_2O suppresses the reaction. However, optimum H_2O/CO_2 should be under consideration to obtain the higher photocatalytic activity. Similarly, Sasirekha et al. [20] investigated that that yield of CH_4 increased significantly photocatalytic reduction of CO_2 with H_2O when titania is doped on the support SiO_2 material.

Chapter 1

1.2.8 *Ti–oxide anchored on zeolite materials*

The Ti–oxide anchored onto zeolite, Ti-oxide/Y-zeolite, the ex-Ti–oxide/Y-zeolite UV-irradiation of powdered TiO_2 and Ti–oxide/Y-zeolite catalysts for CO_2 reduction and H_2O oxidation led to the evolution of CH_4 and CH_3OH at 328 K, along with certain amount of lower hydrocarbon such as C_2H_4 and C_2H_6 were observed [21].

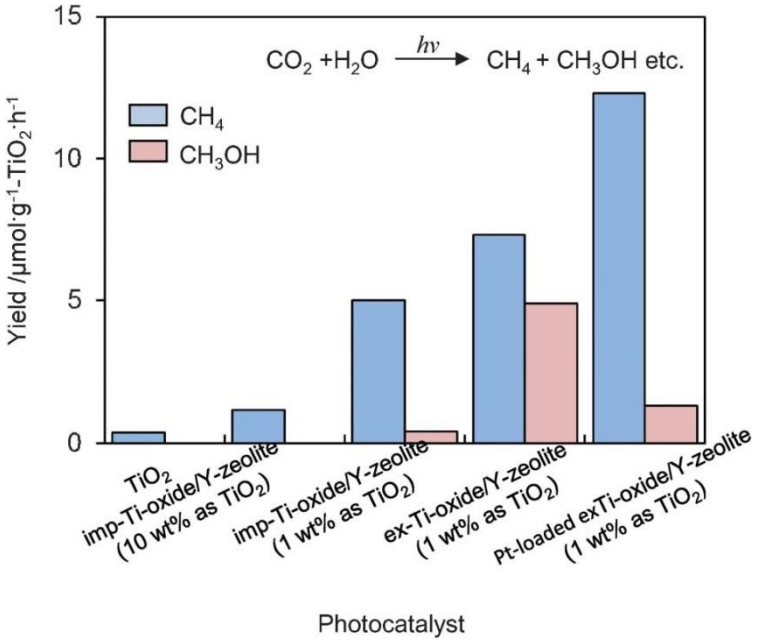

Figure: 1.5 *Photocatalytic reduction of CO_2 with H_2O on anatase TiO_2 powder, Ti–oxide anchored on Y-zeolite prepared by different preparation method with various titania wt% loading (Adapted from Ref [10]).*

The ex-Ti–oxide/Y-zeolite exhibits a high activity and selectivity for the formation of CH_3OH, while the formation of CH_4 was dominated on bulk TiO_2 as well as on the imp-Ti–oxide /Y- zeolite. In addition, improved photocatalytic activity, was observed by deposition of Pt towards CH_4 ($12\mu mol\ g^{-1}\ TiO_2\text{-}h^{-1}$) but the CH_3OH selectivity significantly decreased shown in the Fig. 1.5 which, was observed highest with ($5\mu mol\ g^{-1}\ TiO_2\text{-}h^{-1}$) in ex-Ti oxide/Y-zeolite. However, these finding results indicate that Ti-oxides species serve as active photocatalyst for CO_2 reduction with H_2O and selectivity towards CH_3OH formation.

Chapter 1

1.2.9 Zeolites with Ti-content and mesoporous molecular sieve

Ti–oxide species within the mesoporous silica have revealed a distinctive structure and high selectivity in the oxidation of organic substances with hydrogen peroxide [22]. Moreover Ti-containing zeolites such as TS-1, Ti–Beta and mesoporous molecular sieves Ti–MCM, Ti–HMS, Ti–FSM as shown in the Fig. 1.6 have better photocatalytic activity to CH_4 and CH_3OH formation.

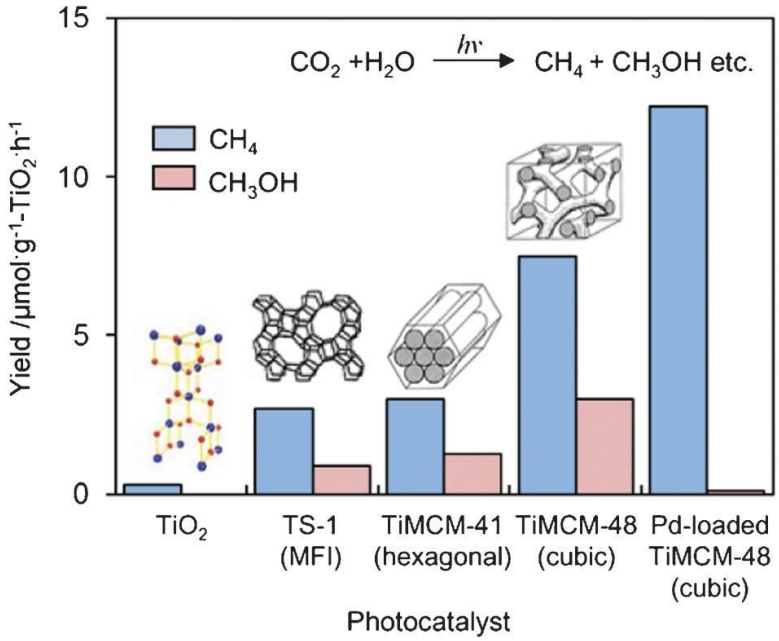

Figure: 1.6 *Photocatalytic reduction of CO_2 with H_2O on TiO_2 powder, TS-1, Ti–MCM-41, Ti–MCM-48, and the Pt-loaded Ti–MCM-48 catalysts CH_4 and CH_3OH formation (Adapted from Ref [10]).*

Furthermore, it was investigated that Ti-oxide in the mesoporous molecular sieve are highly dispersed which is good sign to hydrocarbon formation. Most importantly, CH_4 (more than $13\mu mol\ g^{-1}\ TiO_2\text{-}h^{-1}$) formation was highest in the metal-doped mesoporous molecular sieve but on the other hand selectivity of CH_3OH formation was higher in Ti-MCM 48 (almost $3\mu mol\ g^{-1}\ TiO_2\text{-}h^{-1}$) owing to its 3-D pore structure as well as larger pore size.

Chapter 1

1.2.10 Dye sensitization of titania photocatalyst

Typically, narrow-band semiconductors or visible-light-active molecules (dyes) are used as sensitizing agents. Sensitization with dyes is a commonly used technique in solar cells, where a large number of inorganic or organic dyes have been verified Fig. 1.7. Similarly, coupled semiconductors, for example, CdS and TiO_2, or CdSe and ZnO, have been shown to enhance the efficiency through extension of the absorption range and improvement in the charge separation [23]. The LUMO of the dye has to be higher in energy than the conduction band edge of the semiconductor for the electron transfer to occur.

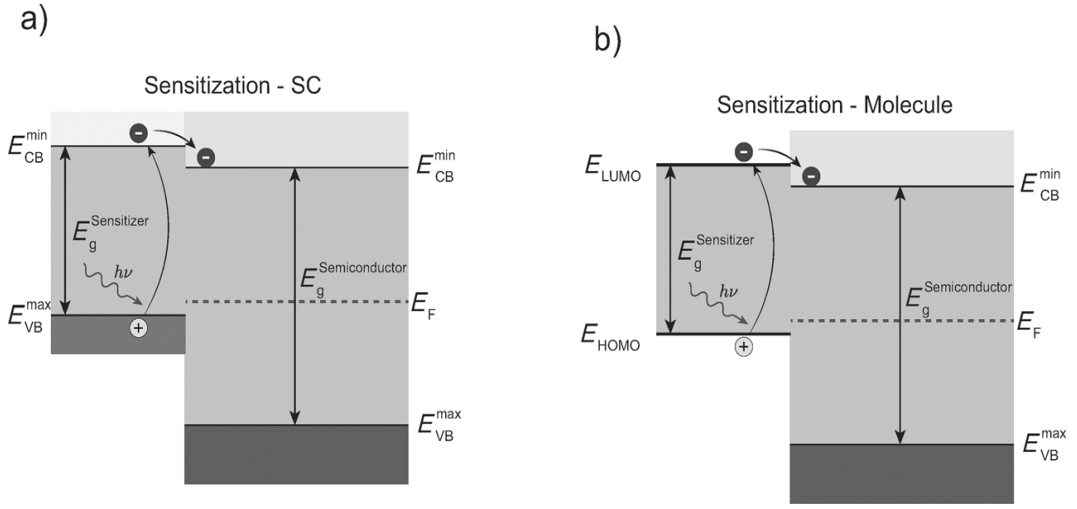

Figure: 1.7 *Sensitization of a wide band gap semiconductor* ***(a)*** *narrow band gap with aligned conduction band* ***(b)*** *a dye that absorbs in the visible region. (Adapted from Ref [24])*

Dye sensitization process is only limited because of narrow band gap, without applying these approaches visible or solar light is insufficient which causes the reduction of photoactivity. Similarly, Wu J C S [19] investigated that the methane production increased from solar to artificial light response. Thus, various light sources effect for N3-dye–Cu (0.5wt%)–Fe (0.5 wt%)/P25 i.e. *(0.617μ mol/g-cat h)* with average concentrated sunlight intensity of 60 mW/cm^2 and N3-dye–Cu (0.5wt%)– Fe (0.5wt%)/P25 *(0.84 μ mol/g-cat h)* with artificial light in the range of 320–500 nm with the intensity of 225 mW/cm^2 for CO_2 reduction.

In addition, Lee et al. [25] used the nanoporous TiO_2 and study its application, to dye-sensitized solar cells (DSSCs). They proposed that the energy conversion efficiency of the DSSC prepared from nanoporous structured TiO_2 was approximately 8.71% with the N719 dye under 100mWcm^{-2} simulated light. When a dye molecule absorbs light, electrons on the HOMO orbital are excited to an electronically excited state, LUMO orbital. The electron is then transferred to the conduction band of TiO_2. Therefore, the energy difference between the HOMO orbital of the dye and the conduction band of TiO_2 was examined. With nanoporous TiO_2 having a shorter band gap than nano-sized TiO_2, it is easier to move excited electrons from the valence band to the conduction band on the surface. Therefore, nanoporous TiO_2 is a better material in DSSC than nano-sized TiO_2.

1.3 Key role of photocatalysis with greenhouse gas (CO_2)

From last few decades, *photocatalysis* is playing a significant role in different fields such as H_2O splitting, environmental pollution control, water and air purification, self-cleaning surfaces, and reduction of atmospheric CO_2 concentration *etc*., which is considered to be the most crucial concern regarding global warming issues as well as to overcome the health problems of human being. Despite, approximately more than 80% of the world's energy supply is derived from combustion of the fossil fuel, which causes the pollution and contributes to the green house effect. However, the recent atmospheric concentration inclination of carbon dioxide (CO_2), which is considered a primary greenhouse gas amongst those gases such as methane (CH_4), chlorofluorocarbons (CFCs), and nitrous oxide (N_2O) threaten a meaningful role in global warming along with also raised various environmental harms associated with human activities and is currently considered a key challenge for the world [26].

On one side, key emission sources of CO_2 are mostly due to the burning of fossil fuel such as oil, natural gas, coal *etc*., which not only accelerated the greenhouse effect but human activity which generates about 37 billion tons of CO_2 emissions each year, with about 30 Gt of this coming from energy-related emissions. Twenty years ago, total emissions were less than 25 Gt and are projected to rise to over 50 Gt. However, burning 1 t of carbon in fossil fuels releases more than 3.5t of carbon dioxide [27]. Due to such adverse effect, the Earth's surface temperature has risen by approximately 0.6 K in the past century, with particularly significant warming trends over the past two decades. On the other hands, depletion of the fossils fuel

worldwide is dramatically increasing every year because of strong energy demands of human being. Consequently, to fulfill the energy demand and to prevent the globe to being heat up, a lot of strategies have been made by numerous researchers, scientists, and investigators from last more than four decades. Therefore, CO_2 reduction to valuable compounds or chemicals is the most widely used technology to overcome these issues and to provide energy for future progeny simultaneously.

1.4 Capture of CO_2 from atmosphere by various technologies

However, various technologies have been adopted for capturing of CO_2 from atmosphere and then utilized CO_2 to formation of energy bearing products or renewable fuel.

- *CCS (Carbon Capture and Storage):* This technique involves the capture of CO_2 from the atmosphere, the generation of a highly concentrated stream of CO_2, which then participate in transportation phenomena and finally storage takes place in geological formations including oil, gas reserves, and on the bottom of the oceans. In particular, before being stored in the appropriate sites, it can be used directly for industrial purposes; the carbon dioxide is purified, compressed and liquefied. The main disadvantage is that each of these steps (separation, purification, compression, transport and storage) requires a lot of energy. This technology can be used for CO_2 emissions from power plants and industries, which does not allow the capture of carbon dioxide from the transport sector or the residential area.
- *DAC (Direct Air Capture):* This process of the CO_2 capturing from air is very sensitive. In this technology the flow of air is taken from the environment, which further is used to separate from another atmospheric gases such as N_2 and O_2, the separated gas is compressed and finally transported to storage.
- *SCPP (Solar Chimney Power Plants):* In this process collected CO_2 is circulated by fireplace very top of the center of the manifold. Where the air enters into the collector and the sun continuous heats it for specific period of time. Afterward, the traveling around the collector reaches the mouth of the fireplace, where a turbine produces electricity to purify this captured CO_2 gas for further utilization [21]. In addition, different other methods has been used for capturing of CO_2 involve Post combustion, pre-combustion and oxy-combustions *etc*.

- *Postcombustion:* Includes solvant scrubing, biological capture by algae ponds, high temperature solid sorbent, membrane separation technology (separation of CO_2 from flue gases).

- *Precombustion*: Includes sorbent enhanced reforming using carbonate looping, integrated gasification, membrane separation technology (H_2 separation from synthesis gas).

- *Oxy-combstion:* Chemical combustion looping by using solid metal oxygen carrier, oxy-fuel boiler with oxygen separation from nitrogen by cryogenic air separation, membrane separation (for O_2 separation from N_2 with ion-exchange membrane). However, these are not economically feasible [28].

1.4.1 CO_2 conversion approaches

The previous work on photocatalysis by Honda-Fujishima, sparked the a lot of research which has been carried out to exploring the new ways of applications in reduction of CO_2 such as electrochemical CO_2 reduction [29], photovoltaic [30], self-cleaning coatings [31], electro chronic display devices [32]. Moreover, thermal CO_2 photocatalytic reduction [33], biological reduction by plants [34], and photoelectrochemical reduction of CO_2 previously reported by Halmann et al. [35], by using an electrochemical cell. Unfortunately, an electrochemical cell for CO_2 conversion has disadvantages because of its very slow kinetics as well as very high energy intensive [36, 37]. Afterward, the initial work on CO_2 photocatalytic reduction by various semiconductors under UV light illumination was carried out by Inoue et al [38]. This not only provided a new glimpse and excitement as well as encouraged the various studies to boost this technology. In addition to these above-mentioned methods, photocatalysis technology has been extensively studied for *reduction of CO_2* to valuable fuel products owing to its advantageous such as

- Its input energy consumption is very low
- Profitable products formation, and
- The use of renewable energy makes it more challenging [39, 21].

Moving on, to photocatalysis technologie, a lot of investigators have used various semiconductors photocatalysts. Generally, semiconductors are particularly useful as

photocatalysts because of its combination of electronic structues, light absorption, charge transport proprety as well as excited-state lifetimes characteristics. In addition, to proceed this technology, for accomplish the desired products certain photocatalysts are needed to hasten the chemical reactions. Photocatalysts are considered solids or in suspension that can stimulate reactions in the presence of light source either UV or solar light without being consumed catalyst itself [40]. However, different photocatalysts oxides and non-oxides, such as titanium dioxde (TiO_2), cadmium sulphide (CdS), zinc sulphide (ZnS), silicon carbide (SiC), towngston oxide (WO_3), iron oxide (Fe_2O_3), zirconium oxide (ZrO_2), gallium oxide (Ga_2O_3), zinc oxide (ZnO), and magnesium oxide (MgO_2), have been used extensively for photocatalytic reduction [41]. Amongst all above-mentioned photocatalysts titanium dioxide (TiO_2) is particularly noteworthy due to its unique properties. Wide band-gap TiO_2 photocatalyst (3.2 eV) is considered the most convenient candidate for these applications. Additionally, this is an environmentally friendly material which shows a good oxidation power, strong resistance to chemicals and photocorrosion, non-toxicity, superior charge transport properties, a low operational temperature, low cost, and significantly low energy consumption [42-44]. All of these photocatalysts have led to relevant applications in various eras specifically for fuel production. Still, photocatalysis is an its embryonic stage, further progressive works and strategies for the development of new photocatalyst, or modification, design/configuration *etc*. are needed to be consideration substantially improving the photocatalytic activity and selectivity towards the renewable fuel formation for future progeny. In fact, an efficient catalyst must have a sufficient redox potential to reduction of CO_2 and oxidation of H_2O on reduction band and valence band respectively. Additionally, a good photocatalyst must have a highest specific surface area which increases the adsorption of reactants on the surface of catalyst, along with smaller particle size, highest crystallinity, an adequate band gap of photocatalyst to absorb the sufficient light, lower chance of recombination of a pair of e^-/h^+, higher mobility of charges distribution, and longer life time stability as well as selectivity towards the products formation are necessary parameters should be in consideration to start the photocatalysis process for CO_2 reduction.

1.5 Applications of photocatalysis

Heterogeneous photocatalysis has been demonstrated as a low cost and sustainable technology, which plays a significant role in the various areas starting from households to

commercial products. Some of them are listed as:

- *Water purification:* Globally, 1 billion people lack access to safe water supplies and 2.6 billion are without access to basic sanitation. Similarly, growth in the global population, the deficiency of supply of clean, which are strong link between quality of water and human health are the major concerned, connected with globe thus, need for clean water. Nanotechnology is one of the most promising emerging technologies for efficient, economical and environmentally friendly water and wastewater treatment offering great potential for manufacturers in Europe. Photocatalysis can also be used to destroy bacteria and viruses. The increasing incidence of algal blooms in fresh water supplies and the consequent possibility of cyanobacterial microcystin contamination of potable water *Microcystin toxins* are also degraded on immobilized titanium dioxide catalyst. Photodisinfection sensitized by TiO_2 had some effect on the degradation of the green algae. This is being used to great advantage in many developed and developing nations to treat water especially in remote and disaster areas without portable water supply or electricity. In addition, water can be purified by applying various possible ways through photocatalysis for lakes and water-storage tanks, fish feeding tanks, drainage water and industrial wastewater along with river water by using titania as a photocatalyst.
- *Air cleaning:* This technology had a wide range of applications as a air cleaning purpose indoor (room air cleaner, interior air cleaner for factories) as well as exterior air cleaner (highways, building walls, roadways and footpaths, tunnel walls, soundproof walls *etc*.
- *Self-cleaning*: TiO_2 coatings to buildings as a self-cleaning purposes is of the significant interest. If a TiO_2 film is prepared with a certain percentage of SiO_2, which, shows super hydrophilic properties after UV illumination. In this case, electrons and holes are still produced but they react in a different way than normal photocatalysts. The electrons tend to reduce the Ti (IV) cations to Ti (III), and the holes oxidize the O^{2-} anions resulting production of OH groups that tend to make the surface more hydrophilic. The longer the surface is irradiated with UV light, the smaller the contact angle of water becomes. However, in such a way this application is applies in all the self-

cleaning purposes in residential places for instance kitchen and bathrooms and offices, curtains an interior furnishings, highway tunnel lamp cover glass, tunnel wall, soundproofed wall, traffic signs and reflectors, tent materials, cloth for hospital garments, cleaning the mirrors of the cars *etc.*

- *Self-sterilization hospital*: Used in the wall of the operating room, tiles of floor, rat-breeding rooms and in the rest rooms to protect from infection.
- *Anti-fogging agent:* Due to its super hydrophobicity, used in mirrors for bathrooms, heat exchangers for air conditioners and high-voltage electric transmission equipment, glass films, general-purpose paints and coatings and optical lenses.
- *Removal of trace metals:* The environmental applications of heterogeneous photocatalysis include removing heavy metals from the water which is very important for human health and to improve the quality of water e.g. Chromium (Cr), Lead (Pb), Arsenic (As), Nickel (Ni), Copper (Cu) and Cadmium (Cd) *etc.*
- *Removal of organic and inorganic compound:* Photocatalysis has been used for the destruction of organic compounds such as alcohols, carboxylic acids, which is then converted to into harmless products, for example, carbon dioxide, water, and simple mineral acids. In addition inorganic species such as bromate, or chlorate, nitric oxide, palladium, rhodium and sulfur species can be decomposed. Some metal salts such as $AgNO_3$, and organometalic compound (e.g., CH_3HgCl), cyanide, and thiocyanate, can be removed from water to make it free from some dangerous compound.
- *Medical application:* Photocatalysis application in medical field by using TiO_2 Fabrics is very important which is used to disinfect microbes, viruses and bacteria *etc.* Hospital garments especially, in Japan are TiO_2 fabricated, which are used during operations, which protect from hospital infection including MRSA (*Staphylococcus)*
- *Applications in construction:* In some European countries TiO_2 cement (pellite cement) has been used in road during road construction that protects the emissions of NO (nitrous oxide) and NO_2 (nitric oxide) cause the atmospheric pollution. By applying such process other pollutants present can be eliminated at some extent and provides the positive sign for environmental protection.
- *Degradation of pesticides:* Pesticides, which includes herbicides, insecticides, and

fungicides, have been developed to exhibit an envisioned efficacy to specific pests, fungal diseases and weeds. Pesticides are considered cumulative and very toxic species. However, their presence as contaminants in aquatic environments may cause serious problems for human beings and other organisms. Therefore, the use of TiO_2 for decomposition of organic compounds is an excellent approach for environment to cleanup through photo-oxidation.

- *Production of hydrogen fuel:* Photocatalysis using solar energy has been widely studied as a possible system to produce hydrogen from water. So, water splitting with a system in which an n-type TiO_2 semiconductor electrode was connected through an electrical load to a platinum black counter electrode. When the surface of the TiO_2 electrode was irradiated with near-UV light, photocurrent flowed from the platinum counter electrode to the TiO_2 electrode through the external circuit, resulting the decomposition or splitting of water to produce oxygen and hydrogen.

In this study, an attempt has been made to synthesize novel mesoporous materials such as SBA-15S and KIT-6 by a hydrothermal treatment method. Furthermore, these materials were used for the synthesis of Ti-SBA-15 and Ti-KIT-6 materials with different Si/Ti ratios (200, 100, 50 ratios) both in dried and calcined forms. Besides, these mesoporous photocatalysts were primarily characterized by BET, SEM, UV-Vis, TEM, XPS and FT-IR analysis technique to observe the physical and chemical properties of the synthesized photocatalysts. Furthermore, these Ti-based mesoporous materials were tested for photocatalytic activity of CO_2 reduction with H_2O vapor towards methane as well as other fuel produtcs for optimized Ti-KIT-6 calcined Si/Ti = 100. Moreover, mesoporous TiO_2 was prepared by nanocasting or template method and characterized by BET specific surface area, FE-SEM, XRD and SAXS *etc* and photocatalytic activity of CO_2 reduction was compared with titania nanoparticles (TNPs) and Evonik P25 which showed the improved results towards fuels production. However, various key parameters e.g. various UV light sources, UV light intensities, H_2O/CO_2 ratios, different shapes of photocatalyst, and the effect of water vapor as well as activation/regeneration of photocatalyst and reaction mechanism and pathways of CO_2 reduction have been elucidated for Ti based and Meso. TiO_2 which, strongly influenced the production rate. In addition, nanostructured TiO_2/KIT-6 series with different wt% titania loadings (1, 5, 10, *20*, 30, 50, 70, 90%) were prepared successfully and

characterized by using different techniques such as by N_2 Adsorption/desorption, FE-SEM, XRD, and UV-Vis. Amongst the TiO_2 series catalysts screening was made to obtain the best percentage for CO_2 reduction. Consequently, 20wt% TiO_2/KIT-6 was found to be the optimized photocatalyst for CO_2 reduction towards the fuel production as compared to the other wt% TiO_2/KIT-6 nanocomposite. Various calcination temperatures effect for optimized photocatalyst to observe the change in structure and its correlation with photocatalytic activity of CO_2 reduction, as well as proposed reaction mechanism/pathways has been discussed.

Chapter 2

2 Research objective and scope

As it has already been discussed in Chapter 1 that photocatalytic reduction of carbon dioxide with water to fuel or energy bearing products (such as methane, methanol, hydrogen and carbon monoxide *etc*.,) is an emerging area of research to utilize CO_2 as a feedstock as well as production of some energy to overcome the problem of energy crisis. The work on photocatalysis of CO_2 reduction started from last few decades, but right now scientists, investigators and researchers are facing various challenging to improve this technology in order to find reliable fuels. Still, CO_2 photocatalytic reduction is in its embryonic stage. Therefore, different approaches and various reaction parameters, reaction mechanism and pathways have been under investigation.

The main purpose of this work is to produce the energy bearing renewable fuel products by applying photocatalysis technology of CO_2 reduction with H_2O vapor by UV light irradiation. The objective of this research is based on two approaches. One approach is to investigate the new catalyst formulations that can improve the fuel production rate from CO_2 over H_2O vapor. The catalysts investigated so far include:

- Synthesis of novel mesoporous support materials and further exploration for Ti or isolated species which are more photocatalytic active and selectivity is also higher than bulk type titania.
- Synthesis of titatia nanoparticles TNPs with greater surface area with enhanced adsorption property of the reactant (CO_2 + H_2O), which is crucial step for CO_2 reduction process to increase the efficiency of the photocatalytic process.
- Meso. TiO_2 photocatalyst with higher surface area, pore volume as well as 3-D pore structure, which efficiently regulate the reactants, enhanced light adsorption capacity and reduce the chance of e^-/h^+ recombination.
- Comparison of the commercial titania Aeroxide P25 which is less active and production rate is lower than that of TNPs and Meso. TiO_2.

Chapter 2

- Titania nanocomposite, TiO_2(x)/KIT-6 series with various titania content dispersed on KIT-6 along different calcination temperature optimization investigation is the indication of improved photoactivity from CO_2 reduction to renewable fuels.

Generally, for all catalyst materials, a high surface area is an advantage in terms of concentration of active sites per square meter and this generally leads to higher reactivity. Therefore, these investigations were based to develop the more *active site* for support i.e. KIT-6 mesoporous material by modifying it with various components of titania, towards CO_2 photocatalytic reduction. KIT-6 (3D) mesoporous support material is superior than 1D or 2D MCM-41/SBA-15 materials.

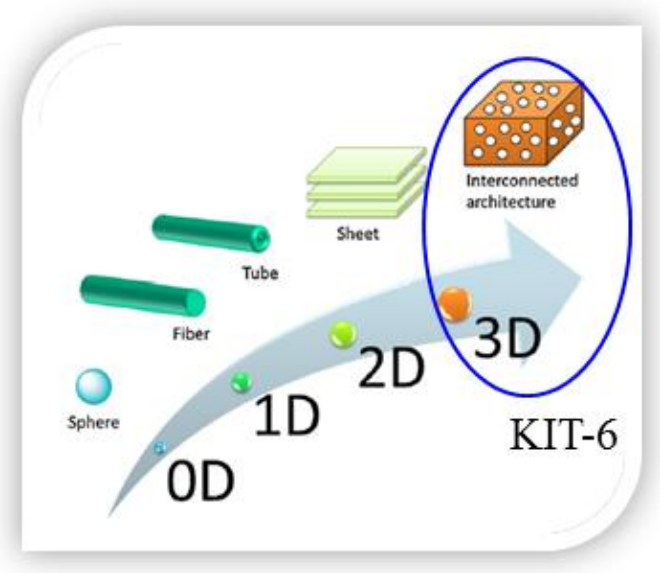

Figure: 2.1 *Structural dimensions of various materials*

However, materials having (zero-dimensional, one-dimensional, two-dimensional) structure also have a high surface area, a high pore volume but due to the unidimensional channels of these materials, the pores are blocked, which inhibit the diffusion of the reactants which caused to decrease the activity. While on the other hand 3-D pore structure of support (KIT-6) as shown in the Fig. 2.1 due to its greater surface area, it has interconnected pores which, provides the good diffusion of reactants (CO_2 and H_2O), better light absorption and most importantly, having the tendency to reduce the rate of e^-/h^+ recombination and enhance the life

time of photoactivity. Hence, the support structure preservation is the main aspect of this objective to boost the reaction. Thanks to these properties, exhibiting a greater surface area accessible to the reagents and enhanced absorption of the radiation within the catalyst itself.
Furthermore, to the complicated reaction mechanism and pathways of CO_2 reduction with H_2O vapor, less attention has been given to understand the phenomena of CO_2 reduction and H_2O oxidation in the conduction and valence bands, respectively. Still, mechanism is very complex, further comprehensive study is needed to make it more tremendous.

Another approach is to reduce the atmospheric concentration of CO_2, which has threatened the world as a global warming issue. In such a way, the atmospheric level of greenhouse gas (CO_2) can be overcomed at some extent or decreased by reduction of CO_2 emission into atmosphere. However, photocatalytic reduction of CO_2 is the only plausible way to provide sufficient energy to the future generation and to reduce the risk of CO_2 emission.

One driving force for perusing on TiO_2 investigation is its extensively used applications and expectations to drive this material will help on fundamental level with further improvement and reaction set up in many fields. According to reference scenario projections or the 'business as usual' scenario from the International Energy Agency (IEA), to meet the needs of populations in 2030, the world will need over 55% more primary energy than in 2005, with an increase in global carbon dioxide (CO_2) emissions of 57%. At present, according to IEA data for 2009 observation, the emission of CO_2 was reduced by 6.5% in developed countries while on the other side this emission has been seen to increasing continuously in developing countries about more than 3.3% (specifically, in Asia and the Middle East). Scientific studies, on CO_2 reduction by semiconductor photocatalyst has been extensively used from last more than forty years ago, because of peculiarities of this technology is only promising opportunity to find the solution of lack of energy for future generation as well as to protect the global to being heat up. Regarding CO_2, which is considered a main contributor amongst the greenhouse gases and causing the environmental, health problems to the human being. However, reduction of these risks and to provide clean energy to the system is the better solution to control the greenhouse CO_2 emission. However, this could be only possible by converting CO_2 (as a raw material) in such a ways that it recycled again into enviable products or organic substances but extra energy input required to fulfill this demands either by sunlight or artificial sources/UV light in the presence of semiconductor photocatalyst to boost the reaction. However, 21^{th} century will depend mostly on

the fossil fuels resources due to increased level of population worldwide to have desired energy. This would be promising by using the CO_2 as feedstock. If we have a look on Fig. 2.2 a recent research trend of CO_2 photocatalytic reduction, it is obvious increasing dramatically from 2000-2014. Publications on this topic during the period 2000-2004 were merely 11.50% but during next four years this reached to 19.62%. Surprisingly, in the period of 2010-2014, it shifted more than three times higher, almost 68.88% than previous five years.

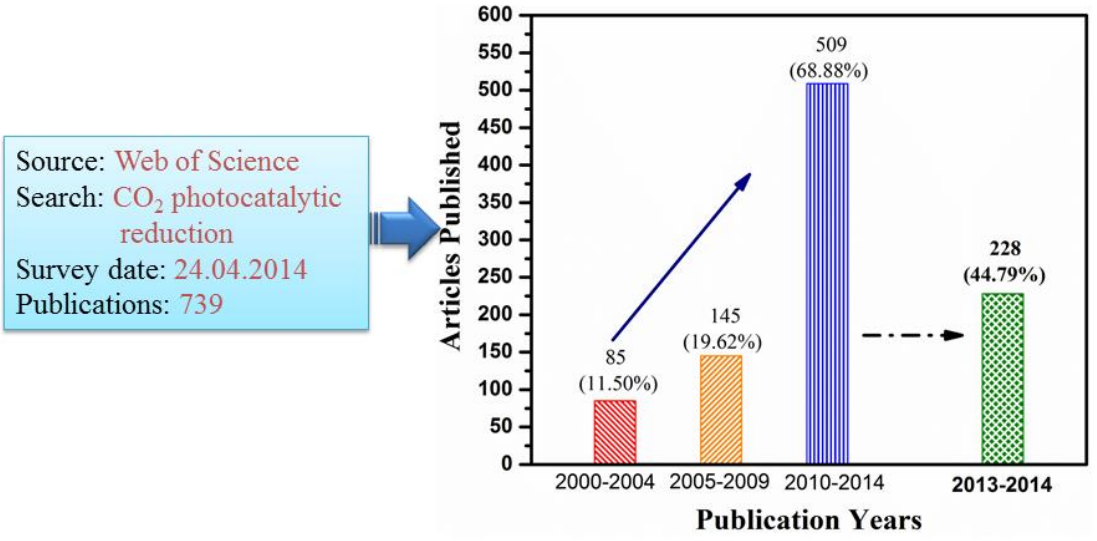

Figure: 2.2 *Articles publications on CO_2 reduction photocatalysis dramatically increasing trend since 2000-2014.*

In addition, there has been a great attention on the long-term projects regarding this field especially in Europe, North America, and Asia to tackle CO_2 issue as well as regarding its economy. Therefore, the main objective of this study is to focus on increasing level of atmospheric CO_2 to reduce it into valuable energy bearing fuels products through a chemical process. Thus, plenty of efforts have been made to reduce the concentration of CO_2 by using the various novel synthesized photocatalysts to obtain the renewable fuels listed hereafter.

It is expected that an understanding of the photocatalytic activity of these synthesized photocatalytic materials based on the good photo-physical characteristics and understanding the reaction mechanism would lead towards development of superior active catalysts.

Chapter 3

3 CO_2 utilization for renewable fuels formation

The increasing level of carbon dioxide (CO_2) to the atmosphere is not only causing a challenging steps in all over the world but has forced the many scientists, investigators, and a researchers to explore various approaches to find the better solution of the energy crisis. Therefore, much more attention has been taken by huge amount of various researchers to grip this concentration as well as to convert it to valuable chemicals or fuels. If we have a look on the topic *"CO_2 conversion*" in the period of 2003, publications including books, journals review and patents *etc*., were over 195 but after ten years intervals these publications has raised to more than 700 at the end of 2013. Moreover, the chemical utilization of CO_2 have increased over the last few years and owing to this increasing tendency, chemicals industries are taking part to convert CO_2 to produce more higher energy density compounds such as fuel products. Notwithstanding with its positive aspects furthermore, CO_2 has a negative effect on the earth atmosphere due to its increased concentration, which is significantly considered a greenhouse gas effect (GHG) and also triggering many environmental problems associated with human activities. Likewise, a future object is to overcome these complications that our society is facing such as climate change, sanctuary environment, and use of renewable energy, replacement of fossil fuels, from last few years [45]. Additionally, recycling or reuse of CO_2 not only addresses the balance of the atmosphere carbon dioxide but also represent the valuable carbon source for renewable fuel formation. As well as chemical industries are being taking part for CO_2 conversion. Recently various studies have been carried out on the economic point of view for the future of chemical industry [46-48]. However, the major products of CO_2 conversion must be fuels to reduce CO_2 emissions significantly and to generate great economic value renewable products. Various options have been adapted for CO_2 conversion such as Hydrogenation of CO_2 to form oxygenates and/or hydrocarbons are the most intensively investigated area of CO_2 conversion. Methanol synthesis from CO_2 and H_2 has been proposed and other possibility is the production

of dimethyl ether (DME), which is considered a clean burning fuel and most importantly, photocatalytic reduction of CO_2 to fuel by semiconductor catalyst is one of the most significant technique to obtain energy bearing products. Therefore, there are various possibilities to activate and to convert CO_2, but it is necessary to overcome a thermodynamic barrier. For this reason, providing the sufficient energy for the reaction is the critical aspect in evaluating the alternative routes for CO_2 conversion. For such conversion of CO_2 to chemicals reducing agents as well as intermediates species are need to complete this reaction. For instance, production of methanol from CO_2 hydrogenation [49, 50] by using protons and electrons consecutively [21]. Another possible route is syngas (CO/H_2) formation, which is produced from CO_2 conversion and then converted to chemicals or clean fuels [51]. Generally, there are some approaches which should be keep in mind for CO_2 conversion to meet the energy demands [52] along with starting materials should be energy richest, unsaturated, and organometallic compounds such as

- Lower energy synthetic material could be better for oxidation
- There must be an equilibrium towards the products sides by removing a particular compound
- There should be supply of energy from any light source or electricity.

3.1 Sources and costs of CO_2 for chemicals production

Carbon dioxide (CO_2) purification and recovery are always remained the problems in term of cost. But these are not critical one, instead there are many other sources of rather pure CO_2 in refinery, chemical process such as ammonia formation, H_2 production, ethylene oxide synthesis, synthesis of liquefied natural gas, Fisher-Tropsch coal synthesis and from bio refineries, (Fermentation process) [53]. It is estimated that globally around 500 million ton of low cost and high concentration (US $ 20/ton) CO_2 is obtainable as a by-product from fertilizer plants, industrial sources as well as from natural sources. On the other hand, diluted CO_2 is emitted at higher cost 18,000 million tons, which could be captured from power, cement and steel plants *etc*. There is a hope, that by introducing the limitation of CO_2 all around the world, the cost of CO_2 captured as well as the market price for CO_2 will decrease [54] in near future.

Chapter 3

3.2 *CO_2 hydrogenation*

Hydrogenation of CO_2 over catalytic beds at elevated temperatures and pressures to produce hydrocarbons such as methane, or oxygenated hydrocarbons such as dimethyl ether and methanol, is a viable approach only if the hydrogen is produced from water electrolysis is derived from sunlight and energy can be supply by using the solar panel [55]. Another strategy is to couple the reverse gas shift reaction with hydrogenation to form methanol or dimethyl ether [37]. Hydrogenation of CO_2 to lower carbon products such as (CH_4, CH_3OH) as well as to higher molecular weight alkanes, alkenes and alcohols through C–C bond formation could be produced [56]. A variety of products such as methanol, dimethyl ether (DME), and other carboxylic acids (formic and acetic acids) could be possible products. Moreover, various homogeneous and heterogeneous catalysts have been used for CO_2 hydrogenation. Additionally, CO_2 hydrogenation involves multi steps routes for instance, H_2 is produced by water electrolysis using electrical energy from renewable sources then further it is used in catalytic process or H_2 can be produced by electro or photocatalysis process by using electrons and protons simultaneously which are produced during the reaction from catalyst. Furthermore, this hydrogen is being used for CO_2 hydrogenation. However, the reverse water-gas shift (RWGS) reaction is very important in catalytic hydrogenation of CO_2 which is considered a mildly endothermic reaction with enthalpy $\Delta H_{298\ K}$ = 41.2 kJ/mole and Gibbs free energy $\Delta G_{298\ K}$ = 28.6 kJ/mol. The RWGS is the primary step in CO_2 hydrogenation for fuel production.

$$CO_2 + H_2 \rightleftharpoons CO + H_2O \qquad (3.1)$$

For example, iron-chromium catalysts are considered very active at 400˚C or greater temperature, but a significant problem arises as a low equilibrium constant in driving the RWGS reaction for its completion. The equilibrium can be shifted to the right by increasing the CO_2 concentration, higher H_2 concentration to complete CO_2 consumption as well as removing water vapor from the reactor for driving the reaction to the right. In addition, different catalysts have been studied for WGS reaction [57]. Copper-based catalysts, particularly CuO/ZnO oxides modified by alumina, zirconia, titania and/or silica [58], Iron-based catalysts, but in iron-based catalysts reaction temperature required above 400 ˚C and are not suited for RWGS reaction and also cerium-based catalysts etc. Thus, CO produced by RWGS reaction, could be further used for

hydrogenation towards methanol formation or Methanol could be synthesized from a feed of CO_2 and H_2 under feasible conditions. However, recently a book has been published by Nobel Laureate Olah [59]. Termed as ‘‘*Methanol Economy’’*, which emphasize the production of methanol or dimethyl ether. Similarly, many studies have indicated that CO_2 is the best-feed component for methanol formation than that of CO for hydrogenation process.

$$CO_2 + 3H_2 \rightleftharpoons CH_3OH + H_2O \qquad (3.2)$$

The RWGS reaction cause rapid conversion of H_2 and CO_2 to CO and H_2O. However, water acts as an inhibitor on the catalyst resulting the slowing down the consecutive step of methanol formation. However, to overcome this critical issue some improved catalysts have been used for CO_2 hydrogenation to methanol production [60]. In addition multicomponent systems ($Cu/ZnO/ZrO_2/Al_2O_3/SiO_2$) illustrated the better performances and a stable productivity but the productivity is typically 3–10 times lower using pure CO_2 feed with respect to a CO/CO_2 feed it is because of higher oxidation power of CO_2 and its negative effect on the catalyst than that of CO. Besides, dimethyl ether (DME), which is clean burning alternate for diesel, could be produced from methanol dehydration over an acidic catalyst.

$$2CH_3OH \rightleftharpoons CH_3OCH_3 \qquad (3.3)$$

There are another two possibilities for the production of dimethyl ether. For example,

$$2CO + 4H_2 \rightleftharpoons CH_3OCH_3 + H_2O \qquad (3.4)$$

$$2CO + 4H_2 \rightleftharpoons CH_3OCH_3 + CO_2 \qquad (3.5)$$

Thermodynamic stability of CO_2 is greater than that of H_2O. However, synthesis of DME is more favorable from syngas as compared to methanol formation. Thermochemical process involves direct decomposition of CO_2 to carbon monoxide and oxygen.

$$CO_2 + energy \longrightarrow CO + 1/2\ O_2 \qquad (3.6)$$

The reaction is endothermic, and it involves a free energy change ($\Delta G0$) of 257 kJ/mol. For a 100% conversion of CO_2, the reaction should be carried at a minimum temperature of about

3075°C, at which $\Delta G0$ becomes zero. However, in principle, the CO yield can be as high as 30% at temperatures near 2400°C but unfortunately yield is very low and backward reaction may occurs.

3.2.1 Advantages of producing methanol and its uses

Production of methanol from CO_2/H_2 is a renewable fuel as recognized by Renewable Energy Directives of the European Union. However, renewable energy sources used for the methanol synthesis either electrolysis or bio-routes, using semiconductor photocatalysts. Methanol formation has more advantages than other solution (such as FT hydrocarbons synthesis) *etc*. Its benefits are, Synthesis process is very simple with higher selectivity and flexibility as well as with reducing transport cost. Methanol could be further used as a raw material in process industry for synthesis of olefins *etc.* In addition, methanol fuelled due to their greater stability and flexibility used in turbine fuel. Owing to its low emission rate, with higher output power e.g., some pilot units have proved that by using methanol-fuelled decreased the NOx emission around 30% than that of CH_4 used as feed [61]. Another benefit of methanol used is that, small water contents present in the methanol further caused the reduction of NOx emission. Furthermore, methanol can be used multipurpose such as chemicals, power generation as well as for transportation.

3.3 Urea synthesis

Urea is synthesized from ammonia and CO_2, which is well established on large scale. Urea boosting technology indicates that capturing of fossil fuel CO_2 for urea production not only solve the problem of reduction of (GHG) emission but on the other hand participate in an integrated ammonia-urea manufacturing plant, that use natural gas as a feedstock in the reforming process to produce CO_2 and NH_3. An excessive amount of NH_3 can be produced by using the surplus of natural gas (CH_4). Generally, ammonia is synthesized from hydrogen (from natural gas) as well as nitrogen (from the air). Firstly, natural gas is converted to hydrogen:

$$CH_4 + H_2O \rightleftharpoons 3H_2 + CO \qquad (3.7)$$

$$CH_4 + 2H_2O \rightleftharpoons 4H_2 + CO_2 \qquad (3.8)$$

Similarly, air is mixed with gas stream to give hydrogen: nitrogen ratio 3:1. Furthermore, hydrogen and nitrogen are treated at higher temperature/pressure in the presence of iron catalyst to produce ammonia, which is very crucial component in the urea synthesis.

$$N_2 + 3H_2 \rightleftharpoons 2NH_3 \qquad (3.9)$$

The ammonia and carbon dioxide are fed into the reactor at higher temperature and pressure to produce urea, which is involved into two steps. In first step ammonium carbamate an intermediate product is formed which than further dehydrates to produce urea.

Ammonium carbamate formation:

$$2NH_3 + CO_2 \rightleftharpoons H_2NCOONH_4 \qquad (3.10)$$

Urea formation:

$$H_2NCOONH_4 \rightleftharpoons H_2NCONH_2 + H_2O \qquad (3.11)$$

Urea is used as fertilizer with richest nitrogen component. Therefore, it is of great importance agriculture fields and also used in the manufacturing of resins for timber processing as well as in yeast manufacturing process. Additionally, the synthesis of substituted urea is also making great attention on industrial scale [62] and is being applied in various fields such as in refinery process, pharmaceuticals use, agrochemicals and petrochemicals industries as well.

3.4 Electrochemical conversion of CO_2

A plenty of work have been done on the use of electro catalysts to split CO_2 dissolved in liquids. Various products such as simplest forms CO to very complex, oxygenated hydrocarbons of high-energy content can be directly synthesized. This technology has some positive aspects because of its compatibility with well-established water electrolysis technology and the possibility of using photovoltaic derived electricity. In aqueous electrolytes such as $NaHCO_3$ and $KHCO_3$, water and carbon dioxide reduction processes take place simultaneously at the cathode due to the proximity of their reduction potentials (H^+/H_2O potential is – 0.41 V *vs.* NHE whereas

CO/CO_2 potential is – 0.52 V *vs.* NHE at pH = 7). However, a wide range of hydrocarbons can be produced by co-electrolysis of water and carbon dioxide.

3.5 Use of CO_2 in biotechnological routes

CO_2 utilization in the bio catalytic industries plays a significant role and provides a variety of opportunities for synthesis of chemicals. For instance, Evonik is pursuing acetone fermentation process by using CO_2. In this process industrial waste gas streams contained CO, H_2 and CO_2.as well as genetic modified acetone such as (*Clostridium ljungdahlii, Clostridium carboxidivorans, Clostridium aceticum)* that are used for acetone synthesis with CO_2. In addition, using glucose and CO_2 is producing Bio-succinic acid. In some process Escherichia coli (E. coli) strain developed specifically to produce succinic acid along with wheat-derived glucose, which is used as substrate. Moreover, longer chain alcohols could be produced by metabolic pathway by using CO_2. In some studies engineered bacteria are being used for alcohol synthesis process by conversion of CO_2 for example genetically modified *E. coli* bacteria is used to produce variety of alcohols and isobutanol formation is carried out by modified cyanobacterium [63]. Additionally, another possibility to CO_2 conversion is non-natural metabolic pathway. In this process branched chain amino acid are protracted to produce abiotic longer chain keto acids as well as alcohol (carbon chain 5 to 8 number) in the presence of 2-isoproplylmalate synthase and enzyme, *etc*. [63]. But the optimization of this technique was found of synthesis 6-carbon alcohol i.e. (S)-3-methyl-l-pentanol. However, biosynthesis route for CO_2 utilization to syngas fermentation is another interesting approach, which is widely acceptable on the industrial scale to use (CO/H_2) rather than pure CO_2, consequently, modification lead to use CO_2 directly. In this process, Carbon Monoxide Dehydrogenase (CODH) from *clostridium thermoaceticum*

Catalyze the reversible oxidation of CO to CO_2 by using an iron (Fe) and nickel (Ni) containing metalloenzyme or this enzyme can be coupled with semiconductor catalyst such as TiO_2 (its conduction band have good reducing ability) which produces the electrons for reduction process. In addition, TiO_2 nanoparticles after the modification with Carbon Monoxide Dehydrogenase (CODH) and a photosensitizer under the illumination of visible light on specific reaction condition produce CO (250µmol (g $TiO_2)^{-}1/h^{-}1$) [64-66]. The formation of fuels and chemicals through syngas fermentation propose an ideal way over metal catalytic conversion

owing to its some advantages such as the higher specificity of the biocatalyst, lower energy costs, and greater resistance to catalyst poisoning, and independence of a fixed H_2: CO ratio. On the other hand, there is a drawback, it is very costly. Although, numerous microorganisms, suc as *acetogens including Clostridium ljungdahlii, Clostridium autoethanogenum, Eurobacterium limosum* etc have been reported, which can produce fuels and chemicals by syngas utilization [67].

3.6 CO_2 conversion by using biomass

Another feasible approach for CO_2 conversion through is very significant aspect to produce fuel via recyclying of CO_2 [68]. However a plenty of feed stocks are being used for biofuel production. Use of microalgae appears the most promising route to biofuel production. The oil content of algae is significantly higher than that of crops. Similarly, many algal species have dry weight oil content of more than 30%, while the oil content can go as high as 80% in some strains like *Schizochytrium* sp. and *Botryococcus braunii*. [69] Algae itself fixes carbon dioxide and facilitate carbon recycling without any assistance.

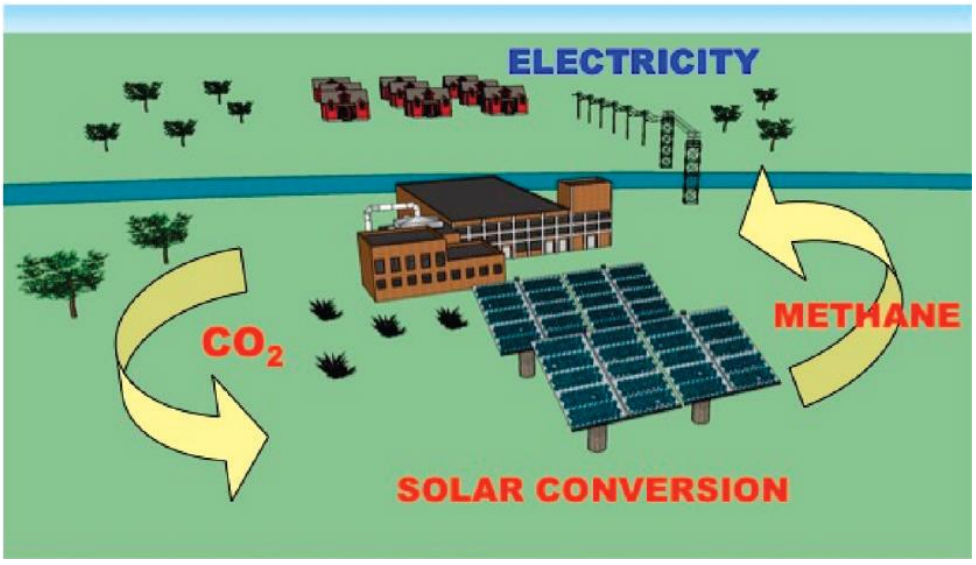

Figure: 3.1 *Solar fuels system for CO_2 conversion with H_2O to fuel. Fuels can be stored, transported or recycled CO_2 passing through photocatalytic process to again fuels formation [70].*

Moreover, bioethanol is commonly produced from sugar or starchy crops such as sugar cane and from plant cellulose using fermentation processes. Similarly, biodiesel are being produced from oil crops for examples, corn, soybean, canola, coconut, oil palm, *etc*. in the presence of microalgae. Typically, in this trans esterification process triglycerides oil reacts with methanol in the presence of catalysts such as sodium hydroxide or potassium hydroxide. Biodiesel can be used in the combustion process by blending with petro diesels. However, biodiesel produced from microalgae is considered a significant source of global energy. Moreover, world fuel production from biomass is rapidly increasing (3.91 quadrillion Btu from biomass in 2008, Department of Energy statistics), the sunlight to fuel energy conversion efficiency of photosynthesis is approximately 1%, [71]. It appears that biofuels will be a part of the future energy infrastructure but are unlikely to have a decisive role.

3.7 Thermochemical conversion of CO_2

Capturing of CO_2 from the atmosphere through various capturing technologies, CO_2 involved from one or a series of chemical reaction for production of energy bearing products. CO_2 capture and conversion are high intensive energy process. However, direct reduction of carbon dioxide using concentrated sunlight by thermochemical cycles is one of the most encouraging approaches for the production of hydrocarbons from CO_2 reduction with H_2O. Moreover, thermochemical process involves direct decomposition of CO_2 to carbon monoxide and oxygen.

$$CO2 + energy \longrightarrow CO + \frac{1}{2}O2 \qquad (3.12)$$

The reaction is highly endothermic, with free energy change (ΔG^0) of 257 kJ/mol. Similarly, 100% conversion of CO_2, the reaction should be carried at a minimum temperature of about 3075°C, with zero ΔG^0. However, the CO yield can be as high as 30% at temperatures near 2400°C, but the yield is much lower because of back ward reactions. Galvez *et al.* carried out a second law thermodynamic analysis of Zn/ZnO and FeO/Fe_3O_4 cycles [72].

$$ZnO \Leftrightarrow Zn + \frac{1}{2}O_2 \quad (3.13)$$

$$\Delta H°25℃ = +350.5\frac{KJ}{mol} \quad (3.14)$$

$$Zn + CO_2 \Leftrightarrow Zn + CO \quad (3.15)$$

$$\Delta H°25℃ = -\frac{67.5KJ}{mol} \quad (3.16)$$

[Equ, (3.13)] reaction is highly endothermic and requires a temperature of about 1700°C to form gas phase zinc and oxygen. After the separation of O_2 from equation reaction (3.13) CO is the only product as shown in the [Equ, (3.15)], which is highly exothermic, and temperature is suggested between 425 and 725 °C to operate this reaction with 39% an efficiency under concentrated solar radiation.

3.8 New opportunities for CO_2 utilization

There has been a prodigious curiosity for CO_2 utilization by using new approaches from last more than two years under homogeneous photocatalyst. For instance, methane or methanol can be poduced by CO_2 conversion with hydro silanes under the zirconium phenoxide borane complexs or N-heterocyclic carbenes as catalyst [73, 74]. However, CO_2 hydrogenation in homogeneous is considered an important step by using Frustrated-Lewis pairs [75]. Methanol can be produced from CO_2 hydrogenation by using non-metal homogeneous catalysts [76]. In addition, Hydrogenation of carbonates, carbamates, and formats by indirect CO_2 conversion to methanol synthesis in the presence of Ru pincer complexes as catalyst is very significant aspect [77]. Furthermore, CO_2 can also be used in the organic synthesis for example, the catalytic hydro carboxylation of styrene, and hydrocarboxylation of alkynes by copper-catalysis using carbon dioxide in the presence of a hydro-silane [78]. But unfortunately the reactions have very low production rate.

Moreover, electrolysis is another novel approach to produce small organic molecules, which are used in conjunction or as valuable synthetic products. However, two promising ways

for synthesis of methanol or other long chain alcohols by using conventional metal type electrodes operating in liquid phase or in gas phase [79] in the presence of molecular catalyst such as pyridinium ion. Similarly, another attractive route by using non-conventional electrolytes such as ionic liquid can be useful for CO_2 conversion process [80]. However, recently novel electrocatalysts have revealed for example a nanoporous silver electrocatalyst that is able to electrocatalytically reduce CO_2 to CO. In addition to these novel opportunities, there is a great attraction of new notions and prospects for conversion of CO_2 or reuse of CO_2 in the era of catalysis and industrial chemistry. Though, many of the recent discoveries specifically in the field of homogeneous photocatalysis and electrocatalysis have been exploited at industrial level. But unfortunately, some of them are still far from industrial viability because of some limitations of their stability particularly in electrocatalysts.

3.9 Photocatalytic reduction of CO_2 to renewable fuels

Photocatalytic reduction of CO_2 to fuel has been an attractive approach from last few decades owing to its benefits as compared to other technologies. CO_2 is easily available as a feedstock and can be used infinite for fuel synthesis. However, reaction can be carried out at mild conditions to obtain short chain hydrocarbons photocatalytic products from CO_2 reduction to solve the problem of energy crisis as well as to protect the environment at some extent, simultaneously. *"**Hunting two birds with one stone in terms of saving the environment and supplying future energy"**.* Moreover this technology would be more favorable replacing the fossil fuels CO_2 as C source in chemical industry. However, the pioneering works by Fujishima and Honda, which is known as "*Honda-Fujishima* effect". On photocatalytic splitting of water by TiO_2 electrodes in 1972 opened the door for future generation in the field of photocatalysis [3]. After this discovery, a curiosity in this research field has been focused not only in specific era but a lot of researchers exploited their work in different applications from a laboratory to industrial scale.by using semiconductors TiO_2 catalysts and photocatalysis approaches. Moreover, the innovative work on the photocatalytic reduction of CO_2 in aqueous solution was carried out by Inoue et al. [38]. to produce energy bearing products such as formaldehyde (HCHO), formic acid (HCOOH), methyl alcohol (CH_3OH), and trace amounts of methane (CH_4),

Carbon monoxide (CO) etc, by using various semiconductors such as titanium dioxide (TiO_2), tungsten trioxide (WO_3), zinc oxide (ZnO), cadmium sulfide (CdS), gallium phosphide (GaP), and silicon carbide (SiC) under illumination of Xenon and mercury-lamp. Moreover, various catalysts oxides and non-oxides such as TiO_2, ZrO_2, Fe_2O_3, WO_3, ZnO, MgO_2, CdS, ZnS and SiC have been extensively used for photocatalytic reduction. Photocatalytic reduction of CO_2 by using semiconductor catalysts such as TiO_2 in aqueous or gases phase by using various UV light sources have been shown in *Chapter 4* and *Table 4.2* since 1994-2014.

Photocatalytic reduction of CO_2 is still in an embryonic stage. Further, improvement and modification in this technique are needed to boost this process. But most importantly, selection of the best catalyst is primary step to enhance the photo activity.

3.10 The perception of CO_2 utilization on the future of society

The CO_2 utilization has a great perception on the society but rather it would be more interesting to observe the public perception, CO_2 reuse into chemical or fuel is considered the more pertinent than that of carbon sequestration (CSS). One reason is that, catalysts not intricate in CO_2 sequestration and on the other hand, it is also considered a less energy efficient technology while CO_2 reuse is more efficient in terms of sustainable feedstock. Similarly, aspirin is also a less relevant extent to sustainable catalysts regarding the marketing values. However, CO_2 utilization is a widely used technology than that of (CSS) it is because of a positive aspect for investigators or scientists to boost the synthesis of novel renewable or chemicals products for future progeny to fulfill the energy demands which is considered a big challenge in the 21 century. Moreover, CO_2 reuse is considered a major contributor in the low-carbon economy but still catalysis technology is measured as in an embryonic stage. However, to move to the low-carbon economy, it should be in consideration that resources and energy must be more efficient as well as use of novel technologies for renewable [81, 82]. Furthermore, it is very essential to increase the scientific efforts not only to develop the new routes but also to efficiently assess the problems associated with ideas to innovation. Along with, public and privates funds are necessary parameters to reach this goal. From this perspective, SPIRE initiative [83], which indicates that CO_2 utilization, is one of the most important pillars to boost the sustainable, as well

as competitive step for the future of chemical industry.

3.11 Assessment of CO_2 utilization

There are various criteria associated with assessing the different routes for CO_2 utilization. For instance

- Potential development is the major criterion, which indicates the duration of primary industrial facility liked with R&D efforts.
- Economic perspective is another criteria, which represent the perceptions to find the economic return.
- External use of energy is a very huge criterion, which assesses the energy consumption for product formation. The consumption of energy in the form of thermal or electrical associated with the manufacture of the reagents as well as energy requirements with this process. However, this energy is a main issue particularly, for dry reforming and mineralization. For example, photo-electro catalysis or microalgae uses the direct sunlight (in the form of energy) but productivity is very low.
- Potential volume of CO_2 utilization is important criteria, which represent the supreme amount of CO_2 use by 2050 but the released of CO_2 during the process on industrial scale in not taken into consideration.
- Sequestration of time is a significant step, which is noted before to reenter or reintroduced the CO_2 into atmosphere.
- Environmental impacts, this criterion is associated with use of some toxic substances or solvent having toxicity during the process released to the atmosphere causes the pollution and another disease associated with human being, as well as use of catalysts with negative impacts on the environment etc.

However, implementation of all resolutions will depend on the techno-economic but all these criteria mentioned above should be consideration to achieve the better efficiency of CO_2 utilization for photocatalysis or another possible way.

Chapter 4

4 Literature survey on photocatalytic reduction of CO_2 with titanium based materials

4.1 Research background

The previous work on the photocatalytic reduction of CO_2 in aqueous solution was carried out by Inoue et al. [38] to produce energy bearing products such as formaldehyde (HCHO), formic acid (HCOOH), methyl alcohol (CH_3OH), and trace amounts of methane (CH_4), carbon monoxide (CO) *etc*. by using various semiconductors such as titanium dioxide (TiO_2), tungsten trioxide (WO_3), zinc oxide (ZnO), cadmium sulfide (CdS), gallium phosphide (GaP), and silicon carbide (SiC) under illumination of Xenon and mercury-lamp boosted the photocatalytic technology by numerous investigators operating the CO_2 as a reducing agent with H_2O vapor as well as another solvents [84, 16, 85-89, 20, 90-94]. In addition, the list of literature survey for CO_2 is shown in *Table 4.2*. Photocatalytic reduction of CO_2 to sustainable fuels is a challenging and promising application owing to its many advantages. For instance,

- Reaction can be carried out in moderately mild condition such as room temperature and pressure
- CO_2 is easily available as key carbon source which can be used infinite and clean solar energy
- Short chain hydrocarbons photocatalytic products can be obtained by CO_2 reduction process, which can overcome the energy crisis problem at some degree.
- This technology would be favorable replacing the fossil fuel CO_2 as C source in chemical industry.

Therefore, reduction of atmospheric CO_2 with H_2O to valuable fuel products would be like killing two birds with one stone in term of saving energy supplying as well as protection of environment [95]. Currently, the concentration of Carbon dioxide (CO_2) in the atmosphere is not only triggering global warming issues but also raised many environmental problems

associated with human activities. [26] Key sources to the emissions of carbon dioxide are mostly due to the burning of fossil fuels such as oil, natural gas, coal, *etc*., which strongly influence the greenhouse effect. According to a recent study, regarding US emission of CO_2 in the atmosphere have led to the acceleration of carbon sources in different forms such as gases, liquids, solids, flaring and cements *etc*., which are the major contributor to the inclination of the global temperature. Almost, 920 billion tons of carbon have been released due to burning of fossil fuels and cement production since 1951s but half of this increased has dramatically shifted at the mid of 1970s.to 2006 [96]. However, according to a report that CO_2 is present in atmosphere with 377ppm (parts per million by volume) as of December 2004 [97]. Furthermore, this dramatically increased concentration of CO_2 into atmosphere is rising continuous every year. For example, from Oct 2011-Oct 2013, CO_2 concentration was reported as 388.96ppm, 391.01 ppm and 393.66ppm respectively. In addition, carbon-containing substances produce CO_2 during combustion, which directly goes to the atmosphere and commencing very serious problems. Unfortunately, CO_2 is thermodynamically very stable but less energy assessment compound. Therefore, it is very difficult to decompose or reduced to CO_2 under normal conditions without being supplying any reaction conditions. Thus, energy can be supplied through a direct ways using solar energy or via chemical reaction in the presence of the catalyst, which stimulates the reaction and provides the sufficient energy to splits CO_2 molecules. In other words, it needs intensive amount of energy to breakdown of carbon dioxide. In fact, CO_2 is a colorless and odorless gas. The molecule is linear with a double bond between the carbon and oxygen atoms (O=C=O). However, CO_2 is naturally occurring compound which assists as a source of carbon for photosynthesis of plants by using natural sunlight. Nevertheless, CO_2 plays a significant role in the earth's carbon cycle, and is considered to be as an essential component in the life cycle of animals and plants [98, 99].

Moreover, CO_2 can also be used in industrial applications such as metal industry, paper, pulp and electronics, healthcare and environment contamination, foodstuffs, beverages, laboratory analysis and safety purpose as well as most importantly *chemicals* or fuel syntheses process. On the other side, it has some detrimental effects on the environment and to overcome this limitation, the only plausible ways is photocatalytic conversion of CO_2 with H_2O vapor, seems to be a more promising technique when appropriate energy for instance, UV and or visible light used as a excitation source for the production of higher energy photons which creates a pair

of e^-/h^+ to followed by intermediates species which further facilitates the final energy bearing products/renewable fuel. Such as carbon monoxide (CO), methane (CH_4), methanol (CH_3OH), hydrogen (H_2), formaldehyde (HCHO), and formic acid (HCOOH) [100, 5, 101, 94]. In recent years, much effort has been paid to the conversion of CO_2 to hydrocarbons or renewable fuel in liquid or in gaseous phase. Most importantly, a lot of research has been focused in gaseous phase [102-106, 17, 107-113, 10, 114] by using various semiconductors photocatalysts under different UV light sources to overcome the global heat problems and to fulfill the energy demands for the future progeny simultaneously. The pioneering work by Fujishima and Honda, which is known as "*Honda-Fujishima effect*" on photocatalytic splitting of water by TiO_2 electrodes in 1972 opened the door for future generation in the field of photocatalysis [3]. Afterward, a curiosity in this research field has been focused not only in specific era but a lot of researchers exploited their work in different applications from a laboratory to industrial scale by using semiconductors TiO_2 catalysts under the photocatalysis approaches. However, a massive scientific research on photocatalytic reduction of CO_2 to enviable chemicals revealed that better efficiency towards desired products could be accomplished but still this technique is in an embryonic stage because of lack of proficiency and yields discrimination is very low for commercialization.

Furthermore, various photocatalysts oxides and non-oxides, such as Titanium dioxide (TiO_2), cadmium sulphide (CdS), zinc sulphide (ZnS), silicon carbide (SiC), tungsten oxide (WO_3), iron oxide (Fe_2O_3), zirconium oxide (ZrO_2), gallium oxide (Ga_2O_3), zinc oxide (ZnO), and magnesium oxide (MgO_2), have been used extensively for photocatalytic reduction [41].
However, some of these catalysts have limitations such as ZnO is highly unstable as it dissolved in the water immediately to form Zn $(OH)_2$ which cause the inactivation of catalyst [115]. In addition, Fe_2O_3, and WO_3 have conduction band edge below the reversible hydrogen potential, thus an external electrical bias is needed to complete the splitting of H_2O for H_2 production [116]. Therefore, the major criteria for an efficient semiconductor photocatalyst are that the redox potential of the e^-/h^+ should lies within the band gap domain of photocatalyst to obtain the better efficiency of the CO_2 reduction. Accordingly, amongst all these above-mentioned catalysts, TiO_2 accomplished all these characteristics that a good photocatalyst must have. However, TiO_2 are widely used semiconductors due to its adequate reduction potential value for CO_2 reduction (-0.24V) towards methane formation. [117]. As well as, its holes are strongly oxidizing and redox selective. In addition, TiO_2 is an environmentally friendly material which

shows a good oxidation power, strong resistance to chemicals and photo corrosion, non-toxicity, superior charge transport properties, a low operational temperature, low cost, and significantly low energy consumption.

Up to date, a lot of investigations have been focused on this area to obtain the better efficiency of the products but still this approach is very far to get desired products. Furthermore, development of new ways and choosing the best catalyst might be only one option to enhance the photocatalytic activity. The research objectives are highlighted to establish not just efficient but along with cost effective, robust technologies and materials to be used for this application.

4.2 Research on Titanium dioxide (TiO_2) based materials as semiconductor photocatalysts

4.2.1 Background of Titanium dioxide (TiO_2)

Titanium dioxide with chemical formula (TiO_2) was first discovered in 1791 by William Gregor, in England during the studying of mineralogy he studied this substance and after he was assured that it was a mineral, named it *menachanite*. After four years of this discovery in 1795, Martin H. Klaproth, recognized a new chemical element in this mineral, he later named it *Titanium*. It is also known as titanium (IV) oxide, titania, titanium white or pigment used in the building paints, and food industry as a additive E171 in food coloring such as icings, salad dressings and sweets *etc*. The oxide of titanium is naturally occurring as three different forms such as anatase, and rutile and brookite. On commercial scale it has been manufactured as white pigments in building since 1916. Moreover, E. Kedel noticed photoactivity of TiO_2 initially in 1929 [118]. But most importantly, previous scientific research work on TiO_2 was published in 1932-1934 [119, 120], which raised the many questions. Furthermore, in 1938 photocatalytic activity results on TiO_2 as "*photo sensitizer*" were significant [121]. But K. Hoshimoto et al. first used the term "Photocatalyst" for TiO_2 in 1956 [122], for the oxidation of organic compounds under UV light irradiation. The pioneering studies on photo electrolysis were carried out by Fujishima et al 1972 (related to photocatalysis) of H_2O by TiO_2 semiconductor called "*Honda-Fujishima effect"* lead to the evolution of H_2 boosted the application of TiO_2 [38]. Furthermore,

in 1977, Frank and Bard [123] observed the reduction of CN in water by using this technology. In 1978, the first organic photosynthetic reaction was described by Kolbe reaction ($CH_3COOH \rightarrow CH_4 + CO_2$), which opened the door for photosynthetic reaction [124]. In 1986, Fujishima et al. [125] extended their research by using TiO_2 for the treatment of tumor cells called (HeLa cells) in the presence of light irradiation.

In 2000, Fujishima et al. [126] found the super hydrophilic properties of TiO_2 film under the UV light illumination. In 2002, Watson et al. [127] prepared the novel magnetic TiO_2 photocatalyst using sol-gel method by application of external magnetic field from slurry type photo reactor. In 2005, Sreethawong et al. [128] synthesized nano crystalline mesoporous TiO_2 by sol-gel techniques for photocatalytic H_2 production from an aqueous methanol solution [104, 129, 130]. However, a lot of many investigators used the TiO_2 as photocatalyst for CO_2 reduction under UV light irradiation towards fuel formation. Since then, TiO_2 has been extensively used in many applications, starting from its basic research results, to industrial photocatalytic activity in 20^{th} century makes it stronger to enter in 21 century which would be considered the bright future of TiO_2 for further innovation. Additionally, there are already a number of commercial photocatalytic TiO_2 products available on the market. The most used commercial photocatalyst is P25, from Evonik (Germany), composed by anatase and rutile (*70% and 30 %*.). This semiconductor is being used as a standard reference in several photocatalytic researches works for instance [43].

4.2.2 Physical aspects and photocatalytic activity of TiO_2

TiO_2 surfaces are rich in structures variations that directly impact the chemistry and photochemistry. The richness in structures is seen both in the arrangement of atoms (physical structure) and distribution of state (electronic structure). Basically, physical properties of TiO_2 have polymorphs but there are three most important phases e.g. Anatase, rutile, and brookite. It is very difficult to the prepare brookite crystals in laboratory scale. However, two out of three (anatase and rutile) crystals forms plays a significant role in photocatalysis specifically anatase because it is easy to prepare. Anatase is always found as small, isolated and sharply developed crystals, it crystallizes in the tetragonal system. The mineral was named, by René Just Haüy in 1801, from the Greek *anatasis*, "extension or the greater length of the usual pyramid compared with other tetragonal minerals. Rutile was discovered two years later after the discovery of

anatase in 1803. Rutile is similar tetragonal in morphology to that of anatase but thermodynamically it is more stable, and slightly better whitening abilities than anatase and brookite. Moreover, owing to this ability it can be widely used for industrial paints, domestic and artistic purposes. At higher temperature anatese and brookite can be converted to rutile instead rutile remains stable at higher temperature.

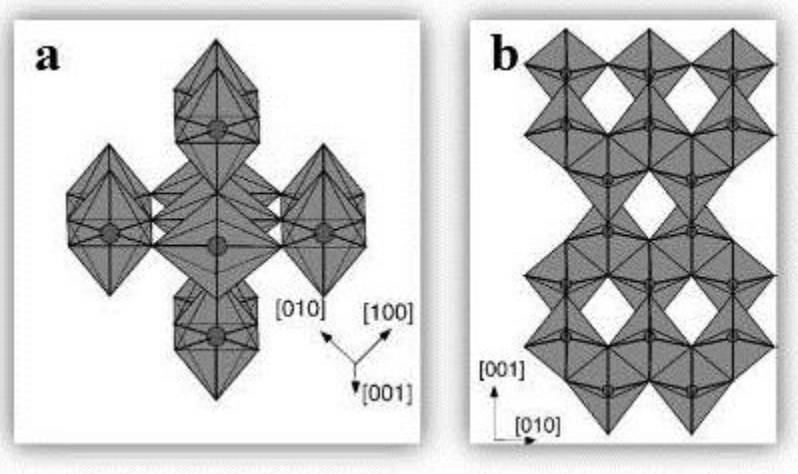

Figure: 4.1 *Crystal structures of TiO_2* ***(a),*** *Rutile and* ***(b),*** *anatase phases (Adapted from Ref [131] modified form).*

On the other hand, anatase form is softer and less abrasive, and therefore is considered the most popular for healthcare products and foods as well as photocatalysis applications. Anatase form is considered the best photocatalyst because of its certain additional properties such as Fermi level of anatase is higher about 0.1eV than that of rutile phase which reduced the oxygen affinity and resulting in the formation of greater number of hydroxyl groups on the surface of titania [132] which enhance the photocatalytic activity. Hence, a lot of research has proposed that the photoactivity of TiO_2 is due to its crystalline forms [133]. Photocatalytic activity of rutile is very poor and it depends on its preparation parameters, which strongly effect its activity or inactivity [134]. Crystalline TiO_2 dioxide i.e. mixture of two phases (anatase + rutile) have dissimilar photocatalytic activity toward the reduction of CO_2. Generally, improvement in the photocatalytic activity by using the combination of two catalysts is considered due to the greater charge separation and reduced the chances of recombination of photogenerated charges i.e., electron/holes. In such a way, electron transfers from rutile to anatase at the interface, which produced the defective sites. These defective sites play a

significant role for higher reactivity because of a better accommodation for adsorption of reactants as well as efficient charge trapping properties [135, 136].

***Table 4.1**: Differences between Anatase and Rutile forms*

Anatase	Rutile
It is optically negative	It is optically positive
Soft/less hard with 5.5-6vs Mohs	Firm/ more hard 6-6.5vs Mohs
Refractive index is 2.5-3	Refractive index is 3.87
Band gap energy for anatase is 3.23 eV	Rutile has band gap energy 3.02eV
It only absorbs the UV light	It does absorb some visible light
Less dense with specific gravity 3.9	More dense with specific gravity 4.2
It is an excellent photocatalyst	It is a not good photocatalyst
Anatase can be converted to rutile at higher temperature	Rutile has no any transformational property It remains stable
Anatase has higher Fermi level	Fermi level of rutile is less
Mobility of electrons is higher, so that 10 times higher photocatalytic property due to less recombination of e^-/h^+ pairs	Less mobility of electrons which show less photocatalytic property due to higher chance of recombination of e^-/h^+ pairs

In addition reduction is associated with the reductive TiO_2 surface sites in the presence of UV light resulting in the formation of higher reactive charge transfer excited state i.e. (Ti^{3+} - O^-) of the tetrahedral coordinated titanium oxide species on the catalyst surface [137]. Photocatalytic reaction takes place on the surface of the catalyst; in such a way, that surface phase of TiO_2 play a key role in photoactivity which should be more crystalline to enhance the photoactivity. Moreover, phase transformation from anatase to rutile is effected by particle size of the catalyst [138]. However, specific surface area is indirectly proportional to the particle size. If TiO_2 nanoparticles size decreased from 29-14nm, which led to the higher production of CH_4 and CH_3OH, it is due to greater absorption of photonic energy by smaller particles [137]. Similarly, TiO_2 powder prepared by sol-gel method having the particle size ranges from 8-15nm gives the

higher photocatalytic activity as compared to greater particle size about 150nm of commercial TiO_2 [139]. An optimum particle size might be exist between 25-40nm, having all other properties such as greater specific surface area, generation of efficient charge carrier and good absorption/scattering of light, which is challenging effect for CO_2 reduction [140]. By further decreasing the particle size less than 5nm CO_2 photocatalytic activity decreased harshly because of change in optional and electronics properties of the catalyst inhibit the CO_2 reduction process. Overall, TiO_2 has been one of the most attractive and convenient candidates for photocatalytic application from last few decades and still are at the top position from all another types of photocatalysts amongst oxides and non-oxides due to its superior characteristics. For instance, its commercial availability, nontoxicity, photochemical stability, good oxidation power, strong resistance to chemicals, low cost, a low operational temperature, appropriate electronic and optical potentials, low energy consumption as well as an environmentally friendly material all of which have led to relevant applications for fuel production. In addition, various TiO_2 advance technologies have been adapted such as TiO_2 nanoparticles. Modified TiO_2 nanoprticles with metals [19] titanium doped with Pt metal, Pt/TiO_2 nanotubes [141] and hetero structured TiO_2 [142] as well as Cu/TiO_2 nanorods [100]. Dispersed nanoparticles on mesoporous silica support materials [10]. Among all these nanostructures materials 3 dimensional (gyroid cubic Ia3d) KIT-6 materials demonstrate the superior photocatalytic activity than 1 or 2dimentional SBA-15S or MCM-41 photocatalysts, it might be because of not only its higher surface area, but large pore structure and pore size, with multi pore channels provides the enough space for dispersion of materials on the support, as well as better light dispersion which creates a sufficient number of a e^-/h^+ pairs to promote the photocatalytic activity for CO_2 reduction.

Consequently, titanium dioxide semiconductors are considered the paramount photocatalysts for CO_2 reduction because under the UV light illumination, photogenerated electrons in the bottom of the conduction (CB) band can have sufficient negative redox potential to motivation of CO_2 reduction, while on the other hand photogenerated holes in the top most level of the valance band (VB) can be more positive to oxidize the H_2O towards the O_2 formation and superoxide (−0.2V) simultaneously. TiO_2 exhibits almost all of the required properties for an efficient photocatalyst must have for photocatalysis process, but only with the limitation of not absorbing visible light.

Chapter 4

4.2.3 Photocatalytic reduction of CO_2 on TiO_2 based materials and the application as semiconductor photocatalysts

Titanium dioxide (TiO_2) has drawn much research attention in recent years due to its potential applications specifically, photoreduction of CO_2 over TiO_2 based materials from last few years and this trend is dramatically increasing every year owing to its unique properties and easily availability. However, TiO_2 can be used in its pure form (bare), doped with different metals and non-metals as well as highly dispersed form within mesoporous or zeolites materials to enhance its photoactivity as shown in *Table 4.2*. Moreover, the surface phase of TiO_2 should be responsible for its photoactivity because the photocatalytic reaction takes place on the surface of catalyst though; the surface phase of TiO_2, particularly during the phase transformation has not been well investigated. Additionally, the phase transformation from anatase to rutile is influenced by particle size [138]. UV Raman spectroscopy is found to be more sensitive to the surface phase of a solid sample when the sample absorbs UV light [143]. This outcome signs use to study the crystalline phase in the surface region of TiO_2 by UV Raman spectroscopy as TiO_2 strongly absorbs UV light and further try to correlate the surface phase of TiO_2 and its photoactivity. TiO_2 has very wide band gap (3.2eV for anatase) and it is only active in the UV range spectra below than 400nm. However, during CO_2 reduction, photo-generated electrons in the bottom of the conduction band can have sufficient negative redox potential to drive CO_2 reduction, while the photo-generated holes in the valence band can be sufficiently energetic (positive holes) to act as acceptors and oxidize water to O_2. But luckily, in our present context TiO_2 was used under the UV region and satisfactory results were obtained from CO_2 reduction with H_2O vapor by using various nanostructured photocatalytic titania materials.

Chapter 4

Table 4.2: *Literature survey of photocatalytic reduction of CO_2 on the bare and doped or highly dispersed TiO_2 based materials*

Photocatalysts	***Reductants***	***Light source***	***Products***	***References***
Cu/TiO_2	H_2O	450 Xe lamp	CH_4, C_2H_4	Adachi et al. (1994) [84]
TiO_2	H_2O	75 W high-pressure Hg	CH_4, CH_3OH, CO	Anpo et al. (1995) [16]
TiO_2	H_2O	75 W high-pressure	CH_4, CH_3OH, CO	Yamashita et al. (1995) [85]
TiO_2	H_2O, 0.2M, NaOH solution	4.5kW Xe lamp	HCOOH, CH_3OH, CH_4, C_2H_6OH, C_2H_4, C_2H_2	Mizuno et al. (1996) [144]
TiO_2	H_2O, liquid CO_2	990W Xe lamp	HCOOH	Kaneco et al. (1997) [145]
Pt-TiO_2/Y zeolite	H_2O	75 W high-pressure Hg lamp λ> 280 nm,	CH_4, CH_3OH	Anpo et al. (1997) [86]
TiO_2 nanocrystals SiO_2 matrices	1M 2-propanol, solution	500W high-pressure Hg arc lamp	$HCOO^-$, CO	Liu et al. (1997) [146]
TiO_2 (P25)	Isopropyl alcohol	4.2 Kw Xe lamp	CH_4, HCOOH	Kaneco et al. (1998) [147]
Ti-MCM-41, Ti-MCM-48	H_2O vapor	High-pressure Hg lamp, λ> 280 nm	CH_4, CH_3OH	Anpo et al. (1998) [87]
Rh/TiO_2	H_2	Ultra high pressure Hg lamp λ = 290-450	CH_4	Kohno et al. (1999) [148]
TiO_2	Methano, ethanol 2-propanol, nitric, hy drochloric, and phosphoric acid	0.96wK Xe lamp	HCOOH	Kaneco et al. (1999) [149]
TiO_2/SiO_2, Ti-MCM-41	H_2O	100W high-pressure Hg lamp	CH_4, CH_3OH	Ikeue et al. (2002) [150]
Ti/Si hexagonal and cubic	H_2O	100W high-pressure Hg lamp	CH_3OH CH_4	Shioya et al. (2003) [151]
TiO_2(P25)	aqueous $NaHCO_3$	15W (365nm)	CH_4, CH_3OH	Ku et al. (2004) [152]
Ti-SBA-15	H_2O	Mercury lamp	CH_4, CH_3OH	Hwang et al. (2004) [153]
TiO_2 suspension	H_2O	λ=350nm	CH_4	Dey et al. (2004) [154]
Cu/TiO_2	H_2O	UV light	CH_3OH	Wu et al. (2005) [155]
TiO_2 pellets	H_2O	UV light	CH_4	Tan et al. (2006) [90]
TiO_2(P25)	H_2O, H_2	15W UVA λ= 365nm	CH_4, CO, C_2H_6	Lo et al. (2007) [156]
TiO_2	H_2O vapors	UVC 253.7nm	CH_4, CO, H_2	Tan et al. (2007) [104]
TiO_2	H_2O	15W UVA lamp, λ=365nm	CH_4, C_2H_6OH, HCOOH	Xia et al. (2007) [91]
TiO_2	H_2O vapor	200W Hg/Xe lamps	H_2, CH_4	Tan et al. (2008) [129]
Pure TiO_2 anatase	H_2O	8W Hg lamp, λ=254nm	CH_4, CH_3OH	Koci et al. (2009) [117]
Cu/TiO_2-SiO_2	H_2O	Xe lamp	CO, CH_4	Li et al. (2010) [100]
Ag/TiO_2	H_2O	8W Hg lamp, λ=l254nm	CH_4, CH_3OH	Koci et al. (2010) [157]
TiO_2	H_2O	UV light	CO	Dimitrijevic et al. (2011) [158]

Ti-SBA-15	H_2O vapor	120W high pressure Hg lamp	CH_4, C_2H_4, C_2H_6	Yang et al. (2011) [111]
Bulk TiO_2, Ti Oxide	H_2O	UV lamp	CH_4, CH_3OH	Mori et al. (2012) [10]
Cu(I)/TiO_{2-x}	H_2O vapor	150 W Solar simulator	CO,	Liu et at. (2012) [159]
Cu-I/TiO_2	H_2O vapor	UV light	CO, CH_4, CH_3Cl	Zhang et al. (2012) [160]
Pt/TiO_2	H_2O vapor	100W high pressure Hg lamp	CH_4	Uner & Oymak (2012) [161]
Ce/TiO_2 SBA-15	H_2O vapor	UV Xe lamp	CO, CH_4	Zhao et al. (2012) [162]
R/TiO_2 modified A/TiO_2 nanorods	H_2O vapor	UV Hg lamp	CH_4, CH_3OH, H_2, CO	Wang et al. (2012) [163]
Ti-KIT-6	H_2O vapor	UV 300W	CH_4	Hussain et al. (2013) [164]
Au/Ti/SBA	H_2O	200W Hg lamp	CH_4	Mei et al. (2013) [165]
Montmorillonite/TiO_2	H_2O vapor	200W mercury lamp	CH_4, CO	Tahir et al. (2013) [166]
Ti-KIT-6	H_2O vapor	UV light	CH_4, CH_3OH, H_2, CO	Akhter et al. (2014) [167]

In addition, there is an extremely wide range of applications of TiO_2 because it is well known material due to its versatile characteristics which has been widely used in different environmental application [168, 169] water purification [170], decomposition of organic compounds, [171-174] self-cleaning purposes, air conditioners, purification of sewage water, air cleaner and anti-bacterial [175] including tiles, tents and variety of glass wares which have been widely used in Japan, in railway tracks, tunnels, roads, *etc*. Furthermore, TiO_2 materials are being extensively used in our daily life such as households goods, (clothes, sprays, fibers *etc*.) cosmetics, toothpaste, painting, even foodstuffs so on. Generally, in self-cleaning phenomena, TiO_2 materials show the super hydrophilic property by using of natural sunlight and rainwater. Some other applications, such as protection from corrosion of materials [176], medicals implantations, [177, 178] anti-fogging agent for cleaning the surface of glass and mirrors *etc.* Thus, TiO_2 is non-toxic and safe material, and can be dispersed easily. In pure form it is also used as a food additive [179] in pharmaceuticals, and in cosmetic products [180].

Furthermore, novel applications of TiO_2 photocatalyst such as wettability patterning, offset printing plates recently have been applied by Nakata and Fujishima [181]. But the most importantly, TiO_2 plays a very crucial role in the field of photocatalysis, specifically in the reduction of CO_2 to fuel production.

Chapter 4

4.3 CO_2 problems and global strategies for energy crisis

Emission of carbon dioxide (CO_2) has become a great challenge in all over the world due to the increasing level of CO_2 in atmosphere, which is being considered the main contributor amongst the greenhouse gases. *French scientist Jean Baptiste Fourier first observed greenhouse effect* in 1827. However, this effect caused by the greenhouse gases, the top most gas carbon dioxide (CO_2), water vapor, ozone (O_3), methane (CH_4) and nitrous oxide (N_2O), *etc*. The increase in the greenhouse effect constitutes about 70% of CO_2 24% CH_4 and about 6% of N_2O. Furthermore, this increased concentration of carbon dioxide in the atmosphere is mainly due to burning of fossil fuels such as oil, coal, natural gas (land-use changes and cement manufacturing and deforestation also contribute which release about 6 gig tons (Gt) of carbon to the atmosphere each year). According to a climate simulation, [182] the atmospheric temperature raises about 6ºC average at the end of this century. On the other side, IPPC has stated that global greenhouse gases (GHG) emissions should be reduced by 50 to 80% by the year 2050 [183].

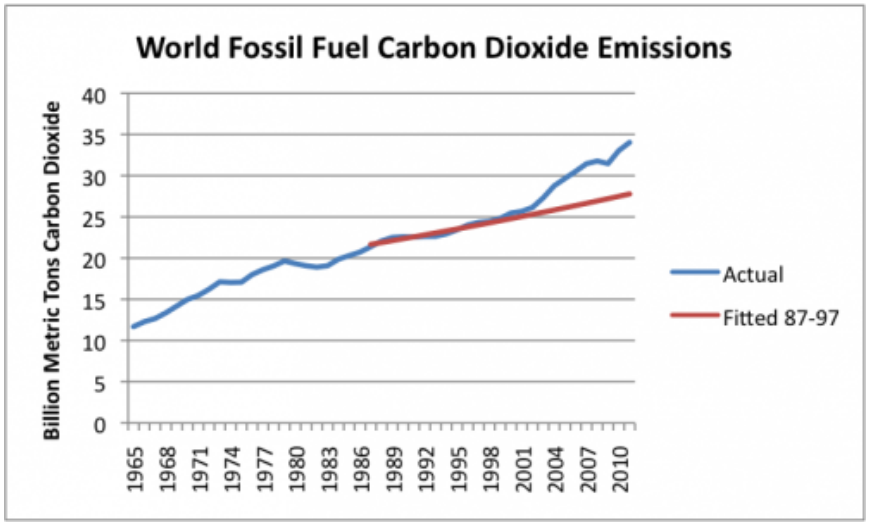

Figure: 4.2 *Actual world carbon dioxide emissions from fossil fuels, as shown in BP'S 2012.Statasitical Review of World Energy. Fitted line is expected trend in emission based on actual trend in emission from 1987-1997, equal to about 1 %per year.*

Moreover, there is a slight alteration of release of CO_2 into atmosphere over the period of 1000 years to 20th century. Since in 1000 (280ppmv) to (295ppmv) in 1900 [184] statistics based on antarctica ice core but suddenly increased in 1958 (315 ppmv) and further in 2004 (377 ppmv) based on actual analysis in Hawaii [185]. CO_2 intensities gradually increasing every year by year such as recently data figure out since October 2011-2013 the CO_2 concentration shifted to (388.96, 391.01, 393.66ppmv) respectively. On the other hand, depletion of the energy sources is mainly concerned due to rapid increase in population worldwide, rise in public transportation, increase in economic, and the construction of plenty of industries, which released the toxic substances causes health as well as environmental problems [186]. In addition, other key cradles, which cause the CO_2 emission, are the use of large amount of CO_2.on industrial scale. However, CO_2 is being used for a lot of applications such as metal industry, pulp, paper and electronics, health and chemicals *etc*. According to the Kyoto Protocol in 1997, if CO_2 emission has risen at the average rate that they did during the 1987 to 1997 period (about 1% per year) thus, emissions in 2011 would be 185 lower than they actually were.

While there were many other things going on at the same time that much higher rise in emissions in recent years is not an encourage sign. The Earth's energy requirements are estimated at 14 TW/y. By considering, the economic development, high consumption of fuel and constantly increasing number of people in the world, it is estimated that energy demand in 2050 will be amount 28-30 TW/y. It is estimated, that in case of continued use of traditional energy sources by 2030, carbon dioxide levels will rise to 40 billion Mg per year.

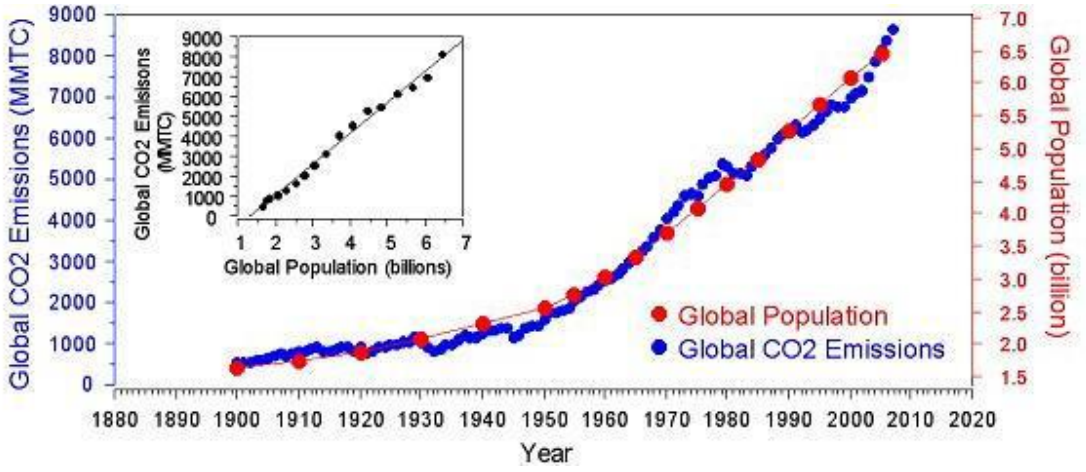

Figure: 4.3 *The correlation of CO_2 emissions with the world's population [187].*

Chapter 4

The correlation of carbon dioxide emissions from the world's population is shown in Fig. 4.3. Consequently, CO_2 has two aspects, on one way it is very crucial for life existence, such as photosynthesis of plants, carbon cycle, many useful industrial applications, as well as on the other hand it has some drawbacks for instance, higher emission causes the global warming which currently has become a challenging phase for scientists, investigators and researcher *etc*. To tackle this problem, a lot of investigation has been carried out from last few decades by applying different technologies to control CO_2 emission and convert it into valuable energy products. However, various possible strategies, which participate to conversion of CO_2, are of great interest such as by physicochemical approaches, sustainable (or renewable) methanol synthesis and production of syngas (CO/H_2) derived from flue gases, from coal, gas, or oil-fired electric power stations, as well as photochemical production of synthetic fuel [27]. To prevent a global warming issue, atmospheric scientists suggested that there should be reduction of our current level of CO_2 emissions by about 60% while on the other hand, another study have proposed that not only greenhouse CO_2 gas emissions reduction is the solution of this problem but organic matter associated with the fossil fuels combustion have greater impact on the climate change [188]. According to estimation, total emission of CO_2 from the fossil fuels is about 23 Gt /year all around the world. Primarily source of this emission are connected with public electricity and heat production which are the main contributor of CO_2 release almost 35%, along with public transport also discharge 24%, but another 40.1% of CO_2 emission occur from manufacturing, industrial energy use, auto producers and other sectors *etc*. [92]. Nevertheless, photo technology is considered the most encouraging way to relief from CO_2 emission. This higher concentration of CO_2 in the atmosphere could be captured and stored by engaging various technologies [189]. Therefore, currently different modes are being applied for capturing of CO_2, such as chemical and physical adsorption, [190] cryogenic process, [191] membrane separation, [192]. Moreover, newest way for CO_2 capturing “ammonia scrubbing” is being established which in realization would improve the efficiency of this process [193]. Nonetheless, amongst all these technologies to reduce the CO_2 emission, photocatalysis has been extensively used to tackle this problem as well as to provide sufficient energy for future. In this study, CO_2 photocatalytic reduction was carried out with H_2O vapor by using well known semiconducting catalyst titanium dioxide

(TiO_2) under the UV light illumination to develop energy bearing products such as methane (CH_4), methanol (CH_3OH), hydrogen (H_2) and carbon monoxide (CO) *etc*.

4.4 CO_2 conversion to fuel thermodynamics and kinetics aspects

Carbon dioxide (CO_2) is thermodynamically stable and chemically inert molecules with closed shell electronic configuration as well as linear geometry [194, 44]. CO_2 photoreduction is not a single-step reaction. Upon transfer of one electron, the structure changes from linear to bent form. However, an extensive input of energy, optimized reaction conditions along with very active catalyst are needed for any chemical conversion of CO_2 to fuel. Despite that, chemical reactions are motivated only by difference in Gibbs free energy between reactants and products of the reaction process. A relationship between G-H i.e. Gibbs–Helmholtz is given as

$$\Delta G0 = \Delta H0 - T\Delta S\ 0 \qquad (4.1)$$

However, CO_2 can be used as chemical feed stock to obtained the valuable products thus it should be noteworthy the relative stability of the final reaction products, as compared to the reactants. However, the bond between carbon and oxygen are very strong and significant energy must be input for their cleavage in terms of carbon reduction. Similarly, the entropy term ($T\Delta S^0$) does not participate to the thermodynamic driving force for any reaction of CO_2 conversion. Significantly, one can then take the enthalpy term (ΔH^0) as a good initial director for assessing thermodynamic stability and feasibility of any CO_2 conversions. Therefore, ΔG^0 only provides information as to the yield of products at equilibrium through the relationship and the kinetics of

$$\Delta G0 = -RT\ In\ K \qquad (4.2)$$

such a process is favorable for conversion of CO_2 to CO. For instance, metal surfaces, or some other catalytic material, e.g. nanoscale metal particles encapsulated in nano-and mesoporous hosts [195, 54]. Additionally, conversion of CO_2 is endothermic reaction e.g. the steam reforming of hydrocarbons to yield syngas and hydrogen [27].

Chapter 4

$$CH_4 + H_2O \rightarrow CO + 3H_2 \qquad \Delta H0 = +206.3KJ/mol - 1 \quad (4.3)$$

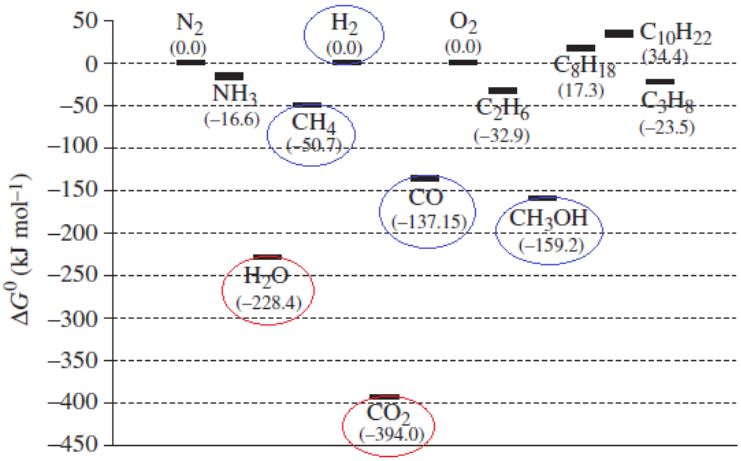

Figure: 4.4 *Gibbs free energy for selected chemicals formation [27]*

The consistent CO_2 reforming of CH_4 (so-called 'dry reforming') illustrates the important reaction of CO_2 with a hydrocarbon, which will be of central importance to our considerations of converting CO_2 in flue gases to yield a chemical fuel.

$$CH_4 + CO_2 \rightarrow 2CO + H_2 \qquad \Delta H0 = +247.3KJ/mol - 1 \qquad (4.4)$$

Almost more than 20% energy is needed to convert CO_2 reforming of CH_4 than that of steam reforming process. Aforementioned, that the reaction give rise syngas but with different CO/H_2 molar ratio. By considering if thermodynamically CO_2 is used as a co-reactant with another substance that has a higher (i.e. less negative) Gibbs free energy, e.g. H_2 or CH_4.

$$CO_2 \rightarrow CO + \frac{1}{2}O_2 \qquad \Delta H0 = +293KJ/mol - 1 \qquad (4.5)$$

<u>Reaction of CO_2 with H_2</u>

$$CO_2 + H_2 \rightarrow CO + H_2O \qquad \Delta H0 = +51KJ/mol - 1 \qquad (4.6)$$

Photocatalytic reduction of CO_2 with H_2O into hydrocarbon fuels such as CH_4 and CH_3OH is an

uphill reaction with a highly positive change in Gibbs free energy. These hydrogen-bearing energy carrier products have their intrinsic chemical energy to promote the conversion of CO_2,the enthalpies of reaction for conversion of CO_2 to CO, CH_3OH and CH_4 are illustrated below

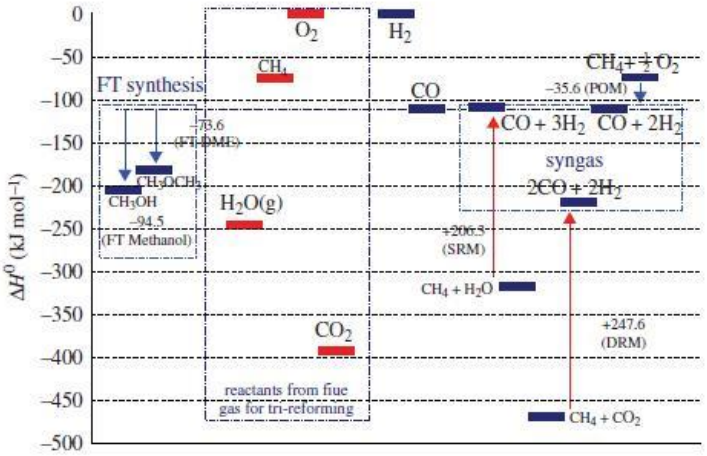

Figure: 4.5 *Gibbs free energy of formation for selected chemicals. ΔH^0 for the constituent elements is taken as the reference point [27].*

<u>Reaction of CO_2 with H_2O</u>

$$CO2 + 2H2\,O \rightarrow CH3OH + \frac{3}{2}O2 \qquad = +702.2KJ/mol - 1 \qquad (4.7)$$

$$CO2 + 2H2O \rightarrow CH4 + 2O2 \qquad = +818.3KJ/mol - 1 \qquad (4.8)$$

For CO_2 photocatalysis reducing agents are very crucial because of photocatalytic reaction depends on the reduction potential of reactants. The reduction potential of H_2O to produce H_2 is considerably lower (E^{O}_{red} = 0 V) than the standard reduction potential of CO_2 to generate CO^{-}_{2} (E^{0}_{red} = −1.9 V). However, H_2O play a significant role as an excellent reducing agent than that of other reducing agents. Similarly, the fraction of formate increases and CO decreases by increasing the dielectric constant of the solvent. If high dielectric constant solvent is used the CO_3^- anion radicals are stabilized by solvent which causes the weak interaction with

photocatalytic surface. Therefore, one, two, four, six and eight electron required for CO_2 reduction and H_2O oxidation at reduction potentials vs. NHE at pH 7 in gaseous and aqueous systems [44]. Similarly, reaction scheme of reduction/oxidation of CO_2 and H_2O with reduction potential values have been shown in the activation, dissociation of CO_2 and decomposition of H_2O (part below) on the catalyst surface. Therefore, any process, which inhibits electron-hole recombination, would greatly increase the efficiency of CO_2 photoreduction. The kinetics of CO_2 photoreduction is also dependent upon many other factors such as incident light intensity, absorption of photon flux by the photocatalyst, reaction condition, the specific surface area and particle size of the photocatalyst *etc*. However hydrogen formation is kinetically faster than methane formation, because eight protons and electrons are required for CH_4 formation [146, 196].

4.5 General principle and reaction mechanisms of TiO_2 for CO_2 reduction

Generally, photocatalysis is a process in which light radiations having energy (*hv*) equal to or greater than the band gap energy (Eg) of a semiconductor photocatalyst reaches on its surface resulting the generation of an electron (e^-) /hole (h^+) pairs [197, 198, 5]. Band gap is defined as "*the distance between the top of the filled level of valence band (VB) to the bottom of the vacant conduction band (CB).*"

Generation of electron and hole

$$TiO_2 \xrightarrow{h\nu} (CB)e^- + (VB)h^+ \qquad (4.9)$$

Recombination of electron and holes

$$e^- + h^+ \longrightarrow heat\ (unproductive) \qquad (4.10)$$

Where, h is the Planck's constant (h = 6.63.10^{-34} J s^{-1}), v is the frequency, e^-represents a conduction band electron, and h^+ represents a hole in the valence band.

However, the photogenerated electrons and holes participate in various oxidation and

reduction processes for and H_2O and CO_2 respectively. This process proceeds simultaneously on the catalyst surface by competing with intermediate products to give rise final products. Moreover, if the charges fail to find any trapped species on the surface or their band gap energy is too small, then they recombine immediately releasing unproductive energy as heat [199]. Taking into consideration all these situation TiO_2 catalysts are extensively studied for CO_2 reduction owing to its wide variety of properties. The rate of charge transfer depends on band edge position of the band gap and redox potential of the adsorbate species. Photogenerated electrons migrate to the surface and after they are trapped at the edge of the CB, they serve as reduction centers; the semiconductor donates electrons to acceptors. Likewise, the holes being trapped at the VB edges serve as oxidizing sites, photogenerated hole than reacts with electrons from donor species. If these electrons and holes could not find any proper place as trap center than they recombine in the volume of semiconductor called "*volume recombination*" or on the surface of catalyst is known as "*surface recombination*" [21].

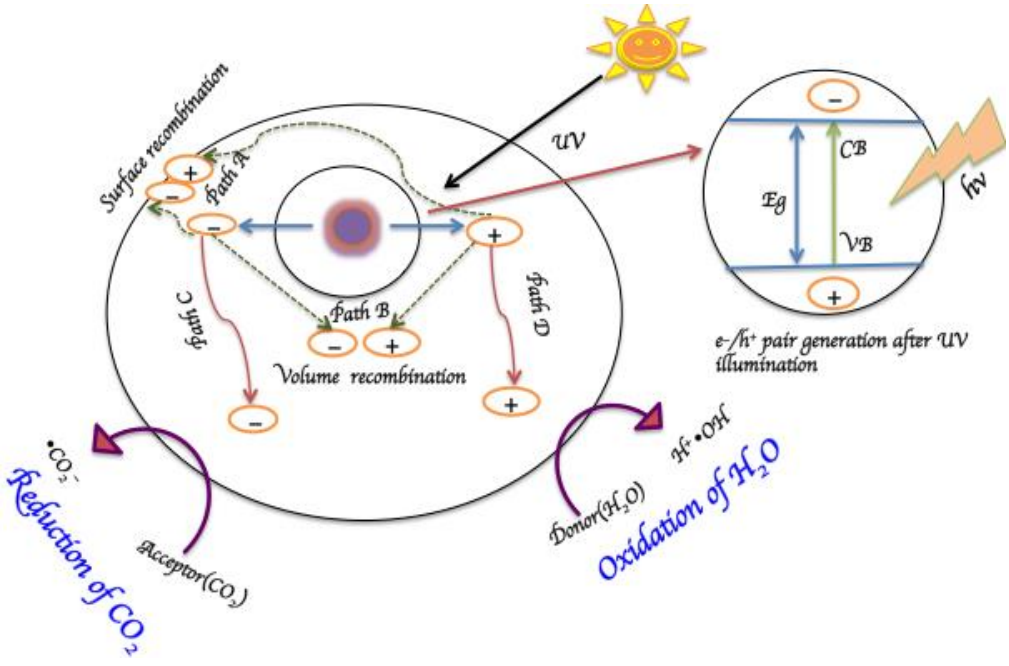

Figure: 4.6 *Mechanism and pathways for photocatalytic reduction and oxidation processes on the surface of semiconductor photocatalyst.*

However, the rate of recombination of e^-/h^+ pair is two or three orders of magnitude faster than that of charge separation or charge transportation [200]. Hence, this is the major limiting step for reducing the efficiency of CO_2 photoreduction. Although, any strategy that could inhibit the recombination of *e-/h+* and participate the better transportation of the photogenerated charges will encourage the CO_2 reduction. On the other hand, upon UV light excitation in Ti-isolated species or Ti-oxide moieties is brought by an electron transfer from the oxygen (O^{2-}) to (Ti^{4+}) ions, resulting in the formation of pairs of trapped hole centers (O^{2-}) and electron centers (Ti^{3+}). These photogenerated e^-/h^+ pair is located very close to each other than the bulk TiO_2 $e^-/h+$ pair that are separated to conduction band and valence band respectively under the light irradiation. Thus, isolated Ti-oxide plays a vital role in photocatalytic reduction of CO_2. The band gap of the semiconductor photocatalyst increases by decreasing the particle size. Accordingly, e^-/h^+ generation by UV light irradiation in the small particle size and highly dispersed titanium dioxide species show distinctive property and higher activities as compared to that e^-/h^+ produced in lager particle size TiO_2 photocatalyst.

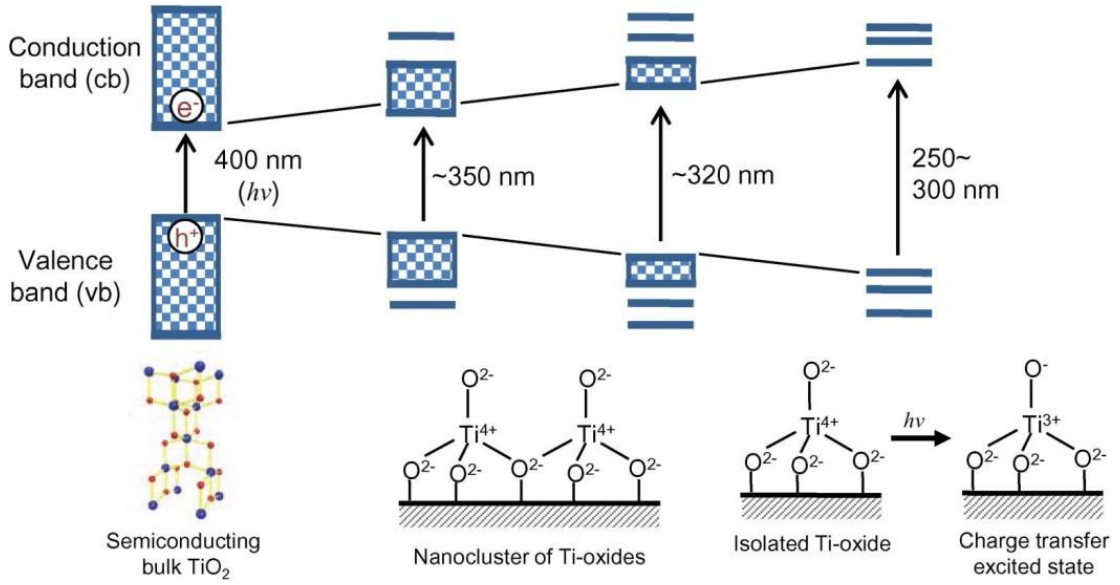

Figure: 4.7 *TiO_2 electronic state changes from bulk to isolated molecular species [10].*

Chapter 4

4.6 Adsorption of reactants (CO_2 & H_2O) on the surface of the photocatalyst

Reactants are very crucial components for photocatalysis process but most importantly, the efficiency of adsorption on the surface of photocatalyst plays a significant role to produce organic compounds. During this photocatalysis reaction prior to start the reaction there must be equilibrium between the reactants such as CO_2 and H_2O. Moreover, H_2O is the primary reactant since it is readily available, inexpensive, and nontoxic. However, H_2O as reactant along with TiO_2 offers a green chemistry approach for photocatalytic conversion of CO_2 to fuel. Moreover, H_2O is considered the excellent reducing agent than that of other solvents because of its high dielectric constant, which ultimately decreases the photocatalytic activity by making weak interaction with photocatalytic surface [148, 201]. The efficiency of reaction strongly depends on the molar ratio of H_2O/CO_2. With increasing the H_2O/CO_2 ratio photocatalytic activity of CO_2 increase linearly. But on the other hand, excessive amount of H_2O suppress the activity. According to Anpo et al. the optimized ratio for CO_2 conversion to fuel is 5.0 [16]. Furthermore, the yield of methane increased with increasing the H_2O/CO_2 ratio [202]. If H_2O is used in very small amount, the production rate will decrease. Therefore, there should be an appropriate amount of H_2O for CO_2 reduction to fuel, which is very critical and significant step for photocatalysis. Instead, adsorption of CO_2 in neglected in most of the literature, although CO_2 adsorption is also very crucial likewise H_2O adsorption, so both of these reactants adsorption should be under consideration to start the reaction. However, these are primary steps, which intensely affect the photocatalysis reaction. Besides, CO_2 and H_2O under the UV light illumination undergo competition for reduction and oxidation process simultaneously on the catalyst surface to produce CO, CH_4, CH_3OH *etc*, on the conduction band as well as H_2O oxidize to give rise H^+, OH^- and O_2 on valence band. Furthermore, these intermediates react with each other to form final photocatalytic products.

Chapter 4

4.7 Activation, dissociation of CO_2 and decomposition of H_2O on the catalyst surface

The CO_2 photocatalysis is not only a single step reaction but it involves a series of steps before to endure photoreaction such as CO_2 adsorption, activation, and dissociation ultimately to reach the final products formation. As it has been already mentioned, that the adsorption of CO_2 is also a very important alike that of H_2O adsorption. After a good adsorbed surface of the catalyst, lead to activation of CO_2. However, activation of chemically stable CO_2 molecule begins multistep reactions. Similarly, when photocatalyst surface is excited by UV light irradiation, during this activation a photogenerated electron is transferred from photocatalyst (TiO_2) surface to the lowest molecular orbital (LUMO) of CO_2 to form $CO_2^{\bullet-}$ where the linear structure of CO_2 is changed to bent form due to repulsion between a lone pair of electron on the oxygen atom as well as an unpaired electron on the electrophilic carbon atom [203]. Additionally, it is reported that the non-linear structure of CO_2 molecule on the surface of solid bases is destabilized than that of linear structure of CO_2 [204, 194]. Likewise, breakage takes place between C–O bond and newly C–H bond formation occur. However, some investigators have anticipated that CO_2 activation to formation of a negatively charged $CO_2^{\bullet-}$ species involves are 23 electron radical anions consecutively, [194] and various technologies have been applied for detection of formation of $CO_2^{\bullet-}$ species such as (IR) spectroscopy, [205] electron paramagnetic resonance (EPR) spectroscopy [206]. Nevertheless, activation of CO_2 is a multi-electron transfer process rather than a single electron transfer process. However, in the heterogeneous photocatalysis (gas-solid interface) an electron is transferred from CB of TiO_2 to CO_2 [Eq. (4.11)] to form of carbon dioxide anion radical $CO_2^{\bullet-}$ at potentials as negative as –1.9 which is highly endothermic and mainly connected with negative adiabatic electron affinity of gaseous CO_2 as well as the interaction between CO_2 and H_2O [194, 44]. Additionally, CO_2 after activation dissociate to give transitional product such as CO and O. Although, two electron and two protons are needed for the formation of CO, which is very important and most common, step in CO_2 reduction [Eq. (4.12)]. However, it may be desorbed on the catalyst surface or further participate as an intermediate by-product to produce C•, which is active species towards

hydrocarbons formation such as CH_4, CH_3OH, C_2H_6 and other lower chain alkanes.

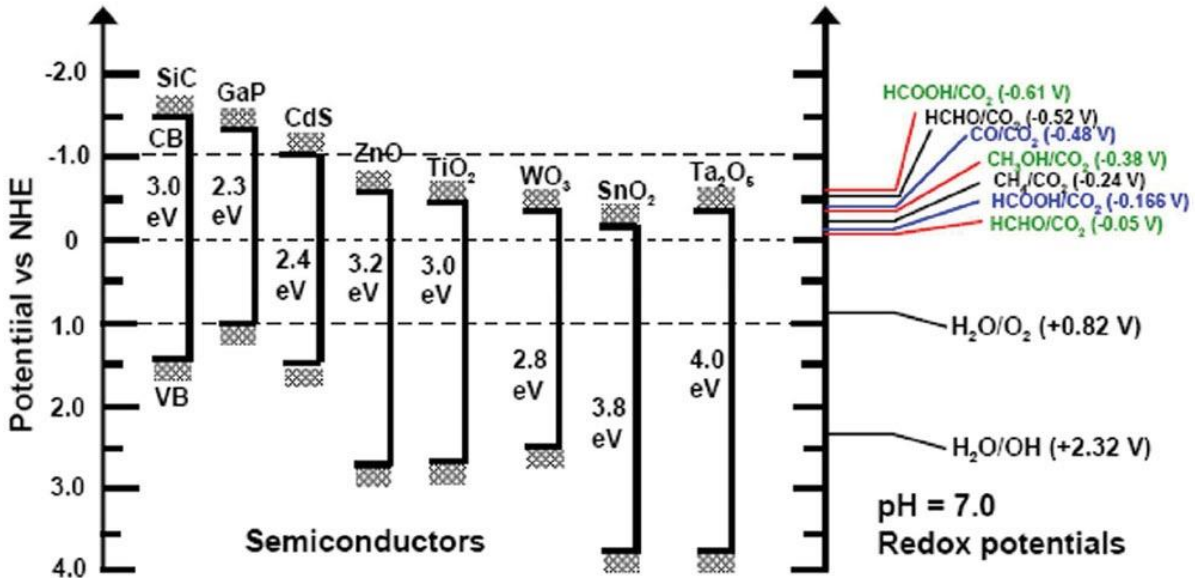

Figure: 4.8 *Conduction band and valence band potentials, and band gap energies of various semiconductor photocatalystss relative to the redox potentials at pH = 7 of compounds involved in CO_2 reduction. (Adapted from Ref [207]).*

Photo reduction of CO_2 E^0_{redox}*/V vs. NHE*

$$CO_2 + e^- \rightarrow CO_2^{-\cdot} \quad = -1.90 \quad (4.11)$$

$$CO_2 + 2H^+ + 2e^- \rightarrow CO + H_2O \quad = -0.53 \quad (4.12)$$

$$CO_2 + 6H^+ + 6e^- \rightarrow CH_3OH + H_2O \quad = -0.38 \quad (4.13)$$

$$CO_2 + 8H^+ + 8e^- \rightarrow CH_4 + 2H_2O \quad = -0.24 \quad (4.14)$$

$$2H^+ + 2H^+ + 2e^- \rightarrow H_2 \quad = -0.41 \quad (4.15)$$

Methane formation

$$CO + 6H^+ + 6e^- \rightarrow CH_4 + H_2O \quad (4.16)$$

$$CH_3OH + 2H^+ + 2e^- \rightarrow CH_4 + H_2O \quad (4.17)$$

Photo oxidation of H_2O

E^0_{redox}*/V vs. NHE*

$$H_2O + 2h^+ \rightarrow H^+ + OH^{\cdot} \quad 0.82 \quad (4.18)$$

Chapter 4

Oxygen formation from H_2O decomposition

$$2H_2O + 4h^+ \rightarrow O_2 + 4H^+ \qquad (4.19)$$

***Scheme 4.1**: Reaction scheme of reduction/oxidation of CO_2 and H_2O with reduction potential*

Similarly, H_2O is oxidized to H^+ and OH^- on the catalyst surface. CH_4 and CH_3OH are formed with 8 or 6 protons and electrons respectively. There might be another possibility for CH_4 formation by multi steps reaction [Eqs. (4.16, 4.17)]. However, several reaction schemes for photocatalytic reduction of CO_2 with H_2O on the TiO_2 photocatalysts have been reported by numerous researchers [84, 147, 89, 20, 10, 24]. Wide band gap semiconductors like (TiO_2) are the most suitable photocatalysts for CO_2 photoreduction, because they provide sufficient negative and positive redox potentials in conduction bands and valence bands, respectively. In addition to these desired redox reactions, CO_2 photoreduction becomes more complex by some backward reactions. For example, the strong oxidation power of the photoexcited holes, protons, OH radicals, or O_2 could oxidize the intermediates and products to form CO_2.

4.8 Reaction intermediates and products formation pathways

Various studies have been reported to investigate the surface reaction intermediates in the CO_2 photocatalysis techniques over bare TiO_2, micro or mesoporous titania silicates, and modified TiO_2. Reaction intermediates strongly depend on the reaction media e.g. in solid-gas phase, CO_2 reduction with the water vapor under the UV light irradiation involve the formation of CO_2^-, C•, CO, HCO_3^-, are the primary intermediates. Furthermore, (carbon radical) C• formed from CO. On the other hand, H_2O decomposed simultaneously to produce H^+ OH^- radical owing to oxidation capability of holes or may produce O_2. Then H^+ reacts with electron to form $H^\bullet$ radical. These radicals are considered the more active species which than reacts with $CO_2^{\bullet-}$ to give C. Therefore, this could be possible that C combined H^+ consecutively along with

multi electrons to form of $CH_3^{\bullet}$ radical. Here are two possibilities for $CH_3^{\bullet}$ radical to reacts with $OH^{\bullet}$ to form of CH_3OH or $CH_3^{\bullet}$ radical further reacts with $H^{\bullet}$ to form CH_4.

$$CO_2^{-\cdot} + H^{\cdot} \rightarrow C + + OH^{-} \quad (4.20)$$

$$C + H^{\cdot} \rightarrow CH^{\cdot} \quad (4.21)$$

$$CH^{\cdot} + H^{\cdot} \rightarrow CH_2^{\cdot} \quad (4.22)$$

$$CH_2^{\cdot} \rightarrow CH_3^{\cdot} \quad (4.23)$$

$$CH_3^{\cdot} + H^{\cdot} \; or \; OH^{\cdot} \longrightarrow CH_4 \; or \; CH_3OH \quad (4.24)$$

Moreover, (carbon monoxide) CO is considered as an intermediate product which might be desorbed on the catalyst surface or go to final product formation as CO. Additionally, $H^{\bullet}$ can reacts with each other to form of H_2 as a main fuel product and generated free oxygen [Eq. (4.19)] can participate in re-oxidation of methane which led to formation of CO_2 in reverse reaction [104]. Consequently, photocatalytic products such as CH_4, CH_3OH, CO, H_2 or O_2 obtained from CO_2 reduction with H_2O vapor under UV light irradiation as shown in the *reaction mechanism scheme 7.9.* On the other hand, Yang et al. [111] reported the reaction intermediates (CO, HCOH) in the isolated Ti mesoporous materials such as Ti-SBA-15. However, O_2 formation was also observed by many researchers but unluckily, in our work, we were unable to detect the O_2 formation because of GC limitation although it is obviously produced during the reaction because photocatalyst deactivation and regeneration emphasized its formation.

Chapter 5

5 Synthesis of photocatalytic materials for CO_2 reduction

5.1 Materials and chemicals

Pluronic, triblock copolymer (P123) poly (ethylene oxide)-poly (propylene oxide)-poly (ethylene oxide) as structure directing agent, P123 ($EO_{20}PO_{70}E_{20}$, Aldrich), hydrochloric acid (HCl, 37%, Sigma Aldrich), tetraethyl orthosilicate (TEOS, 98%, Aldrich), potassium chloride (KCl, 99%, Sigma Aldrich), mesitylene (Aldrich), 1-butanol (99.5%, Fluka), and titanium tetra-isopropoxide (TTIP, 98% Sigma Aldrich), Iso propanol (99.9% Sigma Aldrich, Ethanol (99.9% Sigma Aldrich), distilled water (DW), and commercial titania Degussa or Aeroxide P25 was obtained from Evonik. All these materials were used directly without any purification.

5.2 *Designs of photocatalysts by applying various synthesis routes*

A variety of photocatalysts have been successfully synthesized in this study by using different synthesis routes to enhance the photoactivity of CO_2 reduction with H_2O. These process involved hydrothermal treatment method, sol-gel method, Nano-casting/template method and incipient wetting method by following the sol-gel hydrolysis condensation of titania *etc*.

5.3 *Synthesis of mesoporous materials*

5.3.1 Background and photocatalytic properties of mesoporous materials

According to the IUPAC definition, solids porous materials are classified into three groups based on their pores diameter [208].

Chapter 5

Pore size distribution according to (IUPAC) system

Micropores/<2nm ***Mesopores/2-50nm*** ***Macropores/>50nm***

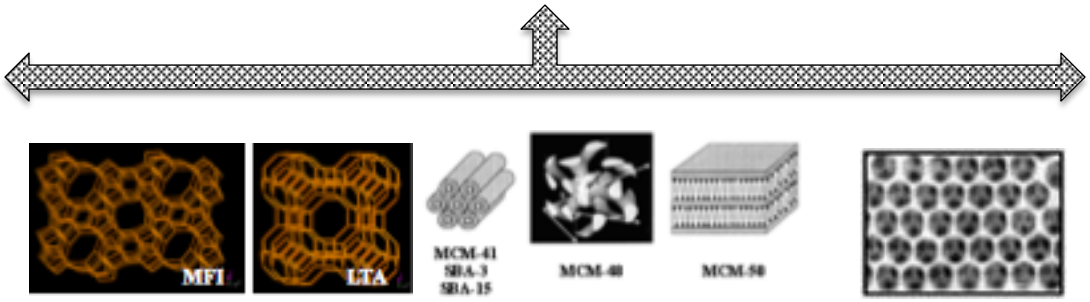

Zeolite, Activated Carbon, Metal Organic framework

Mesoporous Silica, activated Carbon

Sintered metals and Ceramics

However, synthesis of mesoporous materials was first demonstrated by Chiola et al [209]. In 1992, scientists in Mobil Oil Corporation reported a new group of mesoporous silicate molecular sieves, known as MCM41, which opened the new area in research field [210, 211]. Moreover, a lot of attention has been focused in the synthesis and further apply these materials for various applications [212-221]. Mesoporous materials have been widely used due to its various compositions in which the most important mesoporous titania is extensively accepted material and shows great potentials in various applications. Mesoporous structures with well-defined morphology and owing to its better performance in photocatalysis are well known materials than that of non-mesos tructures materials [222-226]. However, hierarchical structures are responsible to enhance the interactions with numerous species as well as multiscale pores, which allow for the mass transportation. Moreover, the coexistence of multiscale pores enhances the diffusion of molecules through the porous matrices [227, 228]. Generally, surfactant-assisted self-assembly is crucial step for the synthesis of mesoporous materials with the well-designed composition, pore configuration and morphology [229]. Therefore, variety of surfactants with varied morphologies including micelles, vesicles, liquid crystals and other assemblies have been used by the interactions with co-templates such as hydrogen bonding, van der Waals forces, and electrostatic interaction [230]. However, mesoporous structures play a significant role in photocatalysis to the transportation of photo-generated e^-/h^+ as well as prevent the recombination

of this charge carrier species. However, higher crystallinity, crystal structure distortion and the defects sites of the materials affect this characteristic. In addition, morphological properties such as surface area, particle size, surface structure and active sites on the surface are very important for photocatalysis. Despite, the various modification routes for mesoporous materials have been adapted to enhance photoactivity. Moreover, it has been proposed that a decrease in particle size could lead to a higher efficiency in photocatalysis [231, 232]. Theoretical models determine that particle size is an important factor for TiO_2 photoactivity. However, an optimum particle size might exist between 25 and 40 nm, which is a result of competing effects of effective particle size on light absorption and scattering efficiency, charge trasportation, and higher surface area of photocatalyst [233]. A lot of mesoporous materials have been studied for photocatalysis but the previous works on the MCM-41 was carried out by Kresge et al. [234] due to its high specific surface area of the mesporous material which facilitate the more reactive sites at the surface of the photocatalyst and nano-scale channel wall of mesopores can assist the transfer of photogenerated electrons and holes to the surface, and inhibit the recombination in the bulk [235]. Such as many mesoporous titania based and other photocatalytic materials have been used in photocatalysis technique for H_2 production from water splitting [235, 236-240] which indicates the better charge separation and transportation due to its wall thickness property, which reduced the duration of charge carrying as well. Consequently, mesoporous materials are considered the promising candidates for photocatalysis process.

5.3.2 Synthesis of SBA-15-S and KIT-6 mesoporous materials

Mesoporous materials Santa-Barbra-Amorphous-Spherical shaped (SBA-15-S) and Korean advanced Institute of Science and Technology-6 silica (KIT-6) were synthesized by hydrothermal treatment method. However, SBA-15-S was obtained according to the procedure reported by Wang et al. [241]. In a typical synthesis process, the molar ratio of the reactants was 1TEOS:0.017 P123:0.6 mesitylene, xKCl: 5.85 HCl: 165 H_2O, where x = KCl/TEOS molar ratio. 4 g of P123 and a certain amount of KCl (x = 2) was dissolved in 120 g of H_2O and 23.6 g of concentrated HCl at room temperature until the solution became transparent, then 3 g of mesitylene was added. After stirring for 2 h, 8.5 g of TEOS was added drop wise and stirred vigorously for 10 min. The mixture was then kept under static conditions at 35°C for 1 day,

followed by another 24 h at 100°C. The resultant precipitate was filtered, washed, dried and calcined at 550°C for 5 h so that it could be used as a support. Furthermore, Korean advanced institute science and technology (KIT-6) material was synthesized according to the procedure reported in literature [242, 243] and also shown in Scheme 5.1.

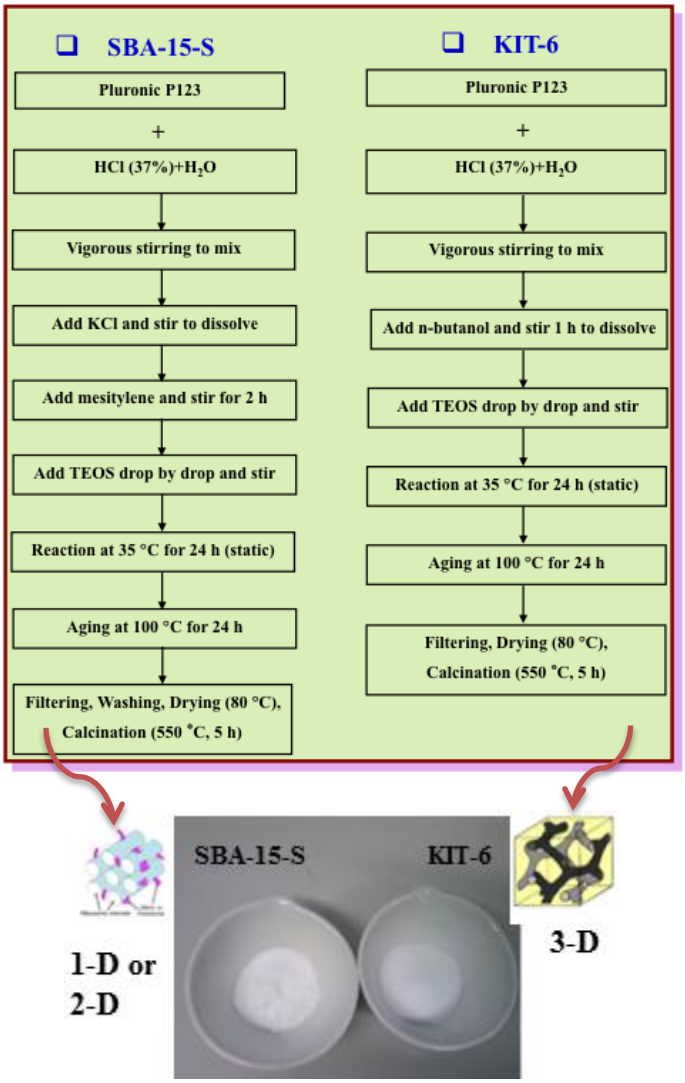

Scheme: 5.1 *Synthesis of SBA-15-S and KIT-6 mesoporous materials by hydrothermal treatment method.*

Typically, in this process, 6 g of P123 was dissolved in 217 g of distilled water and 11.8

g of concentrated HCl, and 6 g of 1- butanol was added under stirring at 35°C. After 1h of stirring 12.9 g of TEOS was added drop wise at 35°C. The mixture was stirred for 24 h at 35°C. The final solution was transferred to a Teflon bottle and heated at 100°C for 24 h. The solid product obtained after the hydrothermal treatment was filtered, dried and calcined at 550°C for 5 h so that it could be utilized as a support material.

5.3.3 Synthesis of novel Ti-SBA-15-S and Ti-KIT-6 materials

The purpose of synthesis of Ti based mesoporous materials was to investigate the two variables, increasing the Ti ratio and effect of calcination temperature on mesoporous materials. However, Novel Ti-SBA-15 & Ti-KIT-6 materials were prepared after the hydrothermal treatment of (SBA-15 and KIT-6) respectively, and was filtered, dried and/or calcined at 550 °C for 5 h mesoporous materials with different Si/Ti ratios such as (200, 100, 50). The dried and calcined KIT-6 materials were then treated with Titanium (IV) iso propoxide (98%) at different Si/Ti ratios (200, 100 and 50) and finally calcined to achieve Ti-KIT-6 following the roughly procedure 1 g SBA-15 was dissolved in 80 ml solvent (ethyl alcohol absolute (C_2H_5OH) by using the titanium precursor i.e. titanium isopropoxide (TTIP), while different amount of TTIP were diluted and thoroughly mixed in 10 ml absolute ethanol. This solution was then added to the suspension and stirred continuously, for 30 min to avoid agglomerates formation. Furthermore, by using a static stirrer, the solution was heated at 60-70°C to promote evaporation of the solvent. Afterward, paraffin film was used to cover the mouth of the beaker protect solution from environmental pollutants by constantly heating and stirring for next 30 mints. Subsequently, the solution were transferred into a Teflon bottle and situated in the Rota vapor at 80°C overnight to complete the solvent vaporization. Finally, the solid product obtained after hydrothermal treatment was calcined at 550 °C for 5h with a heating ramp of 3°C/minute as shown in the scheme: 5.2. Thus, Ti-SBA-15 dried and calcined materials with various ratios (200, 100, 50) were obtained successfully which were further utilized for photocatalytic reduction of CO_2 to fuel formation. Similarly, Ti-KIT-6 mesoporous materials were synthesized according to procedure recently reported in [244] both dried and calcined form having the same

molar ratio of Si/Ti (200, 100, 50) but notably KIT-6 mesoporous material was used instead of SBA-15 to obtained the final Ti-KIT-6 mesoporous photocatalyst. Mesoporous silica, KIT-6 possesses large pores with thick pore walls, high hydrothermal stability, high specific surface area (800m^2/g) and large pore volume (almost 1 cm^3/g). However, all these characteristics of KIT-6 material showed the better photoactivity than of SBA-15 material, which are 1-D, or 2-D mesopores structures.

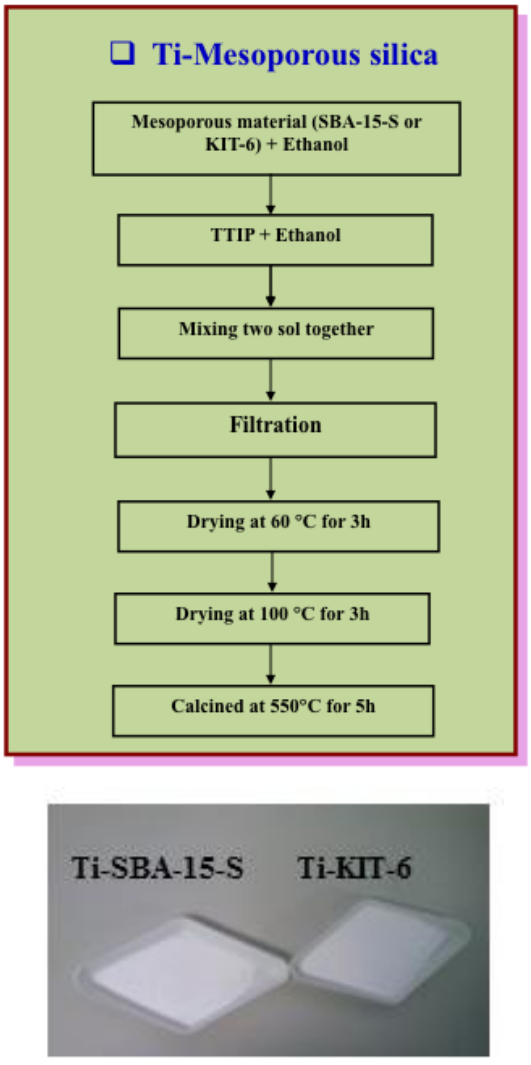

Scheme: 5.2 *Synthesis of Ti-SBA-15-S and Ti-KIT-6 mesoporous materials.*

5.3.4 Synthesis of titania nanoparticles (TNPs)

Titania nanoparticles (TNPs) were synthesized by sol-gel method. Generally, the sol-gel method has been extensively used amongst the other variety of methods for synthesis process. It is because of many advantageous of relatively low cost, very flexible applicability to obtained wide range of sizes and shapes of the materials. In this process, the dispersion of colloidal particles suspended in Brownian motion within a fluid matrix then first converts to viscous gels and subsequently to solid material during the sol-gel process [245]. Titanium dioxide (TiO_2) on small scale (200 mL gel) was synthesized by following the procedure published by Hussain et al. [43]. Typically, synthesis process involved by homogeneously mixing a solution of micro-filtered water (Milli-Q) with isopropanol as well as a solution of titanium tetra iso propoxide (TTIP) in isopropanol. The solutions were prepared separately under nitrogen flux to control alkoxide reactivity with humidity and moreover, hydrochloric acid (HCl) was added at different initial concentrations as a hydrolysis catalyst and de-agglomeration agent. TTIP/isopropanol concentration was taken equal to 1M/L to obtain the maximum TiO_2 yield (1M), whereas the water and hydrochloric acid concentration were chosen in order to obtain a water to precursor ratio as following $W=[H_2O]/[TTIP]=4$ while acid to precursor ratio, $H=[H^+]/[TTIP]$ was set to 0.5. The two solutions of TTIP and water in isopropyl alcohol were stored in four identical syringes and fed at equal flow rates in the *Vortex reactor* where were mixed by using this set-up as shown in the Fig. 5.1. Equal volumes of reactant solutions (i.e.100 ml) were mixed at equal flow rates at 25°C in a Vortex reactor (VR) and then for both configurations the solutions exiting the reactor were collected in a small vessel gently stirred. The VR used in this work is constituted by a cylindrical chamber of 12 mm in diameter and 3mm in height; four reactant streams are fed tangentially at opposite sides of the reactor through four pipes of 3 mm of diameter, whereas the mixed solutions leave the reactor from the bottom through an outlet pipe of 3 mm of diameter. The TTIP conversion into TiO_2 through hydrolysis and condensation can be summarized into the following global chemical reaction:

$$Ti\,(OC_3H_7)_4 \rightarrow TiO_2 + 2H_2O + 4C_3H_7OH \qquad (5.1)$$

Chapter 5

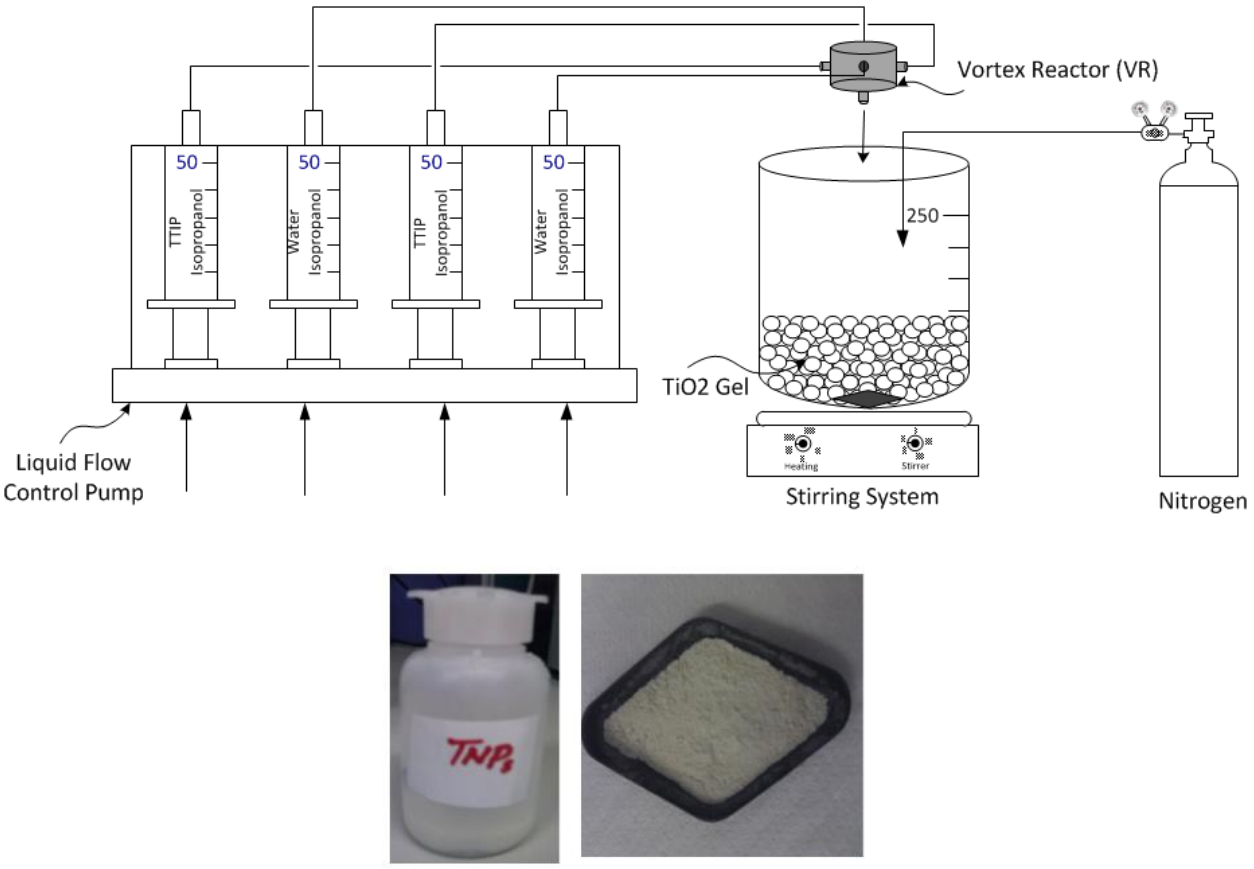

Figure: 5.1 *Schematic diagram for synthesis of titania nanoparticles (TNPs) by Sol-gel method (Adapted from Ref [43] modified form).*

As it is well known, that a very fast chemical reaction characterized by equilibrium completely shifted toward the products, as TiO_2 is a thermodynamically very stable substance, thus resulting in almost 100% yield. The mixed solutions (i.e. gel) were then dried using a Rota vapor. Complete drying was obtained at 150°C overnight. The resulting dried powders were eventually calcined at 500°C for 3h to obtain the solid/powder titania nanoparticles.

Chapter 5

5.3.5 Synthesis of Meso.TiO_2 photocatalyst by Nanocasting/template method

Mesoporous TiO_2 /KIT-6 photocatalytic material was synthesized by using mesoporous silica KIT-6 as template as shown in the scheme 5.3.

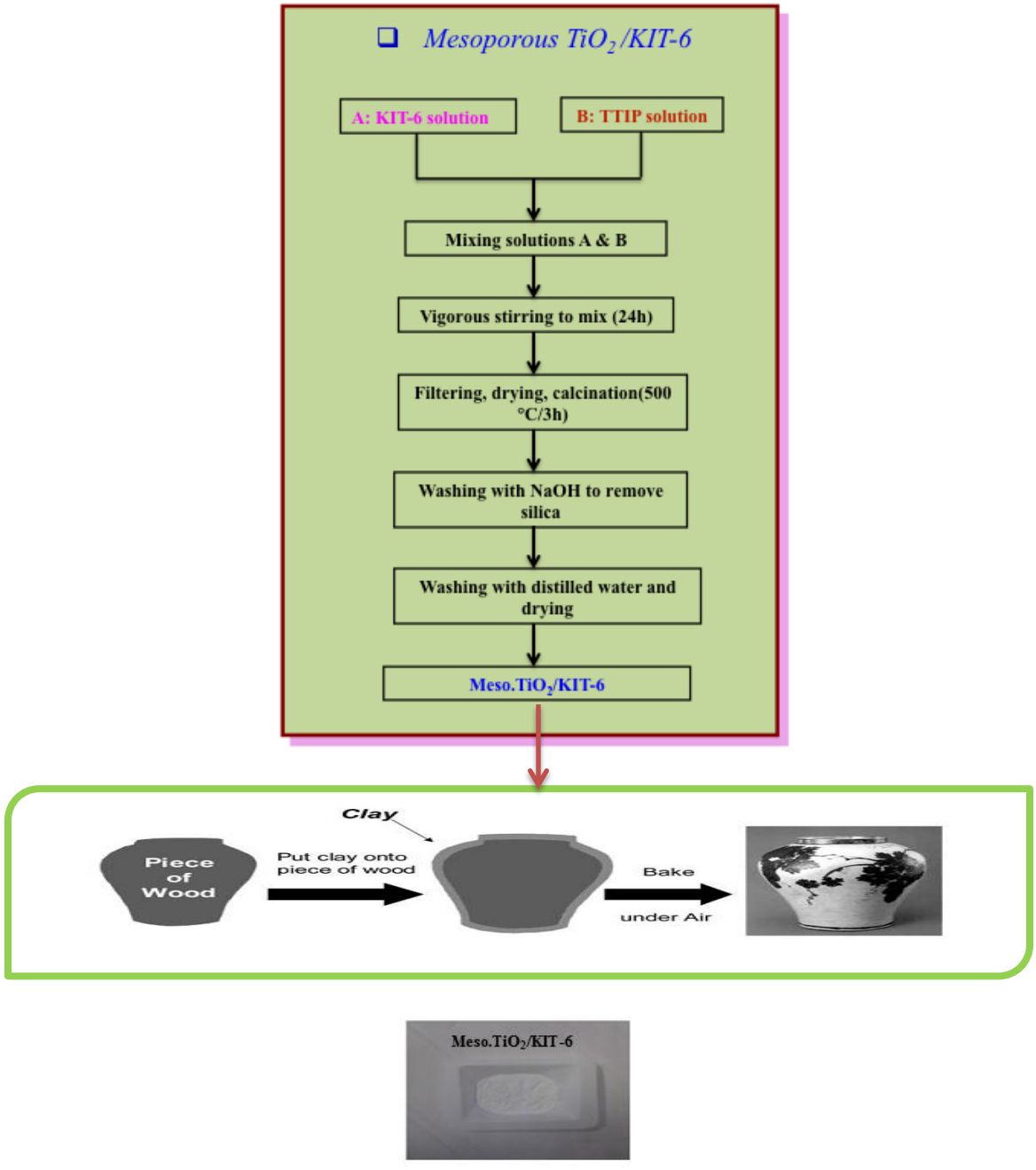

Scheme: 5.3 *Synthesis of Meso. TiO_2/KIT-6 materials by nanocasting/template method [247].*

Chapter 5

KIT-6 mesoporous silica material, after passing the hydrothermal treatment, solid products was filtered, dried and finally calcined at 550°C for 5h. Furthermore, Meso.TiO_2 obtained by using KIT-6 replication according to the following procedure reported in the literature [246] but notably meso porous silica i.e. KIT-6 was used in this study instead of SBA-15 as a silica template and Titanium (IV) isopropoxide (TTIP, Sigma Aldrich.98%) was used as the TiO_2 precursor. However, the solid products obtained was filtered, dried and calcined at 500 °C/3h. Afterwards, the samples were washed with 2M NaOH solutions as well as with distilled water to remove the silica impurities and then subsequently dried to obtain final Meso.TiO_2/KIT-6 material. Meso.TiO_2/KIT-6 material is the exact copy of the template KIT-6 material as reported by Lee et al. [247].

5.3.6 Synthesis of mesostructured TiO_2/KIT-6 nanocomposite series

Mesostructured TiO_2/KIT-6 nanocomposite titania series were synthesized by sol-gel hydrolysis and condensation of TTIP, applying different wt% of the TiO_2 using, titanium (IV) isopropoxide (TTIP, Sigma Aldrich.98%) as a precursor. To obtain the supported TiO_2/SiO_2 materials, the required amount of titanium tetra isopropoxide (TTIP) such as 1, 5, 10, 20, 30, 50, 70, and 90wt% was used with silica KIT-6 materials. Typically, synthesis process was followed by according to procedure reported in [248] instead SBA-15, KIT-6 mesoporous material was used as a support due to its 3D pore structures which provides the enough space for the dispersion of TiO_2 into meso porous channels. The mixture obtained, was centrifuged or filtered and the recovered solid was dried at 110^oC. . The synthesis procedure is shown in scheme 5.4 as well as in Fig. 5.2. Furthermore, 20% TiO_2 has been found to be the optimized photocatalyst for CO_2 photo reduction with H_2O vapor under the UV light illumination to renewable fuel products such as CH_4, CH_3OH, CO and H_2. Moreover, optimized 20%TiO_2/KIT-6 was calcined further at different calcination temperature (e. g 500, 600 700, and 800^oC/3h) to acquire the higher crystallinity as well as tested for CO_2 photocatalytic activity. Satisfactory results were obtained shown in the results and discussion part.

Chapter 5

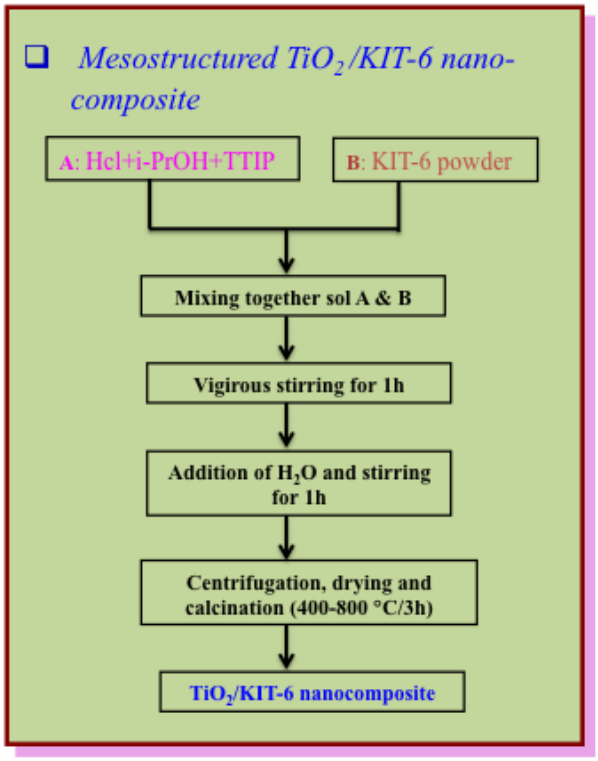

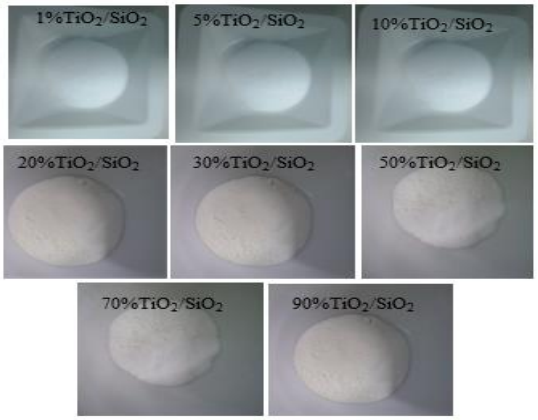

Scheme: 5.4 *Synthesis of nanostructured TiO_2/KIT-6 materials.*

Chapter 5

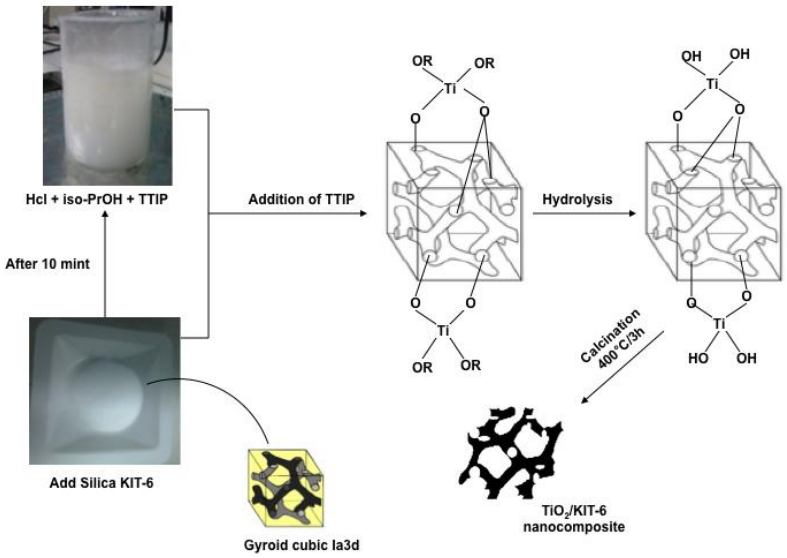

Figure: 5.2 *Synthesis routes for nanostructured TiO_2/KIT-6 photocatalysts.*

Chapter 6

6 Characterization of synthesized photocatalytic materials

6.1 Textural structural properties of the synthesized photocatalytic materials

6.1.1 N_2 adsorption/desorption analysis

The textural properties of the synthesized photocatalytic materials have been observed by Micromeritics Tristar II, USA (surface area and porosity) instrument. The BET specific surface area (S_{BET}), pore volume (PV) and average pore diameter (APD) were measured on the powder materials which had previously been outgassed at 150°C for 2h using Micromeritics Flow Prep 060, USA (sample degas system), by means of N_2 sorption at 77 K shown in Fig.6.1. N_2 adsorption/desorption is important phenomena, which is very useful to characterize porous materials allowing for the determination of specific surface area, pore size distribution and pore volume. Generally, in physio sorption (physical adsorption), there is a weak Van der Waals attraction between the adsorbate and the solid surface. When a gas or vapor phase is brought into contact with a solid and part of it is taken up and remains on the outside attached to the surface in the form of mono, bi or multilayer formation is called "*adsorption"* and the reverse process is called *"desorption"*. Specific surface area was measured by S_{BET} measurement, pore size distribution, were calculated by using the Brunauer-Emmet-Teller (BET), BJH, adsorption/desorption isotherms of the mesoporous materials showed the type IV isotherm obtained from Barrett-Joner-and Halenda (BJH) adsorption and desorption calculation.

Chapter 6

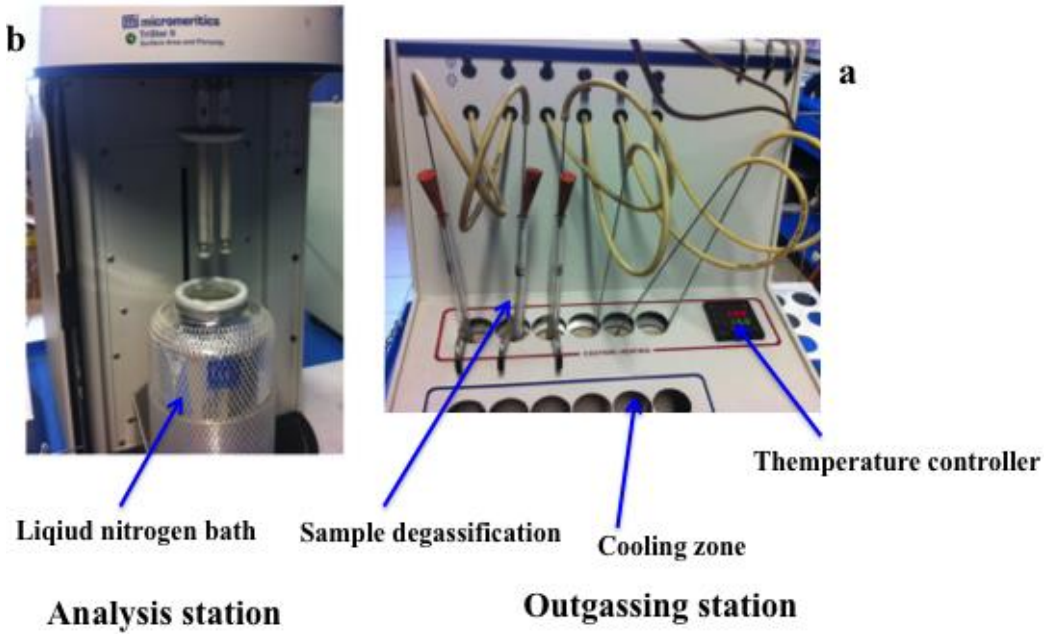

Figure: 6.1 *N_2 adsorption/desorption analysis apparatus* ***(a, right)*** *outgassing station,* ***(b, left)*** *analysis station.*

6.1.2 Field Emission Scanning Electron Microscopy (FE-SEM) analysis

Field emission microscopy is an analytical technique used to investigate the molecular surface structures and their electronic properties. However, Leo Supra 55 field emission scanning electron microscopy (FE-SEM, Zeiss Merlin) was used to observe the morphology of the synthesized photocatalytic materials. Typically in a field-emission, cathode in the electron gun of scanning electron microscope provides narrow probing beam at low and high electron energy, resulting in both resolution samples is being protected from charging as well as damage. In such a way, high quality, low voltage images are obtained with very negligible electrical charging of sample. In addition, SEM also provides some information about the pore size and the connectivity of the pores but it is rarely used for pore analysis.

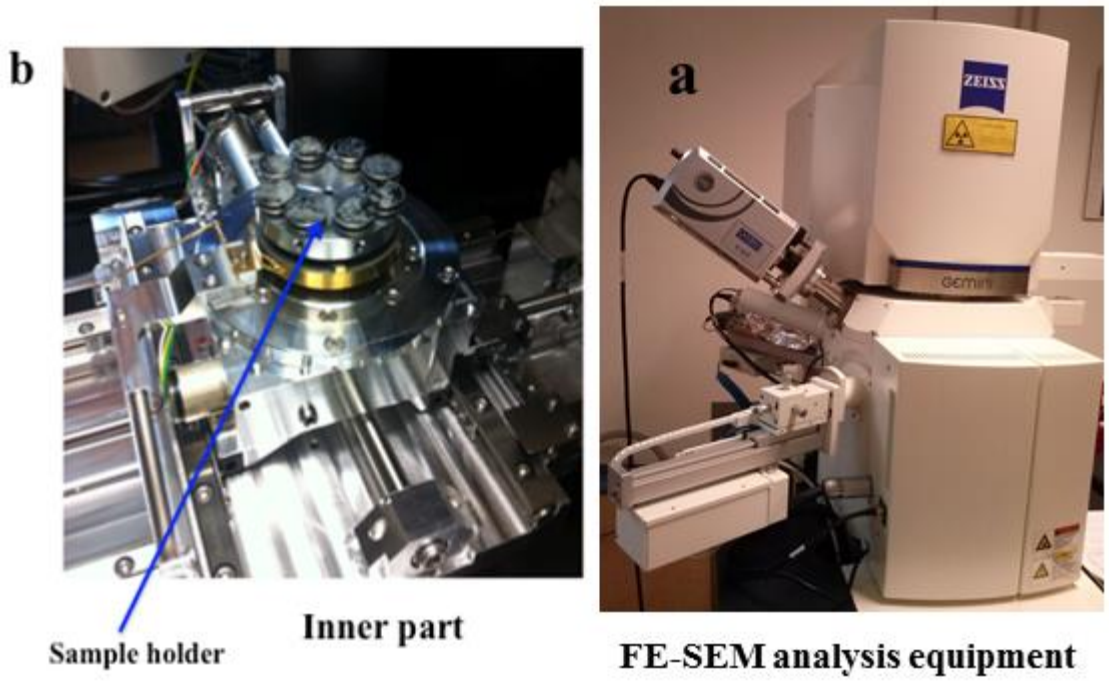

Figure: 6.2 *FE-SEM analysis technique:* ***(a, right)*** *analyzer* ***(b, left****) sample holder.*

6.1.3 X-ray Diffraction (XRD) analysis

XRD is analytical technique used to identify the crystallinity of the crystalline materials. However, the powder X-ray diffraction (XRD) patterns of modified titania mesoporous materials were recorded by X'Pert Phillips diffraction using Cu Kα (λ=1.54173Å) radiation, under the following conditions: 2θ, (10–90°) with step size =0.02 for WAXS. Moreover small-angle X-ray scattering (SAXS) patterns of the materials were recorded on a Phillips instrument at 2θ=0.2–3.5° in order to determine the different polymorphs or crystallinity of the samples.

Chapter 6

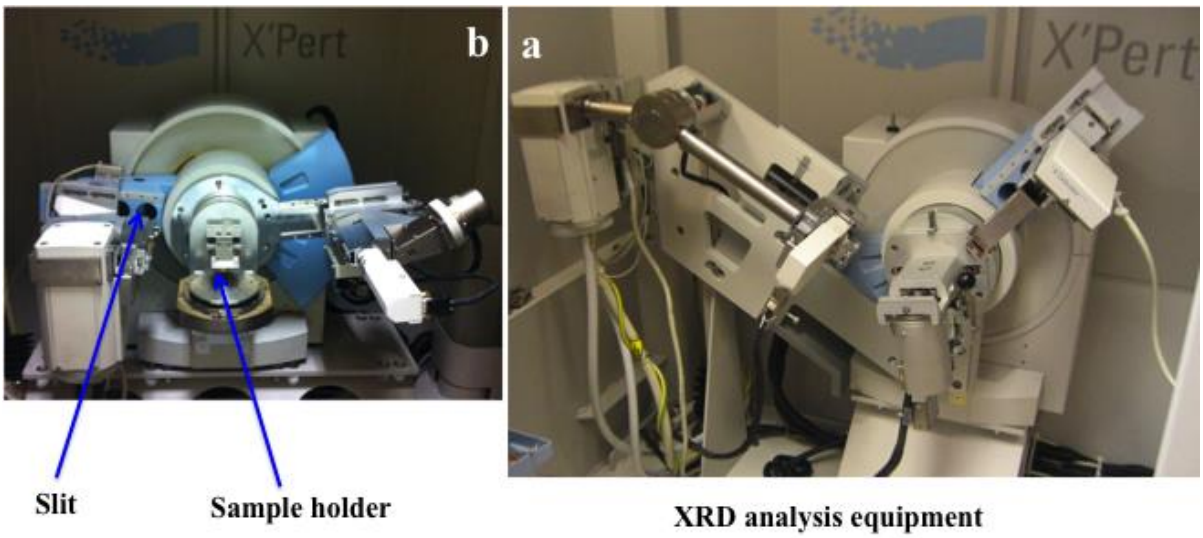

Figure: 6.3 *XRD analysis technique* ***(a, right)*** *external view* ***(b, left)*** *internal components with sample holder.*

6.2 Chemical, structural properties of synthesized photocatalytic materials

To investigate the chemical structural and electronic properties of synthesized photocatalytic materials various technologies for instance, UV-Vis, TEM, XPS, FT-IR, technologies have been applied to further investigate the chemicals properties of the photocatalyst.

6.2.1 Ultraviolet-Visible Spectroscopy (UV-Vis) analysis

To observe the absorption or transmission of UV-Vis light, the UV-Vis diffuse reflectance spectra of TiO_2/KIT-6 nanocomposite were recorded using a Varian model Cary 500 spectrophotometer with a quartz cell suitable for measuring powders. The accurate absorption of the UV-Vis light can be calculated by using the following equation.

$$\Delta E_{bg} = \frac{hc}{\lambda} = \frac{1239.95}{\lambda} \qquad (6.1)$$

E_{bg} = Band Gap energy in eV

h = Planck's constant = 6.63 x 10^{-34} Js

c = speed of light = 3 x 10^{8} m/s

λ = wavelength in nm

When photons are absorbed by the photocatalyst in a certain range of wavelengths, after the absorbance in the ultraviolet photons you may get a trend of the absorbance as a function of wavelength, generally the curve increases to a maximum and thereafter decreases rapidly making the tangent that best approximates the curve in the descending tract is possible to derive the value of the characteristic wavelength. Consequently, the band gap energy between the valence band and conduction band can be derived using the above equation.

6.2.2 Transmission Electron Microscopy (TEM) analysis

Transmission electron micrographs (TEM) of the support material and Ti-based mesoporous samples were collected from the thin edges of the sample particles using a TEM Philips CM12, with a LaB6 filament, double tilt holder, operating at 120 kV. Generally, TEMs work by using a tungsten filament or LaB6 filament, which produces an electron beam in a vacuum chamber. The emitted electrons are then accelerated through an electromagnetic field, operating at 120 kV that also narrowly focuses the beam. The beam is then passed through the very thin sample material (less than 100nm). Then electrons that pass through the sample hit a phosphor screen, CCD or film and produce an image, which can be observed by on the screen. If the sample has less density, more electrons get through and the image is brighter and clearly can be seen. On the other hand, a darker image is produced in areas where the sample is denser and therefore, less passage of electrons could ‘not produce the clear image. TEM provides the important information regarding the pore size; pores connectivity of the samples having less than 5nm pore size can be measured easily if sample contains the ordered pores.

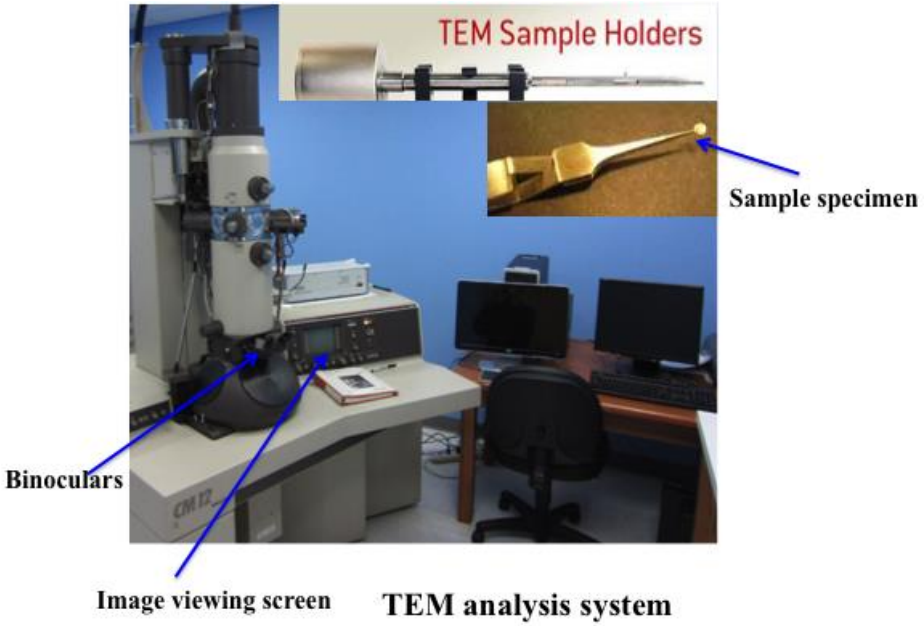

Figure: 6.4 *TEM analysis technique.*

6.2.3 *X-ray Photoelectron Spectroscopy (XPS) analysis*

Elemental composition of the mes porous titania samples were recorded using a PHI 5000 Versa Probe (USA), with a scanning ESCA microscope fitted with an Al monochromatic X-ray source (1486.6 eV, 25.6 W), a beam diameter of 100 μm, a neutralizer at 1.4 eV, 20 mA, and in FAT analyzer mode.

6.2.4 Fourier Transforms Infrared (FT-IR) analysis

Fourier transforms infrared (FT-IR) spectra of the support and Ti-KIT-6-mesoporous materials were collected at a resolution of $2cm^{-1}$ on a Perkin Elmer FT-IR spectrophotometer equipped with an MCT detector to determine the structures of molecules with the molecules' characteristic absorption of infrared radiation such as the information about the nature of the surface oxygen or hydroxyl groups. Infrared spectrum is molecular vibrational spectrum. When exposed to infrared radiation, sample molecules selectively absorb radiation of specific wavelengths, which causes the change of dipole moment of sample molecules. Consequently, the vibrational energy levels of sample molecules transfer from ground state to excited state. The

frequency of the absorption peak is determined by the vibrational energy gap. The number of absorption peaks is related to the number of vibrational freedom of the molecule. The intensity of absorption peaks is related to the change of dipole moment and the possibility of the transition of energy levels. The common used region for infrared absorption spectroscopy is 4000~500 cm^{-1} because the absorption radiation of most organic compounds and inorganic ions is within this region.

6.3 Primary photocatalytic reaction system set-up

The schematic representation of the experimental system set-up is shown in Fig. 6.5.

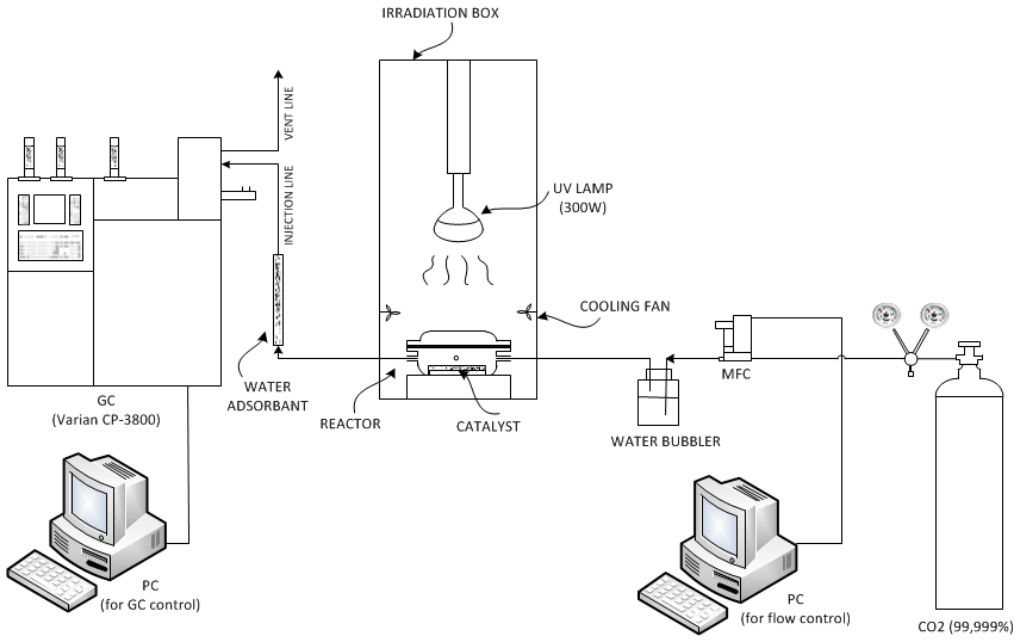

Figure: 6.5 *Schematic diagram of primarily CO_2 photocatalytic reduction system set-up.*

Photocatalytic reaction system set-up consists of a *Pyrex glass reactor* (transparent to UV light). From one side it is connected to a *Gas Chromatograph* (Varian CP-3800) equipped with capillary column (CP7381, fused silica) and flame ionization detector (FID) with a patented ceramic flame tip for ultimate peak shape and sensitivity used to analyze composition of gas products and from other side it has connection with *water (H_2O) bubbler* which allow to pass

water vapor passing from reactor along with gas (CO_2) making a homogeneous mixing to establish the equilibrium. Glass reactor with a photocatalyst dispersed at its bottom is located inside an *irradiation box* where there is an UV lamp (Osram Ultra Vitalux, 300 W has a mixture of light of UVA with a range of 320-400 nm and UVB with 290-320 nm wavelength which produces 13.6 and 3.0 W radiations respectively, is situated at the top of the irradiation box.

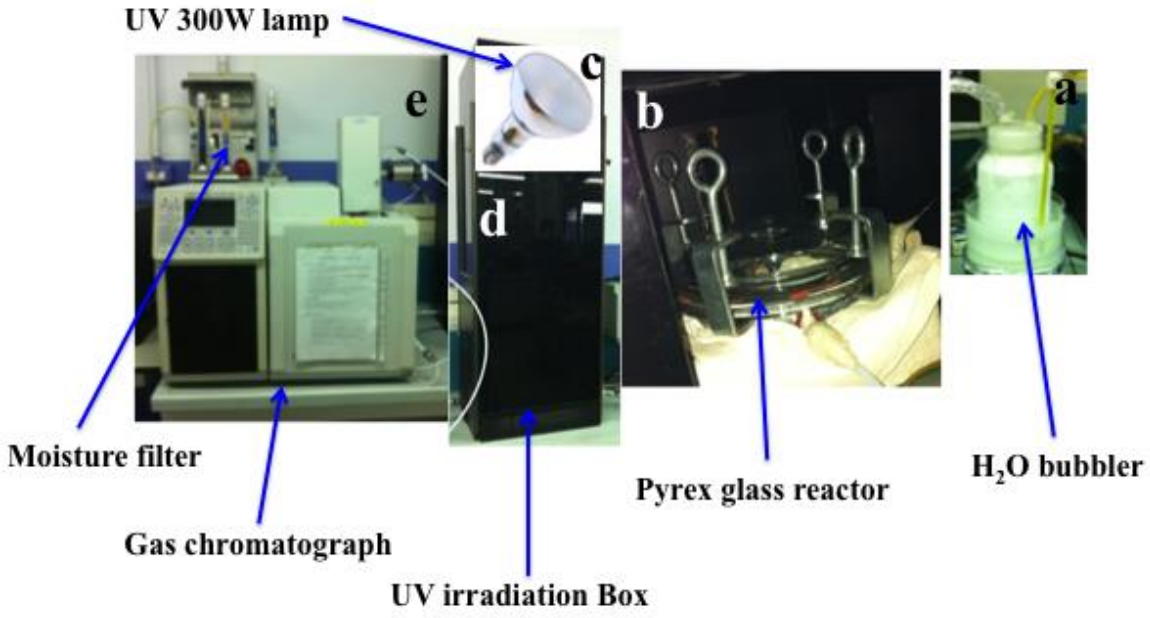

***Figure: 6.6**. Major components of primarily CO_2 photocatalytic reduction system set-up: **(a),** water bubbler **(b),** Pyrex glass reactor **(c),** UV light source **(d),** UV irradiation box **(e),** GC (only FID detector).*

However, the moisture silica adsorbent filter was used to adsorb the moisture contents to avoid damage of GC devices. Furthermoreover, reactor was connected to a Teflon bottle containing de ionized water and a gas cylinder supplying a highly purified *carbon dioxide (99.999%) gas*. Hence, the water bubbler permits to feed the enough amount of water vapor necessary to the CO_2 reduction but excess of water vapor suppressed the photocatalytic reaction The temperature in the reactor was measured by a *thermocouple* while a *mass flow controller* (MFC, Bronkhorst high tech) was used to regulate CO_2 flux to the reactor.

Chapter 6

6.4 Modification of the photocatalytic reaction system set-up

Photocatalytic reaction system set-up has been modified to synthesize hydrocarbons such as CH_4 and CH_3OH (which were the main products obtained from primarily reduction system) and another valuable fuel products (H_2, CO) after modification by using TCD detector. However, there were several deficiencies in the previous system set-up to get all these desired products, modification of reaction system was very necessary step to improve the photocatalytic efficiency from CO_2 reduction is shown in the Fig. 6.7 and 6.8. This set-up includes a *Pyrex glass reactor*, *connectors*, *mass flow controllers* (Bronkhorst, High-Tech), a *water bubbler* and a *UV lamp* (Newport/Oriel Instrument USA 200 W with focusing lens assembly or Osram Ultra-Vitalux 300 W).

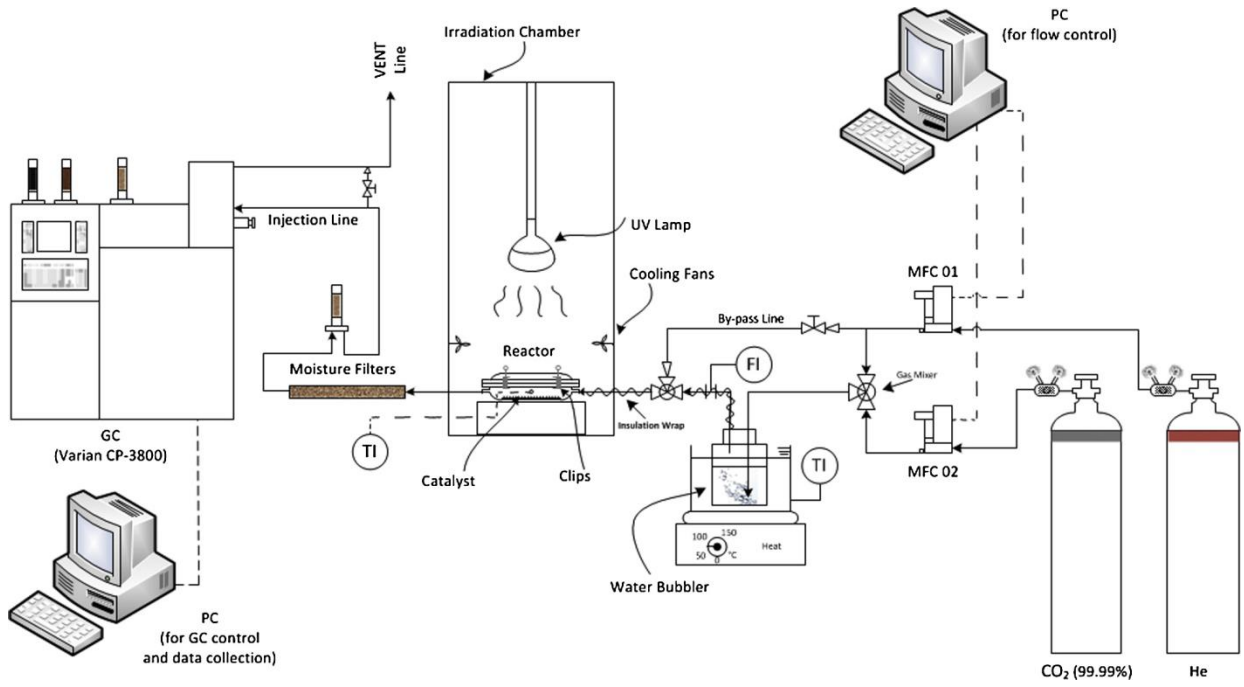

Figure: 6.7 *Schematic diagram of optimized photocatalytic reaction system set-up for CO_2 reduction.*

The set-up also includes a *CO_2 gas cylinder (99.99 %)*, and a *Hellium (He)* gas cylinder, a *gas chromatograph* (GC, Varian CP-3800) equipped with a capillary column (CP7381), a *flame ionization detector (FID)* and a *thermal conductivity detector (TCD)*.

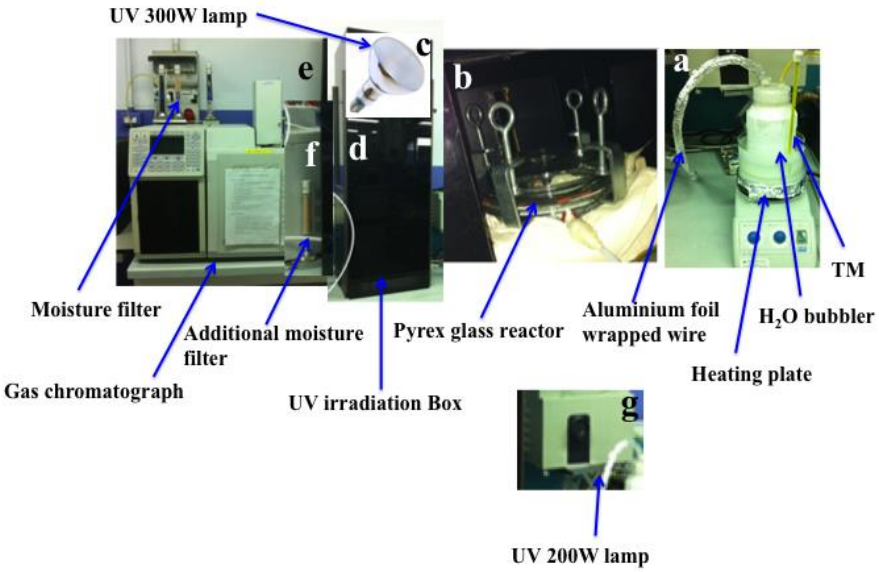

Figure: 6.8 *Additional components of modified CO_2 Photocatalytic reduction system set-up:* ***(a),*** *water bubbler* ***(b),*** *Pyrex glass reactor* ***(c),*** *UV 300W* ***(d),*** *UV irradiation box* ***(e),*** *GC with FID+TCD detectors* ***(f),*** *Additional moisture filter* ***(g)*** *UV 200W lamp. TM*(Thermometer).*

A photocatalytic reaction was performed in the reactor, which contained 0.2 or 0.5 g of photocatalyst. The reactor and lines were purged with a He flow to remove the trapped air and the impurities. CO_2 gas 100 % pure or after dilution (20 %) with He, was introduced into the reactor after having passed through the water bubbler and ensuring it was adsorption-desorption balanced in order to saturate the catalysts with CO_2 and H_2O. Heating system was used to maintain the water bubbler temperature (controlled by thermometer) to produce enough amount of water vapor.

Furthermore, an additional moisture filter was used to prevent the moisture, which could damage the GC components. However, an improved photocatalytic CO_2 reduction results were

attained after the modification of photocatalytic reaction system set-up. Moreover, when equilibrium was reached, the UV light was turned on and the reaction products were analyzed by means of GC. Blank tests were also conducted to ensure that the products were due to the photocatalytic reaction. The blank tests consisted of a UV-illumination without the photocatalyst and a reaction in the dark with the photocatalyst. Additionally, 200W UV source was used for comparison of the activity tests in Meso.TiO_2/KIT-6 materials.

6.5 Gas chromatographic analysis (GC)

Gas chromatography (GC) is a gas separation technique in a chemical analysis. This process is based on the principle, that the analyses compounds separated are dispersed through two different phases; one is "mobile phase" (a gas chromatograph uses gas as mobile phase which is called carrier gas and is stored in a high pressure cylinder) and another "stationary phase" respectively. However, GC permits to separate the gas and volatile substances. In a single process, mixture can be separated into its individual components and through a detector (FID) to identify the hydrocarbons and (TCD) detector is used to see the hydrocarbons as well as non-hydrocarbons as well. However, a known amount of gas is injected and fixed (so "instantaneous") in column (formed by a capillary tube in numerous windings until arriving to a length of several meters) and eluted in it by means of the carrier gas (carrier gas that should be inert with respect to the other components present). The column has a filling fixed bed that interacts with components of the test gas with adsorption and desorption. The affinity of each component with the fixed phase determines a speed of elution (and thus a residence time in the column). Having the rate of elution various components, they will come out from the column at different times [249] to identify and quantify each compound. For a good analysis it is therefore necessary to adjust the parameters GC, in particular the temperature of the oven (which affects the volatility of the components, on elution times and the index of resolution R, which defines the overlap / distance between two peaks) and the flow rate of the carrier gas. Analyzer is then used to the individual components and it allows measuring the quantity. There are several methods: TCD, FID, ECD, FPD and others. In this case we make use of two methods TCD and FID [250].

FID: (Flame Ionization Detector); the carrier gas and the hydrogen component are mixed

with the output of a nozzle and then ignited in the presence of a stream of air. The combustion produces ions that are collected by a pair of polarized electrodes, producing an electrical current that represents the signal. This analysis is destructive and therefore not applicable to inorganic compounds that do not burn the precisely, hydrocarbons such as CH_4 and CH_3OH *etc*.

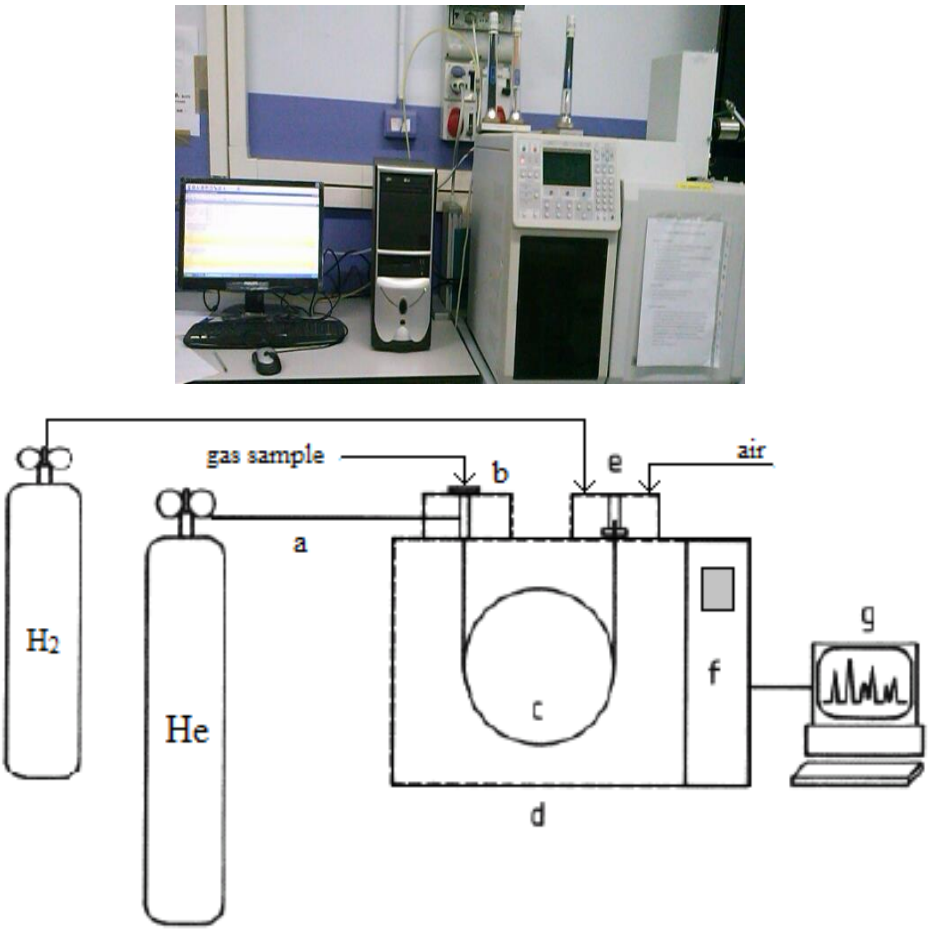

Figure: 6.9 *Schematic diagram of gas-chromatography system set-up* ***(a)****, carrier gas* ***(b)****, syringe injection,* ***(c)****, column, (****d****), column oven, and analyzer, (****f****), control panel, (****g****), computer for data storage.*

TCD: (Thermal Conductivity Detector) is a method able to detect any component (in particular inorganic molecules, but also hydrocarbons) and non-destructive. However it is used to

measures the difference in thermal conductivity between the component and the carrier gas through measures of electric resistance, and is therefore able to determine the amount present. The potential variation due to the variation of thermal conductivity represents the signal such as H_2, N_2, O_2, CO, CH_4 and CO_2 *etc*. Oxygen and nitrogen derived from the air that inevitably remains trapped in the system and are monitored as a rebuttal of leaks.

Moreover, a column chromatography system consists of the following constituents such as a mobile phase, a pump, a column, a detector and a system to analyze data, as shown in the Fig. 6.9. The abscissa to which it has the maximum of the peak identifies the elution time of the substance, which allows for the qualitative identification; calculating the area under the peak, however, one can derive the amount of substance eluted. It is therefore required careful preliminary calibration to identify the characteristic time is injected into the GC pure component, and to convert the value of the area (in volts / sec) in the number of moles (or ppm) samples are carried out at different known concentrations, thus obtaining an equation of conversion. The main problems of this type of analysis are therefore the distance between the peaks, which must be sufficient so as to have no loss of resolution; the background noise of the signal, in fact, the GC is able to detect very small amounts, but these may be covered by the noise on the signal; the incompatibility with the water, so it is necessary to place a filter at the entrance of the sample gas with the risk that this also withholds other substances of interest. [251]. In addition to, there are two types of gas chromatography.Gas-liquid chromatography (GLC) and Gas-solid chromatography (GSC). GLC is the chromatography type used for most GC analyses. There are several non-volatile compounds that can be separated with both GC and LC but these need to be derivative before GC separation. The capillary columns in GC have higher separation efficiencies than LC columns. This is the reason why GC is used to handle multicomponent mixtures. The most common carrier gas, used to transport volatile substances through the column, is helium, nitrogen and hydrogen. These gases are inert and do not react with sample or the stationary phase. For GC separation, several detectors have been developed and can be employed; these can be classified in two main types, Concentration sensitive detectors and Mass sensitive detectors. Nowadays, the most used detectors, in combination with gas chromatography, are mass spectrometer (MS).

Chapter 7

7 Results and discussion

7.1 Photocatalytic activity tests for highly dispersed isolated Ti mesoporous materials for methane and other fuel products

7.1.1 Characterization of synthesized mesoporous photocatalytic materials

Primarily, characterization of the synthesized mesoporous silica materials were made by Brunauer–Emmett–Teller (BET) specific surface area (S_{BET}), pore volume (PV), average pore diameter (APD), isotherms and pore size distributions on the powder materials, which had previously been outgassed at 150 °C using a Micromeritics FlowPrep 060, USA (sample degas system), by means of N_2 sorption at 77 K on a Micromeritics Tristar II, USA (surface area and porosity) instrument.

The physical and textural properties of the mesoporous materials (SBA-15-S, KIT-6) and Ti-mesoporous silica series were obtained by means of N_2-sorption and are shown in Table 7.1 SBA-15-S and KIT-6 have shown different and large surface areas (S_{BET}), pore volumes (PV) and average pore diameters (APD) on the basis of their characteristics. However, there was a significant decrease in the surface area (S_{BET}), pore volume (PV) and average pore diameter (APD) of SBA-15-S in the Ti-SBA-15-S-calcined series of photocatalysts, which is due to the increased Ti content in the rigid 1-dimensional or 2-dimensional (1-D or 2-D) calcined structure of SBA-15-S. A similar decreasing trend in the physical properties was also observed in Ti-SBA-15-dried series. However, due to the dried bulk structure, there was easy incorporation of Ti. Since due to the restructuring and final calcination, the overall physical properties were higher in this case.

A noticeable decrease can be seen in the physical properties of KIT-6, after Ti incorporation with different Si/Ti ratios. The S_{BET} and PV of the Ti-KIT-6 (dried) materials were slightly higher than those of the Ti-KIT-6 (calcined) ones, which might be due to the easy incorporation of Ti in the dried weak structure of KIT-6.

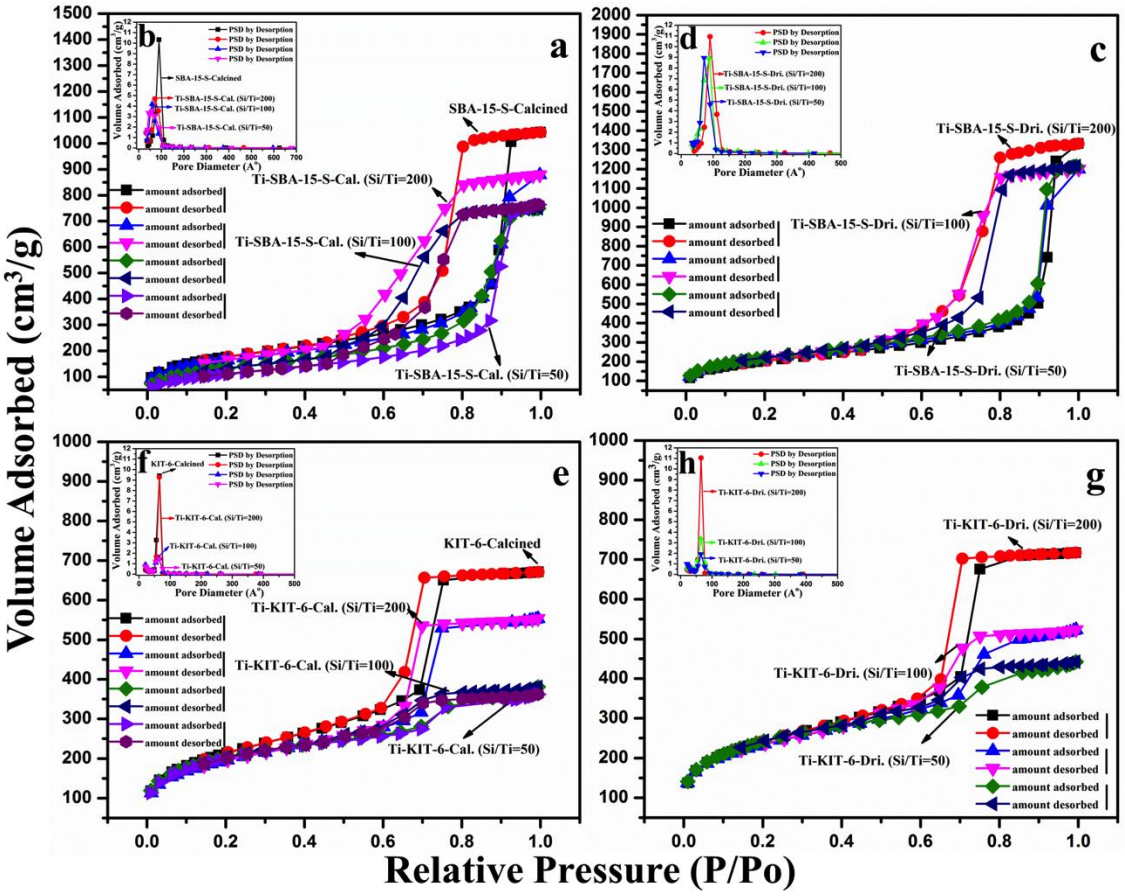

Figure: 7.1 *N_2 adsorption/desorption isotherm and pore size distribution trends of:* ***(a, b)*** *SBA-15-S calcined and Ti-SBA-15-S-calcined series,* ***(c, d)*** *Ti-SBA-15-S-dried series,* ***(e, f)*** *KIT-6 calcined and Ti-KIT-6-calcined series* ***(g, h)*** *Ti-KIT-6-dried series.*

However, Ti can be trapped in the bulk of the dried KIT-6 material, but not in that of the rigid structure of the calcined KIT-6 one. The average pore diameter did not change significantly and remained uniform, which might be due to the three-dimensional (3-D) pore structure of KIT-6, which is able to accommodate the uniform isolated-Ti dispersion. The porous and textural

properties of the mesoporous silica and Ti-mesoporous silica materials were examined by means of N_2 adsorption/desorption isotherms at 77 K and pore size distribution (PSD), as shown in Fig. 7.1. SBA-15-S and KIT-6 before Ti incorporation showed the typical reversible type IV adsorption isotherms defined in IUPAC [252]. The type IV isotherm also provides useful information on the mesoporous structure through its hysteresis loop [252, 243].

***Table: 7.1**: Physical properties of the synthesized mesoporous materials*

Samples	S_{BET}	PV	APD
Spherical SBA-15 (S-15) Calcined	638	1.62	10.1
[Ti-S-15(Calcined) (Si/Ti=200)] Calcined	591	1.36	7.3
[Ti-S-15(Calcined)(Si/Ti=100)] Calcined	481	1.17	6.1
[Ti-S-15(Calcined)(Si/Ti=50)] Calcined	403	1.15	5.9
[Ti-S-15(Dried) (Si/Ti=200)] Calcined	794	2.06	9.0
[Ti-S-15(Dried) (Si/Ti=100)] Calcined	776	1.90	8.8
[Ti-S-15(Dried) (Si/Ti=50)] Calcined	731	1.52	7.1
KIT-6 (K-6) Calcined	772	1.04	6.49
[Ti-K-6(Calcined) (Si/Ti=200)] Calcined	726	0.95	6.45
[Ti-K-6(Calcined) (Si/Ti=100)] Calcined	700	0.85	6.40
[Ti-K-6(Calcined) (Si/Ti=50)] Calcined	684	0.73	6.41
[Ti-K-6(Dried) (Si/Ti=200)] Calcined	865	1.11	6.55
[Ti-K-6(Dried) (Si/Ti=100)] Calcined	767	0.80	6.48
[Ti-K-6(Dried) (Si/Ti=50)] Calcined	730	0.67	6.45

S_{BET} (BET specific surface area in m^2/g); PV (cumulative pore volume in cm^3/g); APD (average pore diameter in nm)

According to the IUPAC classification of adsorption hysteresis, SBA-15-S and Ti-SBA-15-S showed a type IV isotherm, but hysteresis of the H_2 type, with a sharp inflection at a

relative pressure in the 0.6–0.9 range, which is indicative of a high quality mesoporous material with uniform mesopores, as shown in Fig. 7.1a, c. However, unlike the Ti-SBA-15-S-dried series, there was a significant decrease in the volume adsorbed of the Ti-SBA-15-S-calcined series and the hysteresis loops were slightly changed, which are in accordance with the physical properties shown in Table: 7.1. However, a similar decreasing trend in case of PSD has been observed as shown in Fig.7.1b, d. Unlike SBA-15-S, the adsorption branch of each isotherm in KIT-6 and Ti-KIT-6, showed a sharp inflection at a relative pressure in the 0.5–0.80 range, which means a typical capillary condensation within uniform pores with a typical H1 type hysteresis loop, and which points out large channel like pores with a narrow pore size distribution as can be seen in Fig. 7.1e, g. Although there was decrease in the volume adsorbed by increased Ti content, however, all the Ti-KIT-6 materials preserved the hysteresis shapes and positions. Similarly, regardless of the decrease in volume due to Ti addition, the Ti-KIT-6 materials also preserved the PSD due to the 3-D pore structure, which can be seen in Fig. 7.1f, h and are in agreement with the results shown in Table 7.1.

Fig. 7.2 shows the morphologies of the mesoporous silica and the Ti-mesoporous silica (calcined or dried, Si/Ti=100). As shown in Fig. 7.2a, b, SBA-15-S has a spherical morphology in agreement with Wang et al [241]. It has well-dispersed microspheres with a limited dispersion of the particle size in the 2–3 μm range, together with a high yield of almost 100 %. However, Ti incorporation in SBA-15-calcined (Si/Ti=100) not only changed the morphology of SBA-15-S, in which the particles were much grown to larger spherical rigid particles, but also Ti was not dispersed uniformly and many agglomerates could be seen within the spherical rigid silica particles Fig. 7.2c, d. Unlike to the Ti-SBA-15-calcined (Si/Ti=100), the Ti-SBA-15-dried (Si/Ti=100) has shown more uniform morphology with comparatively better-dispersed Ti Fig. 7.2e, f which is in agreement with the results discussed in Table 7.1 and Fig. 7.1. The morphology of KIT-6 is shown in Fig. 7.2g, h and is consistent with that shown in the literature [253]. As shown in Fig. 7.2i–l, after Ti incorporation, no significant difference was observed in the morphology of KIT-6, which indicates that Ti was very well dispersed within the 3-D structure.

In optimization point of view, Ti-KIT-6-calcined series have been found better than all other materials, both in characteristics, as well as in activity (which will be discussed hereafter).

Chapter 7

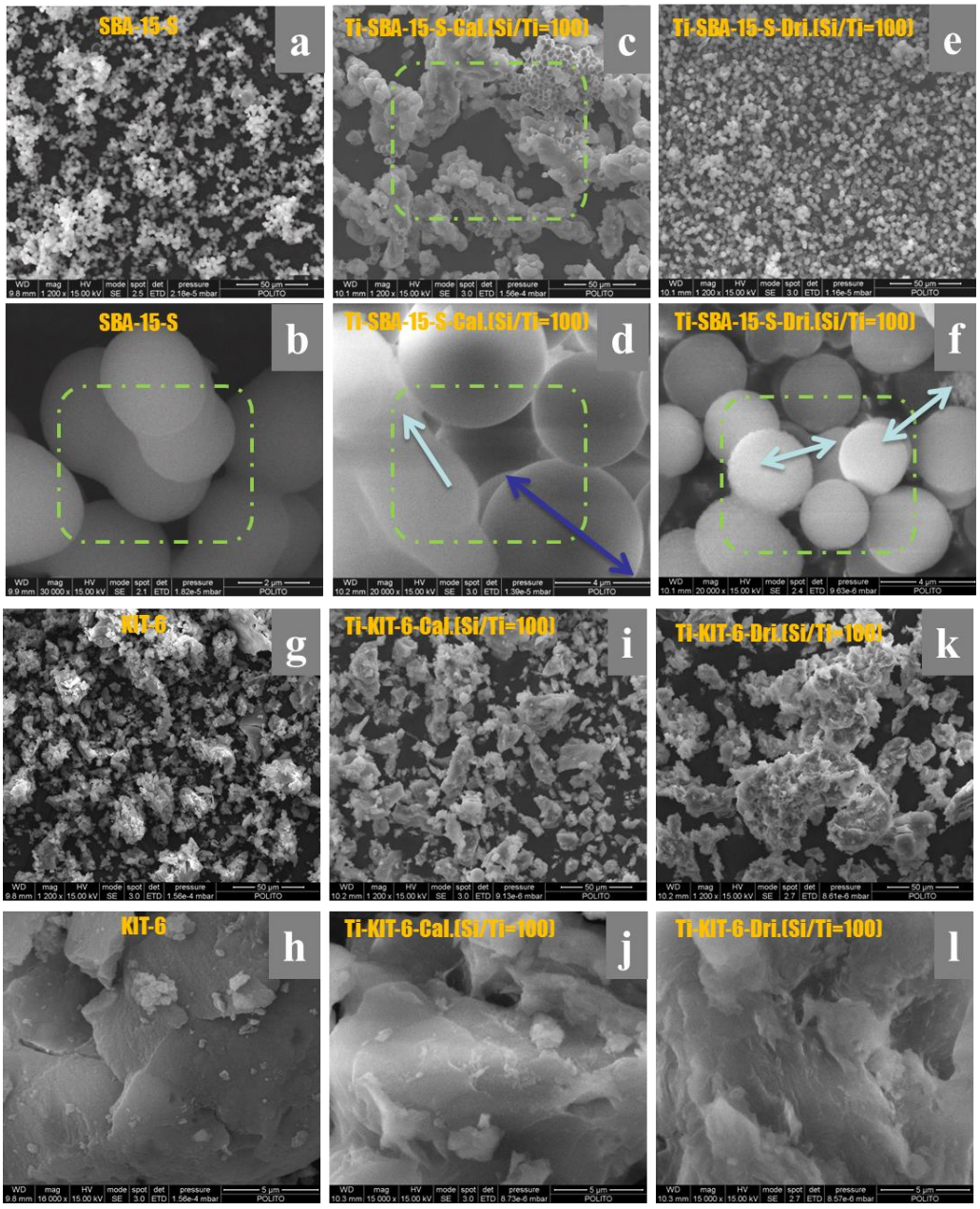

Figure: 7.2 *FE-SEM images of bare and Ti incorporated mes porous materials:* ***(a, b)*** *SBA-15S,* ***(c, d)*** *Ti-SBA-15S calcined Si/Ti=100,* ***(e, f)*** *Ti-SBA-15S dried Si/Ti=100* ***(g, h)*** *KIT-6,* ***(I, j)****, Ti-KIT-6 calcined Si/Ti=100,* ***(k, l)*** *Ti-KIT-6 dried Si/Ti=100.*

Therefore, further characterizations have been done only for the Ti-KIT-6-calcined series to explore the most optimized Si/Ti ratio out of 200, 100 and 50 ratios for further optimization. The UV-Vis. spectra of the Ti-KIT-6-calcined (Si/Ti=200, 100, 50) are shown in Fig. 7.3.

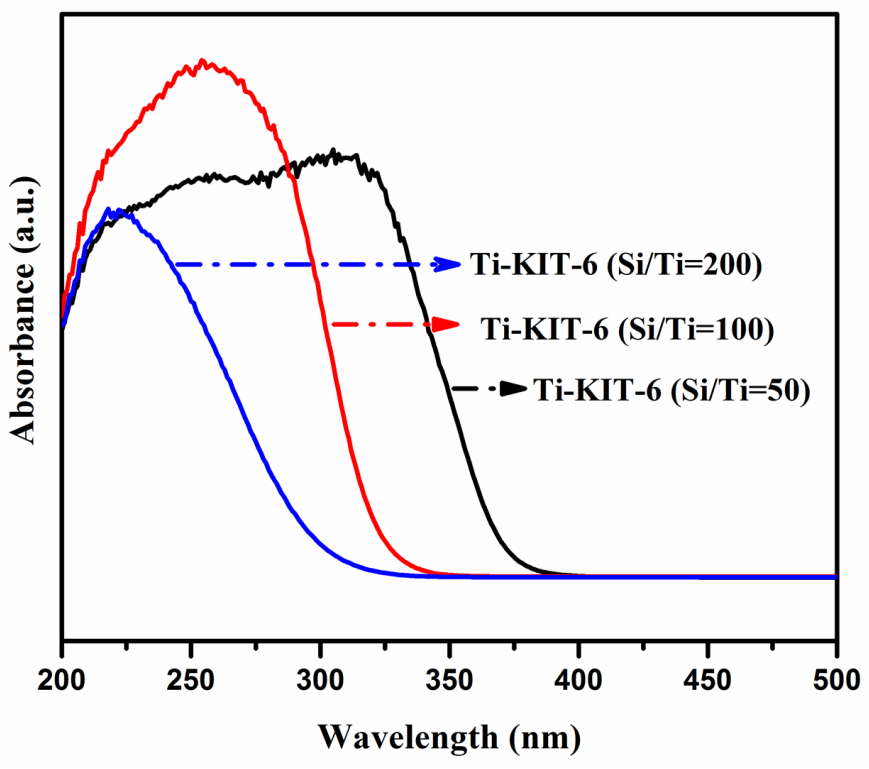

Figure: 7.3 *UV-Vis spectra of Ti-KIT-6 photocatalysts with different Si/Ti (200, 100, 50) ratios.*

It has been observed that, with the increased Ti content, the absorption spectra are shifted to higher wavelengths for an absorption edge wavelength change from 320 to 372 nm data shown in Table 7.2 that is moving towards the trend of pure TiO_2. Therefore, it can be observed that this increased Ti might also have more chance of making the agglomerates of TiO_2 with the moisture present during the synthesis. The band gap energies of the Ti-KIT-6 materials, corresponding to a band gap of 3.33-3.87 eV, which is the characteristic band gap of Ti-silica, are shown in Table 7.2. The variation in the band gap is due to the TiO_2 agglomerates that have formed, as already mentioned, and which will be dealt with in more detail hereafter. Mesoporous structure in the KIT-6 material has been confirmed by TEM analysis, which also shows isolated Ti dispersion within the KIT-6 structure. The successful formation of the KIT-6 structure with an ordered array of mesopores can be seen in Fig. 7.4a, which shows the centers of two adjacent pores about 10 nm apart; a pore diameter of 6 nm can also be seen. APD finding is also in accordance with the results obtained from N_2-sorption Table 7.1 as well as with that reported in literature [242].

Chapter 7

Table: 7.2 *Comparison of band gap energies, surface hydroxyl groups and Ti ($2p_{3/2}$) and O (1s) atomic concentrations of different Ti-KIT-6 materials.*

Sample name	Absorption edge wave length by UV-Vis., λ (nm)	Band gap energy by UV-vis., E (eV)	Amount of OH group by FT-IR (nm^{-1})	Ti ($2p_{3/2}$) atomic concentrations (%) by XPS		O (1s) atomic concentrations (%) by XPS	
				459.9 (eV)	458.0 (eV)	533.1 (eV)	530.8 (eV)
				A	B	C	D
Ti-KIT-6 (Si/Ti=200)	320	3.87	1.5	n.d	n.d	n.d	n.d
Ti-KIT-6 (Si/Ti=100)	330	3.75	2.0	84.5	51.5	99.7	0.3
Ti-KIT-6 (Si/Ti=50)	372	3.33	1.2	77.6	22.4	98.6	1.4

n d (not determined)

The TEM images of Ti-KIT-6-calcined (Si/Ti ratios of 200,100 and 50) have been shown in Fig. 7.4b, c, d. Ti-KIT-6 (200) shows a uniform Ti dispersion with hardly any Ti agglomeration, which indicates the preserved structure of the KIT-6, as is confirmed by the mesoporous channels of KIT-6, which are shown in Fig. 7.4b. Ti-KIT-6 (100) has a similar tendency to Ti-KIT-6 (200) in which a good dispersion of isolated Ti and mesoporous structure preservation is obvious Fig. 7.4c

Unlike to Ti-KIT-6 (200) and Ti-KIT-6 (100), it can also be observed that the mesopore structure of KIT-6 is partially collapsed/damaged in Ti-KIT-6 (50), (top right corner in Fig. 7.4d. due to the higher Ti content than for the other two ratios. However, higher Ti contents cause the structure or morphology of the material collapse which has adverse effect on the photocatalytic activity of CO_2 reduction.

Chapter 7

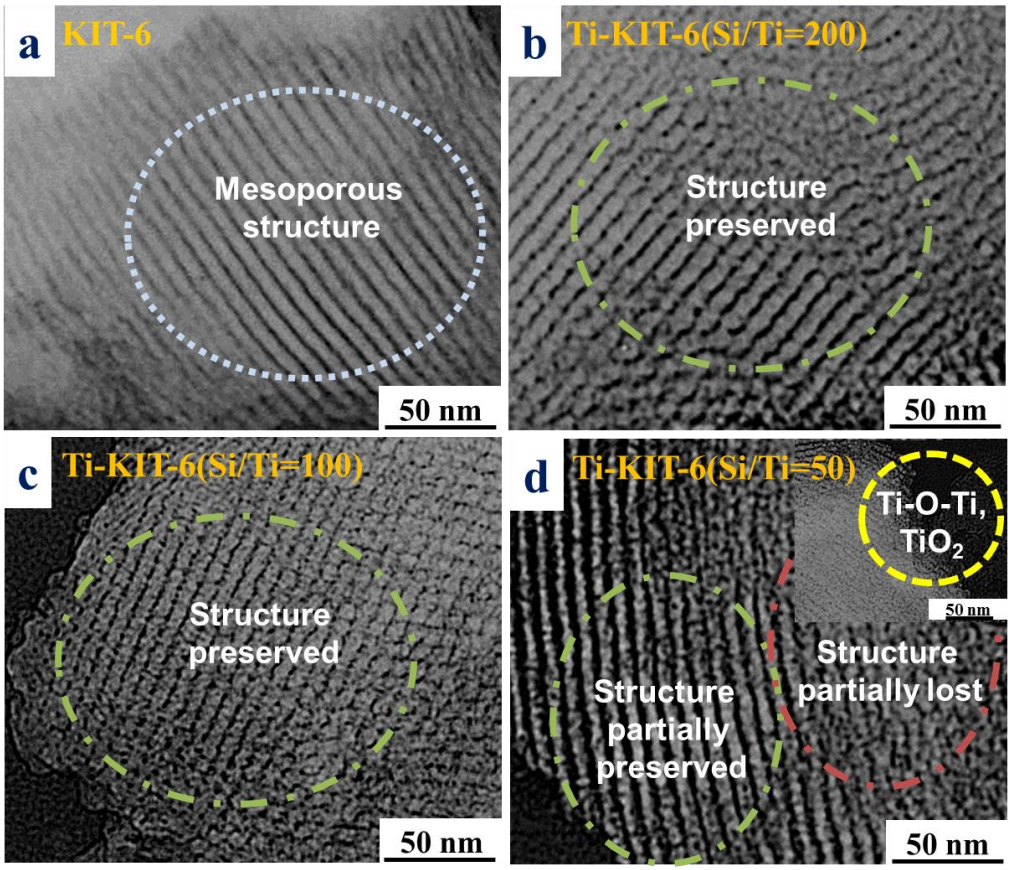

Figure: 7.4 *TEM images of:* ***(a)*** *KIT-6-calcined,* ***(b)*** *Ti-KIT-6-calcined (Si/Ti=200),* ***(c)*** *Ti-KIT-6-calcined (Si/Ti=100) and* ***(d)*** *Ti-KIT-6-calcined (Si/Ti=50).*

Despite the isolated Ti species being dispersed on the KIT-6 support material, some Ti-O-Ti/TiO_2 agglomerates which were not seen in Ti-KIT-6 (200, 100), but only in Ti-KIT-6 (50) have also been observed and are shown in the small insert in Fig. 7.4d. This is due to the increased Ti, which is not uniformly dispersed, and either produces Ti-O-Ti agglomerates or forms TiO_2 due to the moisture present during the synthesis.

In order to confirm the TiO_2 formation, which was observed in TEM analysis, XPS analysis of the Ti-KIT-6 materials (Si/Ti ratios of 100, 50) was performed as shown in Fig. 7.5. The overall XPS spectra of the Ti-KIT-6 (Si/Ti=100), Ti-KIT-6 (Si/Ti=50) is shown in Fig. 7.5a and b, respectively. The deconvoluted XPS spectra shown in Fig. 7.5c,d and values in Table 7.2 indicates that, for an increased Ti content of Si/Ti = 50, the Ti ($2p_{3/2}$) line was shifted to 458.0 eV, which is close to the binding energy of Ti ($2p_{3/2}$) of pure TiO_2. It can be seen in Fig. 7.5e, f

and Table 7.2, the deconvoluted XPS spectra of Ti-KIT-6 (Si/Ti ratios of 100 and 50), depicted two peaks at 533 eV, for Si-O-Si and 530.8 eV corresponding to Ti-O-Ti.

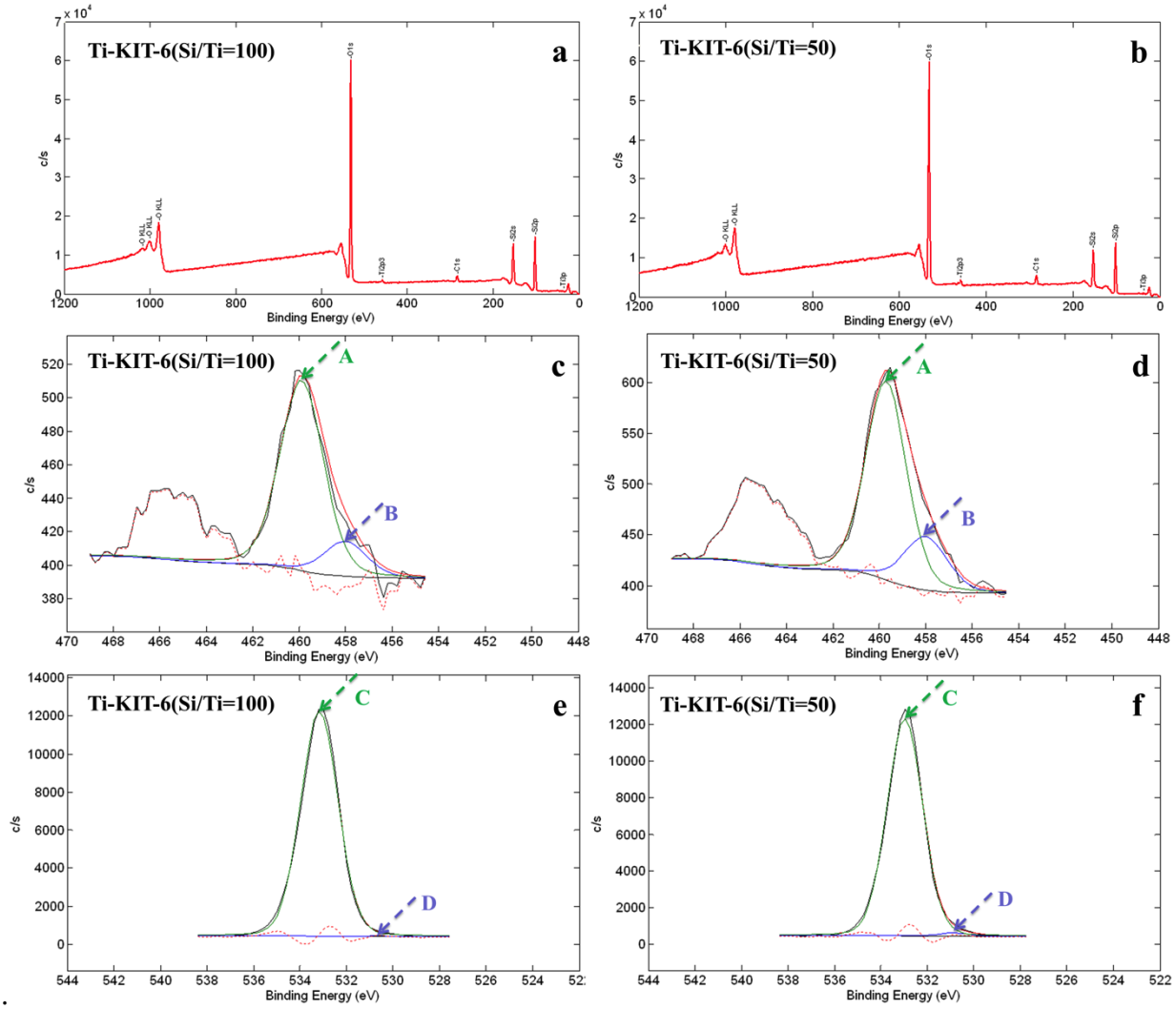

Figure: 7.5 (a, b) *Overall XPS spectra of the Ti-KIT-6 (Si/Ti=100, 50* ***(c, d)*** *Ti ($2p_{3/2}$) deconvolution* ***(e, f)*** *O (1s) deconvolution spectra.*

These indicate that there is more free TiO_2 phase formation in Ti-KIT-6 (Si/Ti=50) than in Ti-KIT-6 (Si/Ti=100) material. This is also in accordance with the findings of the UV-Vis. and TEM analysis techniques. Fig. 7.6 shows the FT-IR spectra of the KIT-6 and Ti-KIT-6 (Si/Ti = 200, 100 and 50) materials. The IR spectra of the KIT-6 mesoporous silica showed bands at 498 and 1268 cm^{-1}, which correspond to Si-O-Si [254]. The band at 1631 cm^{-1} is due to the

OH from the water occluded in the KIT-6 pores, whereas at 961 cm^{-1}, it is from Si-OH. The region from 3100 to 3600 cm^{-1}, which centered in these spectra at 3342 cm^{-1}, should be attributed to hydroxyl groups from silanols as well as OH of adsorbed water, whereas stretching at 3742 cm^{-1} is due to the free OH groups [254, 255].

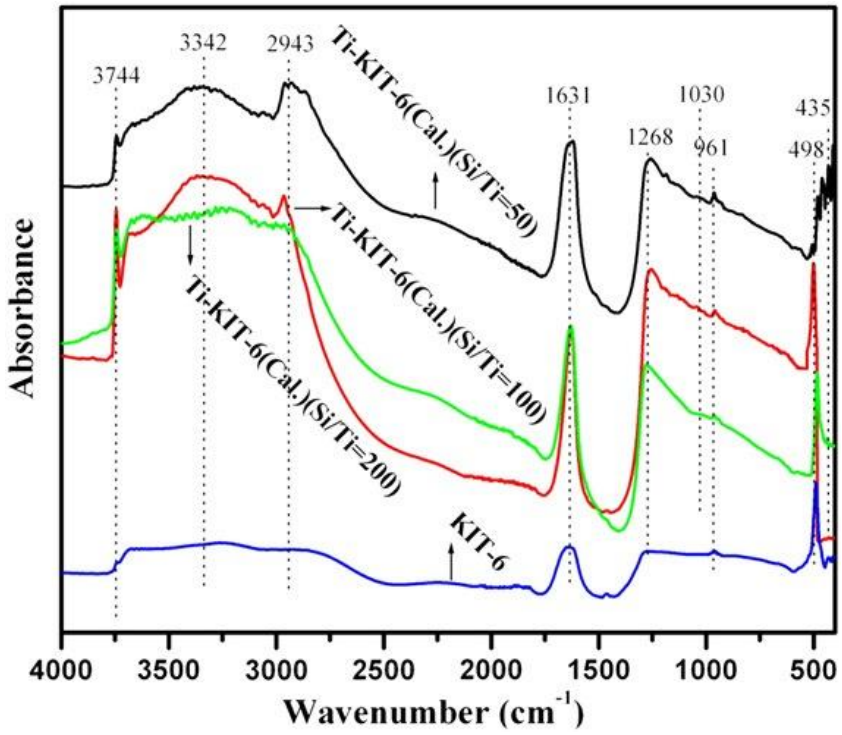

Figure: 7.6 *FT-IR analysis spectra of KIT-6 and Ti-KIT-6 (Si/Ti = 200, 100, 50 ratios) materials.*

The Ti-KIT-6 sample showed an additional stretching at 961 cm^{-1}, which corresponds to Ti-O-Si [254] whereas, Ti was attached through the OH groups of the KIT-6 silica. An increase in the intensity of the peak has been found for an increase in the Ti content for Si/Ti ratios of 200 to 50, which is generally considered as proof of Ti incorporation in the framework of KIT-6. However, an additional stretching of Ti-O-Ti has been observed at 435 cm^{-1}, due to the increased Ti content in Si/Ti = 50. The OH groups that correspond to the adsorption power of the material

were also increased in the Ti-KIT-6 samples from Si/Ti ratios of 200 to 100 and then slightly decreased in the 50 ratio This increase in OH groups might be associated with the good dispersion of isolated Ti species on KIT-6 with Si/Ti = 100 than other ratios, which might increase the adsorption capacity of water or hydro philicity of the material.

7.1.2 Blanks tests or pre illumination of photocatalysts

Primary, photocatalytic reduction set-up is shown in Chapter 6 and Fig. 6.1**.** Blank tests for CO_2 photocatalytic reduction were conducted with catalyst in the absence of UV light or as well as without catalyst under UV light illumination with water vapor and all the other conditions of the reaction remained constant which indicates that no photocatalytic products obtained which, strongly emphasized that the photocatalytic products are only due to CO_2 reduction and H_2O oxidation process in the presence of light. Most significantly, hydrocarbons and other fuel products such as (CH_4, CH_3OH, H_2 and CO) were analyzed the main photocatalytic product in all the reaction experiments from CO_2 reduction with H_2O vapor. However, blank tests have been conducted for all the photocatalyst prepared in this study before to start the photocatalytic reaction. Consequently, in all cases it was proved that no products obtained without incomplete reaction condition.

7.1.3 Photocatalytic activity of CO_2 reduction with H_2O on highly dispersed isolated mesoporous materials to methane formation

Photocatalytic reduction of CO_2 with water vapor on highly dispersed isolated Ti masoporous material (Ti-KIT-6) both in dried and calcined forms showed the better activity towards the methane formation shows the production rate of the CH_4 formation that originated because of the unique properties of the charge transfer excited state, i.e., $(Ti^{3+}–O^{-})^*$ of the tetrahedral coordinated titanium oxide species within the silica frameworks. It can be seen that Ti-KIT-6 (calcined or dried) (Si/Ti = 100) shows higher activity than the Si/Ti ratios of 200 or 50. This is due to the combined contribution of the high dispersion state of the Ti-oxide species, which is caused by the large pore size with a 3D channel structure and the lower formation of Ti-

O-Ti or TiO_2 agglomerates, as was confirmed by TEM and XPS analysis. In addition, Fig. 7.7© shows a high CH_4 production for Ti-KIT-6 (Si/Ti = 100) with more concentrations of OH groups than the other ratios obtained from the FT-IR of the materials, which actually affect the adsorption properties of the water on the catalyst surface [10]. The ratio between H_2O and CO_2 is another parameter that determines the selectivity of CH_4 or CH_3OH. When H_2O/CO_2 is high, the selectivity for CH_4 formation becomes higher [5]. On the basis of the Ti shown in Fig. 7.7(d**)** However**,** it can be stated that the above-mentioned optimized photocatalysts showed better activity than the best commercial TiO_2 (Degussa P25).

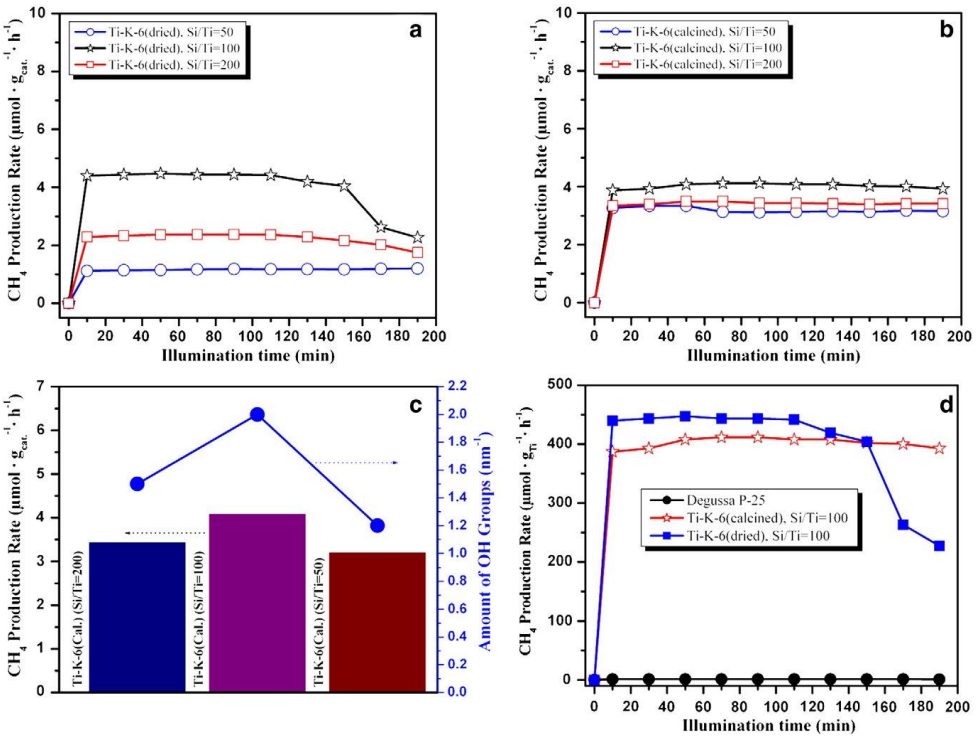

Figure: 7.7*. Methane formation comparison by photocatalytic reduction of carbon dioxide and water* ***(a)*** *Ti-KIT-6 (dried)(Si/Ti = 200, 100, 50 ratios),* ***(b)*** *Ti-KIT-6 (calcined)(Si/Ti = 200, 100, 50 ratios),* ***(c)*** *effect of OH groups on activity and* ***(d)*** *activity comparison on Ti basis with commercial Degussa P25.*

Moreover, the results are comparable with other results reported in literature for TiO_2 as a

photocatalyst [16], Ti-zeolites or Ti-MCM-41 [10] for this application. The optimized Ti-KIT-6 (Si/Ti = 100) showed relatively better CH_4 production than the conventional materials, which indicates its importance in the future research and applications.

7.1.4 Optimization of synthesized mesoporous materials

Mesoporous silica materials SBA-15S and KIT-6 were synthesized successfully by hydrothermal method. Moreover, these mesostructures were used as support material for the synthesis of isolated Ti-SBA-15S and Ti-KIT-6 both in dried and calcined meso structured materials with various Si/Ti ratios (200, 100, 50). Primary characterization and photocatalytic activity of CO_2 reduction showed that Ti-KIT-6 with 100 ratio calcined was superior in activity toward methane production than that of other Ti based materials having Si/Ti other than 200, 50 as can be seen in Fig. 7.7b.

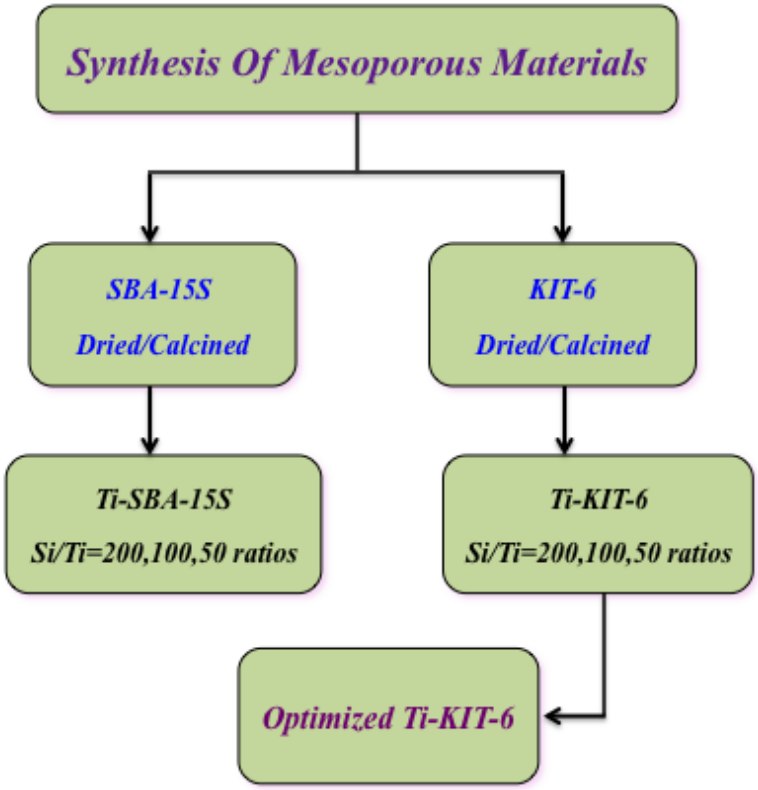

Scheme: 7.1 *Optimization of Ti-mesoporous silica photocatalysts.*

However, further characterization was made only for Ti-KIT-6 calcined Si/Ti = 100 ratio to further explore the chemical properties of the material. Moreover, optimization of the reaction conditions is very helpful to achieve more desired fuel in economical way. Subsequently, Ti-KIT-6 with 100 ratio calcined was found to be the superior in activity not only in methane production but towards the other fuel products such as CH_3OH, H_2 and CO as shown in the Fig. 7.8e.

7.1.5 Photocatalytic activity of CO_2 reduction on highly dispersed isolated Ti mesoporous materials towards fuel formation

The reaction results of the synthesized photocatalysts are shown in Fig. 7.8a, b, c, d, e, f. Blank tests conducted without photocatalysts as well as the reactions in the dark with catalysts have shown no product formation, which indicates that the products obtained during the reaction were merely photocatalyst based. Fig. 7.8a, b, c shows a comparison of the production rate obtained after 3 h of reaction from the CO_2 photocatalytic reduction with H_2O vapors in the presence of Ti-KIT-6 (dried, Si/Ti = 200, 100, and 50 ratios) photocatalysts. As can be seen, CH_4 was the main product, whereas H_2, CO, and CH_3OH (vapors) were also obtained during the reaction when using either Ti-KIT-6 (dried, Si/Ti = 200) or Ti-KIT-6 (dried, Si/Ti = 100) materials. However, H_2 increased and CH_4 decreased when Ti-KIT-6 (dried, Si/Ti = 50) was used. As already mentioned in the characterization part pertaining to the UV-Vis, TEM, and XPS analyses, this phenomenon might be due to the TiO_2 cluster formation caused by the increased Ti content in the Si/Ti ratio of 50, which favors a greater H_2 formation [256]. A similar trend of activity was also observed when Ti- KIT-6 (calcined, Si/Ti = 200, 100, and 50 ratios) was used. However, overall, the Ti-KIT-6 (calcined, Si/Ti = 200, 100, and 50 ratios) materials show higher activity than the Ti-KIT-6 (dried, Si/Ti = 200, 100, and 50 ratios) materials. This might be due to the fact that some of the Ti species in Ti-KIT-6 (dried, Si/Ti = 200, 100, and 50 ratios) materials, which were not accessible on the surface for the reaction, might have been trapped in the bulk dried KIT-6 powder during the synthesis. However, this might not be the problem in the case of Ti-KIT-6 (calcined, Si/Ti = 200, 100, and 50 ratios), where the 3-D pore structure was fully

developed in the calcined KIT-6. Therefore, the greater number of accessible active sites in Ti-KIT-6 (calcined, Si/Ti = 200, 100, and 50 ratios) than that in Ti-KIT-6 (dried, Si/Ti = 200, 100, and 50 ratios) may have caused higher activity. Moreover, it is clear that Ti-KIT-6 (calcined or dried, Si/Ti = 100) shows a higher activity than the Si/Ti ratios of 200 and 50, because of the combined contribution of the high dispersion state of the Ti oxide species, which is due to the large pore size with a 3-D channel structure, and the lower formation of Ti-O-Ti or TiO_2 agglomerates, as confirmed by UV-vis, TEM, and XPS analyses. Moreover, the high production of CH_4 for Ti-KIT-6 (Si/Ti = 100) with greater concentrations of the OH groups (2 nm^{-1}) than the other ratios (Si/Ti = 200 and 50 = 1.5 and 1.2, respectively) obtained from the FT-IR of the materials actually affects the adsorption properties of the water on the catalyst surface [10] Competitive adsorption between the H_2O vapors and CO_2 is another parameter that can determine the selectivity of CH_4 or CH_3OH. CH_4 formation selectivity becomes higher as H_2O vapor adsorption increases due to the greater concentration of OH groups or hydro-philicity of the material [5].

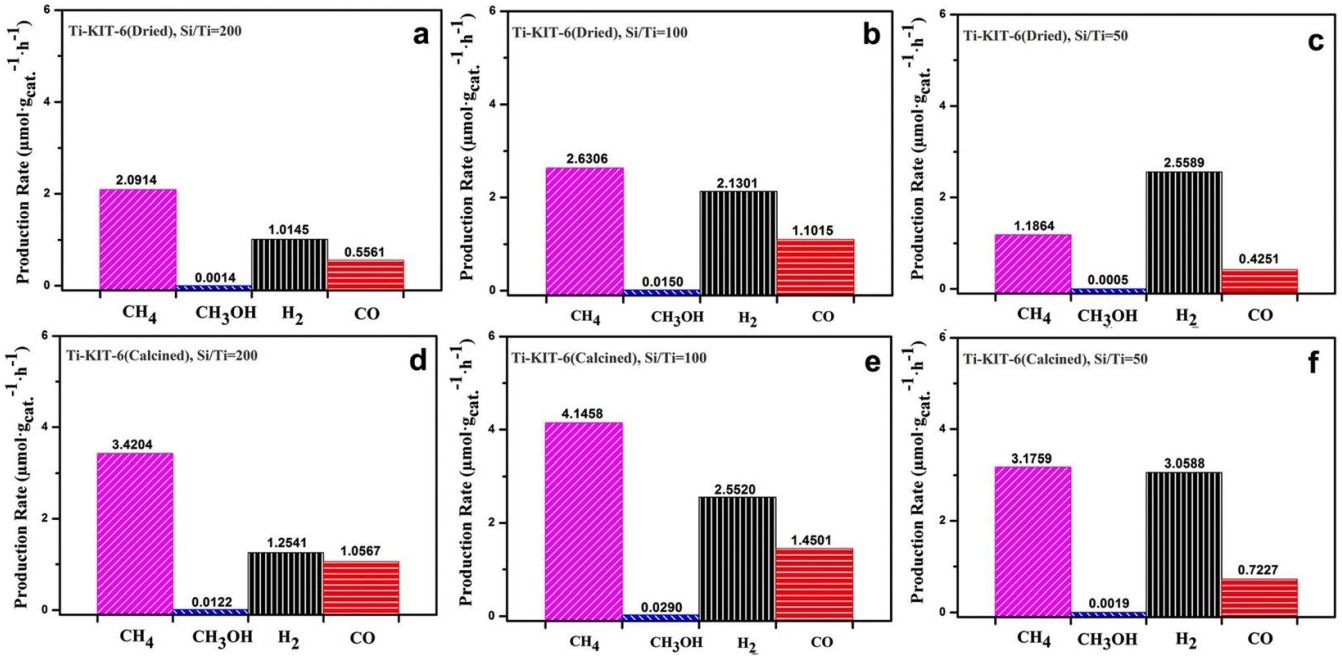

Figure: 7.8 *Comparison of fuel formation after a 3-h photocatalytic reduction of CO_2 and H_2O vapors* ***(a-c)*** *Ti-KIT-6, dried, Si/Ti = 200, 100, and 50 ratios and* ***(d-f)*** *Ti-KIT-6, calcined, Si/Ti = 200, 100, and 50 ratios.*

The main desired product is CH_4 as it has a greater energy or heat content [257] than H_2 or the produced syngas ($CO + H_2$), whereas CH_3OH (vapors) is a minor product. Moreover, these photocatalytic results are comparable with the other results reported in the literature concerning the use of TiO_2 [16]. Ti-zeolites or Ti-MCM-41 [10], were used as a photocatalyst for this application. The optimized Ti-KIT-6 (Si/Ti = 100) showed a relatively better CH_4 production than the conventional photocatalytic materials, a result that is explained more clearly by examining the reaction mechanism.

7.1.6 Photocatalytic proposed reaction mechanism of CO_2 reduction with H_2O to fuel products formation

The photocatalytic reduction mechanism of CO_2 with H_2O vapor is a complex phenomenon, where two aspects regarding the rate-limiting step should be taken into consideration. CO_2 is a thermodynamically stable and chemically inert compound and it is difficult to oxidize or reduce it to various intermediate chemicals under normal operating conditions. As shown in [Eq. (7.1)], a single electron reduction of CO_2 to an anion radical CO_2^- has a very strong negative electrochemical potential of -1.90V [24] which is thermodynamically unfeasible for any semiconducting material to provide a single photo generated electron to a CO_2 molecule.

$$CO_2 + e^- \rightarrow .CO_2^- \qquad (E^0_{redox} = -1.90\ V) \qquad (7.1)$$

$$2H^+ + 2e^- \rightarrow H_2 \qquad (E^0_{redox} = -0.41\ V) \qquad (7.2)$$

$$CO_2 + 2H^+ + 2e^- \rightarrow CO + H_2O \qquad (E^0_{redox} = -0.48\ V) \qquad (7.3)$$

$$CO_2 + 8H^+ + 8e^- \rightarrow CH_4 + 2H_2O \qquad (E^0_{redox} = -0.24\ V) \qquad (7.4)$$

$$CO_2 + 6H^+ + 6e^- \rightarrow CH_3OH + H_2O \qquad (E^0_{redox} = -0.38\ V) \qquad (7.5)$$

Unlike to CO_2, the standard potential of H_2O to generate H_2 is much lower and is viable. Even though it is unfeasible to transfer a single photogenerated electron to a CO_2 molecule, it is possible to conduct the proton-assisted transfer of multiple electrons. Therefore, as it has been

shown in [Eqs. (7.2) and (7.3)], H_2 and CO formation is comparatively favorable as they need a lower number of electrons and protons [158] while CH_4 and CH_3OH require more electrons and protons and are difficult to form as shown in [Eqs. (7.4) and (7.5)]. In this context, the best possible way of activating the inert CO_2 molecule for reduction purposes is to adsorb it on the surface of any semiconductor, which lowers its energy barrier [44].

Therefore, in the current work, the adsorption of CO_2 and H_2O is the main focus. Fig. 7.9 shows the reaction mechanism with the detailed steps and necessary pathways to achieve the required energy bearing products. Hence, before starting the reaction, the CO_2 and H_2O vapors were adsorbed to obtain a good adsorption of these reactants on the photocatalyst surface. However, as can be seen in Fig. 7.9, H_2O, as a polar (1.85D) molecule shows a greater tendency to be adsorbed than CO_2, which has a lower dipole moment (0D); it indicates that both H_2O and CO_2 compete for adsorption. Moreover, the carbene pathway has been found to be well-suited in the present contest, as CO_2 photocatalytic reduction active sites are isolated tetrahedrally coordinated Ti^{+4} centers which are embedded in silica/zeolite matrices [44]

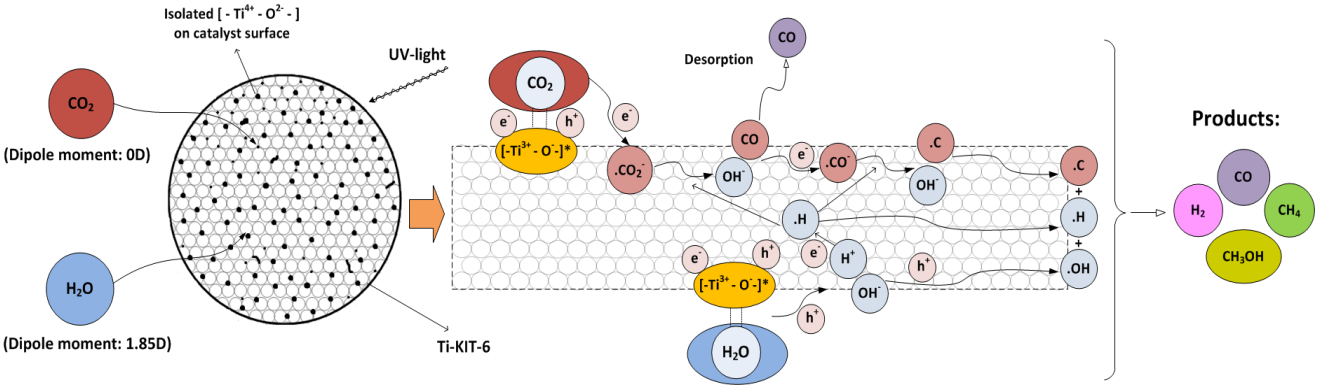

Figure: 7.9 *Proposed reaction mechanism and pathways of CO_2 reduction and H_2O oxidation with Ti isolated titania to fuel formation.*

The quantum confinement effects in these spatially separated 'single-site photocatalysts upon UV light absorption, cause charge-transfer excited states to be formed. Reaction mechanism shown in Fig. 7.9 indicates that, these excited states, i.e., $(Ti^{3+}–O^{-})$*, contain the

photo generated electron and hole which are more localized on neighboring atoms [44, 94] and are very closer than in bulk semiconducting materials, where the charge carriers are free to diffuse. Also, the lifetime of the excited $Ti^{3+}–O^{-}$ is found to be 54 µs [7].

This lifetime is substantially higher than that of bulk TiO_2 powder, which is instead of a nanosecond order. Therefore, these active sites in Ti-KIT-6 materials, i-e, $(Ti^{3+}–O^{-})^*$, are more energetic and longer living than in bulk TiO_2. As shown in Fig. 7.9, CO_2 and H_2O are being adsorbed on the surface of the photocatalyst, with competitive adsorption, due to their different dipole moments. The active sites for the adsorption of the reactants are Ti-OH. As the UV light is turned on, the adsorbed CO_2 and H_2O vapors interact with the photo excited active sites, i.e. $(Ti^{3+}–O^{-})^*$. This induces the formation of intermediates, including CO, which can be an intermediate as well as a released product, which is shown in Fig. 7.9. Ultimately, C, H and OH radicals are formed which can further combine to form other products, such as CH_4, H_2 and CH_3OH. Therefore, the adsorption and the concentration of OH groups play a key role in the reaction mechanism to achieve selective products.

7.1.7 Optimization of the key parameters that influence the reaction activity

The photocatalytic reaction was further improved by using the diluted CO_2 (20 %) in feed to increase the concentration of H_2O vapors in the reaction. The optimization step improved the fuel products; however, optimizing the factors, which affect the photocatalytic activity, further increased the photocatalytic efficiency. These factors including UV light sources and their intensities, H_2O/CO_2 ratios, various catalyst shapes used (powder, pellets, film) along with water vapor play a crucial role for CO_2 reduction therefore the water vapor effect as well as the catalyst activation and regeneration is taken into observation. These factors are briefly explained below.

7.1.7.1 Different UV light sources (200W, 300W)

The main factor that directly affects the initiation of a photocatalytic reaction is light, either it is UV or solar light. In photocatalytic reactions, UV lights are of common sources of illumination and usually provide 100-400 nm range of wavelength. Moreover, usage of light with

a shorter wavelength for irradiation, is definitely more effective but not economical. Therefore, the selection of the optimum light for a specific semiconducting material in a photocatalytic reaction is of vital interest. Two different types of UV lamps with similar UVA and UVB ranges but different in intensities and temperatures and with powers of 200 and 300 W have been exploited in the current work to explore and optimize the effect of light on the catalytic activity. The difference in the production rates and a comparison of the average production rates of the products obtained from optimized Ti-KIT-6-calcined (Si/Ti=100) photocatalyst is shown in Fig. 7.10. The results indicate that the 300 W lamp is more useful in this reaction than the 200 W lamp. The 300 W lamp has more photon power, more UVB intensity and produces a higher temperature, which boosts the CO_2 reduction path. Therefore, more fuel products are produced when the 300 W lamp is used than that of 200W lamp.

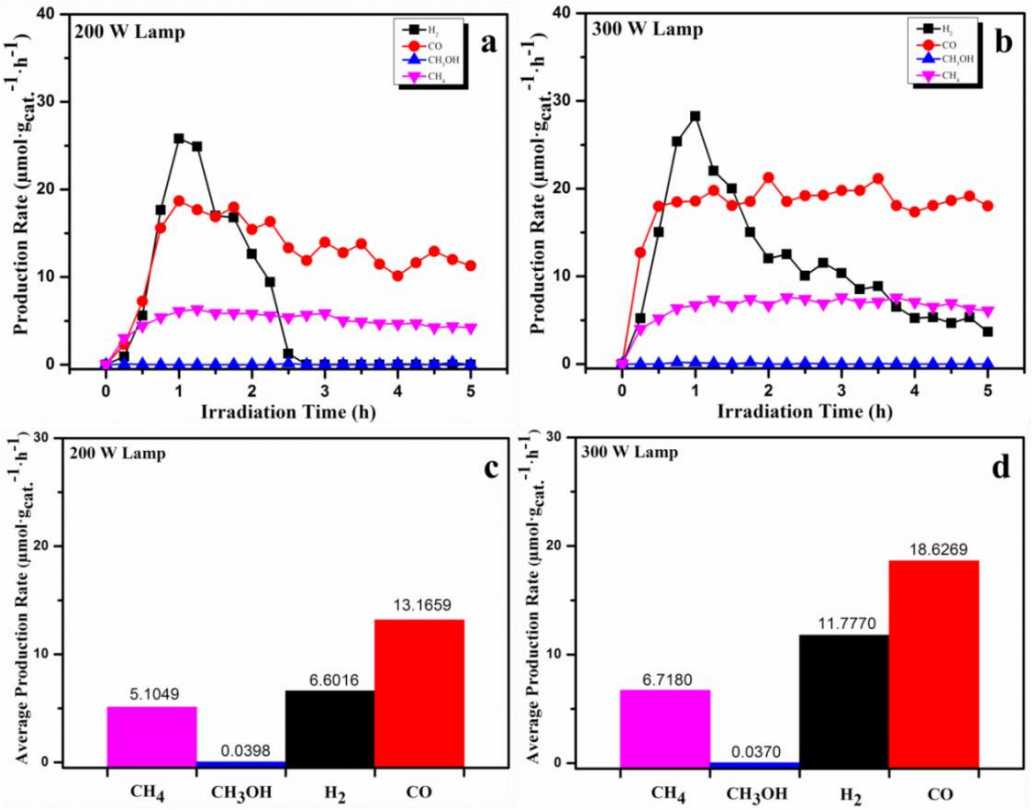

Figure: 7.10 *The UV light source effect on the activity of the optimized Ti-KIT-6-calcined (Si/Ti=100) photocatalyst:* ***(a, c)*** *200 W UV lamp,* ***(b, d)*** *300 W UV lamp, at standard operating conditions with 20 % CO_2, 0.2 g of photocatalyst, 50 mL/min flow rate, H_2O/CO_2=0.1.*

Chapter 7

7.1.7.2 Various UV light intensities effect

Another factor that affects the reaction is the light intensity. As the light intensity increases, the number of generated photons increases, and this leads to more electron-hole pairs being excited with high energy [258] The effect of light intensity on the production rate and average production rate of the products via optimized Ti-KIT-6-calcined (Si/Ti=100) photocatalyst is shown in Fig. 7.11. Three different distances (70, 35 and 10 cm) have been investigated between the lamp and the catalyst in the reactor to acquire different light intensities. As shown in Fig. 7.11a and d, products formation is lower at a distance of 70 cm. Moreover, the reaction kinetics is slower, due to the low light intensity. However, as can be observed in Fig. 7.11b and e, when the distance is reduced to 35 cm, the light intensity increases and the production rate increases remarkably with faster reaction kinetics and long-term product formation stability.

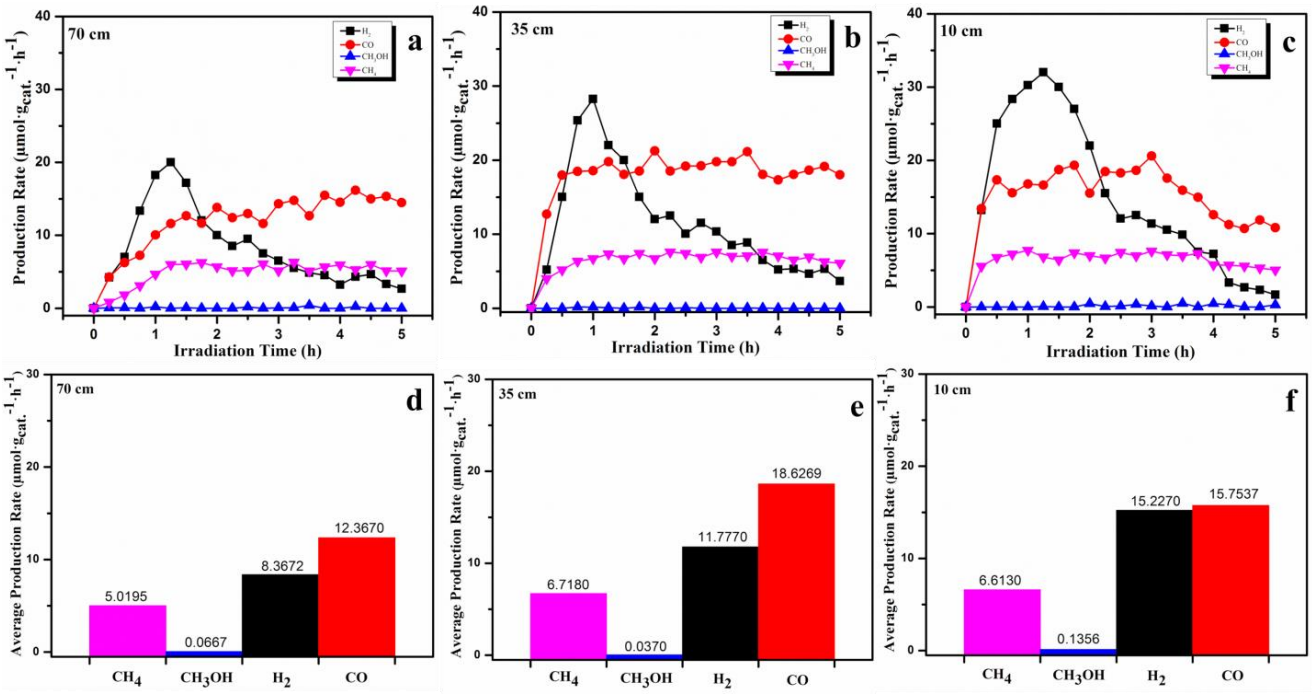

Figure: 7.11 *Effect of different UV light intensities on the activity of the optimized Ti-KIT-6-calcined (Si/Ti=100) photocatalyst:* ***(a, d)*** *70 cm,* ***(b, e)*** *35 cm,* ***(c, f)*** *10 cm, at standard operating conditions with 20 % CO_2, 0.2 g of photocatalyst, 50 mL/min flow rate, H_2O/CO_2=0.1, 300 W UV lamp.*

Fig. 7.11c and f shows that, as the distance is further decreased to 10 cm, the product formation increases and very fast reaction kinetics occurs at the beginning of the reaction process, which is due to the increased light intensity. However, in this case, after 3 h of illumination, the reaction shows a deactivation trend, which could be caused by the rapid saturation of the active sites, due to the fast reaction kinetics and increased temperature from the light.

7.1.7.3 Different H_2O/CO_2 ratios

H_2O is very crucial component in the CO_2 reduction process but an appropriate amount of H_2O with CO_2 could enhance the photoactivity to obtain the photocatalytic products. However, recent research indicates that H_2O vapors have shown a green chemistry approach towards CO_2 reduction to fuels; however, reaction is mainly dependent on the H_2O/CO_2 molar ratio [259].

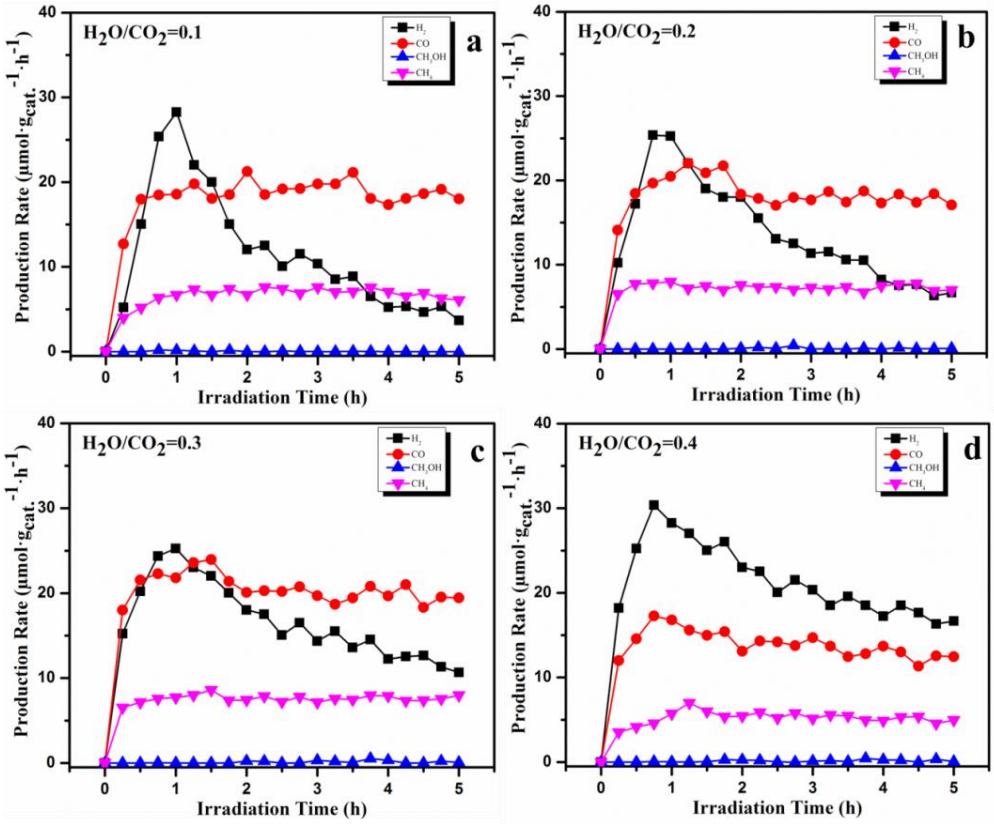

Figure: 7.12 *Effect of different H_2O/CO_2 ratios on the activity of the optimized Ti-KIT-6-calcined (Si/Ti=100) photocatalyst:* ***(a)*** *0.1,* ***(b)*** *0.2,* ***(c)*** *0.3* ***(d)*** *0.4, at standard operating conditions with 20 % CO_2, 0.2 g of photocatalyst, 50 mL/min flow rate, 300 W UV lamp.*

The effect of different H_2O/CO_2 ratios on the activity of the optimized Ti-KIT-6-calcined (Si/Ti=100) photocatalyst is shown in Fig. 7.12. Different ratios were explored to achieve the best ratio to maximize the fuel products. Fig. 7.12a-d indicates that CO_2 conversion increases as the H_2O/CO_2 ratio increases from 0.1 to 0.3, whereas, an excessive amount of H_2O (H_2O/CO_2=0.4) has comparatively suppressed the overall reaction, which is in agreement with the literature [155].

7.1.7.4 Various shapes of photocatalysts (powder, pellets and thin film)

Another key parameter to be optimized is the shape of a catalyst that affects product formation as is the potential use of the catalyst for commercial applications. [260, 90] Photocatalytic activity of CO_2 redution towards fuel formation by powder form catalyst is very lower than that of pellet and thin film. The powder form of the catalyst has been compared with that of pellets (500 micron) and thin film, as shown in Fig. 7.13a-f. The pellets and thin film showed comparatively higher activity than the powder shape of the photocatalyst, which is in accordance with the literature [90, 151]. In pellets and film shapes of the photocatalyst, the better exploitation of the surface that is available for the adsorption of CO_2 and H_2O, and the better penetration of the UV light, which is necessary to initiate a photocatalytic reaction are the main causes of the superior activity. Moreover, better reaction kinetics and better long-term photocatalytic stability have also been observed for the pellets and thin film than for the powder as well as economical point of view, pellets and thin films are more favorable than powder form.

Chapter 7

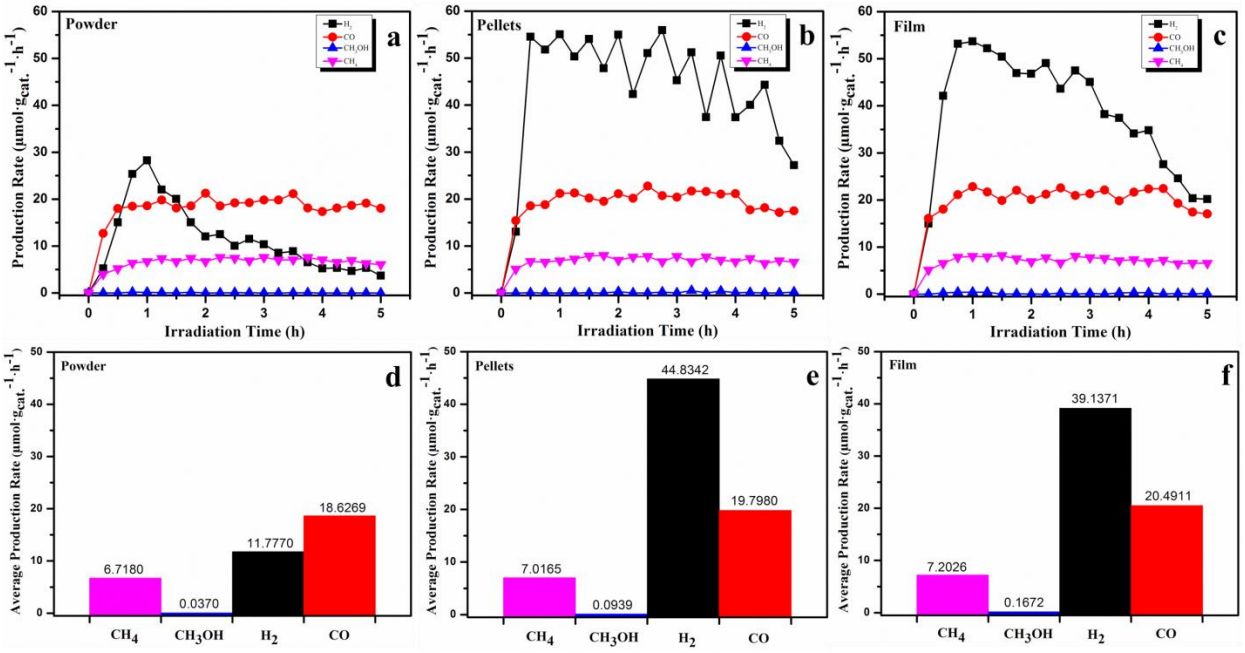

Figure: 7.13 *Effect of different catalyst shapes of the optimized Ti-KIT-6-calcined (Si/Ti=100) photocatalyst on the activity:* ***(a, d)*** *powder,* ***(b, e)*** *pellets,* ***(c, f)*** *film, at standard operating conditions with 20 % CO_2, 0.2 g of photocatalyst, 50 mL/min flow rate, H_2O/CO_2=0.1, 300 W UV lamp.*

7.1.7.5 Confirmation of water vapor effect on the activity and catalyst deactivation/regeneration

Water vapors have a significant role in CO_2 photocatalytic reaction to fuel products. This essential role of water vapor has been confirmed, which is shown in Fig. 7.14. This indicates that the reaction could not pursue in the absence of water vapors as well without UV light. Moreover, as shown in Fig. 7.14, the color of the photocatalyst changed and a slight photocatalytic deactivation was observed. The deactivation mechanism is not still clear, but could be due to the partial saturation of the active sites for adsorption, on the photocatalyst surface, with intermediate product/by-product/mixture formation. Moreover, after formation, some products as CH_3OH and CO were supposed to be not desorbing fully from the catalysts surface and could be re-oxidized back into CO_2 through the O_2 produced during reaction [100]. The deactivated catalyst was naturally dried for 24 h. After the regeneration, this acquired again more than 90 % of the activity, which indicates that most of the adsorbed species were desorbed away. However,

for a more clear understanding about the deactivation, a separate in-depth study is recommended to explore the exact nature and the causes of these deactivating species.

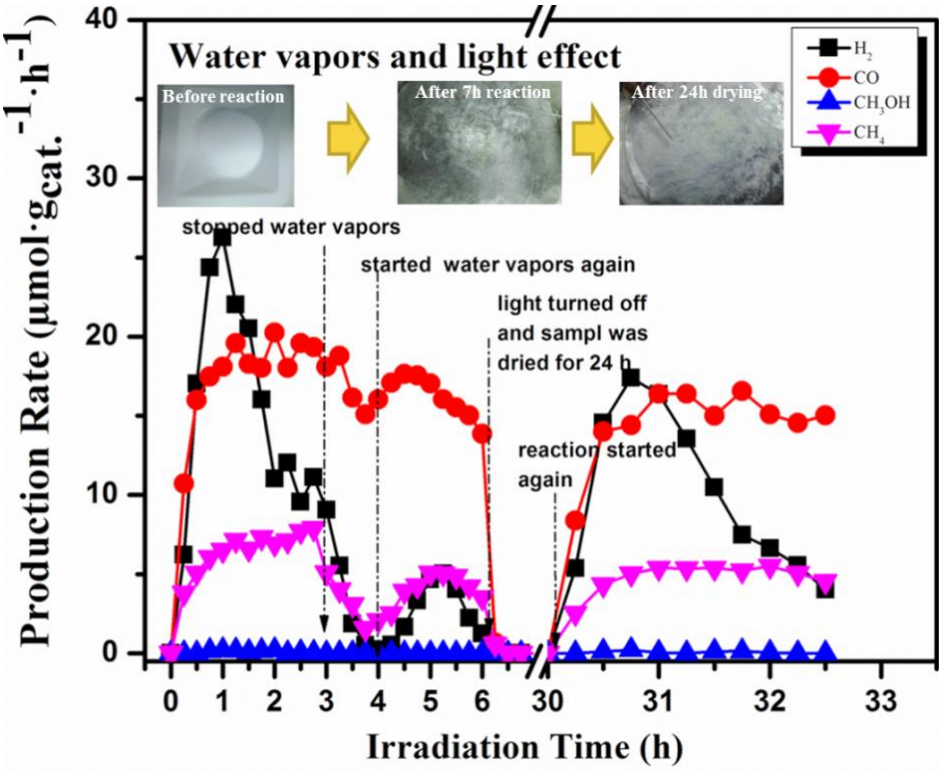

Figure: 7.14 *Confirmatory test of effect of water vapor on the activity of the optimized Ti-KIT-6-calcined (Si/Ti=100) photocatalyst, and catalyst deactivation/ regeneration.*

7.1.7.6 Stability test of optimized photocatalyst

The final stability test of the optimized Ti-KIT-6-calcined (Si/Ti = 100) photocatalyst under the optimized reaction conditions such as with 0.2 g pellets, with 20% CO_2, 50 mL/min flow rate, H_2O/CO_2 = 0.3, and 300W UV lamp with 35 cm distance was performed to observed the stability of the catalyst for extended reaction time of 10 h instead of 5h of the normal reaction time. It has shown in Fig. 7.15, that there is a slow deactivation trend than the reaction under the standard operating conditions. This indicates that the deactivation is not only due to a single factor but various another reaction conditions participate to deactivate the catalyst. Therefore, it

is not yet clear that which factors contribute in the deactivation process. However, a depth-study for understanding the phenomena should be under consideration.

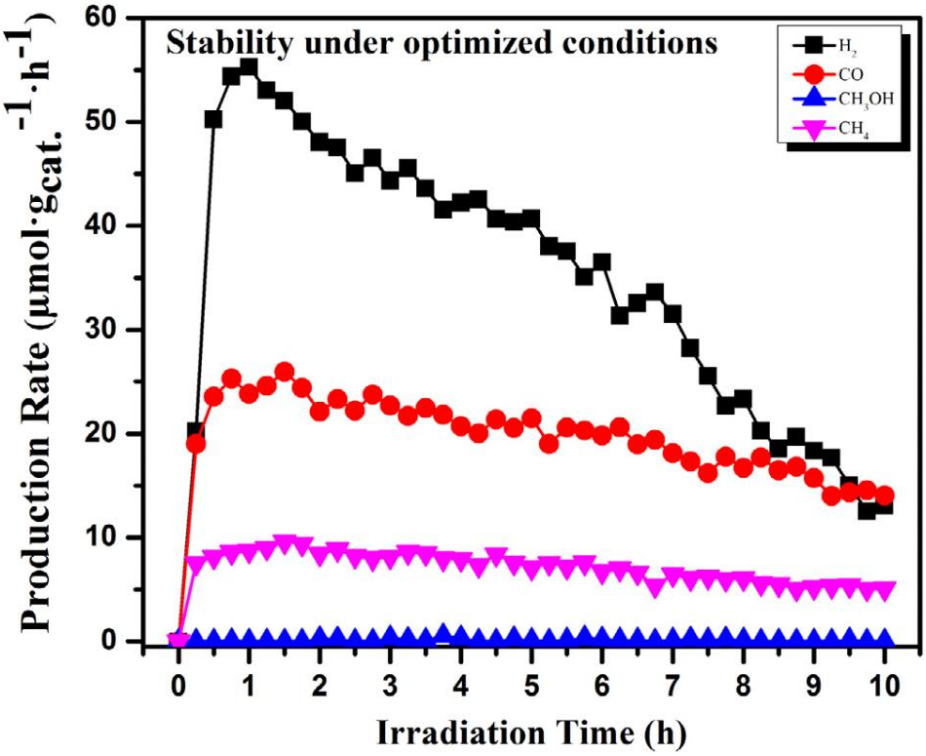

Figure: 7.15 *Stability test of the optimized Ti-KIT-6-calcined (Si/Ti = 100) photocatalyst under the optimized reaction conditions for 10 h of the reaction: 0.2 g pellets, with 20% CO_2, 50 mL/min flow rate, H_2O/CO_2 = 0.3, 300W UV lamp with 35cm distance.*

7.2 Photocatalytic activity tests for Meso. TiO_2 materials towards hydrocarbons and syngas formation

7.2.1 Characterization of Meso. TiO_2 photocatalytic materials

The Brunauer–Emmett–Teller (BET) specific surface area (S_{BET}), pore volume (PV), average pore diameter (APD), isotherms and pore size distributions (PSD) were measured on the powder materials, which had previously been outgassed at 150°C using a Micromeritics Flow Prep 060, USA (sample degas system), by means of N_2 sorption at 77 K on a Micromeritics Tristar II, USA (surface area and porosity) instrument.

Chapter 7

The XRD patterns were recorded in order to determine the different polymorphs, on an X'Pert Phillips diffraction using Cu Kα radiation, under the following conditions: (10–90 °) 2θ, with step size =0.02 as well as the small angle X-ray scattering (SAXS) patterns of the materials were recorded on a Phillips instruments at 2θ=0.2-3.5°. However, the morphology and the meso porous structures of the prepared samples were observed by means of a Leo Supra 55 field emission scanning electron microscopy (FESEM, Zeiss Merlin). The UV-Vis diffuse reflectance spectra were recorded using a Varian model Cary 500 spectrophotometer with a quartz cell suitable for measuring powders. Deep study on TiO_2 shows that the morphology parameters affecting the photo activity include primary and secondary particle size, particle shape and porosity. Moreover, a decrease in primary particle size increases the surface area and has a generally beneficial effect on the photo activity [261]. Therefore, obtaining nano-TiO_2 with high surface area/or porosity was the primary objective of this study to apply further for CO_2 photocatalytic reduction. Table 7.3 shows the physical and textural properties of the three different TiO_2 materials, which were obtained by means of N_2 sorption.

***Table: 7.3**: Physical properties of the various TiO_2 (Degussa P25, TNPs and Meso. TiO_2)*

Samples	**N_2-adsorption/desorption**			**EDX**			**UV-vis.**
TiO_2s	S_{BET}	PV	APD	O%	Si%	Ti%	Band gap energy
Aeroxide P25 TiO_2 (Commercial)	53	n.d.	n.d.	n.d.	n.d.	n.d.	3.25
Titania Nano-particles (TNPs)	150	n.d.	n.d.	n.d.	n.d.	n.d.	3.12
Meso. TiO_2 (by KIT-6 replication)	190	0.32	4.7	66.9	0.6	34.5	3.22

S_{BET} (BET specific surface area in m^2/g); PV (cumulative pore volume in cm^3/g); APD (average pore diameter in nm), E.g. (Band gap energy)

Moreover, as further shown in Table 7.3, EDX analysis of Meso.TiO_2 confirmed that the

silica template (KIT-6) was removed and the resultant material is pure TiO_2. TNPs have a three times higher surface area than the Aeroxide P25 TiO_2, which is due to the smaller nano particles morphology of TNPs than the Aeroxide TiO_2, which will be further discussed in the FE-SEM section. However, mesoporous TiO_2 showed even higher surface area than TNPs and approximately four times higher than Aeroxide P25 due to the meso porosity. The larger surface area is associated with its meso porosity as it contains 4.7 nm average pore diameter. Fig. 7.16 shows the FE-SEM images of the three TiO_2 materials being studied.

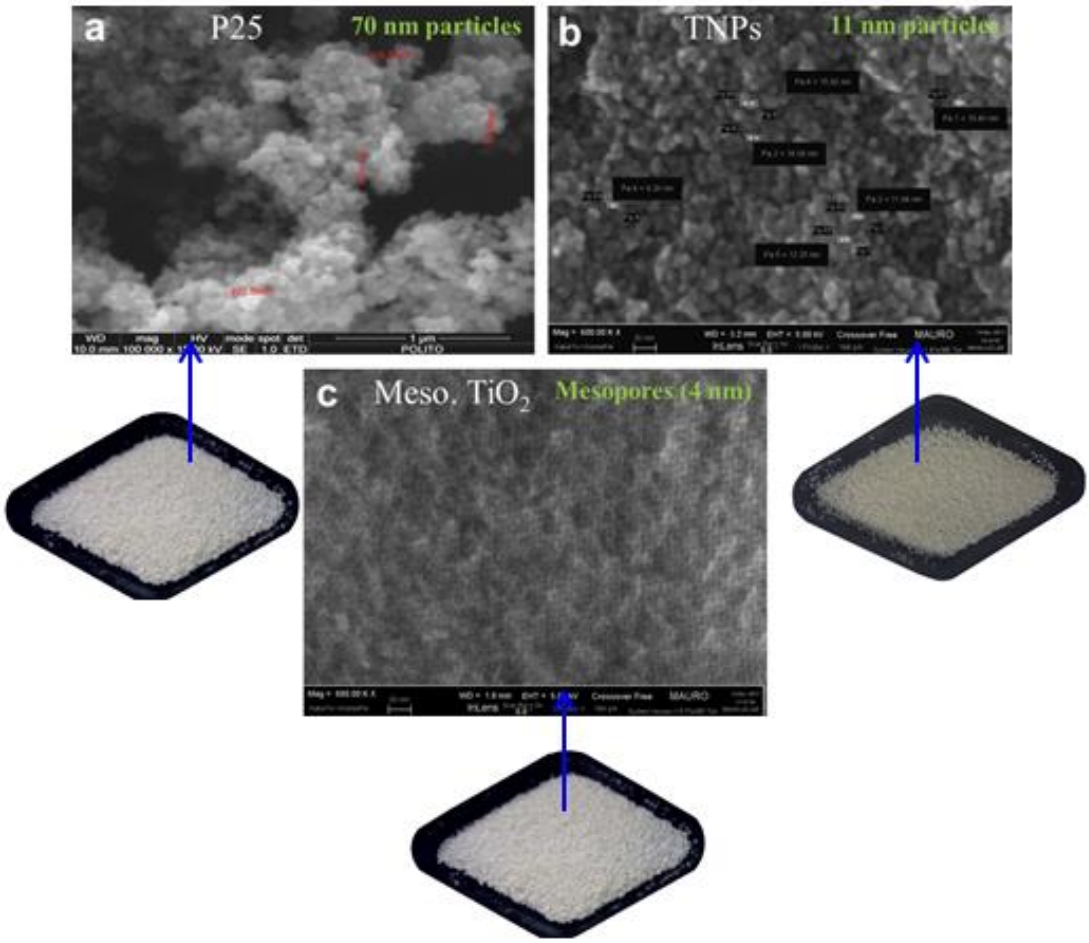

Figure: 7.16 *FE-SEM images showing difference in morphology/structure:* ***(a),*** *Aeroxide P25 TiO_2,* ***(b,)*** *TNPs,* ***(c),*** *Meso. TiO_2.*

In Fig. 7.16a, Aeroxide P25 contains agglomerates of 55-76 nm nanoparticles with an average particle size of 70 nm. However, as shown in Fig. 7.16b TNPs is a combination of 9-15

nm nanoparticles with an average particle size of 11 nm, which is much smaller than Aeroxide P25 TiO_2. Meso.TiO_2 is a porous material same as to KIT-6 silica template and 4 nm meso pores has been observed as shown in Fig. 7.16c.

Fig. 7.17 shows the phase composition by XRD patterns of TNPs, Meso.TiO_2, commercial Aeroxide P25 TiO_2 by Evonik, and 100% anatase TiO_2 by Aldrich as a reference material to compare with other synthesized materials.

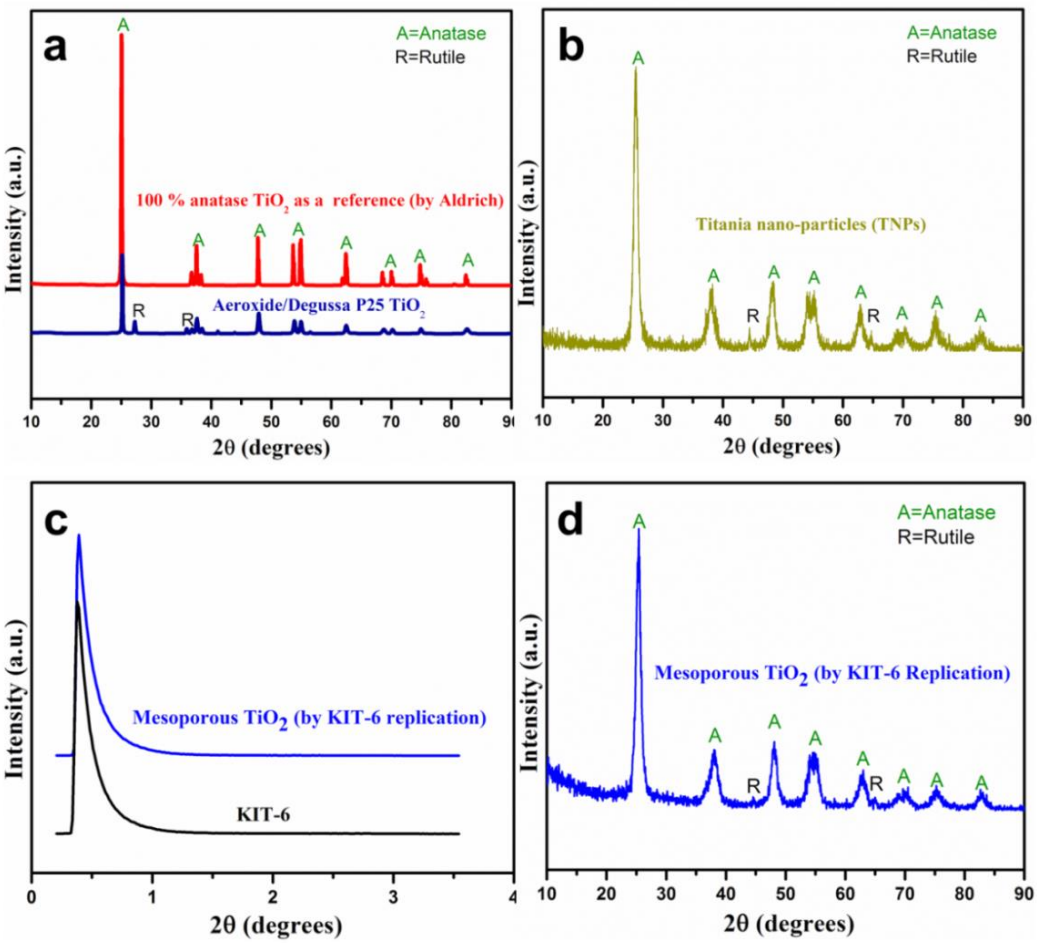

Figure: 7.17 *XRD patterns of different TiO_2 materials:* ***(a)*** *Aeroxide P25 and 100% anatase TiO_2 by Aldrich,* ***(b)*** *TNPs,* ***(c)*** *SAXS analysis of KIT-6 template and replica Meso. TiO_2.* ***(d)*** *Meso. TiO_2.*

It has been observed that P25 TiO_2 is a mixture of anatase and rutile (70:30 %). TNPs show a similar anatase to rutile mixture (80:20 %) as obtained by X'Pert analysis. However,

Meso.TiO_2 also shows anatase-rutile mixture with more anatase and less rutile content (90:10 %). It is generally accepted that anatase shows a higher activity than rutile, for most photocatalytic reaction systems [262]. This enhancement in photoactivity has been ascribed to the fact that the Fermi level of anatase is higher than that of rutile, while rutile is usually less active due to the fact of fast e^- and h^+ recombination [263]. P25 TiO_2 has set the standard for photo reactivity in various applications [264]. This is a non-porous 70:30 % (anatase to rutile) material. Despite the presence of the rutile phase, this material has proved to be even more reactive than single-phase anatase [262]. Therefore, a mixed anatase-rutile phase seems to be preferable to enable some synergistic effects for photocatalytic reactions since the conduction band electron of the anatase partly jumps to the less positive rutile part, thus reducing the recombination rate of the electrons and positive holes in the anatase part. The synthesized TNPs and Meso TiO_2 are actually characterized by the similar anatase-rutile mixture. Moreover, as shown in Fig. 7.17c by SAXS, Meso.TiO_2 is also the exact replica of KIT-6 silica; hence it retains the characteristics of the parent template.

Fig. 7.18 and Table 7.3 show the UV vis. absorption spectra of the three TiO_2 materials and their corresponding band gap energies.

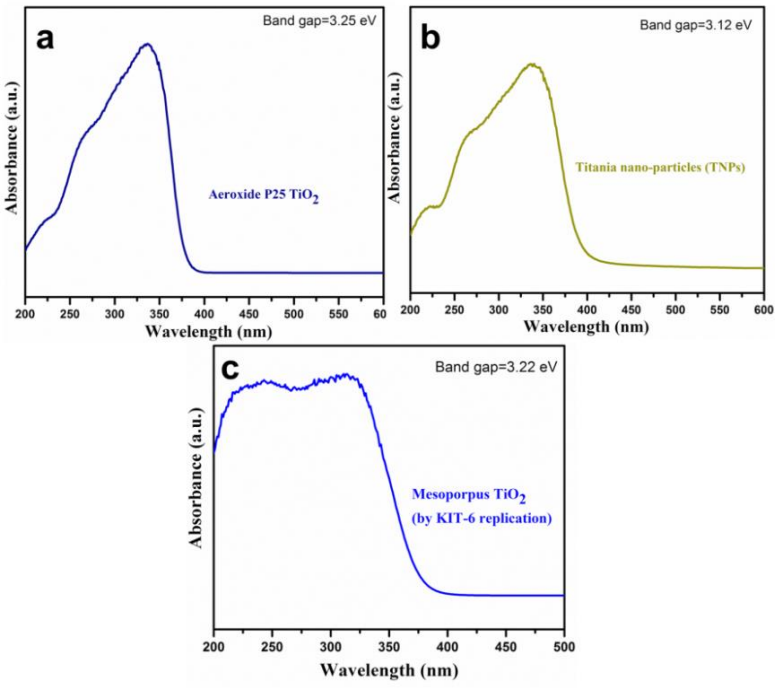

Figure: 7.18 *UV-Vis. spectra of the* ***(a)*** *Aeroxide P25 TiO_2,* ***(b)*** *TNPs,* ***(c)*** *Meso. TiO_2.*

The UV-vis. spectroscopy usually provides some key knowledge between the interactions of the semiconducting materials, for instance TiO_2, with photon energies [265]. The band gap energies of the three TiO_2 samples were calculated using the UV–Vis spectra onset of absorption values with the equation, E (eV)=hc/λ=1239.95/λ [262, 265]. Where, E is the band gap energy (eV), h is Planck's constant, c is the velocity of light (m/s) and λ is the wavelength in nm. The average literature reported band gap energies of the anatase and rutile TiO_2 are 3.2 eV and 3.0 eV, respectively [266]. However, it is demonstrated that the band gap energies of the three types of TiO_2s, obtained in this study, i-e, Aeroxide (3.25 eV), TNPs (3.12 eV), Meso. TiO_2 (3.22 eV) are in agreement with the literature.

7.2.2 Photocatalytic activity of CO_2 reduction with H_2O vapor to hydrocarbons (CH_4 + CH_3OH) and syngas (CO + H_2) formation

The photocatalytic activity results with all the three TiO_2 materials to convert CO_2 with H_2O vapors into various energy-bearing products are shown in Fig. 7.19 The main products obtained after the reaction are hydrocarbons (CH_4, CH_3OH in vapor form) and syngas (CO and H_2), are very useful energy-bearing products [256], Which either can be used directly as energy or to make further more valuable energy products. Fig. 7.19a-c shows the products comparison of the three TiO_2 materials in terms of the reaction kinetics. Aeroxide P25 TiO_2 has comparatively slow reaction kinetics to form the products than TNPs and Meso. TiO_2. The other major difference is that there is no H_2 formation by P25 TiO_2, whereas TNPs forms a significant amount of H_2 and Meso.TiO_2 also produced a reasonable H_2. However, it was gradually decreased with the irradiation reaction time. The production rates of CO and CH_4 by Aeroxide P25 TiO_2 were quickly decreased which are clearly shown in Fig. 7.19a. However, there was higher and stable CH_4 and CO production rates of TNPs than Aeroxide P25 and Meso.TiO_2 showed the highest than the other two TiO_2s. These differences are further clear by the total production comparison after 5h of reaction time, shown in Fig. 7.19d-f. This clearly indicates that TNPs and Meso.TiO_2 are much better than commercial Aeroxide P25 TiO_2, which is due to the higher surface area of TNPs and Meso.TiO_2 than Aeroxide P25 TiO_2. The higher surface area of these materials, as was observed by the characterizations, offers better adsorption of H_2O and

CO_2, which in turn produced the increased fuel products [259]. Moreover, in spite of the basic difference in surface area, the difference in activity may also be due to the different TiO_2 surface effects due to their different morphologies observed by FE-SEM.

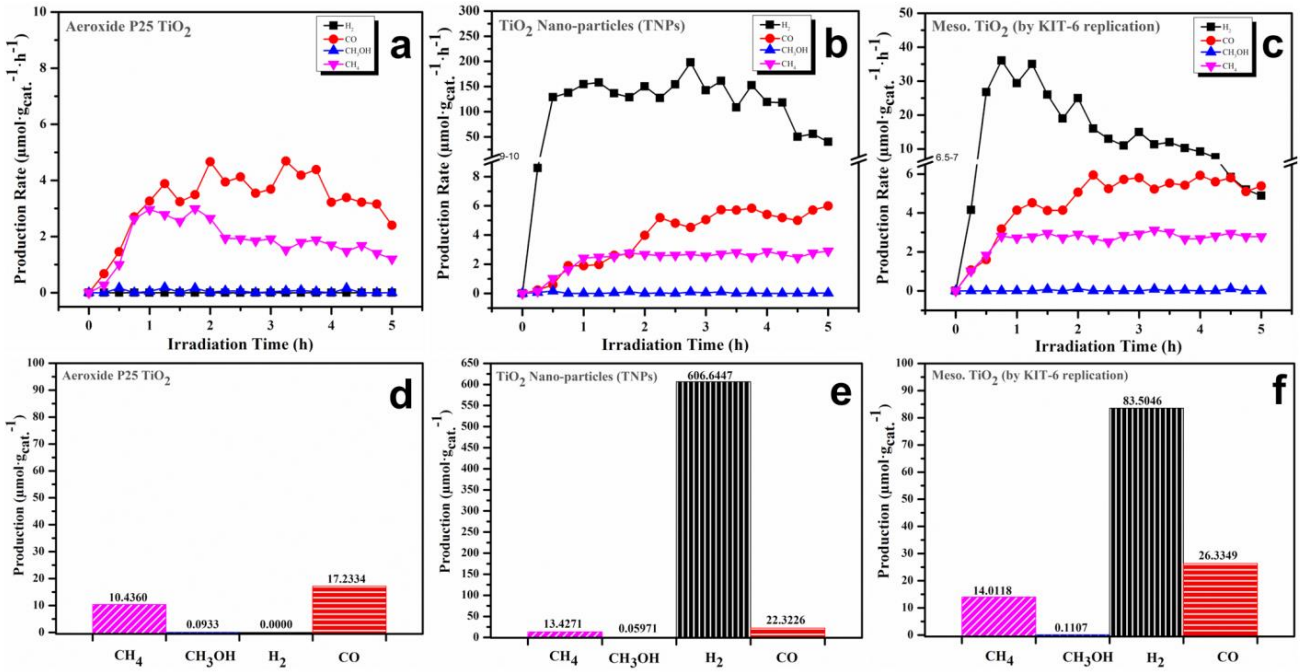

Figure: 7.19 *Photocatalytic activity comparison by the fuels production rate and production in 5h:* ***(a, d)*** *Aeroxide, P25 TiO_2,* ***(b, e)*** *TNPs,* ***(c, f)*** *Meso.TiO_2, at standard conditions of 0.5 g photocatalyst, 50 mL/min flow rate, H_2O/CO_2=0.1, 200 W UV lamp.*

It has been found in literature that CO_2 adsorption varies on different surfaces and structures [267], which may significantly affect the overall reaction due to the difference in adsorption. Therefore, due to meso porosity in Meso.TiO_2, the adsorption of gaseous reactants particularly CO_2 was considered better than the other TiO_2 and also better products desorption due to the easy transportation by the meso pores. Moreover, higher surface area of Meso.TiO_2 showed synergistic effect with this adsorption effect and hence showed overall higher activity. However, more H_2 formation by TNPs also indicates that TNPs favors more H_2O adsorption due to its hydrophilic surface [262, 43]. There is also an effect of competitive adsorption between H_2O and CO_2, which results significantly different products in this reaction and is being further discussed in the mechanism part.

Chapter 7

7.2.3 Proposed reaction mechanism of CO_2 reduction with H_2O to renewable fuel product formation

There are various mechanistic reaction schemes for CO_2 reduction with H_2O (as a reductant) using TiO_2 photocatalysts reported in the literature [44, 258, 261, 117]. The reaction pathways for a conversion are not specific and depend mainly on the reaction conditions applied. Therefore, this is a complex mechanism, which proceeds through branching pathways to produce different products simultaneously. However, the knowledge is still limited and many things are unclear to date, which needs more deep studies. It has been observed that CO_2 is thermodynamically a stable and chemically an inert compound and is difficult to be oxidized or reduced to other useful compounds at normal operating conditions. Therefore, a single electron reduction of CO_2 to an anion radical $\cdot CO_2^-$ has a very strong negative electrochemical potential of -1.90 V [24], which is impossible for any semiconductor to provide a single photo generated electron to stable CO_2 molecule. However, the standard potential of H_2O to generate H_2 is much lower and very feasible. Even it is impossible to transfer a photo generated single electron to CO_2 molecule, the opportunity to proton-assisted transfer of multiple electrons is comparatively easier. H_2 and CO formation is favorable here, as these need lower number of electrons and protons dynamics of CO_2 on selected model surfaces [158] whereas, CH_4 and CH_3OH require comparatively more electrons and protons and complex to be formed. It needs 2 electron and 2 protons and a -0.41 V electrochemical reduction potential to generate H_2. CO_2 to CO requires 2 electrons and 2 protons with -0.53 V electrochemical CO_2 reductions potential. However, CH_4 formation needs 8 protons and 8 elections with -0.24 V and CH_3OH proceeds with 6 protons and 6 electrons with -0.38 V electrochemical CO_2 reduction potentials shown in scheme above mentioned in the section Ti-mesoporous material reaction mechanism. However, to activate the inert CO_2 molecule for reduction, the best way is to adsorb it on surface of any semiconducting material, which lowers its energy barrier [44]. If a high-dielectric-constant solvent is used (e.g. water), the CO_2^- anion radicals can be greatly stabilized by the solvent, resulting in weak interactions with the photocatalyst surface. Similarly, effects of solvents have been observed on titania embedded in SiO_2 matrices [146]. Therefore, before the reaction, CO_2 and H_2O vapors were adsorbed to make good adsorption of these reactants on the catalyst surface. However, as shown in Fig.7.20, H_2O being polar (1.85D) molecule has more tendencies to adsorb than CO_2,

which has lower dipole moment (0D). Therefore, H_2O and CO_2 have a competitive adsorption. Moreover, in this situation, difference in surface area of the three TiO_2 materials is further contributing to have less or more adsorption of the reactants. After the adsorption, upon UV irradiation, electrons and holes are produced and reaction initiates. Electron reached to the adsorbed CO_2 and reduced it to an anion radical $\cdot CO_2^-$ whereas, H_2O oxidation proceeds through the holes, which make H^+, $\cdot OH$ or O_2, which is being desorbed or further, participate in the reaction.

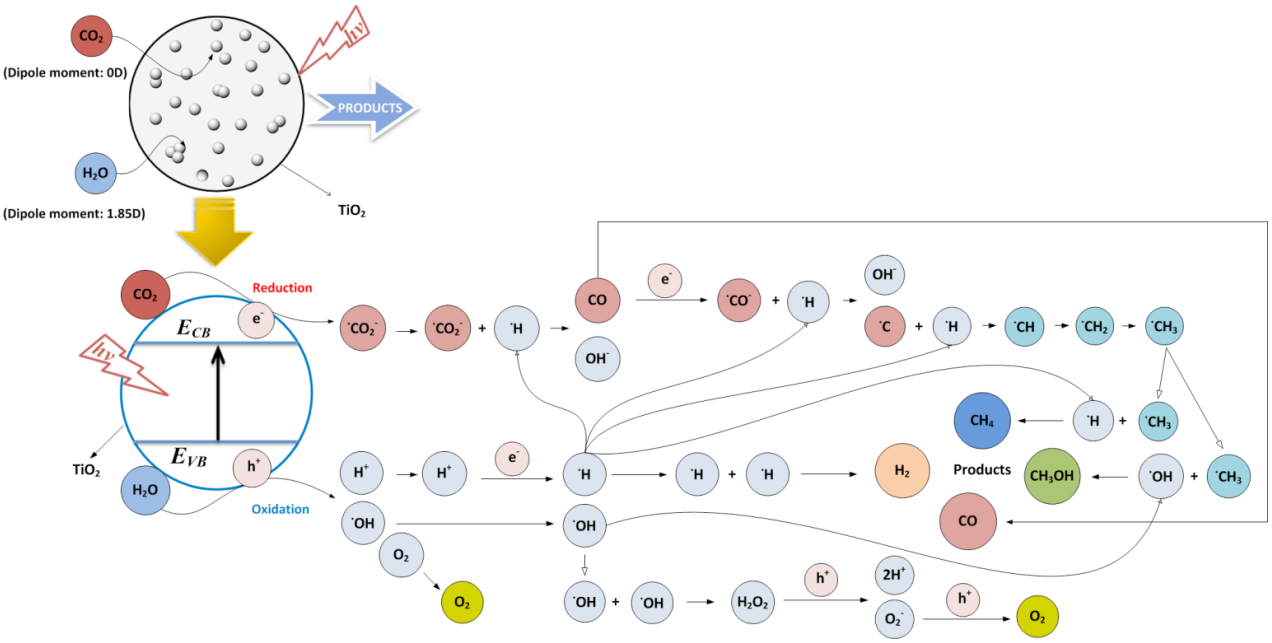

Figure: 7.20 *Proposed reaction mechanism and pathways of the photocatalytic reduction of CO_2 with H_2O vapor on Meso. TiO_2 to hydrocarbons and syngas formation.*

The H^+ further takes electron and form $\cdot H$, which reacts with the $\cdot CO_2^-$ to make CO and OH^-. This CO formation is an easy step as has been described earlier in this section, which either desorb as a product or it is further reduced to $\cdot C$ which makes chain reaction with $\cdot H$ to form $\cdot CH$, $\cdot CH_2$, or $\cdot CH_3$. $\cdot H$ combine together to make H_2, which has been found by TNPs and Meso.TiO_2 might be due to more H_2O adsorption than Aeroxide P25. The $\cdot CH_3$ further reacts with $\cdot H$ to form CH_4.and $\cdot OH$ obtained from H_2O oxidation, either combine together to make O_2, or being directly utilized with $\cdot CH_3$ to CH_3OH as a product, which seems difficult and complex.

Comparing the activity Fig. 7.19 and mechanism Fig. 7.20, under normal operating conditions, due to more hydrophilic nature of TNPs, this favors more water oxidation path to generate H_2, however, under the same conditions, Meso.TiO_2 showed more CO_2 reduction path and produced comparatively more CO and CH_4.

7.2.4 Key parameters that influence the photocatalytic activity of CO_2 reduction towards fuels formation

There are various factors, which strongly affect the CO_2 photocatalytic activity to fuel formation including different UV light sources, UV light intensities, different H_2O/CO_2 ratios, and numerous shapes of photocatalysts *etc*. All these parameters are briefly investigated here:

7.2.4.1 Different UV light sources (200W, 300W)

Light, either UV or solar, is the primary factor which directly affects to initiate the electron and hole pair in photocatalytic reaction. UV lights are common sources of illumination in photocatalytic reactions and have the light wavelength in the range of 100-400 nm. However, threshold wavelength required to promote the excited state, to minimum photon energy for anatase TiO_2 is 387.5 nm [268]. Irradiation using the light with shorter wavelength is more effective but not economical, therefore, to select an optimum light for a specific semiconductor is a key interest. Therefore, in this work, two different UV lamps with similar UVA and UVB range but different intensities, temperature and power of 200 and 300 W has been applied to see the effect of light on the activity. Fig. 7.21 shows the difference in the production rate and average production rate comparison of the products obtained from TNPs and Meso.TiO_2. It has been observed that UV 200 W lamp was favorable for more H_2 production in both TiO_2 which is due to its lower power and lower temperature produced during its functioning, which favors more H_2O adsorption. However, 300W lamp has more photon power, more UVB intensity and produced comparatively higher temperature, which suppress H_2O adsorption and boost the CO_2 reduction path. Therefore, higher CH_4, CO and CH_3OH are produced using 300 than 200 W light source. Meso.TiO_2 again showed better catalytic performance than TNPs under the same operating conditions, which is due to its aforementioned better characteristics.

Chapter 7

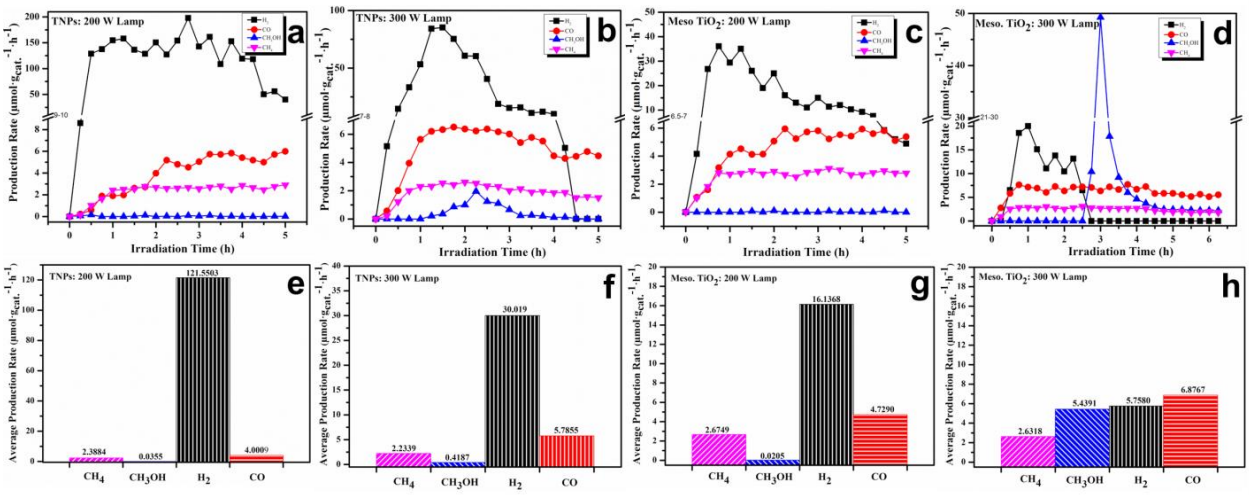

Figure: 7.21. *Effect of UV source on the activity:* ***(a, b)*** *200 W UV lamp/TNPs,* ***(c, d)*** *300W UV lamp TNPs,* ***(e, f)*** *200 W UV lamp Meso.TiO_2,* ***(g, h)*** *300 W UV lamp Meso.TiO_2, at standard conditions of 0.5 g photocatalyst, 50 mL/min flow rate, H_2O/CO_2=0.1.*

7.2.4.2 Various UV light intensities effect

Light intensity is very important element, which directly affects the reaction. As light intensity increases, the number of generated photons increases, which excited more electron-hole pairs with high energy [258]. Fig. 7.22 shows the effect of light intensity on the production rate of the products using TNPs and Meso.TiO_2. Three different distances (30, 20 and 5 cm) between the lamp and catalyst in the reactor have been used to obtain different light intensities. At a distance of 30 cm, shown in Fig. 7.22a, the products formation is low with also low reaction kinetics, which is due to the low intensity of light. However, by reducing the distance to 20 cm, the light intensity is comparatively increased which shows in Fig. 7.22b that the products rate has been increased significantly with higher reaction kinetics and long-time products formation stability. However, as shown in Fig. 7.22c, further decreased distance of 5 cm increased the products formation and very fast reaction kinetics in the beginning of the reaction, due to the increased intensity of light.

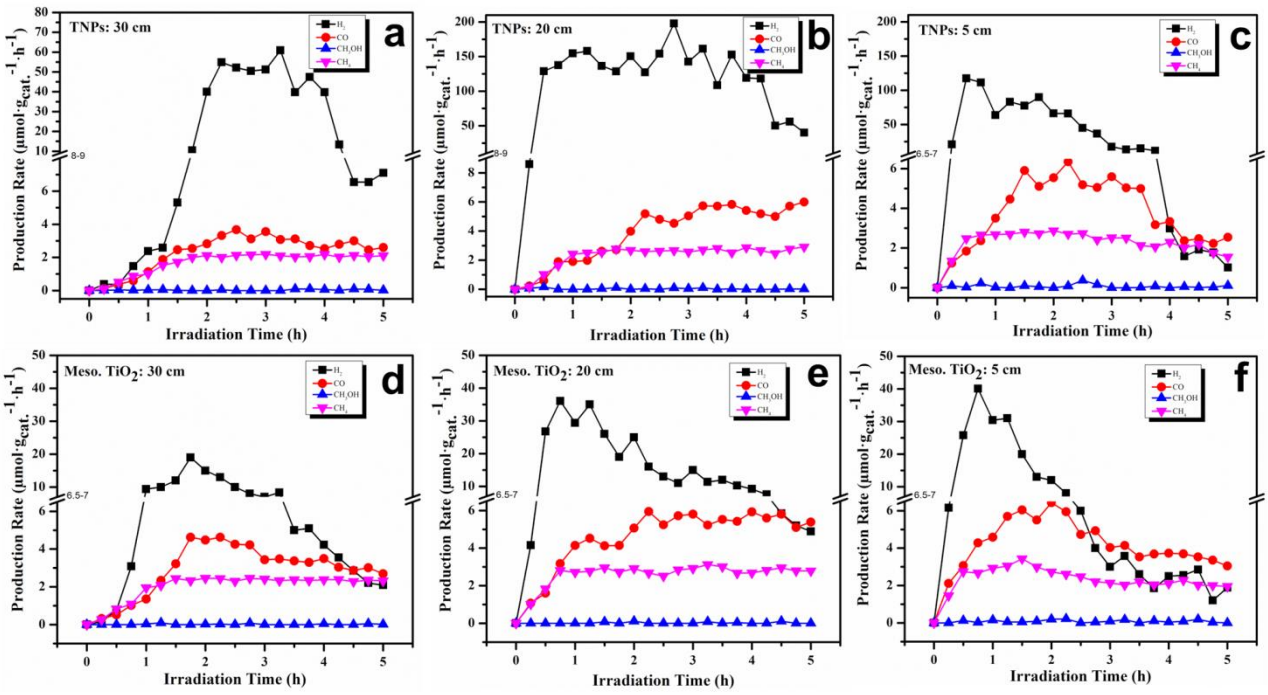

Figure: 7.22 *Effect of different UV light intensities on the activity of TNPs and Meso.TiO_2 photocatalyst:* ***(a-c)*** *TNPs. and* ***(d-f)*** *Meso.TiO_2 30, 20, 5cm, respectively, operating conditions with 20 % CO_2, 0.5 g of photocatalyst, 50 mL/min flow rate, H_2O/CO_2=0.1, 300 W UV lamp.*

However, as shown in Fig. 7.22c, further decreased distance of 5 cm increased the products formation and very fast reaction kinetics in the beginning of the reaction, due to the increased intensity of light. However, in this case, after 3h of illumination time the reaction showed deactivation, which might be due to the rapid saturation of the active sites due to fast reaction kinetics and increased temperature by light. A similar trend has also been observed in Meso.TiO_2 as has been shown in Fig. 7.22d-f.

7.2.4.3 Different H_2O/CO_2 ratios

In the recent research, TiO_2 and H_2O vapors (without any sacrificial hole scavenger) have shown a green chemistry approach towards CO_2 reduction to fuels. However, the reaction is strongly dependent on the molar ratio of H_2O/CO_2 [259]. Similarly, Fig. 7.23 shows the effect of different H_2O/CO_2 ratios on the activity of TNPs and Meso.TiO_2 that have been pursued to obtain the optimized ratio to maximize the fuel products. It can be seen in Fig. 7.23a-c that CO_2

conversion was increased with the increase in H_2O/CO_2 ratio of 0.1 to 0.2, whereas, an excessive H_2O (H_2O/CO_2=0.3) suppressed the overall reaction, which is consistent with literature [16, 155].

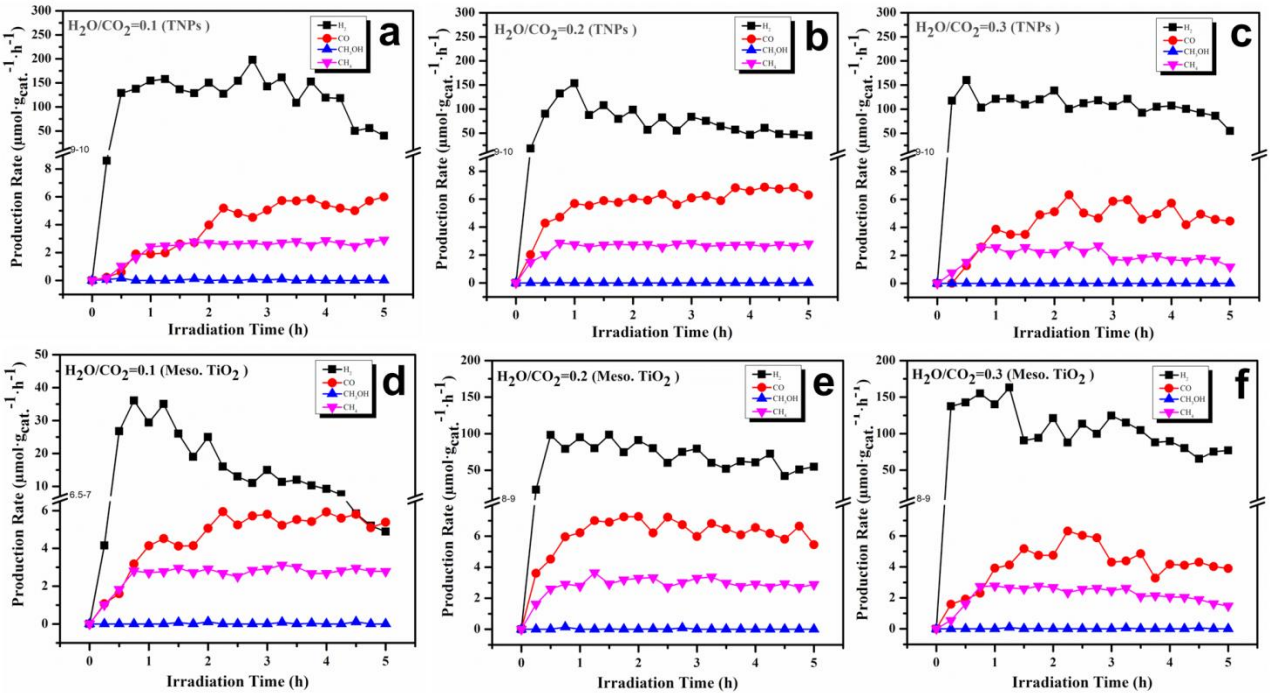

Figure: 7.23 *Effect of different H_2O/CO_2 ratios on the activity:* ***(a)*** *0.1/TNPs,* ***(b)*** *0.2/TNPs,* ***(c)*** *0.3/TNPs* ***(d)*** *0.1/Meso.TiO_2,* ***(e)*** *0.2/Meso.TiO_2* ***(f)*** *0.3/ Meso.TiO_2, at standard conditions of 0.5 g photocatalyst, 50 mL/min flow, 200W UV lamp.*

A similar trend as for TNPs has also been observed for Meso.TiO_2 shown in Fig. 7.23d-f. However, the overall activity of Meso.TiO_2 is comparatively better than TNPs due to its better structure characteristics.

7.2.4.4 Various shapes of photocatalysts (powder, pellets and thin film)

Catalyst shape is another key parameter that affects the products formation as well as the potential use of the catalyst for commercial application [260, 90]. Therefore, various catalysts forms such as powder, thin film and pellets have been investigated in this study for CO_2

reduction. As it can be seen in Fig. 7.24, higher fuels production rates was observed in case of pellets and thin film, it is because of pellet increased the contact areas and adsorption capacity. Their yield was significant when compared to thin film coating technique. [90].

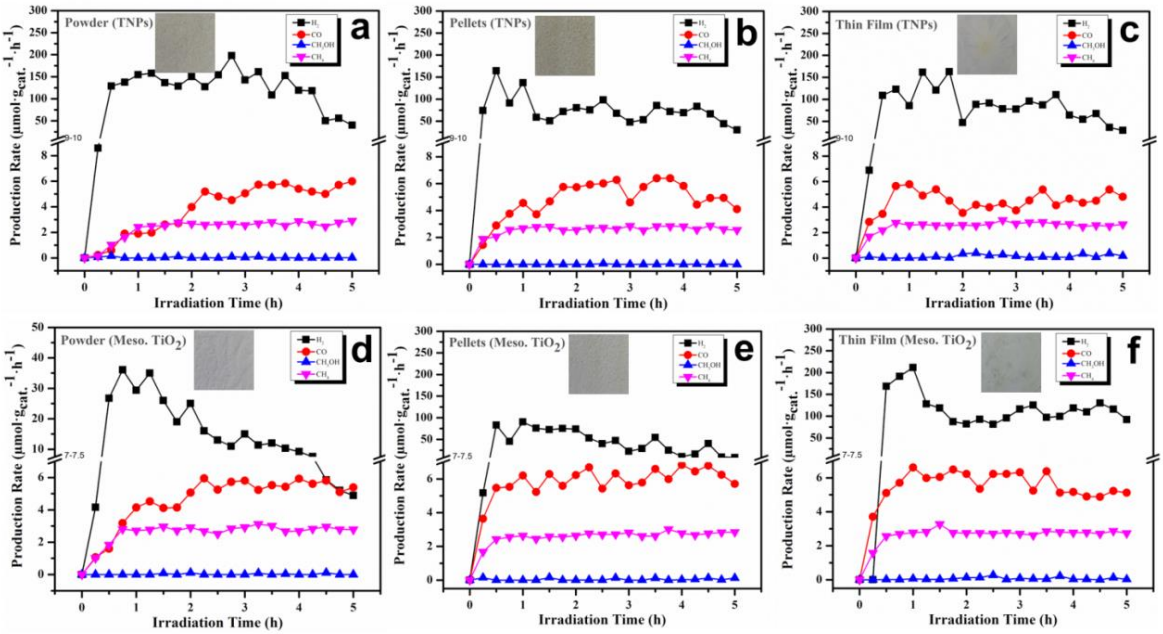

Figure: 7.24 *Effect of different shapes of the catalyst on activity:* ***(a)*** *powder/TNPs,* ***(b)*** *pellets/TNPs,* ***(c)*** *thin film/TNPs* ***(d)*** *powder/Meso.TiO_2,* ***(e)*** *pellets/Meso.TiO_2* ***(f)****, thin film/ Meso.TiO_2, at standard conditions of 0.5 g photocatalyst, 50 mL/min flow rate, H_2O/CO_2=0.1, 200 W UV lamp.*

Therefore, catalyst powder form has been compared with the pellets (100 micron) and thin film, shown in Fig. 7.24a-f compared to the powder, the pellets and thin film showed the highest activity, which is in line with the literature as it already has been discussed in the Ti maso porous mateials section. This is due to the better exploitation of the surface available for adsorption of CO_2 and H_2O, and the penetration of UV light, which is necessary to initiate the photocatalytic reaction. Better reaction kinetics and long-time photocatalytic stability have also been observed by the pellets and thin film shaped than the powder form used.

7.2.5 Deactivation and regeneration of photocatalysts

The blocking of active sites, which inhibit the photocatalytic reaction caused the

deactivation of the photocatalyst. Similarly, taking into account all these important points, many researcher have reported that in some cases the photoreduction of CO_2 tend to get deactivated within short period [20, 269, 270]. While in few cases activity beyond 20 hrs has been reported.

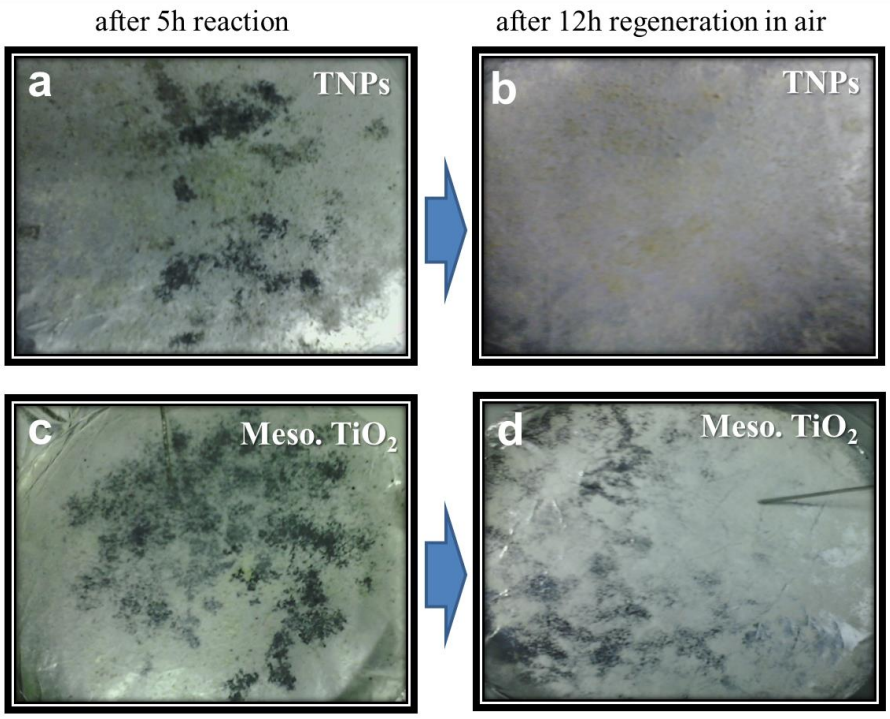

Figure: 7.25 *Catalyst deactivation/regeneration:* ***(a, b)*** *TNPs,* ***(c, d)*** *Meso. TiO_2.*

In this study, the catalysts after 5 h of reaction time were changed partially in color Fig. 7.25, which also showed slight photocatalytic deactivation. The exact mechanism of deactivation is not clear yet, however, the possible reasons of the deactivation are the partial saturation of the active sites for adsorption on the photocatalyst surface with either intermediate products/by-products/complex mixture formation, particularly, CH_3OH formation was absorbed by the powder catalyst, or another possibilities, which might proceed a photo-oxidation back into CO_2 by O_2 produced in the reaction [100]. The used catalysts after the reaction were placed 12 h in an open atmosphere for evaporation of the adsorbed species. More than 90% of the catalyst has been recovered Fig. 7.25b, d that shows that most of the adsorbed species were only physically adsorbed. However, more detailed study is recommended to know the exact nature and causes of these deactivating species, which is important to further understand the reaction mechanism.

Chapter 7

7.3 Photocatalytic activity tests for TiO_2/KIT-6 nanocomposite series towards fuel formation

7.3.1 Characterization of TiO_2/KIT-6 nanocomposite photocatalytic materials

Table 7.4 summarizes the textural properties and average TiO_2 crystal size calculated for these materials. Specific surface area (S_{BET}), pore volume (PV), average pore diameter (APD), and pore size distributions (PSD) were measured on the powder materials, which had previously been outgassed at 150°C for 2h using a Micromeritics Flow Prep 060, by means of N_2 sorption at 77 K on a Micromeritics Tristar II, USA (surface area and porosity) instrument.

The wide range XRD patterns were recorded in order to determine the different polymorphs, on an X'Pert Phillips diffraction using Cu Kα radiation, under the following conditions: (10–90 °) 2θ, with step size =0.02. However, the morphology and the mesoporous structures of the TiO_2/KIT-6 nanocomposites prepared were observed by means of a Leo Supra field emission-scanning electron microscopy (FESEM, Zeiss Merlin).

Fig. 7.25 displays the nitrogen adsorption-desorption isotherms of the different silica supports. It can be observed, all the materials exhibit type-IV nitrogen isotherms. N_2 sorption isotherms at 77 K for calcined samples are presented in Fig. 7.26a and b, which show the corresponding pore size distribution of the TiO_2/KIT-6 samples with various TiO_2 loading wt% such as (1, 5 10, 20, 30, 50, 70, 90 wt%) and optimized 20wt%TiO_2/KIT-6 at different calcination temperature (500, 600, 700, 800 °C) respectively. The isotherms can be classified as type IV according to the IUPAC consideration and are representative of mesoporous materials with pore size in the nano metric range [271]. However, TiO_2/KIT-6 nanocomposite series have shown different and large surface areas (S_{BET}), pore volumes (PV) and average pore diameters (APD) on the basis of their characteristics as shown in the Table 7.4. The use of KIT-6 mesoporous support material appears to control the titania crystal size restricting the growing of the titanium dioxide clusters inside the mesoporous channels.

Chapter 7

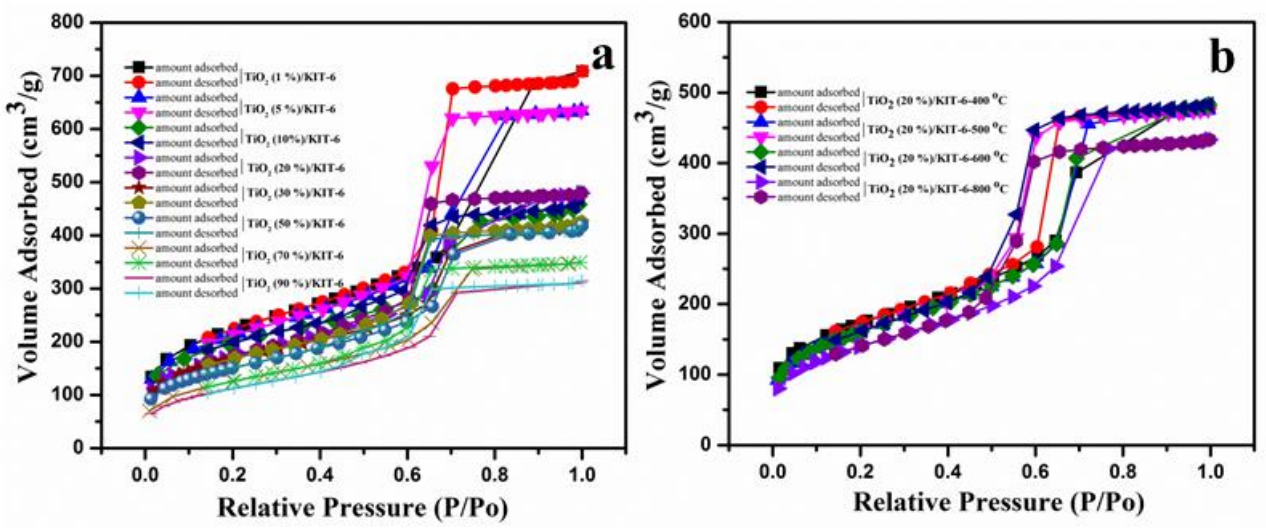

Figure 7.26 *N_2 adsorption/desorption isotherm and pore size distribution trends of:* ***(a)*** *1-90wt%TiO_2/KIT-6 calcined at 400ºC* ***(b)*** *20wt% TiO_2/KIT-6 calcined at 500-800ºC.*

In contrast, the use of an amorphous support persuades to bigger TiO_2 crystals as the titania loading increases [272]. However, specific surface area (S_{BET}), pore volumes (PV) deceases gradually by increasing the Ti contents or titania loading but there is no specific trend on the average pore diameter (APD), which almost remained constant. Additionally, the adsorption branch of each isotherm in TiO_2/KIT-6 series with different titania loading showed a sharp inflection at a relative pressure in the 0.5–0.8, it means a typical capillary condensation within uniform pores with a typical H1 type hysteresis loop, and which points out large channel like pores with a narrow pore size distribution as can be seen in Fig. 7.26.

***Table: 7.4**: Physical properties of various TiO_2 loading and calcination temperature effect on TiO_2/KIT-6 nanocomposite materials.*

Samples	N_2-adsorption/desorption			UV-vis.
TiO_2/KIT-6 series	S_{BET}	PV	APD	Band gap energy
KIT-6 Calcined	770	1.03	5.1	n.d
TiO_2(1wt%/KIT-6)	735	0.58	5.0	3.35
TiO_2(5wt%/KIT-6)	702	0.83	4.9	3.25
TiO_2(10wt%/KIT-6)	637	0.71	4.9	3.23
TiO_2(20wt%/KIT-6)	563	0.68	4.9	3.15
TiO_2(30wt%/KIT-6)	539	0.63	4.8	3.13
TiO_2(50wt%/KIT-6)	431	0.52	4.7	3.11
TiO_2(70wt%/KIT-6)	408	0.45	4.9	3.10
TiO_2(90wt%/KIT-6)	383	0.35	5.0	3.08
TiO_2(20wt%/KIT-6) 400°C	563	0.68	4.9	n.d
TiO_2(20wt%/KIT-6) 500°C	560	0.69	5.0	n.d
TiO_2(20wt%/KIT-6) 600°C	540	0.67	5.0	n.d
TiO_2(20wt%/KIT-6) 700 °C	503	0.65	5.2	n.d
TiO_2(20wt%/KIT-6) 800°C	454	0.60	5.3	n.d

***S_{BET}** (S_{BET} (BET specific surface area in m^2/g); **PV** (cumulative pore volume in cm^3/g); **APD** (average pore diameter in nm) n.d, (not determined)*

Moreover, as the calcination temperature of the TiO_2/KIT-6 composite increased, specific surface area and pore volume decreased more rigorously with such calcination temperature as shown in the Fig 7.26b as well as amount of TiO_2 loading. [118]. Hysteresis loop almost persisted by increasing the calcination temperature. It can be seen that optimized 20%TiO_2/KIT-6 composite calcined at 400-500ºC surface area shows the slightly decreased but by further increasing the calcination temperature 600-800ºC, specific surface area reduced rapidly due to easily dispersion of TiO_2 loading particles into the mesoporous silica KIT-6 support material (its 3-D pore structure) leading to decreased surface area as well as pore volume.

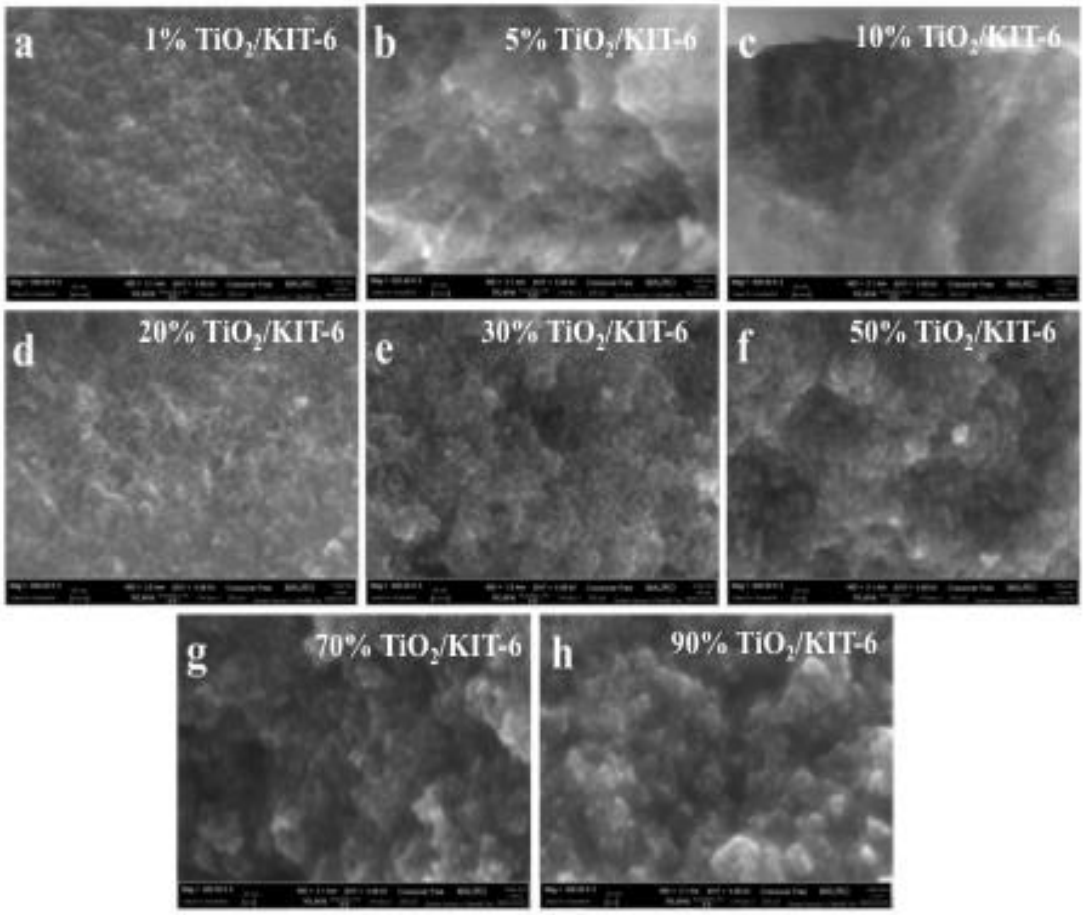

Figure 7.27 *FE-SEM images of the TiO_2/KIT-6 nanocomposites with various TiO_2 loadings:* ***(a)*** *1% TiO_2/KIT-6,* ***(b)*** *5% TiO_2/KIT-6,* ***(c)*** *10% TiO_2/KIT-6,* ***(d)*** *20% TiO_2/KIT-6,* ***(e)*** *30% TiO_2/KIT-6,* ***(f)*** *50% TiO_2/KIT-6,* ***(g)*** *70% TiO_2/KIT-6,* ***(h)*** *90% TiO_2/KIT-6.*

Accordingly, at higher temperature (700-800ºC) an average pore diameter increase, Table 7.4 which might be probably attributed to an increased contribution of the bare titania character in the prepared samples with the increasing of TiO_2 loading, which cause further decrease of surface area, which is probably due to that a little amount of TiO_2 can not result in dramatically change in silica structure. [273] On the other hand, the nanoparticles tend to agglomerate intensively at high calcination temperature, which could make the pore collapsed [274]. Therefore, it is accomplished that the mesostructure is maintained upon TiO_2 addition into the pores of KIT-6 silica materials. From the FE-SEM observation, morphology of the TiO_2/KIT-6 nanocomposite is shown in Fig. 7.27a-h. The images showed that the morphology of the

mesostructured TiO_2/KIT-6 nanocomposite does not change by loading the TiO_2 1-30%. It is conducted that lower amount of titania cause good dispersion into the 3-D pore structures of mesoporous KIT-6 materials but by further increasing the titania loading 50-90wt% a significant change in the morphology of the materials was observed. When the titania loading is low, the titania particles are located inside or within the pore at some extent of titania loading but by further increasing above the optimized limit then titania particles causes the pore blockage or outside the pore [275]. However, greater titania loading tend to agglomerates formation or collapsed the pore structured of the support mesoporous materials shown in the Fig. 7.27 f-h. Moreover, it is conducted that meso structured retained as such to that of support materials KIT-6 even though loading of titania up to 20%. Furthermore, optimized 20wt%TiO_2/KIT-6 was calcined at the various calcination temperatures to observe the change in textural properties of the nanocomposite materials are shown in the Fig. 7 28. At 400ºC calcination temperature, the mesoporosity and morphology of the synthesized TiO_2/KIT-6 materials showed better titania dispersion into the pores of the support materials. By increasing the calcination temperature, up to 500 ºC mesoporosity and the increase in pore size of the synthesized TiO_2/SiO_2 mixed oxides from 4.8 to 5.3nm shown in *Table 7.4*, which facilitates the mass transfer of the reactants (CO_2 and H_2O) as well as reaction intermediates which boosted the photocatalytic activity [276]. Further increase in temperature above 700 ºC causes the phase transformation from anatase to rutile, which was further confermed by XRD. This characteristic together with the high crystallinity and the abundance of the anatase phase in the materials generated allow predicting a good catalyst performance in photocatalytic reactions. Moreover, anatase shows a higher surface area and higher density of active sites [21] and its better crystallinity will favor to enhance the photoactivity. But, higher temperature causes the growth of particles or agglomerates formation, which can be clearly seen in Fig. 7.28 b-d at higher temperature. These agglomerates tend to reduce the light penetration into framework of the mesostructured resulting decreased the photocatalytic activity shown in the Fig. 7.34. Even though, H_2 formation increased with increasing of titania loading but by increasing the higher calcination temperature above the 600 ºC, H_2 formation disappear and other fuel products also decreased significantly which is clearly evidence with the photocataltic activity of these TiO_2/KIT-6 nanocomposite at higher calcination temperature shown in the Fig. 7.34.

Chapter 7

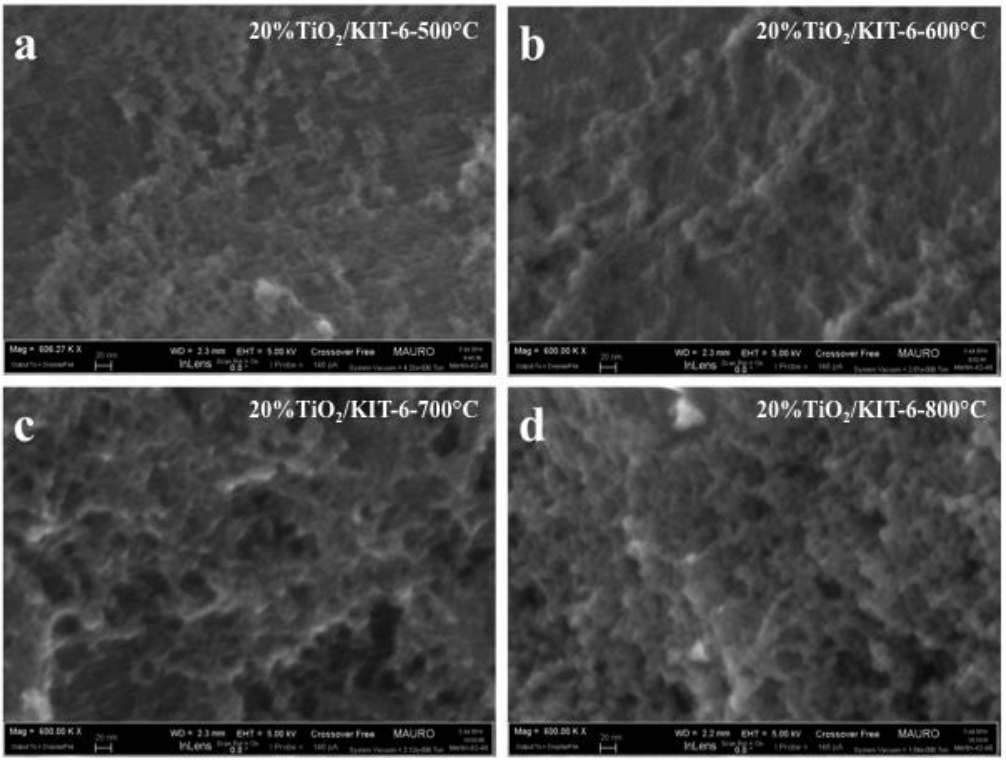

Figure: 7.28 *FE-SEM images of the TiO_2/KIT-6 nanocomposites with various calcination temperatures:* ***(a)*** *20% TiO_2/KIT-6-500ºC,* ***(b)*** *20% TiO_2/KIT-6-600ºC,* ***(c)*** *20% TiO_2/KIT-6-700ºC,* ***(d)*** *20%TiO_2/KIT-6-800ºC.*

Similarly, the wide-angle XRD patterns of the TiO_2/KIT-6 nanocomposite photocatalysts evidenced that anatase was the only titania crystalline phase present in all prepared materials, at 400 ºC calcination temperature. However, it is concluded that less titania contents or higher silica mesoporous material prevents the formation of higher titania crytallinity. Additionally, by further increasing the titania loading into mesoporous silica support material, crystallinity of the titania become more clear and increases with increasing of titania loading as shown in the Fig. 7.29a. Furthermore, XRD patterns of optimized 20wt %TiO_2/KIT-6 was calcined by further increasing the calcination temperature 400-600 ºC and 800 ºC shown in Fig. 7.29b. It was previously suggested, that anatase-rutile transition occur in pure TiO_2 shows at calcination temperatures above 400°C [277]. But another study showed that at higher calcination temperature above than 600 ºC shows mixed phase of anatase and rutile. It is concluded that less titania contents or higher silica mesoporous material prevents the formation of higher titania crytallinity.

Accordingly, Table 7.4 shows the variation of TiO_2 grain (crystal) size with different calcination temperature.

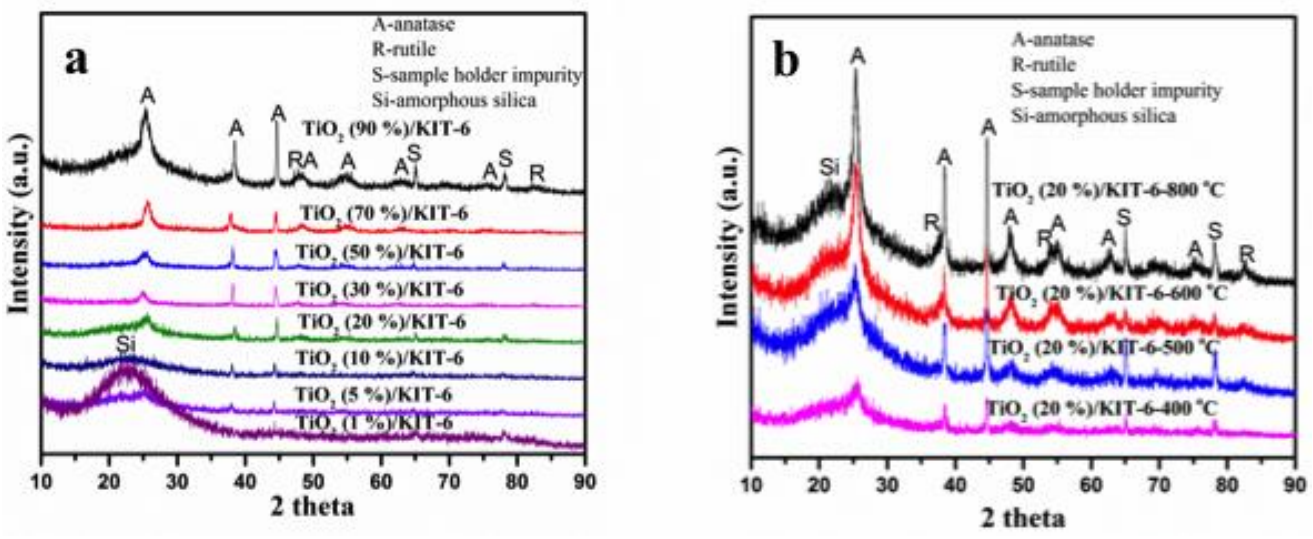

Figure: 7.29 *X-ray diffraction of the nanocomposite materials* ***(a)*** *1-90%TiO_2/KIT-6 with various TiO_2 loading* ***(b)*** *20%TiO_2/KIT-6 with different calcination temperature.*

It was observed that with increase of calcination temperature TiO_2 grain size increases [118] and it was above than that of support KIT-6 mesoporous silica shown in Table 7.4. With further increase of calcination temperature to 800 °C Fig. 7.29b, 20wt% TiO_2/KIT-6 also shows more rutile phase. It has been observed that with increase of calcination temperature more and more rutile phase of TiO_2 appeared in the less content of TiO_2 loading samples. The samples TiO_2/KIT-6 nanocomposite prepared at calcination temperature of 700 °C (not shown in the Fig 6.29b) and 800 °C shows the mixed phase of anatase and rutile [118]. Mixed phase show the better photocatalytic activity than that of pure anatase and rutile phase. Consequently, the increase in calcination temperature leads to a progressive increase of the titania nanoparticles from 4.8 to 5.3 nm particles also confirmed by N_2 adsorption/desorption isotherm, and S_{BET} characterization results.

Similarly, to observe the band gap energies of the TiO_2/KIT-6 nanocomposite materials, a UV-Vis. spectrum was performed as shown in Fig. 7.30. The absorption spectra of these

photocatalysts were shifted to higher wave length by incresing titania loadings 1-90% as shown in Fig. 7.30A. The band gap energies of the TiO_2/KIT-6 materials corresponding to a band gap 3.4-3.1 eV, respectively, from TiO_2 loading 1-90wt%, data shown in the table 7.4. It was observed that with increasing the titania loading the band gap energy decrease shown in Fig. 7.30B. Accordingly, optimized 20wt %TiO_2/KIT-6, with 3.2eV band gap energy indicates that sufficient photogenerated electron−hole pairs could result in higher photocatalytic performance for CO_2 reduction.

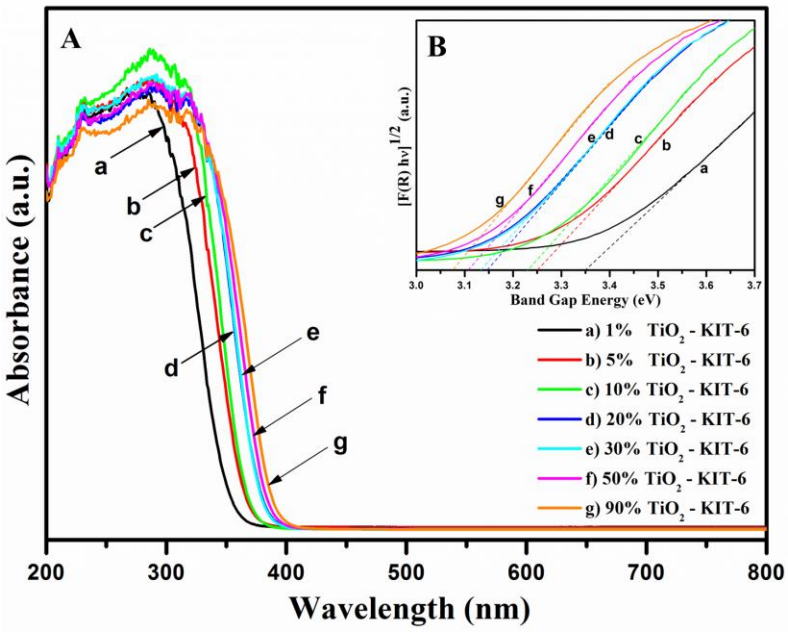

Figure: 7.30 *UV-Vis spectra of TiO_2/KIT-6 nanocomposite with different titania loadings wt%* ***(A),*** *Overall UV spectra* ***(B),*** *band gap energy of nanocomposite titania.*

7.3.2 Photocatalytic activity of CO_2 reduction with H_2O vapor by TiO_2/KIT-6 nanocomposite to fuels formation

The photocatalytic reaction results of the synthesized photocatalysts are shown in Fig. 7.31a-h. Blank tests accompanied without photocatalysts as well as the reactions were conducted in the dark with catalysts have shown no product formation, which suggests that the products obtained during the reaction were merely photocatalyst based. The photocatalytic activity tests with all TiO_2/KIT-6 series with different titania loading wt% to convert CO_2 with H_2O vapors

under the UV light 300W lamp. Various fuel products (CH_4, CH_3OH, H_2 and CO) obtained by CO_2 reduction and H_2O oxidation. CH_4, CH_3OH (in vapors) CO and H_2, all these products obtained in gaseous forms by using FID and TCD detectors.

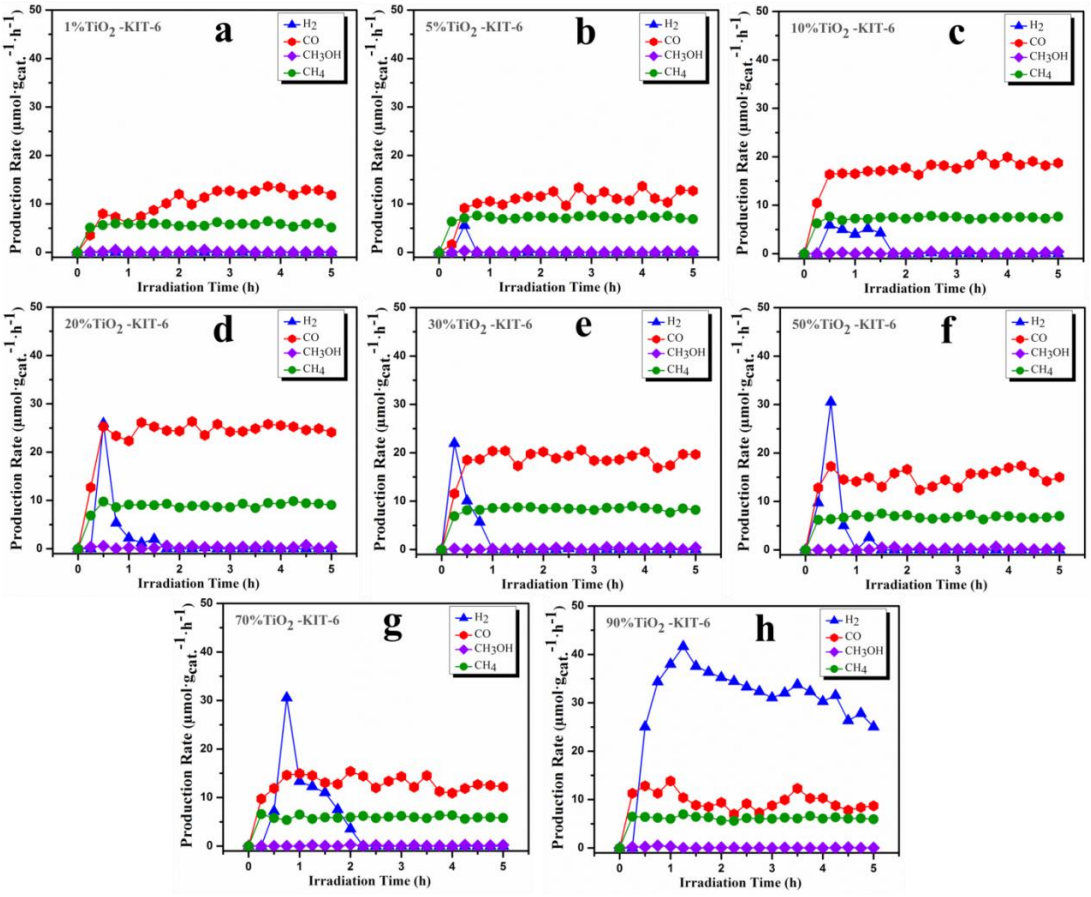

Figure: 7.31 *Photocatalytic activity tests for TiO_2/KIT-6 series* ***(a)*** *1%TiO_2/KIT-6* ***(b)*** *5%TiO_2/KIT-6* ***(c)*** *10%TiO_2/KIT-6* ***(d)*** *20%TiO_2/KIT-6* ***(e)*** *30%TiO_2/KIT-6* ***(f)*** *50%TiO_2/KIT-6* ***(g)*** *70%TiO_2/KIT-6* ***(h)*** *90%TiO_2/KIT-6.*

However, 1wt% titania loading into mesoporous structures (KIT-6) initially, the kinetic of the reaction was very slow and CO as a main product obtained from the CO_2 reduction as shown in Fig. 7.31a. Moreover, by further increasing the titania loading from 5-10wt%/KIT-6, the kinetic of the reaction becomes fast and production rate of the fuel formation increased significantly. But most surprisingly, more H_2 formation was observed by increasing the titania loading as shown in Fig. 7.31b-h. Overall, 20wt%TiO_2/KIT-6 showed higher production of fuel than other titania loading photocatalysts. Higher photocatalytic activity might be due to good

titania dispersion which prevent the titanium agglomerates formation into frame work of support KIT-6 material shown in Fig. 7.31d. By further increasing the titania loading 30-90wt% H_2 formation improved and other products (CH_4, CH_3OH) indicated the long-time stability after the 5h of the reaction. Nevertheless, the deactivation of the photocatalyst was observed at higher titania loading. It might be due to some desorbed CO during the reaction, or by-products formation, and CH_3OH vapor produced during the reaction caused the deactivation of the photocatalyst. Or it might be possible that kinetically, very fast reaction could not stabilize the reaction for long time but still this investigation unclear. A separate depth study is neened to understand the deactivation of the photocatalyst. However, in all these photocatalytic activity tests, standered reaction condition were kept as 0.2 g of photocatalyst, 50 mL/min flow rate, H_2O/CO_2=0.1, 300 W UV lamp, with 20 % CO_2.

Similarly, Fig. 7.32 also showed the fuel production rate by different titania loading content which clearly indicates that by increasing the titania contents the production rate of CH_4, CH_3OH, H_2 and CO gradually increased up to 20wt %TiO_2/KIT-6 (*CH_4 44.55, CH_3OH 1.08, H_2 9.20* and *CO 120.54µmol.g_{cat}^{-1}.h^{-1}* respectively) but by further increasing the titania loading the production rate of all these photocatalytic products decreased except H_2 formation which remain frequently increased even at 90wt%TiO_2/KIT-6. As it has been already mentioned that higher amount of titania favor to H_2 formation, these findings are also in agreement with the results that obtained from Meso.TiO_2 materials whereas, more H_2 is produced than that of other fuel products. However, less titania contents lead to formation of more hydrocarbons such as CH_4, and CH_3OH as results obtained from our optimized Ti-KIT-6 calcined Si/Ti = 100 ratio, but reverse had a adverse effect.

Chapter 7

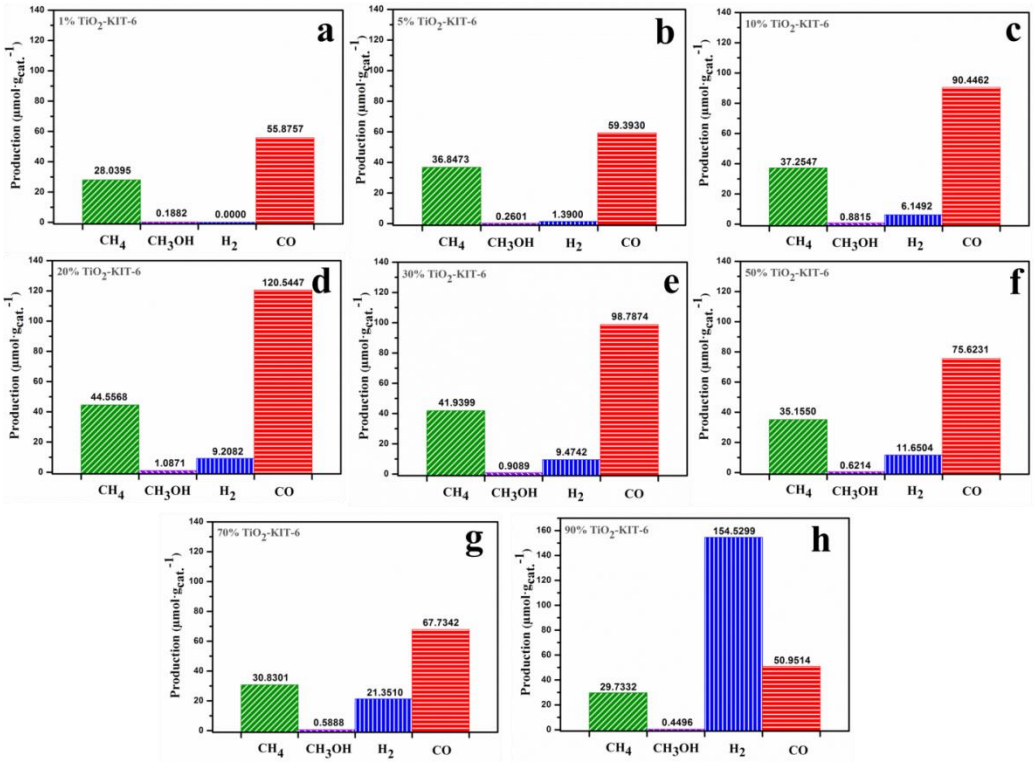

Figure: 7.32 *Production rate of fuel by TiO_2/KIT-6 series* ***(a)*** *1%TiO_2/KIT-6* ***(b)*** *5%TiO_2/KIT-6* ***(c)*** *10%TiO_2/KIT-6* ***(d)*** *20%TiO_2/KIT-6* ***(e)*** *30%TiO_2/KIT-6* ***(f)*** *50%TiO_2/KIT-6* ***(g)*** *70%TiO_2/KIT-6* ***(h)*** *90%TiO_2/KIT-6.*

Therefore, it is determined that higher titania loading favor to H_2 formation from H_2O splitting, photocatalytic pathways and reaction mechanism will be elucidated hereafter to confirm this hypothesis. Actually, more H_2 formation is due to more water adsorption on the catalyst surface than CO_2 adsorption. The CO_2 reduction path way proceed slowly while on the other hand hydrogen radicals formation pathway follow to combine with each other to produce more H_2 as shown in Fig. 7.35, the reaction mechanism and pathways. Consequently, 20%TiO_2/KIT-6 was found to be the optimized photocatalyst with higher CH_4, CH_3OH, H_2 and CO production as compared to another titania loading into mesostructured KIT-6 material. Likewise, selectivity of the titania nanocomposite materials for fuel production are shown in the Fig. 7.33. The photoactivity results indicates that selectivity of fuel, where CO as a major CO_2 photocatalytic reduction product over than 60% was obtained by increasing the loading from 1-50% titania and CH_4 was observed as a primary hydrocarbon from CO_2 reduction with almost

over than 25% until 70%TiO_2 loading but by further increasing the titania loading at 90%, both photocatalytic product CO and CH_4 reduced to 21 and 12% respectively, and H_2 formation increased significantly up to 65% for 90% titania. As it has already been mentioned that CH_3OH vapor indication remained almost constants by increasing the titania loading at the end of the reaction time 5h. However, it was investigated from all the photocatalytic activity tests of the TiO_2/KIT-6 nanocomposite series that, these materials followed the pathways of H_2O oxidation and CO_2 adsorption and activation is comparatively less.

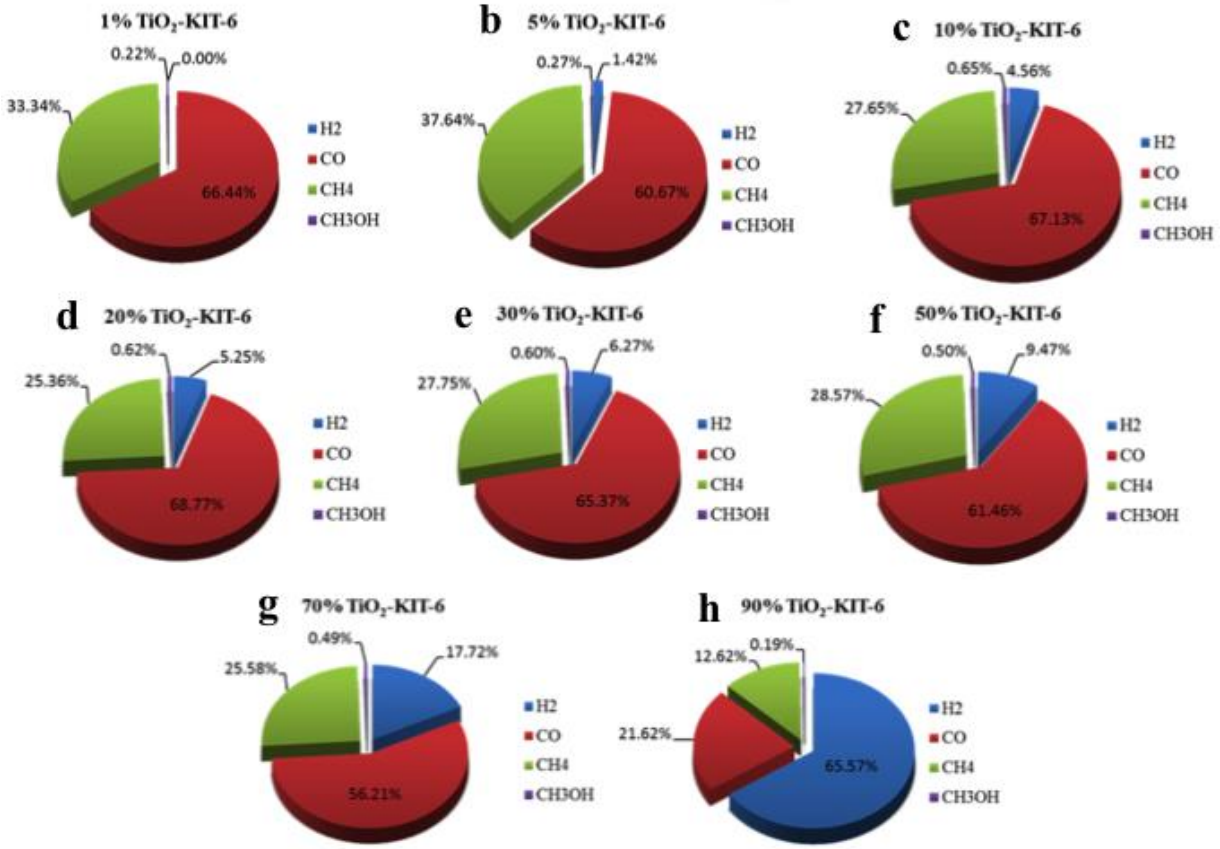

Figure: 7.33 *Selectivity toward fuel formation for TiO_2/KIT-6 series* ***(a),*** *1%wtTiO_2/KIT-6* ***(b),*** *5%wtTiO_2/KIT-6* ***(c),*** *10wt%TiO_2/KIT-6* ***(d),*** *20wt%TiO_2/KIT-6* ***(e),*** *30wt%TiO_2/KIT-6* ***(f),*** *50wt%wtTiO_2/KIT-6* ***(g),*** *70wt%TiO_2/KIT-6* ***(h),*** *90wt%TiO_2/KIT-6.*

Chapter 7

7.3.3 Effect of various calcination temperatures on optimized photocatalyst

Generally, for electron hole pair generation, photon irradiation is the primary step from photocatalyst because the band gap energy is too high for thermal excitation to overcome. Moreover, by increasing the temperature, the collision frequency as well as diffusion rate increased. However, calcination temperature had a strong effect on the size of crystalline TiO_2 nanoparticles. Furthermore, the optimized photocatalyst (20wt%TiO_2/KIT-6) was further calcined at various calcination temperatures 400-800 ºC to observe the change in nanocomposites structures and the effect of photocatalytic activity of CO_2 reduction. It has been mentioned before that by increasing the calcination temperature from 400 ºC to 800 ºC, surface area significantly decreased 563 to 454 m^2/g shown in Table: 7.4 which are evidenced the results obtained from N_2 adsorption/desorption isotherms. However, CO_2 photocatalytic reduction with H_2O vapor at 400 ºC calcination temperature showed the higher kinetic of reaction with increased photocatalytic products formation shown in Fig. 7.34a. Photoactivity gradually increased in all cases of fuel products at 500ºC calcination temperature where H_2 production decreased significantly by increasing the calcination temperature from 600-800ºC shown in Fig. 7.34c-e. Further reduction in CH_4 and H_2 and CO formation was noticed due to higher calcination temperature shown in Fig. 7.34d and e. Moreover, 700-800 ºC calcination temperatures cause the phase transformation from anatase to rutile, which had adverse effect on the photocatalytic activity and reduced the fuel production rate. H_2 formation becomes disappeared and other photocatalytic products also decreased with increasing the calcination temperature above than 500 ºC. Consequently, 400 ºC calcination temperature was found to be the optimized temperature with 20wt%TiO_2/KIT-6 in all reaction conditions which were applied during the photocatalytic reaction for CO_2 reduction.

Chapter 7

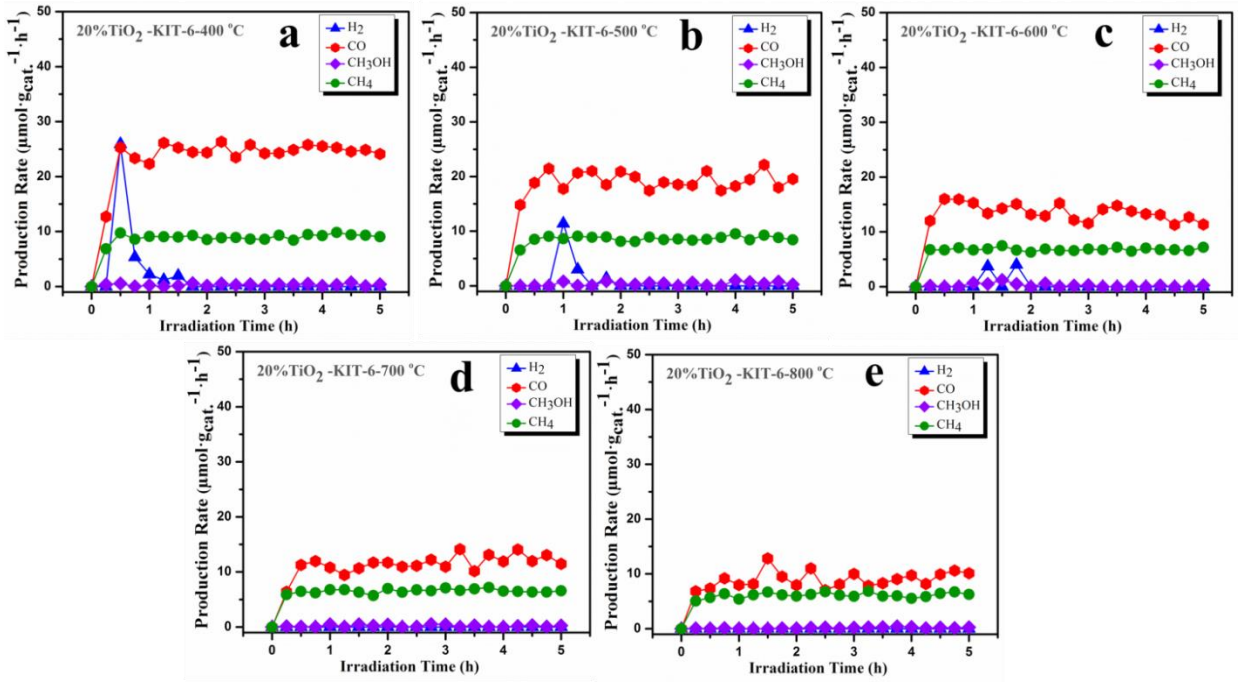

Figure: 7.34 *Various calcination temperature effect on optimized photocatalyst* ***(a),*** *20wt%TiO_2/KIT-6-400 ºC* ***(b),*** *20wt%TiO_2/KIT-6-500 ºC* ***(c),*** *20wt%TiO_2/KIT-6-600 ºC* ***(d),*** *20wt%TiO_2/KIT-6-700 ºC* ***(e)****, 20wt%TiO_2/KIT-6-800 ºC*

7.3.4 Proposed reaction mechanism and pathways for CO_2 reduction and H_2O oxidation on TiO_2/KIT-6 nanocomposite to fuels production

The proposed reaction mechanism of CO_2 reduction with H_2O oxidation has already been discussed in section 7.1 and 7.2 with Ti based titania materials and Meso.TiO_2 respectively. However, there are various pathways and most importantly reaction conditions are very necessarily step to follow the different paths to give fuel products. But in case of TiO_2/KIT-6 nanocomposite, when photocatalyst is irradiated by UV light which, produced e^- /$h+$ pair that migrate to the surface of the solid. The reaction mechanism can be therefore divided into two paths, 1st reduction of CO_2 at the conduction band and 2nd involved the oxidation of H_2O at the valence band respectively. Both reduction of CO_2 and oxidation of H_2O proceed competitively and simultaneously on the surface of photocatalyst.

In the proposed reduction mechanism of TiO_2/KIT-6 nanocomposite CO_2 adsorbed on the surface of the photocatalyst which then is reduced by the electron and form a anion radical $CO_2^{\bullet-}$ with a very strong negative electrochemical potential of -1.90 V [24]. Then latter reacts with the radical $H^{\bullet}$ formed by oxidation of water vapor, and leads to the formation of anion to the CO and OH. The CO can be further reduced by means of an electron to the radical $CO^{\bullet-}$ by reacting with a radical $^{\bullet}H$, leads to the formation of OH^- ion and carbon radical $C^{\bullet}$. Afterward, carbon radical $C^{\bullet}$.react consecutively with hydrogen radical $H^{\bullet}$, to form $CH^{\bullet}$, CH_2,$^{\bullet}$ CH_3,$^{\bullet}$ and finally the final products CH_4 with consectively series of hydrogen radical and CH_3OH. The pathways formation scheme is shown in Chapter 4 and section reaction intermediates product formation as well as here in scheme below.

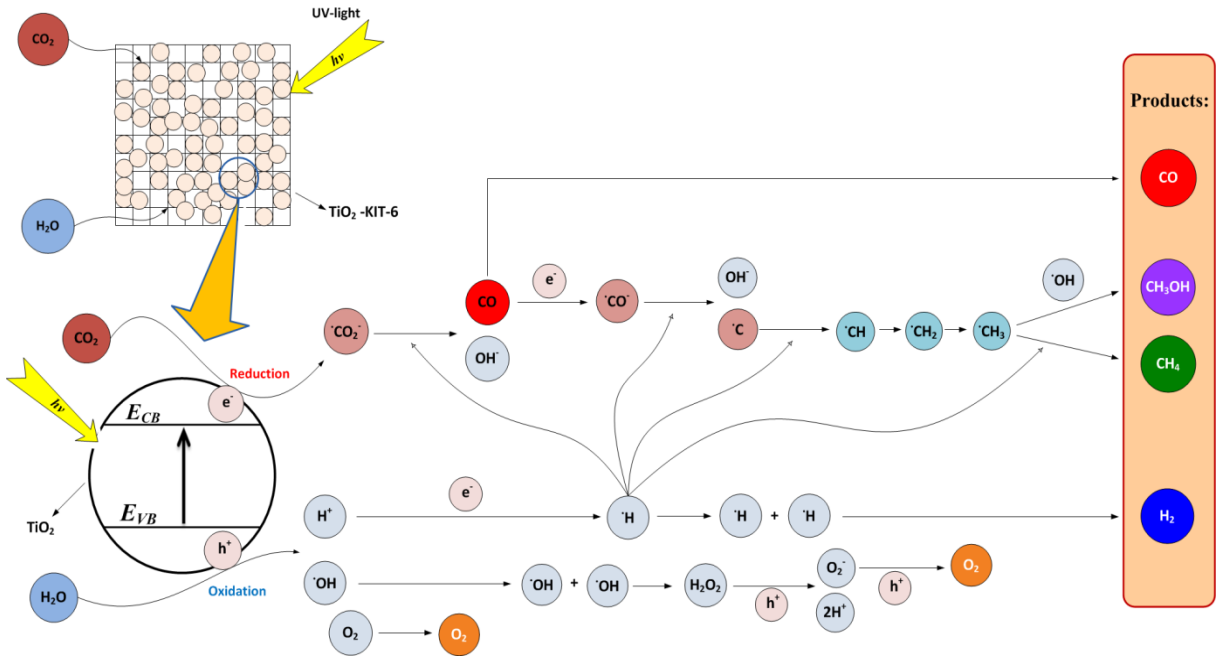

Figure: 7.35 *Proposed reaction mechanism and pathways of the photocatalytic reduction of CO_2 with H_2O vapor on TiO_2/KIT-6 nanocomposite to fuels formation.*

On the other hand, H_2O is oxidized by capturing the hole (h^+) which are produced during the reaction resulting the formation of H^+ and $OH^{\bullet}$. Hydrogen ion (H^+) produced react with an e^- to form radical which facilitate the reduction of CO_2 pathway to form of hydrocarbon products

while in case of $OH^{\bullet}$radicals ,there might be chances to combine two $OH^{\bullet}$ radicals to give rise H_2O_2 or it may produce O_2. TiO_2/KIT-6 nanocomposite favor H_2O splitting pathway to produce more H_2 as compared to another fuel product by increasing the titania loading more than optimized 20%TiO_2/KIT-6 which is clear evidence from photocatalytic activity results. Consequently, less titania content follow to hydrocarbon formation pathway while by increasing the titania CO_2 reduction pathway is slow down and H_2O oxidation dominated to give rise more $H^{\bullet}$radicals which then combine with each other to form H_2 as shown in the Fig.7.35.

$$TiO2/\ KIT-6\ \xrightarrow{h\nu}\ (TiO2/\ KIT-6)\ e^- + (TiO2/\ KIT-6)\ h^+ \quad (7.1)$$

Reduction of CO_2

$$CO_2 + e^- \rightarrow CO\bullet - \quad (7.2)$$

$$CO\bullet - + e^- + H\bullet \rightarrow CO + OH\bullet \quad (7.3)$$

$$CO_2 + 8H^+ + 8e^- \rightarrow CH_4 + 2H_2O \quad (7.4)$$

$$CO_2 + 6H^+ + 6e^- \rightarrow CH_3OH + H_2O \quad (7.5)$$

Oxidation of H_2O

$$2H_2O + 2e^- + 2h^+ \rightarrow O_2 + 2H_2 \quad (7.6)$$

$$H\bullet + H\bullet + 2e^- + 2h^+ \rightarrow H_2 \quad (7.7)$$

$$OH\bullet + OH\bullet + 2e^- + \rightarrow H_2O_2\ or\ O_2 \quad (7.8)$$

Meanwhile, H_2 is produced by the combination of two hydrogen radicals ($H^{\bullet}$). Reaction mechanism is very complicated following the various pathways to produce desired products. In addition, methane and methanol are formed from a series of radical reactions and subsequent products are therefore a lesser amount compared to the CO. and this is also evidence from photocatalytic activity tests that CO formation is higher as compared to other fuel products on optimized photocatalyst.

Chapter 8

8 Conclusions

In this study, different routes have been adopted to achieve highly active photocatalyts for reduction of CO_2 greenhouse gas with H_2O vapor towards energy bearing products. These catalysts have also been characterized by using various characterization techniques (BET, FE-SEM, XRD, UV-Vis, TEM, FT-IR, XPS), to observe the physiochemical properties of these materials and to correlate their characteristics with the photocatalytic activity to achieve the optimized photocatalyst. The different developed photocatalysts, namely novel Ti-KIT, nanostructured TiO_2s and TiO_2(x)/KIT-6 have produced mainly hydrocarbons (CH_4, CH_3OH) and syngas (CO, H_2). However, the overall production as well as the selectivites with these photocatalyst varied. The key findings obtained are summarized below:

- Optimization of the novel synthesized Ti-mesoporous silica (SBA-15-S, KIT-6 calcined or dried) materials with different Si/Ti ratios (200, 100 and 50) has revealed that the Ti-KIT-6-calcined (Si/Ti=100) was the most optimized photocatalyst than the other materials explored in this study, in the activity of CO_2 reduction with water vapors to renewable fuels. This was due to the presence of more accessible surface reaction active sites in the Ti-KIT-6-calcined (Si/Ti = 100), which were due to the lower number of Ti–O–Ti or TiO_2 agglomerates, and to the more isolated Ti species, which were uniformly dispersed on the 3-D KIT-6 mesoporous silica support without collapsing the mesoporous structure. The increased surface concentrations of OH groups found in the Ti-KIT-6-calcined (Si/Ti = 100) also boosted higher activity. The reaction mechanism indicates that the reaction proceeds mainly by the competitive adsorption of CO_2 and H_2O vapors on the catalyst surface. The UV light source, UV intensity, H_2O/CO_2 ratios and catalyst shapes are the key factors that influence the performance of the catalyst, and therefore, these parameters have here been optimized to increase the renewable fuel products. The partial saturation of the active adsorption sites by means of the products or by-products or mixture formation are supposed to be the main possible causes of the deactivation.

The O_2 produced in the reaction is also considered as a redundant, as it might promote the deactivation by means of oxidation of the products back to CO_2. A simple evaporation technique can quickly regenerate the photocatalyst. However, a separate in-depth study is recommended to explore the exact nature and the causes of these deactivating species. Moreover, one of the main hurdles to overcome for photocatalytic reaction to be practical is source of light to initiate the reaction. The wavelength of solar light is not sufficiently short for this scheme. However, CO_2 conversion utilizing solar energy is fundamentally very important for the sustainable future. Therefore, we hope that the development of the photocatalysis with nanomanufacturing will realize CO_2 reduction with solar energy in the near future. These findings indicate that the optimized photocatalyst is a promising candidate for this application in the future research.

- TNPs with an enhanced adsorption capability, due to its high surface area and smaller nano-sized particle morphology, have shown a higher syngas production than commercial Aeroxide P25 TiO_2. However, novel Meso.TiO_2 has shown more hydrocarbons as well as a better syngas production, better reaction kinetics and better stability, due to its superior characteristics than those of the commercial TiO_2 and TNPs. The reaction mechanism indicates that the reaction proceeds mainly by competitive adsorption of CO_2 and H_2O on the catalyst surface. The UV light source, UV intensity, H_2O/CO_2 ratios and catalyst shapes are the main factors that influence the performance of the catalysts, and these parameters have here been optimized to increase the fuel products. Partial saturation of the active adsorption sites by means of the product/by-product/mixture formation are the possible causes of the deactivation. The O_2 produced in the reaction is also believed to promote the deactivation by means of oxidation of the product back to CO_2. The catalysts can be regenerated quickly through a simple evaporation technique. The results indicate that these photocatalysts are also promising for future research and further applications.
- The TiO_2(x)/KIT-6 nanocomposite series with different titania loadings(x) wt% ranging from 1-90 wt% have also been explored for CO_2 reduction to various energy-bearing products (CH_4, CH_3OH, CO, H_2. The catalysts have been explored with characterizations and calcination at different temperatures to make these optimized and effectively explore for the photocatalytic reduction of CO_2 to fuel products. It has been found that TiO_2 showed uniform dispersion within the pores/surface of KIT-6 until 20 wt% TiO_2 loading.

However, TiO_2 agglomeration was accelerated by further increase of TiO_2 wt% ranging 30-90%. A similar behavior has been observed for calcination temperature in which the increased calcination temerpatures (500-800^oC) gradually formed bigger TiO_2 agglomerates due to sintering and also reduced physical properties because of antase to rutile phase formation. Consequently, 20wt% TiO_2/KIT-6 nanocomposite optimized photocatalyst showed the higher fuel production rate than that of other titania wt% series. Moreover, these photocatalysts showed different selectivity of the products based on TiO_2 loadings. More H_2 production in by 90 wt% TiO_2/KIT-6 is the clue that there is more H_2O adsoriton and splitting than CO_2 reduction. These photocatalysts are very promising and could be further explored as well as in other applications.

These findings indicate that the highly dispersed isolated Ti materials favor to higher methane production rate than that of other fuel products while on the other hand, Meso.TiO_2 leads to lower hydrocarbon and improved syngas (CO/H_2) production. TiO_2/KIT-6 nanocomposite produced greater extent of fuel products with improved hydrocarbon as well as syngas production rate than other two above mentioned synthesized photocatalysts and H_2 production rate increased with increasing of titania loadings. Therefore, it is concluded that these nanostructured materials can be considered as promising and effective photocatalyst for CO_2 conversion to fuel and as a suitable candidate for other research activities.

References

[1] Bourikas K, Stylidi M, Kondarides D I, Verykios X E. Adsorption of Acid Orange 7 on the surface of titanium dioxide. *Langmuir*, (2005); 21:9222-9230.

[2] Demeestere K, Dewulf J, Langenhove H V. Heterogeneous Photocatalysis as an Advanced Oxidation Process for the Abatement of Chlorinated, Monocyclic Aromatic and Sulfurous Volatile Organic Compounds in Air: State of the Art. Critical Reviews in *Environ Sci Technol,* **(2007)**; 37:489-538.

[3] Fujishima A, Honda K. Electrochemical Photolysis of Water at a Semiconductor Electrode. *Nature,* **(1972)**; 238:37-38.

[4] Yoshida, H. Heterogeneous photocatalytic conversion of carbon dioxide. In Energy Efficiency and Renewable Energy through Nanotechnology. *Green Energy and Technology*; *Zang, L., Ed.;* Springer-Verlag London Limited: London, UK, (**2011)**; 531–559.

[5] Dhakshinamoorthy A, Navalon S, Corma A, Garcia H. Photocatalytic CO_2 reduction by TiO_2 and related titanium containing solids. *Energy Environ Chem,* (**2012)**; 5:9217–9233.

[6] Navalon S, Dhakshinamoorthy A, Alvaro M, Garcia H. Photocatalytic CO_2 reduction using non-titanium metal oxides and sulfides. *ChemSusChem,* (**2013)**; 6:562–577.

[7] Izumi Y. Recent advances in the photocatalytic conversion of carbon dioxide to fuels with water and/or hydrogen using solar energy and beyond. *Coord Chem Rev*, (**2013)**; 257:171–186.

[8] Corma A, Garcia H. Photocatalytic reduction of CO_2 for fuel production: Possibilities and challenges. *J Catal,* (**2013)**; 308:168–175.

[9] Pirkanniemi K, Sillanpaa M. Heterogeneous water phase catalysis as an environmental application: a review. *Chemosphere,* **(2002)**; 48:1047-1060.

References

[10] Mori K, Yamashita H, and Anpo M. Photocatalytic reduction of CO_2 with H_2O on various titanium oxide photocatalysts. *RSC Advances,* **(2012)**; 2:3165-3172.

[11] Yamashita H, Kamada N, He H, Tanaka K. Ehara S and Anpo M. Reduction of CO_2 with H_2O on TiO_2 (100) and TiO_2 (110) Single Crystals under UV-irradiation. *Chem Lett*, (**1994)**; 23:855–858.

[12] Tahir M, Amin N S. Recycling of carbon dioxide to renewable fuels by photocatalysis: Prospects and challenges. *Renew Sust Energ Rev,* **(2013)**; 25:560–579.

[13] Yamashita H, Nishiguchi H, Kamada N, Anpo M, Teraoka Y, Hatano H, Ehara S, Kikui K, Palmisano L, Sclafani A, Fox M. A and Schiavello M. Photocatalytic reduction of CO_2 with H_2O on TiO_2 and Cu/TiO_2 catalysts. *Res Chem Intermed,* (**1994)**; 20:815–823.

[14] Slamet H, Nasution W, Purnama E, Kosela S and Gunlazuardi J. Photocatalytic reduction of CO_2 on copper-doped Titania catalysts prepared by improved-impregnation method. *Catal Commun*, (**2005)**; 6:313–319.

[15] Wu J C S, Lin H M. Photoreduction of CO_2 to methanol via TiO_2 photocatalyst. *Int J Photoenergy*, **(2005)**; 7:115-119.

[16] Anpo M, Yamashita H, Ichinashi Y, & Ehara S. Photocatalytic reduction of CO_2 with H_2O on various titanium oxide catalysts. *J Electroanal Chem,* **(1995)**; 396:21–26.

[17] Vargheese O K, Paulose M, and Latempa T J. High-Rate Solar Photocatalytic Conversion of CO_2 and Water Vapor to Hydrocarbon Fuels. *Nano Lett*, **(2009)**; 9:731-737.

[18] Michalkiewicz B, Majewska J, Kadziolka G, Bubacz K, Mozia S, Morawski A W. Reduction of CO_2 by adsorption and reaction on surface of TiO_2-nitrogen modified photocatalyst. *J CO_2 Utilization*, (**2014)**; 5:47–52.

[19] Wu J C S. Photocatalytic Reduction of Greenhouse Gas CO_2 to Fuel. *Catal Surv Asia,* **(2009)**; 13:30–40.

[20] Sasirekha N, Basha S J S, & Shanthi K. Photocatalytic performance of Ru doped anatase

References

mounted on silica for reduction of carbon dioxide. *Appl Catal B Environ*, **(2006)**; 62:169–180.

[21] Usubharatana P, McMartin D, Veawab A, and Tontiwachwuthikul P. Photocatalytic Process for CO_2 Emission Reduction from Industrial Flue Gas Streams. *Ind Eng Chem Res*, **(2006)**; 45:2558-2568.

[22] Takewaki S J, Hwang S J Yamashita H, and Davis M E. Synthesis of BEA-type molecular sieves using mesoporous materials as reagents. *Micropor Mesopor Mater*, (**1999)**; 32:265–278.

[23] Serpone N, Borgarello E, Grätzel M. Visible light induced generation of hydrogen from H_2S in mixed semiconductor dispersions; improved efficiency through inter-particle electron transfer. *J Chem Soc Chem Commun*, **(1984)**; 342–344

[24] Habisreutinger S N, Schmidt-Mende L, and Stolarczyk J K. Photocatalytic Reduction of CO_2 on TiO_2 and Other Semiconductors. *Angew Chem Int Ed*, (**2013)**; 52:7372–7408.

[25] Lee Y, Kang M. The optical properties of nanoporous structured titanium dioxide and the photovoltaic efficiency on DSSC. *Mater Chem Phys*, **(2010)**; 122:284–289.

[26] Roy S.C, Varghese O.K, Paulose M, Grimes C.A. toward solar fuels: photocatalytic conversion of carbon dioxide to hydrocarbons. *ACS Nano*, **(2007)**; 4:1259–1278.

[27] Jiang Z, Xiao T, Kuznetsov V.L, Edward P P. Turning carbon dioxide into fuel. *Phil Trans R Soc A*, **(2010)**; 368:3343–3364.

[28] Schlaich J, Bergermann R, Schiel W, Weinrebe G. Design of commercial solar updraft tower systems-utilization of solar induced convective flow for power generation. *J Solar Energy Eng*, (**2005)**; 127:117–124.

[29] Abe T, Yoshida T, Tokita S, Taguchi F, Imaya H and Kaneko M. Factors Affecting Selective Electro Catalytic CO_2 Reduction with Cobalt Phthalocyanine Incorporated in a Polyvinylpyridine Membrane Coated on a Graphite Electrode. *J Electroanal Chem*, **(1996)**; 412:125–132.

References

[30] Regan B.O, Gratzel M. A low-cost, high-efficiency solar cell based on dye-sensitized colloidal TiO_2 films. *Nature,* **(1991)**; 353:737–740.

[31] Blossey R. Selfcleaning surfaces-virtual realities. *Nat Mater*, **(2003)**; 2:301–306.

[32] Bach U, Corr D, Lupo D, Pichot F, Ryan M. Nano materials-based electrochromics for paper-quality displays. *Adv Mater,* **(2002)**; 14:845–848

[33] Chueh W C, and Haile S M. Ceria as a Thermochemical Reaction Medium for Selectively Generating Syngas or Methane from H_2O and CO_2. *ChemSusChem,* **(2009)**; 2:735–739.

[34] Blankenship R E, Tiede D M, Barber J, Brudvig G W, Fleming G, Ghirardi M, Gunner M R, Junge W, Kramer D M, Melis A, Moore T A, Moser C C, Nocera D G, Nozik A J, Ort D R, Parson W W, Prince R C and Sayre R T. Comparing Photosynthetic and Photovoltaic Efficiencies and Recognizing the Potential for Improvement. *Sci*, **(2011)**; 332:805–809.

[35] Halmann M. Photoelectrochemical reduction of aqueous carbon dioxide on p-type gallium phosphide in liquid junction solar cells. *Nature,* (**1978)**; 275:115–116.

[36] Michele A. Carbon Dioxide as Chemical Feedstock. Weinheim: *Wiley-VCH*. (**2000)**.

[37] Olah G A, Goeppert A, Prakash G K S. Chemical recycling of carbon dioxide to methanol and dimethyl ether: from greenhouse gas to renewable, environmentally carbon neutral fuels and synthetic hydrocarbons. *J Org Chem*, (**2009)**; 74:487-498.

[38] Inoue T, Fujishima A, Konishi S, & Honda K. Photoelectro catalytic reduction of carbon dioxide in aqueous suspensions of semiconductor powders. *Nature*, **(1979)**; 277:637–638.

[39] Palmisano G, Augugliaro V, Pagliaro M, Palmisano L. Photocatalysis: a promising route for 21st century organic chemistry. *Chem Commun,* (**2007)**; 33:3425-3437.

[40] Bhatkhande D S, Pangarkar V G, Beenackers A A C M. Photocatalytic degradation for environmental applications. a review. *J Chem Technol Biotechnol*, **(2001)**; 77:102–116.

[41] Kitano M, Matsuoka M, Ueshima M, Anpo M. Recent developments in titanium oxide based photocatalysts. *Appl Catal A,* **(2007)**; 325:1–14.

[42] Fox M A, Dulay M T. Heterogeneous photocatalysis. *Chem Rev,* **(1993)**; 93 341–357.

References

[43] Hussain M, Ceccarelli R, Marchisio D L, Fino D, Russo N, Geobaldo F. Synthesis, characterization, and photocatalytic application of novel TiO_2 nanoparticles. *Chem Eng J,* **(2010)**; 157:45–51.

[44] Indrakanti V P, Kubicki J D and Schobert H H. Photoinduced Activation of CO_2 on Ti-based Heterogeneous Catalysts: Current State, Chemical Physics based Insights and Outlook. *Energy Environ Sci*, **(2009)**; 2:745–758.

[45] Centi G, Perathonar S. Facing the Energy Challenge Through Chemistry in a Changing World, in The Chemical Element: Chemistry's Contribution to Our Globe Future, Garcia-Martinez, J, Serrano-Torregrosa, E. (Ed.s) *Wiley-VCH Pub, Weinheim (Germany)* (**2011)**; Ch. 8, 269-307

[46] KPMG International. The Future of the European Chemical Industry. (**2010)**. Publication number:1001503.(http://www.kpmg.com/Global/en/IssuesAndInsights/ArticlesPublications/Lists/ Expired/The-Future-of-the-European-Chemical-Industry.pdf 41.A).

[47] Kearner T. Chemical Industry Vision 2030: A European Perspective. (**2012)**. (https://www. atkearney.com/documents/10192/536196/Chemical + Industry + Vision + 2030 + A + European + Perspective. pdf/7178b150-22d9-4b50-9125-1f1b3a9361ef).

[48] Deloitte Touche Tohmatsu Chemical Group and Deloitte Research (US). The decadeahead. Preparing for an unpredictable future in the global chemical industry. **(2010)**.(http://www2.deloitte.com/content/dam/Deloitte/global/Documents/Manufacturing/ gx_thedecadeahead_final_lowres_v3.pdf).

[49] Lemonidou A A, Valla J, Vasalos I A. in: Aresta M. (Ed.), Carbon Dioxide Recovery 231. and Utilization, *Kluwer Acad. Pub*. (now Springer-Verlag, Germany), Dordrecht, The Netherlands, (**2003)**; 373.

[50] Saito M. R&D activities in Japan on methanol synthesis from CO_2 and H_2. *Catal Sur Jpn*, **(1998)**; 2:175-184.

[51] Rohde M, Unruh D, Pias P, Lee K W, Shaub G. Fischer-Tropsch synthesis with CO_2-containing syngas from biomass Kinetic analysis of fixed bed reactor model experiments

References

Carbon dioxide utilization for global sustainability. *Stud Surf Sci Catal*, **(2004)**; 153:97-102.

[52] Sakakura T, Choi J C, Yasuda H. Transformation of Carbon Dioxide. *Chem Rev*, **(2007)**; 107:2365-2387.

[53] Centi G, Perathonar S. Catalysis transformation of CO_2 to fuels and chemicals with references to bio refineries. In The Role of Catalysis for the Sustainable Production of Bio-fuels and Bio-chemicals , *Elsevier*, The Netherland, **(2013)**; Ch 16, 529-555.

[54] Centi G and Perathoner S. Opportunities and Prospects in the Chemical Recycling of Carbon Dioxide to Fuels. *Catal Today*, (**2009)**; 148:191–205.

[55] Hashimoto K, Habazaki H, Yamasaki M, Meguro S, Sakaki T, Katagiri H, Matsui T, Fujimara K, Izumiya K, Kumagai H, Akiyama E. Advanced Materials for Global Carbon Dioxide Recycling. *Mater Sci Eng* A, (**2001)**; 304-306:88–96.

[56] Fierro J L G, (Ed.) by J L G Fierro. Metal Oxides Chemistry and Applications, *CRC Taylor & Francis Pub*, Boca Raton, FL, USA, (**2006)**; p 569 (Chapter 18).

[57] Ghenciu A.F. Review of fuel processing catalysts for hydrogen production in PEM fuel cell systems. *Curr Opin Solid State Mater Sci*, **(2002)**; 6:389.

[58] Tanaka Y, Utaka T, Kikuchi R, Sasak K, Eguchi K. CO removal from reformed fuel over $Cu/ZnO/Al_2O_3$ catalysts prepared by impregnation and coprecipitation methods. *Appl Catal A Gen*, **(2003)**; 238:11-18.

[59] Olah A, Goeppert A, Prakash G K S. Beyond Oil and Gas: The Methanol Economy, *Wiley-VCH Pub, Weinheim, Germany*, (**2006)**.

[60] Lachowska M, Skrzypek J. Ga, Mn, and Mg promotedcopper/zinc/zirconia-catalysts for hydrogenation of carbon dioxide to methanol. *Stud Surf Sci Catal*, **(2004)**; 153:173-176.

[61] STOA (European Parliament), Methanol: a future transport fuel based on hydrogen and carbon dioxide. (**2014)**.

[62] Gallou I. Un symmetrical ureas. Synthetic methodologies and application in drug design. *Org Prep Proc Int*, (**2007)**; 39:355-383.

References

[63] Zhang K, Sawaya M R, Eisenberg D S, Liao J C. Expanding metabolism for biosynthesis of non-natural alcohols. *PNAS,* (**2008)**; 105:20653-20658.

[64] Woolerton T W, Sheard S, Reisner E, Pierce E, Ragsdale S W, Armstrong F A. Efficient and Clean Photoreduction of CO_2 to CO by Enzyme-Modified TiO_2 Nanoparticles Using Visible Light. *J Am Chem Soc,* (**2010)**; 132:2132-2133.

[65] Woolerton T W, Sheard S, Pierce E, Ragsdale S W, Armstrong F A. CO_2 photoreduction at enzyme-modified metal oxide nanoparticles. *Energy Environ Sci,* (**2011)**; 4:2393-2399.

[66] Chaudhary Y S, Woolerton T W, Allen C S, Warner J H, Pierce Eh, Ragsdale S W, Armstrong F A. Visible light-driven CO_2 reduction by enzyme coupled CdS nanocrystals. *Chem Commun,* (**2012)**; 48:58-60.

[67] Henstra A H, Sipma J, Rinzema A, Stams A J M. Microbiology of synthesis gas fermentation for biofuel production. *Curr Opin Biotechnol,* (**2007)**; 18:200-206.

[68] Sharma Y C, Singh B, Upadyay S N. Advancements in Development and Characterization of Biodiesel: A Review. *Fuel,* (**2008)**; 87:2355–2373.

[69] Chisti Y. Biodiesel from Microalgae. *Bio-technol Adv,* (**2007)**; 25:294–306.

[70] Roy S C, Varghese O K, Paulose M, and Craig A. Grimes Toward Solar Fuels: Photocatalytic Conversion of Carbon Dioxide to Hydrocarbons. *ACS Nano,* (**2010)**; 4:1259–1278.

[71] Morton, O. Eating the Sun: How Plants Power the Planet; *Harper: New York*, **(2008)**.

[72] Galvez M E, Loutzenhiser P G, Hischier I, Steinfeld A. CO_2 Splitting via Two-Step Solar Thermochemical Cycles with Zn/ZnO and FeO/Fe_3O_4 Redox Reactions: Thermodynamic Analysis. *Energy Fuel,* (**2008)**; 22:3544–3550.

[73] Riduan S N, Zhang Y, Ying J Y. Conversion of carbon dioxide into methanol with silanes over N-heterocyclic carbene catalysts. *Angew Chem Int Ed,* (**2009)**; 48:3322-3325.

References

[74] Matsuo T, Kawaguchi H. From Carbon Dioxide to Methane: Homogeneous Reduction of Carbon Dioxide with Hydrosilanes Catalyzed by Zirconium−Borane Complexes. *J Am Chem Soc*, (**2006)**; 128:12362-12363.

[75] Wesselbaum S, vom Stein T, Klankermayer J, Leitner W. Hydrogenation of Carbon Dioxide to Methanol using a Homogeneous Ruthenium-Phosphine Catalyst. *Angew Chem Int Ed*, (**2012)**; 51:7499-7502.

[76] Ashley A E, Thompson A L, O'Hare D. Non-Metal Mediated Homogeneous Hydrogenation of CO_2 to CH_3OH. *Angew Chem Int Ed*, (**2009)**; 48:9839–9843.

[77] Balaraman E, Gunanathan C, Zhang J, Shimon L J w, Milstein D. Efficient Hydrogenation of Organic Carbonates, Carbamates and Formates Indicates Alternative Routes to Methanol Based on CO_2 and CO. *Nature Chem*, **(2013)**; 609-614.

[78] Zhang Y, Riduan S N. Catalytic Hydrocarboxylation of Alkenes and Alkynes with CO_2. *Angew Chem Int Ed*, (**2011)**; 50:6210–6212.

[79] Ampelli C, Perathoner S, Centi G. CO_2 utilization: an enabling element to move to a resource and energy efficient chemical production. *Phil Trans R Soc A*, **(2014)**. submitted.

[80] Jhong H-R, Ma S, Kenis P J A. Electrochemical conversion of CO_2 to useful chemicals: current status, remaining challenges, and future opportunities, *Curr Opin Chem Eng*, (**2013)**; 2:191–199.

[81] Centi G, Van Santen RA. Catalysis for Renewables: From Feedstock to Energy Production, *Wiley-VCH Pub*: (**2009)**; Germany.

[82] Centi G, Lanzafame P, Parathoner S. Introduction and General Overview, In Catalysis for Alternative Energy Generation, Springer, Germany, **(2012)**; Ch 1:1-28.

[83] SPIRE (Sustainable Process Industry through Resource and Energy Efficiency). Roadmap. **(2013)**.

References

[84] Adachi K, Ohta K, & Mizuno M. Photocatalytic reduction of carbon dioxide to hydrocarbon using copper loaded titanium dioxide. *Sol Energy*, **(1994)**; 53:187–190.

[85] Yamashita H, Shiga A, Kawasaki S, Ichihashi Y, Ehara S, & Anpo M. Photocatalytic synthesis of CH_4 and CH_3OH from CO_2 and H_2O on highly dispersed active titanium oxide catalysts. *Energy Conv Manag*, **(1995)**; 36:617–620.

[86] Anpo M, Yamashita H, Ichihashi Y, Fujii Y, & Honda M. Photocatalytic reduction of CO_2 with H_2O on titanium oxides anchored within micro pores of zeolites: effects of the structure of the active sites and the addition of Pt. *J Phys Chem B,* **(1997)**; 101:2632–2636.

[87] Anpo M, Yamashita H, Ikeue K, Fujii Y, Zhang S G, Ichihashi Y G, Park D R, Suzuki Y, Koyano K, & Tatsumi T. Photocatalytic reduction of CO_2 with H_2O on Ti-MCM-41 and Ti-MCM-48 mesoporous zeolite catalysts. *Catal Today*, **(1998)**; 44:327–332.

[88] Yamashita H, Fujii Y, Ichinashi Y, Zhang S. G, Ikeue K, Park D. R, Koyano K, Tatsumi T, & Anpo M. Selective formation of CH_3OH in the photocatalytic reduction of CO_2 with H_2O on titanium oxides highly dispersed within zeolites and mesoporous molecular sieves. *Catal Today*, **(1998)**; 45:221–227.

[89] Subrahmanyam M, Kaneco S, & Alonso-Vante N. A screening for the photoreduction of carbon dioxide supported on metal oxide catalysts for C1-C3 selectivity. *Appl Catal B Environ*, **(1999)**; 23:169–174.

[90] Tan S S, Zou L, & Hu, E. Photocatalytic reduction of carbon dioxide into gaseous hydrocarbon using TiO_2 pellets. *Catal Today*, **(2006)**; 115:269–273.

[91] Xia X H, Jia Z J, Yu Y, Liang Y, Wang Z, & Ma L L. Preparation of multiwalled carbon nanotube supported TiO_2 and its photocatalytic activity in the reduction CO_2 with H_2O. *Carbon*, **(2007)**; 45:717–721.

[92] Kočí K, Obalová L, & Lacný Z. Photocatalytic reduction of CO_2 over TiO_2 based catalyst. *Chem Pap,* **(2008)**; 62:1–9.

[93] Graves C, Ebbesen S D, Mogensen M, Lackner K S. Sustainable hydrocarbon fuels by recycling CO_2 and H_2O with renewable or nuclear energy. *Renew Sust Energ Rev*, (**2011)**; 15:1–23.

References

[94] Liu and Li. Understanding the Reaction Mechanism of Photocatalytic Reduction of CO_2 with H_2O on TiO_2-Based Photocatalysts: *Aerosol Air Qual Res,* **(2014)**; 14:453–469.

[95] Pichon A A Stretch to Save the World, *Energy Mater*, (**2010)**. (http:// www.Natureasia.com / en / nchina / article / 10.1038 / nchina. 2010.126).

[96] Marland G, Boden T A, Andres R J. Global, Regional, and National CO_2 Emissions, in: Trends: A Compendium of Data on Global Change, Carbon Dioxide Information Analysis Center, Oak Ridge *National. Laboratory*, U.S. *Department of Energy, Oak Ridge*, Tenn., U.S.A, (**2005)**.

[97] Keeling C D, Whorf T P. Atmospheric CO_2 records from sites in the SiO air sampling network, in: Trends: A Compendium of Data on Global Change. Carbon Dioxide Information Analysis Center, Oak Ridge National Laboratory, U. S. *Department of Energy, Oak Ridge*, TN, USA, (**2005)**

[98] Lindsey J S. Carbon Dioxide. *McGraw-Hill Encyclopedia of Chemistry*, second ed., McGraw-Hill, New York, (**1993)**; 157–159.

[99] Pierantozzi R. fourth ed., Carbon Dioxide. Kirk-Othmer Encyclopedia of Chemical Technology, vol. 5, *John Wiley and Sons*, New York, (**1993)**; 35–53.

[100] Li Y, Wang W N, Zhan Z, Woo M H, Wu C Y, Biswas P. Photocatalytic reduction of CO_2 with H_2O on mesoporous silica supported Cu/TiO_2 catalysts. *Appl Catal B Environ,* (**2010)**; 100:386–392.

[101] Anpo M. Photocatalytic reduction of CO_2 with H_2O on highly dispersed Ti-oxide catalysts as a model of artificial photosynthesis. *J CO_2 Utilization,* (**2013)**; 1:8–17.

[102] Thampi K R, Kiwi J, & Grätzel M. Methanation and photo-methanation of carbon dioxide at room temperature and atmospheric-press. *Nature,* **(1987)**; 327:506–508.

[103] Melsheimer J, Guo W, Ziegler D, Wesemann M, Schlogl, R. Methanation and photo methanation of carbon dioxide over Ru/Titania at room temperature exploration for a photoassisted catalytic reaction. *Catal Lett,* **(1991)**; 11:157–168.

[104] Tan S S, Zou L, Hu E. Photosynthesis of hydrogen and methane as key components for clean energy system. *Sci Tech Adv Mater,* **(2007)**; 8:89–92.

References

[105] Marcì G, García-López E I, Palmisano L. Photocatalytic CO_2 reduction in gas–solid regime in the presence of H_2O by using GaP/TiO_2 composite as photocatalyst under simulated solar light. *Catal Commun*, **(2014)**; 53:38–41.

[106] Wu J C S, Wu T H, Chu T, Huang H, Tsai D. Application of Optical-fiber photoreactor for CO_2 Photocatalytic Reduction. *Top Catal*, **(2008)**; 47:131–136.

[107] Liu Q, Zhou Y, Kou J, Chen X, Tian Z, Gao J, Yan S, Zou Z. High-yield synthesis of ultralong and ultrathin Zn_2GeO_4 nanoribbons toward improved photocatalytic reduction of CO_2 into renewable hydrocarbon fuel. *J Am Chem Soc*, **(2010)**; 132:14385–14387.

[108] Asi M A, Hea C, Su M, Xia D, Lin L, Deng H, Xiong Y, Qiu R. Li X Z. Photocatalytic reduction of CO_2 to hydrocarbons using $AgBr/TiO_2$ nanocomposites under visible light. *Catal Today*, **(2011)**; 175:256–263.

[109] Liang Y T, Vijayan B K, Gray K A, Hersam M C. Minimizing graphene defects enhances titania nanocomposite-based photocatalytic reduction of CO_2 for improved solar fuel production. *Nano Lett*, **(2011)**; 11:2856–2860.

[110] Shi H, Wang T, Chen J, Zhu C, Ye J, Zou Z. Photoreduction of carbon dioxide over $NaNbO_3$ nanostructured photocatalysts. *Catal Lett*, **(2011)**; 141:525–530.

[111] Yang C C, Vernimmen J, Meynen V, Cool P and Mul G. Mechanistic Study of Hydrocarbon Formation in Photo catalytic CO_2 Reduction over Ti-SBA-15. *J Catal*, **(2011)**; 284:1–8.

[112] Zhou Y, Tian Z, Zhao Z, Liu Q, Kou J, Chen X, Gao J, Yan S, Zou Z. High-yield synthesis of ultrathin and uniform Bi_2WO_6 square nanoplates benefitting from photocatalytic reduction of CO_2 into renewable hydrocarbon fuel under visible light. *ACS Appl Mater Interfaces*, **(2011)**; 3:3594–3601.

[113] Feng X, Sloppy J D, LaTempa T J, Paulose M, Komarneni S, Bao N, Grimes, C A. Synthesis and deposition of ultrafine Pt nanoparticles within high aspect ratio TiO_2 nanotube arrays: application to the photocatalytic reduction of carbon dioxide. *J Mater Chem*, **(2011)**; 21:13429–13433.

References

[114] Tahir M, Amin N S. Photocatalytic reduction of carbon dioxide with water vapors over montmorillonite modified TiO_2 nanocomposites. *Appl Catal B Environ*, **(2013)**; 142–143:512–22.

[115] Bahnemann D W, Kormann C, Hoffmann M R. Preparation and characterization of quantum size zinc oxide: A detailed spectroscopic study. *J Phys Chem*, (**1987)**; 91:3789–3798.

[116] Sivula K, Formal F L, Grätzel M. WO_3-Fe_2O_3 Photo anodes for water splitting: A host scaffold, guest absorber approach. *Chem Mater*, (**2009)**; 21:2862–2867.

[117] Koci K, Obalova L, Matejova L, Placha D, Lacny Z, Jirkovsky J, Solcova O. Effect of TiO_2 particle size on the photocatalytic reduction of CO_2. *Appl Catal B Environ*, **(2009)**; 89:494–502.

[118] Sahu D R, Hong L Y, Wang S C, Huang J L. Synthesis, analysis and characterization of ordered mesoporous TiO_2/SBA-15 matrix: Effect of calcination temperature *Micropor Mesopor Mater*, **(2009)**; 117:640–649.

[119] Rao G G, Dhar N R. Bulletin of the Academy of Sciences of the United Provinces of Agra and Oudh, Allahabad, India **(1932)**; 1:69–75.

[120] Rao G G. NEWER ASPECTS OF NITRIFICATION: I *Soil Science*, **(1934)**; 38:143–160.

[121] Goodeve C F, Kitchener J A. The mechanism of photosensitisation by solids. *Trans Faraday Soc*, **(1938)**; 34:902–908.

[122] Hashimoto K, Irie H, Fujishima A. TiO_2 Photocatalysis: A Historical Overview and Future Prospects. *Jap J Appl Phys*, **(2005)**; 44 8269–8285.

[123] Frank S N, Bard A J. Heterogeneous photocatalytic oxidation of cyanide ion in aqueous solutions at titanium dioxide powder. *J Am Chem Soc*, (**1977)**; 99:303–304.

[124] Kreutler B, Bard A J. Heterogenous photocatalytic preparation of supported catalyst. Photodeposition of platinum on titanium dioxide powder and other substrates. *J Am Chem Soc*, (**1978)**; 100:4317–4318.

[125] Fujishima A, Ohtsuki J, Yamashita T, Hayakawa S. Behavior of tumor cells on photoexcited semiconductor surface. *Photomed Photobiol*, (**1986)**; 8:45–46.

[126] Fujishima A, Rao T N, Tryk D A. Titanium dioxide photocatalysis. *J Photochem Photobiol C Photochem* Rev, (**2000)**; 1:1–21.

References

[127] Watson S, Beydoun D, Amal R. Synthesis of a novel magnetic photo catalyst by direct deposition of nanosized TiO_2 crystals onto a magnetic core. *J Photochem Photobiol A Chem*, (**2002)**; 148:303–311.

[128] Sreethawong T, Suzuki Y, Yoshikawa S. Synthesis, characterization, and photocatalytic activity for hydrogen evolution of nanocrystalline mesoporous titania prepared by surfactant-assisted templating sol-gel process. *J Solid State Chem*, (**2005)**; 178:329–338.

[129] Tan S, Zou L, Hu E. Kinetic modelling for photosynthesis of hydrogen and methane through catalytic reduction of carbon dioxide with water vapor. *Catal Today*, **(2008)**; 131:125–129.

[130] Tan J Z Y, Fernandez Y, Liu D, Maroto-Valer M, Bian J, Zhang X. Photoreduction of CO_2 using copper-decorated TiO_2 nanorod films with localized surface plasmo behavior. *Chem Phys Lett*, **(2012)**; 531:149–154.

[131] Diebold U. The surface science of titanium dioxide. *Sur Sci Rep*, (**2003)**; 48:53–229.

[132] Lan Y, Lu Y, Ren Z. Mini review on photocatalysis of titanium dioxide nanoparticles and their solar applications. *Nano Energy*, **(2013)**; 2:1031–1045.

[133] Karakitsou K E, Verykios X E. Effects of altervalent cation doping of titania on its performance as a photocatalyst for water cleavage. *J Phys Chem*, **(1993)**; 97:1184-1189.

[134] Sclafani A, Palmisano L, Schiavello M. Influence of the preparation methods of titanium dioxide on the photocatalytic degradation of phenol in aqueous dispersion. *J Phys Chem*, (**1990)**; 94:829–832.

[135] Bouras P, Stathatos E, Lianos P. Pure versus metal-ion-doped nanocrystal line titania for photocatalysis. *Appl Catal B Environ*, **(2007)**; 73:51–59.

[136] Schulte K L, DeSario P A, Gray K A. Effect of crystal phase composition on the reductive and oxidative abilities of TiO_2 nanotubes under UV and visible light. *Appl Catal B Environ*, **(2010)**; 97:354–360.

[137] Liu G, Hoivik N, Wang K, Jakobsen H. Engineering TiO_2 nano materials for CO_2 conversion/solar fuels. *Solar Energy Mater Solar Cells*, **(2012)**; 105:53–68.

[138] Zhang H Z and Banfield J F. Understanding polymorphic phase transformation behavior during growth of nanocrystalline aggregates: Insights from TiO_2. *J Phys Chem* B, **(2000)**; 104:3481-3487.

References

[139] Hao W C, Zheng S K, Wang C, Wang T M. Comparison of the photocatalytic activity of TiO_2 powder with different particle size. *J Mater Sci Lett*, **(2002)**; 21:1627–1629.

[140] Almquist, C B, Biswas P. Role of synthesis method and particle size of nanostructured TiO_2 on its photoactivity. *J Catal*, **(2002)**; 212:145–156.

[141] Yu K, Yu W, Kuo M, Liou Y, Chien S. Pt/titania-nanotube: a potential catalyst for CO_2 adsorption and hydrogenation. *Appl Catal B Environ*, **(2008)**; 84:112–118.

[142] Wang C, Thompson R L, Baltrus J, Matranga C. Visible light photoreduction of CO_2 using CdSe/Pt/TiO_2 heterostructured catalysts. *J Phys Chem Lett*, **(2010)**; 1:48–53.

[143] Li C, Li M. UV Raman spectroscopic study on the phase transformation of ZrO_2, Y_2O_3–ZrO_2 and SO_{42}/ZrO_2. wiley Online Library. *J Raman Spectroscopy*, **(2002)**; 33:301-308.

[144] Mizuno T, Adachin K, Ohta K, Saji A. Effect of CO_2 pressure on photocatalytic reduction of CO_2 using TiO_2 in aqueous solutions. *J Photochem Photobiolo A Chem*, **(1996)**; 98:87–90.

[145] Kaneco S, Kurimoto H, Ohta K, Mizuno T, Saji A. Photocatalytic reduction of CO_2 using TiO, powders in liquid CO_2 medium. *J Photochem Photobiol A Chem*, **(1997)**; 109:59–63.

[146] Liu B, Torimoto T, Matsumoto H, Yoneyama H. Effect of solvents on photocatalytic reduction of carbon dioxide using TiO_2 nanocrystal photocatalyst embedded in SiO_2 matrices. *J Photochem Photobiol A Chem*, **(1997)**; 108:187–192.

[147] Kaneco S, Shimizu Y, Ohta K, Mizuno T. Photocatalytic reduction of high pressure carbon dioxide using TiO_2 powders with a positive hole scavenger. *J Photochem Photobiol A Chem*, **(1998)**; 115:223–226.

[148] Kohno Y, Hayashi H, Takenaka S, Tanaka T, Funabiki T, Yoshida S. Photo-enhanced reduction of carbon dioxide with hydrogen over Rh/TiO_2. *J Photochem Photobiolo A Chem*, (**1999)**; 126:117–23.

[149] Kaneco S, Kurimoto H, Shimizu Y, Ohta K, Mizuno T. Photocatalytic reduction of CO_2 using TiO_2 powders in supercritical fluid CO_2. *Energy*, **(1999)**; 24:21–30.

References

[150] Ikeue K, Nozaki S, Ogawa M, Anpo M. Characterization of self-standing Ti- containing porous silica thin films and their reactivity for the photocatalytic reduction of CO_2 with H_2O. *Catal Today,* (**2002)**; 74:241–8.

[151] Shioya Y, Ikeue K, Ogawa M, Anpo M. Synthesis of transparent Ti-containing mesoporous silica thin film materials and their unique photocatalytic activity for the reduction of CO_2 with H_2O. *Appl Catal A Gen,* (**2003)**; 254:251–259.

[152] Ku Y, Lee W, Wang W. Photocatalytic reduction of carbonate in aqueous solution by UV/TiO_2 process. *J Mole Catal A Chem,* **(2004)**; 212:191–196.

[153] Hwang J S, Chang J S, Park S.E, Ikeue K, Anpo M. High performance photo catalytic reduction of CO_2 with H_2O by Ti-SBA-15 mesoporous material. *Stud Sur Sci Catal,* (**2004)**; 153:299–302.

[154] Dey G R, Belapurkar A D, Kishore K. Photocatalytic reduction of carbon dioxide to methane using TiO_2 as suspension in water. *J Photochem Photobiol A Chem,* **(2004)**; 163:503–508.

[155] Wu J C S, Lin H M, Lai C L. Photoreduction of CO_2 to methanol using optical fiber photoreactor. *Appl Catal A Gen,* (**2005)**; 296:194–200.

[156] Lo C, Hung C, Yuan C, Wu J. Photoreduction of carbon dioxide with H_2 and H_2O over TiO_2 and ZrO_2 in a circulated photocatalytic reactor. *Solar Energy Mater Solar Cells,* **(2007)**; 91:1765–1774.

[157] Kočí K, Matěju K, Obalová L, Krejčíková S, Lacný Z, Plachá D. Effect of silver doping on the TiO_2 for photocatalytic reduction of CO_2. *Appl Catal B Environ,* (**2010)**; 96:239–44.

[158] Dimitrijevic N M, Vijayan B K, Poluektov O G, Rajh T, Gray K A, He H Y and Zapol P. Role of Water and Carbonates in Photocatalytic Transformation of CO_2 to CH_4 on Titania. *J Am Chem Soc*, **(2011)**; 133:3964–3971.

References

[159] Liu L J, Zhao C Y and Li Y. Spontaneous Dissociation of CO_2 to CO on Defective Surface of Cu(I)/TiO_{2-X} Nanoparticles at Room Temperature. *J Phys Chem C*, **(2012)**; 116:7904–7912.

[160] Zhang Q Y, Gao T T, Andino J M and Li Y. Copper and Iodine Co-modified TiO_2 Nanoparticles for Improved Activity of CO_2 Photoreduction with Water Vapor. *Appl Catal B Environ*, **(2012)**; 123–124:257–264.

[161] Uner D. and Oymak M M. On the Mechanism of Photocatalytic CO_2 Reduction with Water in the Gas Phase. *Catal Today*, **(2012)**; 181:82–88.

[162] Zhao C Y, Liu L J, Zhang Q Y, Wang J and Li Y. Photocatalytic Conversion of CO_2 and H_2O to Fuels by Nanostructured Ce-TiO_2/SBA-15 Composites. *Catal Sci Technol*, (**2012)**; 2558–2568.

[163] Wang P Q, Bai Y, Liu J Y, Fan Z and Hu Y Q. One-pot Synthesis of Rutile TiO_2 Nanoparticle Modified Anatase TiO_2 Nanorods Toward Enhanced Photocatalytic Reduction of CO_2 into Hydrocarbon Fuels. *Catal Commun*, **(2012)**; 29:185–188.

[164] Hussain M, Akhter P, Russo N, Saracco G. Novel Ti-KIT-6 material for the photocatalytic reduction of carbon dioxide to methane. *Catal Commun*, (**2013)**; 36:58-62.

[165] Mei B, Pougin A, Strunk J. Influence of photo deposited gold nanoparticles on the photocatalytic activity of titanate species in the reduction of CO_2 to hydrocarbons. *J Catal*, **(2013)**; 306:184–189.

[166] Tahir M, Amin N S. Photocatalytic CO_2 reduction with H_2O vapors using montmorillonite/TiO_2 supported microchannel monolith photoreactor. *Chem Eng J*, **(2013)**; 230:314–327.

[167] Akhter P, Hussain M, Saracco G, Russo N. New nanostructured silica incorporated with isolated Ti material for the photocatalytic conversion of CO_2 to fuels. *Nanoscale Res Lett*, (**2014)**; 9:158.

References

[168] Hoffmann M R, Martin, S T, Choi W, Bahnemann D W. Environmental Applications of Semiconductor Photocatalysis. *Chem Rev*, **(1995)**; 95:69-96.

[169] Thu H B, Karkmaz M, Puzenat E, Guillard C, Herrmann J.From the fundamentals of photocatalysis to its application in environmental protection and in solar purification of water in arid countries. *Res Chem Intermed*, (2005); 31:449–461.

[170] Chong M N, Jin B, Saint C P. Bacterial inactivation kinetics of a photo-disinfection system using novel titania-impregnated kaolinite photocatalyst. *Chem Eng J*, **(2011)**; 171:16–23.

[171] Jwo C, Chang H, Kao M, Lin C. Photo decomposition of volatile organic compounds using TiO_2 nanoparticles. *J Nanosci Nano Technol*, **(2007)**; 7:1947-1952.

[172] Duan X, Sun D, Zhu Z, Chen X, Shi P. Photocatalytic decomposition of toluene by TiO_2 film as photocatalyst. *J Environ Sci Health*: A, **(2002)**; 37:679-692.

[173] Ku Y, Chen J S, Chen H W. Decomposition of Benzene and Toluene in Air Streams in Fixed-Film Photoreactors Coated with TiO_2 Catalyst. *J Air Waste Manag Assoc*, **(2007)**; 57:279–285.

[174] Rezaee A, Pourtaghi Gh H, Khavanin A, Mamoory R S, Ghaniean M T, Godini H. Photocatalytic decomposition of gaseous toluene by TiO_2 nanoparticles coated on activites carbon. Iranian *J Environ Sci Eng*, **(2008)**; 5:305-310.

[175] Fujishima A, Zhang X. Titanium dioxide photocatalysis: present situation and future approaches. *Chimie*, **(2006)**; 9:750–760.

[176] Zubillaga O, Cano F G, Azkarate I, Molchan I S, Thompson G E, Skeldon P. Synthesis of anodic films in the presence of aniline and TiO_2 nanoparticles on AA2024-T_3 aluminium alloy. *Thin Solid Films*, **(2009)**; 517:6742-6746.

[177] Gotfredsen K. Wennerberg A, Johansson C, Skovgaard L T, Hjorting-Hansen E. Anchorage of TiO_2-blasted, HA-coated, and machined implants: an experimental study with rabbits. *J Biomed Mater Res*, **(1995)**; 29:1223-1231.

[178] Kar A, Raja K S, Misra M. Electro deposition of hydroxyapatite onto nanotubular TiO_2 for implant applications. *Surf Coat Technol*, **(2006)**; 201:3723-3731.

[179] Phillips L G, Barbano D M. The Influence of Fat Substitutes Based on Protein and Titanium Dioxide on the Sensory Properties of Lowfat Milks. *J Dairy Sci*, **(1997)**; 80:2726-2731.

References

[180] Hewitt J P. *Cosmet Toiletries*, **(1999)**; 114:59-63.

[181] Nakata K, Fujishima A. Design and applications. *J Photochem Photobiol C Photochem Rev*, **(2012)**; 13:169–189.

[182] IPCC Third Assessment Report-Climate Change. **(2001)**. **(**http://www.grida.no / publications / other / ipcc_tar / ?src /).

[183] Intergovernmental Panel on Climate Change (IPCC), Climate Change, Synthesis report, Cambridge University Press, Cambridge, UK, **(2001)**.

[184] Etheridge D M, Steele L P, Langenfelds R L, Francey R J, Barnola J M, Morgan V I. Historical CO_2 record from the Law Dome DE08, DE08-2, and DSS ice cores (atmospheric CO_2 concentrations, Antarctic ice cores). In: Trends: A Compendium of Data on Global Change, on line at the Carbon Dioxide Information Analysis Center, (http://cdiac.esd.ornl.gov). June (**1998)**.

[185] Keeling C D, Whorf T P. Atmospheric CO_2 records from sites in the SiO air sampling network, in: Trends: A Compendium of Data on Global Change. Carbon Dioxide Information Analysis Center, Oak Ridge National Laboratory, *U. S. Department of Energy*, Oak Ridge, TN, USA, **(2005)**.

[186] Song C. Global challenges and strategies for control, conversion and utilization of CO_2 for sustainable development involving energy, catalysis, adsorption and chemical processing. *Catal Today*, **(2006)**; 115:2–32.

[187] What the Future Holds in Store, in: World Climate Report, The Web's Longest-Running Climate Change Blog, 30 January, **(2008),** available from: (http://www.worldclimatereport.com/index.php/2008/01/30/what-the-future-holds-in-store/).

[188] Jacobson M Z. Control of fossil-fuel particulate black carbon and organic matter, possibly the most effective method of slowing global warming. *J Geophys Res*, (**2002)**; 107:16-22.

[189] Kuramochi T, Ramírez A, Turkenburg W, Faaij A. Techno-economic prospects for CO_2 capture from distributed energy systems. *Renew Sust Energ Rev,* (**2013)**; 19:328–347.

[190] Riemer P. Greenhouse gas mitigation technologies, an overview of the CO_2 capture,

storage and future activities of the IEA Greenhouse Gas R&D programme. *Energy Conv Manag*, **(1996)**; 37:665–670.

[191] Meisen A & Shuai X. Research and development issues in CO_2 capture. *Energy Conv Manag*, **(1997)**; 38:37–42.

[192] Dijkstra J W, & Jansen D. Novel concepts for CO_2 capture. *Energy*, **(2004)**; 29:1249–1257.

[193] Mani F, Peruzzini M, Stoppioni P. CO_2 absorption by aqueous NH_3 solutions: speciation of ammonium carbamate, bicarbonate and carbonate by a 13C NMR study. *Green Chem*, **(2006)**; 8:995–1000.

[194] Freund H J, Roberts M W. Surface chemistry of carbon dioxide. *Surf Sci Rep*, (**1996)**; 25:225–273.

[195] Pan X, Fan Z, Chen W, Ding Y, Luo H. & Bao X. Enhanced ethanol production inside carbon-nanotube reactors containing catalytic particles. *Nat Mater*, **(2007)**; 6:507–511.

[196] Liu B, Torimoto T, Yoneyama H. Photocatalytic reduction of carbon dioxide in the presence of nitrate using TiO_2 nanocrystal photocatalyst embedded in SiO_2 matrices. *J Photochem Photobiol A Chem*, **(1998)**; 115:227–230.

[197] Mikkelsen M, Jørgensen M, Krebs F C. The teraton challenge. A review of fixation and transformation of carbon dioxide. *Energy Environ Sci*, **(2010)**; 3:43–81.

[198] Uner D, Oymak M M, Ipek B. CO_2 utilisation by photocatalytic conversion to methane and methanol. *Int J Global Warming*, **(2011)**; 3:142–161.

[199] Kavita K, Rubina C, Sawhney R L. Treatment of hazardous organic and inorganic compounds through aqueous-phase photocatalysis: a review. *Ind Eng Chem Res*, (**2004)**; 43:7683–96.

[200] Fan W, Zhang Q and Wang Y. Semiconductor based Nano composites for Photocatalytic H_2 Production and CO_2 Conversion. *Phys Chem Chem Phys*, **(2013)**; 15:2632-2649.

References

[201] Chen L, Graham M E, Li G. Gentner D R, Dimitrijevic N M, Gray, K A. Photoreduction of CO_2 by TiO_2 nano composites synthesized through reactive direct current magnetron sputter deposition. *Thin Solid Films*, **(2009)**; 517:5641–5645.

[202] Koppenol W H, Rush J D. Reduction potential of the carbon dioxide/carbon dioxide radical anion: a comparison with other C1 radicals. *J Phys Chem*, (**1987)**; 91:4429-4430.

[203] Indrakanti V P, Schobert H H, Kubicki J D. Quantum mechemical modeling of CO_2 interactions with irradiated stoichiometric and oxygen deficient anatase TiO_2 surfaces: Implications for the photocatalytic reduction of CO_2. *Energy Fuels*, (**2009)**; 23:5247-5256.

[204] Yahaya A H, Gondal, M A. and Hameed, A. Selective Laser Enhanced Photocatalytic Conversion Of CO_2 into Methanol. *Chem Phys Lett*, **(2004)**; 400:206–212.

[205] Hartman K and Hisatsune I C. Infrared Spectrum of Carbon Dioxide Anion Radical. *J Chem Phys*, **(1966)**; 44:1913–1918.

[206] Perissinotti L L, Brusa M A and Grela M A. Yield of Carboxyl Anion Radicals in the Photocatalytic Degradation of Formate over TiO_2 particles. *Langmuir*, **(2001)**; 17: 8422–8427.

[207] Tu W, Zhou Y, and Zou Z. Photocatalytic Conversion of CO_2 into Renewable Hydrocarbon Fuels: State-of-the-Art Accomplishment, Challenges, and Prospects. *Adv Mater*, (**2014)**; 26:4607-4626.

[208] Sing K S W, Everett D H, Haul R A W, Moscou L, Pierotti R A, Rouquerol J, Siemieniewska T. Reporting physisorption Data for Gas/Solid Systems. *Pure Appl Chem*, **(1985)**; 57:603-619.

[209] Chiola V, Ritsko J E, Vanderpool C D. *US Patent* No. 3556725 **(1971)**.

[210] Chen C Y, Li H X, Davis M E. Studies on mesoporous materials: I. Synthesis and characterization of MCM-4. *Micropor Mater*, **(1993)**;2,Issue 1:17–26.

References

[211] Beck J S, Vartuli J C, Roth W J, Leonowicz M E, Kresge C T, Schmitt K D, Chu C T W, Olson D H, Sheppard E W, McCullen S B, Higgins J B, Schlenker J L. A New Family of Mesoporous Molecular Sieves Prepared with Liquid Crystal Templates. *J Am Chem Soc*, **(1992)**; 114:10834-10843.

[212] Corma A. From microporous to mesoporous molecular sieve materials and their use in catalysis. *Chem Rev*, **(1997)**; 97:2373-2419.

[213] Ying J Y, Mehnert C P, Wong M S. Synthesis and Applications of Supramolecular-Templated Mesoporous Materials. *Angew Chem Int Ed*, **(1999)**; 38:56-77.

[214] Thomas J M. Design, Synthesis, and In Situ Characterization of New Solid Catalysts *Angew Chem Int Ed*, **(1999)**; 38:3589-3628.

[215] Davis M E. Ordered porous materials for emerging applications. *Nature,* **(2002)**; 417:813-821.

[216] He X, Antonelli D. Recent Advances in Transition Metal Containing Mesoporous Molecular Sieves. *Angew Chem Int Ed*, **(2001)**; 41:214-229.

[217] Wight A P, Davis M E. Design and Preperation of Organic-inorganic Hybrid Catalysts. *Chem Rev*, **(2002)**; 102:3589-3613.

[218] DeVos D E, Dams M, Sels B F, and Jacobs P A. Ordered Mesoporous and Microporous Molecular Sieves Functionalized with Transition Metal Complexes as Catalysts for Selective Organic Transformations. *Chem Rev*, **(2002)**; 102:3615-3640.

[219] Soler-illia G J D, Sanchez C, Lebeau, B, Patarin J. Chemical Strategies To Design Textured Materials: from Microporous and Mesoporous Oxides to Nanonetworks and Hierarchical Structures. *Chem Rev*, **(2002)**; 102:4093-4138.

[220] Wan Y, Yang H F, Zhao D Y. "Host−Guest" Chemistry in the Synthesis of Ordered Nonsiliceous Mesoporous Materials. *Acc Chem Res*, **(2006)**; 39:423-432.

[221] Wan Y, Zhao D Y. On the controllable Soft-Templating Approach to Mesoporous Silicates. *Chem Rev*, **(2007)**; 107:2821-2860.

[222] Zhang H, Hardy G C, Rosseinsky M J, Cooper A I. Uniform Emulsion-Templated Silica

References

Beads with High Pore Volume and Hierarchical Porosity. *Adv Mater*, **(2003)**; 15:78.

[223] Karkamkar A J, Kim S, Mahanti S D, Pinnavaia T J. Lamellar Mesostructured Silicas with Chemically Significant Hierarchical Morphologies. *Adv Funct Mater Chem*, **(2004)**; 14:507-512.

[224] Andersson J, Johannessen E, Areva S, Baccile N, Azais T, Linde M. Physical properties and *in vitro* bioactivity of hierarchical porous silica–HAP composites. *J Mater Chem*, **(2007)**; 17:463-468.

[225] Sel O, Sallard S, Brezesinski T, Rathousky J, Dunphy D R, Collord A, Smarsly B M. Periodically Ordered Meso and Macroporous SiO_2 Thin Films and Their Induced Electrochemical Activity as a Function of Pore Hierarchy. *Adv Funct Mater*, **(2007)**; 17:3241-3250

[226] Ji Q, Acharya S, Hill P J, Vinu A, Yoon S B, Yu J, Sakamoto K, Ariga K. Hierarchic nanostructure for auto-modulation of material release: mesoporous nanocompartment films. *Adv Funct Mate*r, **(2009)**; 19:1792-1799.

[227] Yoon T J, Kim J S, Kim B G, Yu K N, Cho M H, Lee J K. Multifunctional nanoparticles possessing a "magnetic motor effect" for drug or gene delivery. *Angew Chem Int Ed*, **(2005)**; 44:1068-1071.

[228] Liong M, Angelos S, Choi E, patel K, Stoddart J F, Zink J I. Mesostructured multifunctional nanoparticles for imaging and drug delivery. *J Mater Chem*, **(2009)**; 19(35):6251-6257.

[229] Fukao M, Sugawara A, Shimojima A, Fan W, Arunagirinathan M A, Tsapatsis M, Okubo T. One-Dimensional Assembly of Silica Nano spheres Mediated by Block Copolymer in Liquid Phase. *J Am Chem Soc*, **(2009)**; 131:16344-16345.

[230] Yin H, Zhou Z, Huang J, Zheng R, Zhang Y. Temperature-Induced Micelle to Vesicle Transition in the Sodium Dodecyl sulfate/Dodecyl triethyl ammonium Bromide System. *Angew Chem Int Ed*, **(2003)**; 115:2238-2241.

[231] Hidalgo M C, Aguilar M, Maicu M, Navı´o J A, Colo´n G. Hydrothermal preparation of

highly photoactive TiO_2 nanoparticles. *Catal Today*, **(2007)**; 129:50-58.

[232] Testino A, Bellobono I R, Buscaglia V, Canevali C, D'Arienzo M, Polizzi S, Scotti R, Morazzoni F. Optimizing the Photocatalytic Properties of Hydrothermal TiO_2 by the Control of Phase Composition and Particle Morphology. A Systematic Approach. *J Am Chem Soc*, **(2007)**; 129:3564-3575.

[233] Almquist C B, Biswas P. Role of synthesis method and particle size of nanostructured TiO_2 on its photoactivity. *J Catal*, **(2002)**; 212:145–156.

[234] Kresge C T, Leonowicz M E, Roth W J. Ordered mesoporous molecular sieves synthesized by a liquid-crystal template mechanism. *Nature*, **(1992)**; 359:710-712.

[235] Takahara Y, Kondo J N, Takata T, Lu D, Domen K. Mesoporous Tantalum Oxide.1.Characterization and Photocatalytic Activity for the Overall Water Decomposition. *Chem Mater*, **(2001)**; 13:1194-1199.

[236] Lakshminarasimhan N, Bae E, Choi, W. Enhanced Photocatalytic Production of H_2 on Mesoporous TiO_2 Prepared by Template-Free Method: Role of Interparticle Charge Transfer. *J Phys Chem C*, **(2007)**; 111:15244-15250.

[237] Chen X, Yu T, Fan X, Zhang H, Li Z, Ye J, Zou Z. Enhanced activity of mesoporous Nb_2O_5 for photocatalytic hydrogen production. *Appl Surf Sci*, **(2007)**; 253:8500-8506.

[238] Lin H Y, Huang H C, Wang W L. Preparation of mesoporous In Nb mixed oxides and its application in photo catalytic water splitting for hydrogen production. *Micropor Mesopor Mater*, **(2008)**; 115:568-575.

[239] Zhang Z, Zuo F, Feng P. Hard template synthesis of crystalline mesoporous anatase TiO_2 for photocatalytic hydrogen evolution. *J Mater Chem*, **(2010)**; 20:2206-2212.

[240] Hartmann P, Lee D K, Smarsly B M, Janek J. Mesoporous TiO_2: Comparison of Classical Sol−Gel and Nanoparticle Based Photoelectrodes for the Water Splitting Reaction. *ACS Nano*, **(2010)**; 4:3147-3154.

References

[241] Wang L, Qi T, Zhang Y, Chu J. Morphosynthesis route to large-pore SBA-15 microsphere. *Micropor Mesopor Mater*, **(2006)**; 91:156–160.

[242] Soni K, Rana B S, Sinha A K, Bhaumik A, Nandi M, Kumar M, Dhar G M. 3-D Ordered Mesoporous KIT-6 Sopport for Effective Hydrodesulfurization Catalysts. *Appl Catal B Environ*, **(2009)**; 90:55–63.

[243] Hussain M, Abbas N, Fino D, Russo N. Novel mesoporous silica supported ZnO adsorbents for the desulphurization of biogas at low temperatures. *Chem Eng J*, **(2012)**; 188:222–232.

[244] Peng R, Zhao D, Dimitrijevic N M, Rajh T, Koodali R T. Room temperature synthesis of Ti-MCM-48 and Ti-MCM-41 mesoporous materials and their performance on photocatalytic splitting of water. *J Phys Chem* C, **(2012)**; 116:1605–1613.

[245] Wright J D, Sommerdjik N A J M. Sol Gel Materials: Chemistry and Applications, *Gordon and Breach Science Publishers*. Amsterdam, **(2001)**:33–36.

[246] Kyung-Jun H, Seung-Joon Y, Sung-Soo K, Ji-Man K, Wang-Geun S, Sun-Il K, Jae-Wook L. Photovoltaic Performance of Nanoporous TiO_2 Replicas Synthesized from Mesoporous Materials for Dye Sensitized Solar Cells. *J Nanosci Nanotechnol*, (**2008)**; 8:4976-4981.

[247] Lee J, Han S, Hyeon T. Synthesis of new nanoporous carbon materials using nanostructured silica materials as templates. *J Mater Chem*, (**2004)**; 14:478–486.

[248] Griken V, Aguado R, Lopez-M J. Synthesis of size-controlled silica-supported TiO_2 photo catalysts. *J Photochem Photobiol A Chem*, **(2002)**; 148:315-322.

[249] Marriott P J. GAS CHROMATOGRAPHY Principles; in Encyclopedia of Analytical Science (Second Edition): Reference Model in Chemistry, Molecular Sciences and Chemical Engineering (P. Worsfold, A. Townshend, C. Poole) *Elsevier Ltd.* **(2010)**; 7-18.

[250] Robards K. GAS CHROMATOGRAPHY Overview; in Encyclopedia of Analytical Science (Second Edition): Reference Model in Chemistry, Molecular Sciences and

References

Chemical Engineering (P. Worsfold, A. Townshend, C. Poole,) *Elsevier Ltd*. **(2005)**; 1-7.

[251] Laird C K, Verhappen I. Chemical Analysis: Gas Analysis; inInstrumentation Reference Book (Fourth Edition) (W. Boyes), Butterworth-Heinemann *Elsevier Ltd. Cap*, **(2010)**; 25**:**401-428.

[252] Kaneko K. Determination of pore size and pore size distribution: Adsorbents and catalysts. *J Membr Sci*, **(1994)**; 96:59–89.

[253] Dai W, Zheng M, Zhao Y, Liao S, Ji G, Cao J. Template synthesis of three-dimensional cubic ordered mesoporous carbon with tunable pore sizes. *Nanoscale Res Lett*, **(2010)**; 5:103–107.

[254] Riazian M, Bahari A. Structurw of lattice strain and effect of sol concentration on the characterization of TiO_2 CUO-SiO_2 Nanoparticles. *Int J Nano Dimen*, **(2012)**; 3:127–139.

[255] Socrates G. Infrared and Raman Characteristic Group Frequencies: Tables and Charts, third ed. *John Wiley & Sons Ltd., Chichester*, (**2001)**.

[256] Collado L, Jana P, Sierra B, Coronado J M, Pizarron P, Serrano D P, De la Pena O'Shea V A. Enhancement of hydrocarbon production via artificial photosynthesis due to synergetic effect of Ag supported on TiO_2 and ZnO semiconductors. *Chem Eng J*, (**2013)**; 224:128–135.

[257] Najafabadi T A. CO_2 chemical conversion to useful products: an engineering insight to the latest advances toward sustainability. *Int J Energy Res*, (**2013)**; 37:485–499.

[258] Hussain M, Akhter P, Saracco G, Russo N, "Nanostructured TiO_2/KIT-6 photocatalyts for improved photocatalytic reduction of CO_2 to tunable energy products" *Applied Catalysis B: Environ*, **(2015)**.(In press)

[259] Centi G, Perathoner S. Towards solar fuels from water and CO_2, *ChemSusChem*, **(2010)**; 3:195–208.

[260] Abbas N, Hussain M, Russo N, Saracco G. Studies on the activity and deactivation of novel optimized TiO_2 nanoparticles for the abatement of VOCs. *Chem Eng J*, **(2011)**;

175:330–340.

[261] Kubacka A, Fernandez-Garcia M, Colon G. Advanced nano architectures for solar photocatalytic applications. *Chem Rev*, (**2012)**; 112:1555–1614.

[262] Hussain M, Russo N, Saracco G. Photocatalytic abatement of VOCs by novel optimized TiO_2 nanoparticles. *Chem Eng. J*, (**2011)**; 166:138–149.

[263] Carneiro J T, Savenije T J, Moulijn J A, Mul G. How phase composition influences optoelectronic and photocatalytic properties of TiO_2. *J Phys Chem C*, (**2011)**; 115:2211–7.

[264] Hurum D C, Agrios A G, Gray K A, Rajh T, Thurnauer M C. Explaining the enhanced photocatalytic activity of Degussa P25 mixed-phase TiO_2 using EPR. *J Phys Chem B*, (**2003)**; 107:4545–4549.

[265] Periyat P, Baiju K V, Mukundan P, Pillai P K, Warrier K G K. High temperature stable mesoporous anatase TiO_2 photocatalyst achieved by silica addition. *Appl Catal A*, (**2008)**; 349:13–9.

[266] Fujishima A, Hashimoto K, Watanabe T. TiO_2 photocatalysis: fundamentals and applications. English ed. Tokyo: *BKC Inc*, (**1999)**.

[267] Burghaus U. Surface science perspective of carbon dioxide chemistry-Adsorption kinetics and dynamics of CO_2 on selected model surfaces. *Catal T*oday, (**2009)**; 148:212–20.

[268] Carp O, Huisman C L, Reller A. Photoinduced reactivity of titanium dioxide. *Prog Solid State Chem*, (**2004)**; 32:33–177.

[269] Zhang Q H, Han W D, Hong Y J, & J G, Yu J G. Photocatalytic reduction of CO_2 and H_2O on Pt loaded TiO_2 catalyst. *Cataly Today*, **(2009)**; 148:335-340.

[270] Wang W, Park J, Biswas P. Rapid synthesis of nano structured Cu-TiO_2-SiO_2 composites for CO_2 photoreduction by evaporation driven self-assembly. *Catal Sci Technol*, **(2011)**; 1:593-600.

[271] Sing K S W, Everett D H, Haul R A W, Moscon L, Pierotti R A, Rouquol J. Reporting

References

physisorption data for gas/solid systems with special reference to the determination of surface area and porosity. *Pure Appl Chem*, **(1985)**; 57:603-619.

[272] Lo´pez-Mun˜oz M. J, Grieken R, Aguado J, Marugun J. Role of the support on the activity of silica-supported TiO_2 photocatalysts: Structure of the TiO_2/SBA-15 photocatalysts. *Catal Today*, **(2005)**; 101:307–314.

[273] Zaho Y X, Xu L P, Wang Y Z, Gao C G, Liu D S. *Catal. Today.* **(2004)**; 93–95:583

[274] Yang J, Zhang J, Zhu L, Chen S, Zhang Y, Tang Y, Zhu Y, Li Y. Synthesis of nano titania particles embedded in mesoporous SBA-15: Characterization and photocatalytic activity. *J Hazard Mater B*, **(2006)**; 137:952-958.

[275] Beyers E, Bierman E, Ribben S, Witte K De, Mertens M, Meynen V, Bals S, Van Tendeloo G, Vansant E F, Cool P. Combined TiO_2/SiO_2 mesoporous photocatalysts with location and phase controllable TiO_2 nanoparticles. *Appl Catal B Environ*, **(2009)**; 88:515-524.

[276] Jung K Y, Park S B. Enhanced photoactivity of silica-embedded titania particles prepared by sol–gel process for the decomposition of trichloroethylene. *Appl Catal B Environ*, **(2000)**; 25:249-256.

[277] Jung K Y, Park S B. Anatase-phase titania: preparation by embedding silica and photocatalytic activity for the decomposition of trichloroethylene. *J Photochem Photobiol A Chem*, **(1999)**; 127:117-122.

List of Publications

International Journal Papers:

1. Murid Hussain, Parveen Akhter, Guido Saracco, Nunzio Russo, "Nanostructured TiO_2/KIT-6 photocatalyts for improved photocatalytic reduction of CO_2 to tunable energy products" **Applied Catalysis B: Environmental,** (2015), DOI:10.1016/j.apcatb.2015.01.007, **(Accepted)**.
2. Parveen Akhter , Murid Hussain , Guido Saracco, Nunzio Russo, "Novel nanostructured-TiO_2 materials for the photocatalytic reduction of CO_2 greenhouse gas to hydrocarbons and syngas" **Fuel** (2014), DOI: 10.1016/j.fuel.2014.09.079, **(Accepted)**.
3. Murid Hussain, Parveen Akhter, Guido Saracco, Nunzio Russo, "New optimized mesoporous silica incorporated isolated Ti materials towards improved photocatalytic reduction of carbon dioxide to renewable fuels" **Chemical Engineering Journal**, (2014), DOI: 10.1016/j.cej.2014.08.095, **(Accepted)**.
4. Parveen Akhter, Murid Hussain, Guido Saracco, Nunzio Russo, "New nanostructured silica incorporated isolated Ti material for the photocatalytic conversion of CO_2 to fuels" **Nanoscale Research Letters**, (2014), vol. 9 n. 158, pp. 1-8.
5. Murid Hussain, Parveen Akhter, Debora Fino, Nunzio Russo, "Modified KIT-6 and SBA-15-spherical supported metal catalysts for N_2O decomposition" **Journal of Environmental Chemical Engineering**, (2013), vol. 1 n. 3, pp. 164-174.
6. Murid Hussain, Parveen Akhter, Nunzio Russo, Guido Saracco, "Novel Ti-KIT-6 material for the photocatalytic reduction of carbon dioxide to methane" **Catalysis Communications**, (2013), vol. 36, pp. 58-62.

Conferences proceedings:

1. Parveen Akhter, Murid Hussain, Nunzio Russo and Guido Saracco, "New optimized mesoporous silica materials supported isolated Ti for the photocatalytic reduction of CO_2 to fuels" **ISCRE 23 & APCRE 7**, Bangkok, **Thailand**, September 7-10, 2014.
2. Parveen Akhter, Murid Hussain, Nunzio Russo and Guido Saracco, "Novel Nano-TiO_2 Materials for Photocatalytic Reduction of Carbon Dioxide to Hydrocarbons and Syngas" **International-Mexican Congress on Chemical Reaction Engineering** (IMCCRE 2014), Acapulco, **Mexico**, June 7-13, 2014.

List of Publications

3. Parveen Akhter, Murid Hussain, Nunzio Russo, Guido Saracco, "Photocatalytic conversion of carbon dioxide and water vapor to hydrocarbons and hydrogen" **EMN Spring Meeting (Energy Materials Nanotechnology)**, Las Vegas NV, **USA**, 2014, February 27-March 2.
4. P. Akhter, M. Hussain, N. Russo, G. Saracco, "Novel mesoporous silica incorporated isolated Ti for photocatalytic reduction of CO_2 and H_2O to CH_4" Proceeding of the **XXXVI Meeting of the Italian Section of the Combustion Institute**, Isola di Procida, **Italy**, 2013, June 13-15.
5. P. Akhter, M. Hussain, N. Russo, G. Saracco, "Photocatalytic reduction of CO_2 to methane" Proceeding of the **XXXV Meeting of the Italian Section of the Combustion Institute**, Page 42, Milan, **Italy**, 2012, October 10-12.